ACTIVE CONTROL OF SUPERCONDUCTIVITY BY MEANS OF THE FERROMAGNETIC EXCHANGE INTERACTION

Robert Kinsey

Trinity Hall, Cambridge

A dissertation submitted for the degree of Doctor of Philosophy in the University of Cambridge

April 2001

SUMMARY

Recent theoretical studies have suggested that the observed suppression of superconductivity in superconductor/ferromagnet (S/F) heterostructures could be modulated by controlling the ferromagnetic exchange interaction in the superconductor. The exchange interaction in the superconductor is the sum of the exchange interaction from the ferromagnetic regions, which has a phase and magnitude that depends upon the direction that the ferromagnet is magnetised and the distance. As the exchange interaction has a phase it is possible that the contribution from two regions will cancel out. The exchange interaction, which can be viewed as an imbalance in the spin populations, suppresses superconductivity so any reduction in the exchange interaction will increase the superconducting transition temperature (T_c) of the heterostructure. Thus by changing the magnetisation of the ferromagnetic regions it is possible to control the exchange interaction in the superconductor and so the superconducting properties of the heterostructure.

I have measured the superconducting properties of niobium/cobalt bilayers as a function of the applied magnetic field. I have observed that one component of the superconducting properties is controlled by the net magnetisation rather than the magnitude of the applied field. I have been able to show that this component of the observed change in the superconducting properties is not simply due to stray magnetic field but that the superconductivity is being actively controlled by means of the exchange interaction. This is the first experimental evidence that the superconducting properties of a S/F heterostructure can be controlled in this way, which opens up the possibilities for the construction of future devices.

PREFACE

This dissertation describes work that took place between September 1997 and April 2001 in the Device Materials Group of the Department of Materials Science and Metallurgy, University of Cambridge. It is submitted for the degree of Doctor of Philosophy in the University of Cambridge. Except where specific reference is made, this work is entirely the result of my own work and includes nothing that is the outcome of work done in collaboration. No part of this work has been or is being submitted for any other qualification at this or any other university. Some of the work contained in this dissertation is about to be published, see the appendix.

Robert Kinsey

IRC in Superconductivity

University of Cambridge

April 2002

There are a great many people that I need to thank for their help over the last three and a half years♥. To begin at the beginning, special thanks go to my supervisor Dr. Mark Blamire for all the help he has given and his patience with my inability to string words together coherently. All too often I have completely failed to see the wood in any way, shape or form. I would like to thank Dr. Zoe Barber for all her help, especially with thin film deposition, Dr. Edward Tarte for his help in the clean–room and out of it, and Prof. Jan Evetts for those times I poked my head around his door with 'Just a quick question.' I must also thank my examiners for everything they did to improve this work. The Engineering and Physical Sciences Research Council funded my initial three years of research while the University and my supervisor gave financial support while I overran and for this I am grateful.•

♥ If I fail to mention you by name then please forgive me, this already seems too much like a draft acceptance speech to the Academy — 'You love me, you really do…!' ☺

• I've been checking through my thesaurus to find as many possible variants on thank-you as possible, let's see how I do…

The people that you work with can make all the difference when it comes to enjoying your work. There are five people in particular I feel honoured to have known, and I hope they keep in touch: John (Just because you're paranoid…) Durrell, Phil (The Incredible Hulk) McBrien, Richard (Wild Thing) Moseley, Noel (Wacky Races) Rutter, Neil (California Dreamin') Todd – all of whom are Drs. or else should be soon. I also must thank Drs. Gavin Burnell and Wilfred Booji for everything they taught me around the lab and for keeping the place going. I'd still be there trying to get it to work without you. Around the lab there are many other people who have offered their help and support and I appreciate everything they did.

Thanks go to my housemates for putting up with the often odd hours I've kept, especially Antony Glauser and Dan Wakelin who chose to remain only a wall away. For CUSFS, thanks for being there. You were a welcome distraction. Of course the Reeves (past and present) deserve gratitude for the daylight, though the past few months have been a little disappointing. You'll soon get the hang of it.

'Family alternately delights and infuriates us.' I'm afraid I can't remember the source but, with love, this thesis is as much for them as it is for anyone. There have been times when I have despaired and they have always been there when I needed them. For my parents, grandparents, uncle and aunts, Jan and her parents and most of all for my sister, Helen.

Final thanks and eternal gratitude go to my proof-readers, Dr. Mark Blamire, Dr. Gavin Burnell, Dan Wakelin and my sister Helen Kinsey. Without them this thesis would be far less than it presently is. As usual any mistakes remaining are entirely my own.

CONTENTS

Summary ii
Preface iii
Contents v
Definition of Terms viii

INTRODUCTION **1**
Overview **3**

THEORY OF SUPERCONDUCTORS AND FERROMAGNETS **5**
Basic Superconducting Theory 6
Historical Background **6**
Ginzburg – Landau Theory and Type II Behaviour **7**
BCS Theory **11**
The Proximity Effect **16**
The Josephson Effect **21**
Non-Equilibrium Superconductivity **22**
Basic Magnetic Theory 23
Magnetic Materials **23**
Magnetoresistance **27**
Spin–Polarised Tunnelling **29**
Spin Imbalance in a Paramagnetic Metal **32**

COEXISTANCE OF SUPERCONDUCTIVITY AND MAGNETISM **39**
Magnetic Impurities in Superconductors **40**
The Superconducting Proximity Effect in Ferromagnets **41**
Modelling Superconductor/Ferromagnet Multilayers **45**
Spin-Polarised Quasiparticles in a Superconductor **50**
Suppression of Critical Current by Injection of Spin-Polarised Quasiparticles **53**
The Theory of Spin-Polarised Quasiparticles **55**
Magnetic Superconductors **57**
The Cryptoferromagnetic Phase **59**
Controlling the Exchange Interaction in the Superconductor **62**

EXPERIMENTAL METHODS **64**
Film Deposition **65**
The Kondo Effect 69
Patterning the Device **71**
Modifying the Device Pattern **74**
X-Ray Analysis of the Unpatterned Films **80**
Magnetic Properties of the Cobalt Layer **82**
Electrical Properties of the Heterostructure Device **85**

CHARACTERISATION OF NIOBIUM/COBALT BILAYERS **89**
Measurement of a Niobium Film 92
Critical current vs. applied field for a niobium film **92**
Self field and asymmetry **95**
Crystallite size **100**
Magnetic Structure of the Cobalt Layer 101
Crystallite size **102**
The 'Double Peak' Structure 104
Flux vortices **105**
Stray magnetic field **107**
Ferromagnetic exchange interaction **115**
Voltage criteria **118**
Reproducibility and Barkhousen Noise **119**
Hysteretic Switching in the Critical Current 124
Summary 129
SYSTEMATIC CHANGES **131**
Changes in the Measurement Conditions 134
Maximum applied magnetic field **134**
Magnetic field direction **135**
Superconducting transition temperature vs. applied magnetic field **139**
Change in the cobalt structure with temperature **141**
Change in the critical current with temperature **143**
Structural Changes 148
Track Width **148**
Localising the measurement area 148
The percolation model 155
Changes in track width 157
Thinning the niobium layer 160
Changing the niobium layer thickness **163**
Modelling the change in transition temperature 164
Changes in the critical current 166
Changing cobalt layer thickness **168**
Niobium/iron bilayers **174**
Summary 176
CONCLUSIONS **179**
The 'Double Peak' Structure **180**
Exchange Interaction or Stray Field? **181**
Further Work **184**
BIBLIOGRAPHY **186**

APPENDIX A – PAPER **193**

APPENDIX B – SUPPLEMENTARY DATA **201**

Definition of Terms

e	Charge of an electron = -1.602x10^{-19} C.
eV	Electron Volt = 1.602x10^{-19} J.
$\underline{H}_c$	Critical magnetic field of a type I superconductor.
$\underline{H}_{c_1}$	Lower critical magnetic field of a type II superconductor.
$\underline{H}_{c_2}$	Upper critical magnetic field of a type II superconductor.
$\underline{H}_C$	Coercive field of a ferromagnet.
h_p	Plank's constant = 6.626x10^{-34} Js.
$\hbar$	$\frac{h_p}{2\pi}$ = 1.054x10^{-34} Js.
I_c	Superconducting critical current.
I_{c_f}	The forward critical current, shown as greater than zero on the critical current vs. magnetic field figures.
I_{c_r}	The reverse critical current, shown as less than zero on the critical current vs. magnetic field figures.
I_{c_t}	The total critical current, equal to the sum of I_{c_f} and I_{c_r}.
j	$\sqrt{-1}$
J_c	Superconducting critical current density.
k_B	Boltzmann's constant = 1.38x10^{-23} J/K, links energy to temperature through $E = k_B T$.
M_S	Saturation magnetisation.
n_p	Number of 'superelectrons' in Ginzburg – Landau Theory.
T_c	Superconducting transition temperature, 9.25 K in bulk pure Nb.
T_C	Curie temperature of a ferromagnetic material, 1131°C in bulk pure Co and 770°C in bulk pure Fe.
T_K	The Kondo temperature.
T_N	Néel temperature of an antiferromagnetic material.
Δ	Superconducting gap parameter in BCS theory.
κ	The Ginzburg – Landau parameter, equal to $\frac{\lambda}{\xi}$.
λ_B	London penetration depth.
μ_0	Permeability of free space = 1.257x10^{-6} H/m.

μ_B	The Bohr magneton = 9.274×10^{-24} Am^2 (J/T) = 1.165×10^{-29} Jm/A.
ξ_0	Pippard coherence length.
$\xi_{GL}(T)$	Ginzburg-Landau coherence length.
Φ_0	Flux quantum, equal to $\frac{h}{2e}$ = 2.068×10^{-15} Wb.
$\Psi(r)$	Complex effective superfluid wavefunction in Ginzburg – Landau Theory.

Chapter One

INTRODUCTION

Reason. It is no more reliable a tool
than instinct, myth or dream.

Destruction, Brief Lives, Neil Gaiman

Superconductivity and ferromagnetism involve very different ordering of the electrons in the material. The ordering of the electrons in a material will extend through a good electrical connection into another material: the proximity effect. This ordering is unstable in the second material and so decays with time but the exchange of electrons at the interface leads to a dynamic equilibrium. Around the interface there is a region that has electronic properties which are intermediate between those found in the two separate materials. In most cases, ferromagnetic ordering prevents the formation of superconducting ordering and vice versa. There has been considerable interest in the properties of superconductor/ferromagnet (S/F) heterostructures and the materials that seem to show both sorts of ordering.

Studies have shown that a ferromagnetic layer suppresses the superconducting transition temperature (T_c) of a multilayer far more strongly than a normal metal layer [Hauser 1966]. This led to the use of ferromagnetic materials in superconducting devices, most especially those involving the injection of current to suppress the critical current of the superconductor (I_c) [Chrisey 1997, Dong 1997, Soulen 1997, Vas'ko 1997, Lee 1999, Yeh 1999-II]. The spin-polarised current from the ferromagnet creates a spin-imbalance in the superconductor which strongly suppresses I_c, giving a larger current gain than a normal metal injector. However the performance of current injection devices is limited by the heat generated when the current is driven through the interface. This increase in local temperature also suppresses I_c but the heat must diffuse out of the superconductor before it can return to the original state. As this takes longer than the time required for any spin imbalance to decay or be neutralised, heating significantly increases the switching time of any device.

A new mechanism for controlling the critical current in a superconductor that avoids the problem of interfacial heating has been proposed [Oh 1997, Tagirov 1999]. These devices are based upon S/F multilayers, where the ferromagnetic exchange interaction extends into the superconductor and reduces the superconducting gap parameter (Δ), and so reduces T_c and I_c. The exchange interaction has a phase that depends upon the direction of the magnetisation in the ferromagnet. In the proposed devices there are two ferromagnetic layers and the magnitude of the exchange interaction in the superconductor depends upon whether the magnetisation of the ferromagnetic layers is parallel or antiparallel. The magnetisation, and so the T_c and I_c, of a suitable ferromagnetic layer can be controlled with a small magnetic field. The devices described in the theoretical studies require extremely precise control of the layers in the heterostructures as a tiny variation in, for example, the thickness would change the phase of the exchange interaction at a point in the superconductor. A more robust system involves a single ferromagnetic layer and a single superconducting layer. If the ferromagnetic layer forms domains with antiparallel magnetisations at the coercive field then the same effect should be observed as predicted in the theoretical studies.

Overview

This work aims to show that the critical current of a superconductor can be controlled with a small magnetic field through the medium of the exchange interaction. The work attempts to prove the concept rather than building a fully functioning device. A careful analysis of the results was necessary as the magnetic field itself will suppress the critical current and stray field from a ferromagnetic layer can give a strong local magnetic field.

Chapter two presents a brief overview of the basic theories behind superconductivity and ferromagnetism. This includes a brief description of the basic macroscopic and microscopic theories describing superconductivity and superconductor heterostructures, for more in depth coverage the author found books by Gray, Poole and Tinkham to be useful [Gray 1981, Tinkham 1996, Poole 2000]. The basic properties of magnetic materials are described, primarily the interaction between the magnetic and electrical properties – magnetoresistance – and the injection of spin into a normal metal.

In chapter three the basic theories are extended to examine the influence of ferromagnetic materials on superconductors. Beginning with the effect of magnetic impurities in the superconductor I move on to a discussion of the proximity effect and the properties of superconductor/magnetic material multilayers. Next I consider active superconductor/ferromagnet devices where the spin polarised current from the ferromagnet is used to suppress the superconducting critical current. Finally I discuss magnetic superconductors and the devices based on active control of the ferromagnetic exchange interaction in the superconductor that they have inspired.

Chapter four concerns the fabrication and methods of measurement of the devices. Both electrical and magnetic measurements and the capabilities of the available equipment are discussed. The chapter includes a discussion of the variations in film thickness across an individual film and the concentration of magnetic impurities in the films.

Chapter five discusses the effect of applying a magnetic field, parallel to the current flow, on the superconducting properties of niobium/cobalt bilayers. In particular I discuss the four components that are observed in the critical current vs. applied magnetic field behaviour, focussing on the 'double peak' structure. The critical current depends upon the magnetic history of the film, with the magnetisation of the cobalt layer, and this component contains the effect of the exchange interaction. In order to understand this behaviour I also consider the behaviour of a plain niobium film and the structure of the cobalt layer. The chapter also contains a discussion of the reproducibility of the measurement of an individual track and the causes of noise within the data.

In chapter six I discuss the systematic changes in the measurement conditions and the structure of the S/F bilayers in order to clarify the degree to which the exchange interaction causes the changes in the critical current as the magnetic field is changed. I begin with changes in the measurement conditions of a single track as this increases the reliability of comparison between the measurements. Different tracks have different magnetic structures and so the behaviour with small magnetic field will not be identical even if all other properties are the same. After discussing the effect of changes in maximum magnetic field strength, magnetic field direction and temperature I then discuss the structural changes – changing the track width, the thickness of the individual layers and changing the ferromagnet.

Finally I present the conclusions drawn from the data in chapter seven. Although these conclusions have been discussed in chapters five and six they are drawn together here and the implications for further work are discussed. A paper accepted for publication in *IEEE Trans. Magn* is included as an appendix.

Chapter Two

THEORY OF SUPERCONDUCTORS AND FERROMAGNETS

Few subjects in science are more difficult to understand than magnetism.

Encyclopaedia Britannica, 15th edition 1989

This chapter introduces the basic concepts of superconductivity and ferromagnetism required to understand the theory of superconductor/ferromagnet heterostructures. Beginning with the discussion of superconductivity, a brief historical overview and the concepts of superconducting penetration depth and coherence length. This is followed by the macroscopic theory of Ginzburg and Landau and the quantized flux vortex, then the microscopic theory of Bardeen, Cooper and Schriffer which describes superconductivity in terms of pairs of electrons with opposite spins. The discussion of the basic properties of superconductors is brought to a close with superconductor heterostructures, in terms of the proximity effect, the Josephson effect and non-equilibrium superconductivity.

The discussion of ferromagnetic materials begins with the basic definition and properties of ferromagnetic materials, including domain structure. This is followed by a discussion of how magnetism relates to electrical properties, both in terms of magnetoresistance and the injection of spin into a normal metal. This chapter is no more than a brief overview of the vast body of work on these materials and the devices that can be made from them, however there are numerous textbooks which are available if the reader seeks a fuller understanding. The books by Gray, Poole and Tinkham [Gray 1981, Tinkham 1996, Poole 2000] have been useful in discussions of superconductivity.

BASIC SUPERCONDUCTING THEORY

Historical Background

In 1911, three years after liquefying helium, H. Kameling Onnes observed that the electrical resistance of pure mercury immersed in boiling helium fell to a value that he was unable to measure. A year later he found that a sufficiently large applied current (the critical current, I_c) or magnetic field (the critical field, $\underline{H}_c$) would destroy the superconducting state causing the mercury to exhibit electrical resistance once again. After the discovery of superconductivity in mercury other researchers discovered that a number of elements, intermetallic compounds, oxides and organic materials also become superconducting when cooled below a critical transition temperature (T_c), different for each material. The most obvious superconducting property tends to be perfect conductivity. A current can flow in a superconducting ring without measurable losses over a period of years.

Superconducting materials also show perfect diamagnetism, actively expelling magnetic flux when cooled below T_c if the field is sufficiently low – the Meissner effect [Meissner 1933]. This property cannot be explained in terms of perfect conductivity. Any change in magnetic flux penetrating a material induces an electric field and in a perfect conductor this would generate an opposing current which would maintain the flux density. The Meissner effect explains thermodynamically why superconductivity is suppressed by a sufficiently large magnetic field. If the magnetic energy ($\frac{H^2}{8\pi}$ per unit volume) exceeds the difference in the Helmholtz free energy between the normal and superconducting states then the superconducting state will no longer be stable.

An initial explanation for the properties of superconductors was given by H. and F. London in 1935. They theorised that some of the electrons in the superconductor form a conducting superfluid of 'superelectrons' which carries the electrical current without losses. This phenomenological model gave two main results, first that the 'superelectrons' can carry a steady current without any applied electric field. Second an external magnetic field decays exponentially at the surface of the superconductor over a characteristic length scale, the London penetration depth (λ_L), which is a function of the density of 'superelectrons'. The concept was refined by Pippard in 1953 who proposed a characteristic length scale, the coherence length (ξ_0), over which the local electric field would effect a 'superelectron'. The Pippard coherence length could be derived by assuming that the 'superelectrons' have an energy within k_BT_c of the Fermi level and applying the uncertainty principle.

Ginzburg – Landau Theory and Type II Behaviour

Second order phase transitions are characterised by a continuous first differential of some order parameter that increases from zero at the transition temperature to a limiting value at absolute zero. Near the transition temperature this behaviour is described by Landau's theory as a power series in the order parameter. This theory was extended to superconductivity by Ginzburg and Landau in 1950, with the number of 'superelectrons' used as the order parameter. The number of 'superelectrons' (n_p)

can also be equated as the magnitude of some complex effective superfluid wavefunction $\Psi(\underline{r})$ giving:

$$F_s = F_n + \alpha|\Psi|^2 + \frac{\beta}{2}|\Psi|^4 + \gamma\left|\underline{\nabla}\Psi + \frac{2e}{\hbar}.\underline{A}\Psi\right|^2 + \frac{1}{2\mu_0}\left(\underline{B} - \underline{B}_E\right)^2 \qquad (2\cdot1)$$

where: F_S is the free energy of the superconducting state.

F_n is the free energy of the normal state.

α, β and γ are parameters used to fix $|\Psi|^2 = n_p$.

$\underline{\nabla} \wedge \underline{A}$ is the magnetic flux, $\underline{B}$.

μ_0 is the permeability of free space.

$\underline{B}_E$ is the external magnetic flux.

In addition to the power series terms there is also a 'strain' term and a field term. The strain term represents the additional energy involved in any non-uniform magnitude or phase of Ψ. The field term is the magnetic self-energy of any current flowing in the superconductor. The theory is semi-empirical, it assumes that Ψ exists and that the free energy depends upon it, but makes no assumptions about the microscopic explanation for superconductivity. This is one reason why Ginzburg-Landau theory has been so successful in describing the behaviour of a whole range of superconducting materials near to T_c.

The above equation is then minimised with respect to both Ψ and $\underline{B}$ to give the Ginzburg-Landau equations with a boundary condition that prevents supercurrent crossing a free surface:

$$\begin{aligned} \frac{1}{2m}\left(-i\hbar\nabla + 2e\underline{A}\right)^2\Psi + \left\{\alpha + \beta|\Psi|^2\right\}\Psi = 0 \\ \left(-i\hbar\nabla_n + 2e\underline{A}_n\right)\Psi = 0 \end{aligned} \qquad (2\cdot2)$$

where: the index $_n$ indicates the component normal to the surface.

m is the mass of an electron.

Taking into account the effect of magnetic field on the 'superelectrons' the second Ginzburg-Landau equation is obtained:

$$\underline{J}_S = \nabla \wedge \frac{B}{\mu_0} = \frac{ie\hbar}{m}\left(\Psi^\dagger\nabla\Psi - \Psi\nabla\Psi^\dagger\right) - \frac{4e^2}{m}\underline{A}|\Psi|^2 \qquad (2\cdot3)$$

where: $\Psi^\dagger$ is the complex conjugate of Ψ.

This gives a characteristic length that can be identified as the shortest length over which Ψ can change significantly, the Ginzburg-Landau coherence length $\xi_{GL}(T)$. In a pure superconductor this tends to the Pippard coherence length at absolute zero but diverges as $(T - T_c)$ near to T_c.

In the case where the superfluid wavefunction has been suppressed to a value much less than the value infinitely far from any peturbation, i.e. $|\Psi|^2 << \Psi_\infty^2 = -\frac{\alpha}{\beta}$, it is possible to linearize the Ginzburg-Landau equations. The $|\Psi|^4$ term in equation 2·1 then becomes negligibly small giving the linearized form of equation 2·2:

$$\left(\frac{\nabla}{i} - \frac{2\pi \underline{A}}{\Phi_0}\right)^2 \Psi = -\frac{2m\alpha}{\hbar^2}\Psi \equiv \frac{\Psi}{\xi^2(T)} \tag{2·4}$$

where: Φ_0 is the flux quantum, see below for more details.

Additional simplification arises from the fact that all screening supercurrents give effects that are proportional to $|\Psi|^2$ and so can be inserted into the linearized approximation, decoupling equation 2·4 from equation 2·3.

In 1957, Abrikosov investigated the properties of superconductors with a coherence length considerably shorter than the penetration length. He found that the energy spent in creating a normal region was more than compensated for by the magnetic energy, i.e. a negative surface energy. The type II superconductor, so called to distinguish them from the type I superconductors which show perfect diamagnetism as long as they are superconducting, could subdivide into regions limited by the length ξ. If the normal regions were any smaller than ξ the strain term in equation 2·1 would become so large that the region would become energetically unfavourable. The nature of the superconductor, type I or type II, can be characterised using $\kappa = \frac{\lambda}{\xi}$, which is not temperature dependent as both λ and ξ have the same $(T - T_c)$ dependence. If $\kappa > \frac{1}{\sqrt{2}}$ the superconductor is type II, such as the cuprate superconductors, niobium and its alloys. Type II behaviour must have been observed before Abrikosov established his model but was not reported and may have been put down to instrumental error.

Type II superconductors differ from type I in two critical factors. First, instead of a discontinuous breakdown in superconductivity at the critical field ($\underline{H}_c$), there is a gradual penetration of flux starting at the lower critical field ($\underline{H}_{c_1}$) and increasing until the superconductor is fully penetrated and so normal at the upper critical field ($\underline{H}_{c_2}$). The critical fields are vectors as some superconductors, most notably the cuprates, are anisotropic. This partial penetration by magnetic flux lowers the diamagnetic energy and superconductivity can persist to much higher fields, in fact $H_{c_1} = \frac{H_c}{\sqrt{2}\kappa}$ while $H_{c_2} = \sqrt{2}\kappa H_c$. In some cuprate superconductors κ is so large that the Earth's magnetic field is larger than $\underline{H}_{c_1}$. In addition the demagnetising effects of a thin film can concentrate the magnetic flux at the edge of the film, which can cause some flux to penetrate. It should be stressed that nothing actually occurs at $\underline{H}_c$ in a type II superconductor though it can be determined from thermodynamic measurements. Second, above $\underline{H}_{c_1}$ current flow can require a potential difference, although superconductivity persists. The localised normal regions experience a Lorentz force as a bulk supercurrent flows past them and the resulting motion of magnetic flux lines induces an opposing electric field. The system develops electrical resistance with dissipation occurring amongst the normal electrons in the normal regions. In any real sample there will be some sort of pinning force opposing the motion of the normal regions and no resistance will be observed until the Lorentz force exceeds this limit. In many applications pinning centres are artificially created to increase the maximum useful current.

The magnetic flux within a type II superconductor forms vortices, each with a single quantum of magnetic flux (Φ_0). Thus Φ_0 is the minimum amount of flux possible within a type II superconductor. The flux is quantised in this way as the phase of Ψ must be single valued at all points but equally must change around the normal region to generate the current loop required to screen the bulk of the superconductor from the flux. Thus the phase must increase by an integer multiple of 2π and, as the surface energy is negative, the amount of flux within a vortex will be the minimum possible so as to give the maximum number of vortices and so the maximum surface. The value of the flux quantum can be calculated by considering a superconducting ring with some magnetic flux passing through it and integrating around a loop deep within the bulk of the superconductor where the 'superelectrons' are not moving. This gives $\Phi_0 = \frac{h_p}{2e}$, approximately 2x10^{-15} Wb. The flux vortices tend to repel each other and so form a triangular flux lattice, though this lattice is easily distorted by anisotropy in the superconductor or by pinning centres. The motion of flux vortices has been observed by decorating the surface of the superconductor with magnetic powder. When the magnetic field is reversed vortices remain trapped at the pinning sites until new vortices with the opposite field direction enter the superconductor and the pairs mutually annihilate.

BCS Theory

Bardeen, Cooper and Schrieffer proposed a microscopic mechanism for superconductivity in 1957. In BCS theory the lattice of positively charged ions is so strongly deformed by the charge carrying electrons that it screens the negative charge of the electron and attracts other electrons. In 1956, Cooper had demonstrated that any attractive interaction between electrons would be sufficient to form at least one electron pair, known as a Cooper pair, at sufficiently low temperature. A Cooper pair is a boson not a fermion and so a single wavefunction can describe all the Cooper pairs in a superconductor.

One way to describe the BCS ground state is to consider the Fermi sea by creating pairs of electrons inside the Fermi surface of equal and opposite momentum and spin:

$$\Psi_{Fermi} = \prod \left(c^{\dagger}_{\underline{k}\uparrow} c^{\dagger}_{-\underline{k}\downarrow} \right) |0\rangle \tag{2·5}$$

where: $c^{\dagger}_{\underline{k}\uparrow}$ creates a spin-up electron at k.

$c^{\dagger}_{-\underline{k}\downarrow}$ creates a spin-down electron at –k.

$|0\rangle$ is the empty state.

$\underline{k}_F$ is the reciprocal lattice vector corresponding to the Fermi energy, E_f.

The BCS ground state is then:

$$\Psi_{BCS} = \prod \left(u_{\underline{k}} + v_{\underline{k}} c^{\dagger}_{\underline{k}\uparrow} c^{\dagger}_{-\underline{k}\downarrow} \right) |0\rangle \tag{2·6}$$

The pairs are still present but near the Fermi surface there is a probability that the state is empty, given by $u_{\underline{k}}^2$, and a probability the state is filled, given by $v_{\underline{k}}^2$. Of course $u_{\underline{k}}^2+v_{\underline{k}}^2=1$ and $v_{\underline{k}}^2$ falls from one within the Fermi surface to zero outside it, over a range on the order of k_BT_c which is much less than the Fermi energy. The ground state is assumed to be a singlet state where the two electrons in each Cooper pair have opposite spin states.

The energy of the BCS state is given by:

$$\langle E\rangle = 2\sum \varepsilon_{\underline{k}} v_{\underline{k}}^2 + \sum V_{\underline{kk}'} u_{\underline{k}} v_{\underline{k}} u_{\underline{k}'} v_{\underline{k}'} \qquad (2\cdot7)$$

where: $\varepsilon_k = \dfrac{\hbar^2 k^2}{2m} - \mu$.

μ is the chemical potential of the electrons.

$V_{\underline{kk}'}$ is the interaction potential within a pair.

The first term gives the kinetic energy with respect to the reservoir, which is higher than that of the Fermi sea but the attractive pairing interaction may more than compensate for this by decreasing the potential energy of the system. If the pairing interaction is not strong enough then the Fermi sea is the lowest energy state and the material is not superconducting. A simplifying approximation is made that $V_{\underline{kk}'}$ is constant and equal to $-V$ for all electron states with energy ε_k up to a typical phonon cut-off energy (ε_c) and zero otherwise. Minimising with respect to energy gives the following results:

$$\Delta \equiv \sum V_q u_{\underline{k}'} v_{\underline{k}'} = 2\varepsilon_c e^{\frac{-1}{NV}} \qquad (2\cdot8)$$

$$E_{\underline{k}}^2 = \varepsilon_{\underline{k}}^2 + \Delta^2 \qquad (2\cdot9)$$

$$F_N - F_S(0) = \frac{B_c^2(0)}{2\mu_0} = \frac{N\Delta^2}{2} \qquad (2\cdot10)$$

$$\begin{aligned} u_{\underline{k}}^2 &= \frac{1}{2}\left(1 + \frac{\varepsilon_{\underline{k}}}{E_{\underline{k}}}\right) \\ v_{\underline{k}}^2 &= \frac{1}{2}\left(1 - \frac{\varepsilon_{\underline{k}}}{E_{\underline{k}}}\right) \end{aligned} \qquad (2\cdot11)$$

where: Δ is the gap parameter.

$E_{\underline{k}}$ is the excitation energy for the momentum state $\underline{k}$.

N is the density of electron states at the Fermi level.

NV is the BCS coupling parameter.

$F_N - F_S(0)$ is the condensation energy per unit volume at T = 0.

Δ is the minimum value of $E_{\underline{k}}$, giving an energy gap in the excitation spectrum, which explains how a supercurrent can persist without decaying. Current flow within a material can be described as a shift of the occupied states by some vector $\underline{q}$, which describes the tendency of the electrons to flow in one direction. In a normal metal it is easy for electrons to be elastically scattered into the states emptied by this shift and so, unless a constant potential difference is applied, the current rapidly dies away. In a superconductor the presence of the gap in the density of states above the Fermi level prevents this.

The BCS ground state, like the Fermi sea, has single-particle excitations, which constitute the normal fluid. These excitations can have an electron-like or hole-like character and near E_F, the character is mixed, though each has a definite energy ($E_{\underline{k}}$), a definite momentum ($\hbar\underline{k}$), and a definite spin ($^{\hbar}/_{2}$). They are fermions and obey the Fermi distribution, which gives the occupation at finite temperatures. The excitations are considered in terms of quasiparticles in one of the pair states, for example an electron present in the $\underline{k}$ state but not in the $-\underline{k}$ state. If an empty state above E_F is filled by a quasiparticle it is said to be electron-like, and behaves like an electron, as the absence of an electron at $-\underline{k}$ makes very little difference but the presence of one at $\underline{k}$ is very obvious. Equally if the state is below E_F, the absence of an electron will be obvious and the quasiparticle is said to be, and acts, hole-like. If the quasiparticle is scattered it can change character, allowing relaxation of any excess charge. The different excitations are shown schematically in figure 2·1.

The density of states for the quasiparticles can be derived by remembering that they are fermions and there is a one to one correspondence between the normal metal electron states and the superconductor quasiparticle states. This gives:

$$N_s\left(E_{\underline{k}}\right)\mathrm{d}E_{\underline{k}} = N_n\left(\xi_{\underline{k}}\right)\mathrm{d}\xi_{\underline{k}} \Rightarrow \frac{\mathrm{d}\xi_{\underline{k}}}{\mathrm{d}E_{\underline{k}}} = \frac{N_s\left(E_{\underline{k}}\right)}{N_n\left(\xi_{\underline{k}}\right)} \qquad (2{\cdot}12)$$

where: N_s is the number of quasiparticles in the superconductor.

N_n is the number of electrons in the normal state.

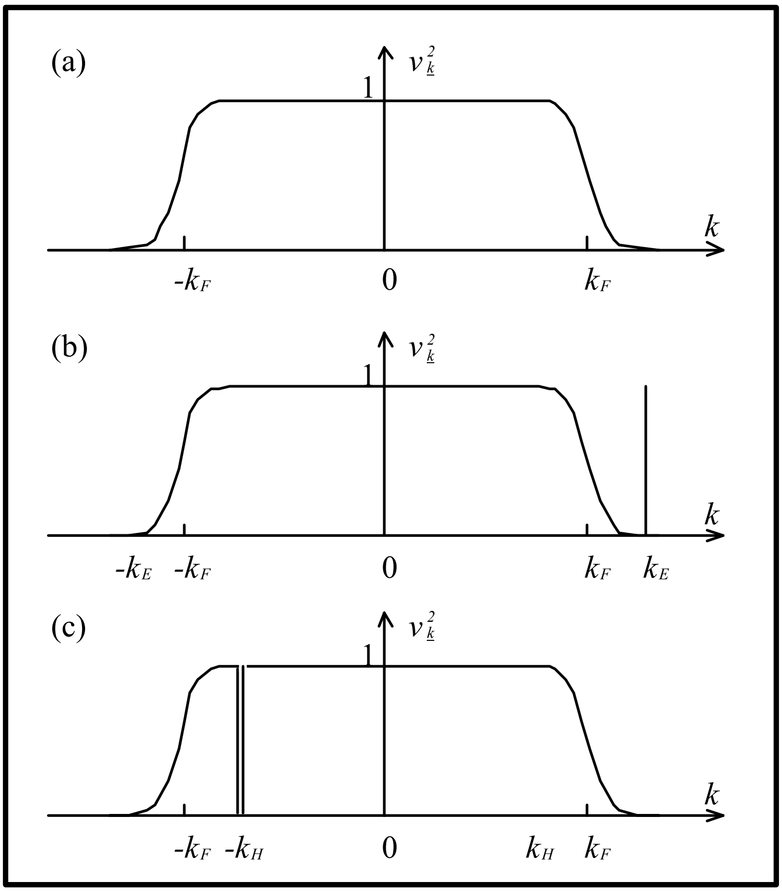

Figure 2·1 Probability of occupation vs. wave number in BCS theory.

a) shows the BCS ground state.
b) shows an electron-like excitation.
c) shows a hole-like excitation.

For energies close to the Fermi surface, within a few meV, we can assume that $N_n(\xi_{\underline{k}})$ is a constant $N(0)$, allowing the easy solution of equation 2·12 to give the BCS density of states:

$$N_s(E_{\underline{k}}) = \begin{cases} N(0)\dfrac{E_{\underline{k}}}{\sqrt{E_{\underline{k}}^2 - \Delta^2}} & E_{\underline{k}} > \Delta \\ 0 & E_{\underline{k}} < \Delta \end{cases} \qquad (2\cdot13)$$

The BCS density of states, shown in figure 2·2, has a discontinuity at Δ and an increased number of states just above Δ.

The excitations become important when BCS theory is extended beyond absolute zero to finite temperatures. The gap parameter Δ of the superconductor is related to the

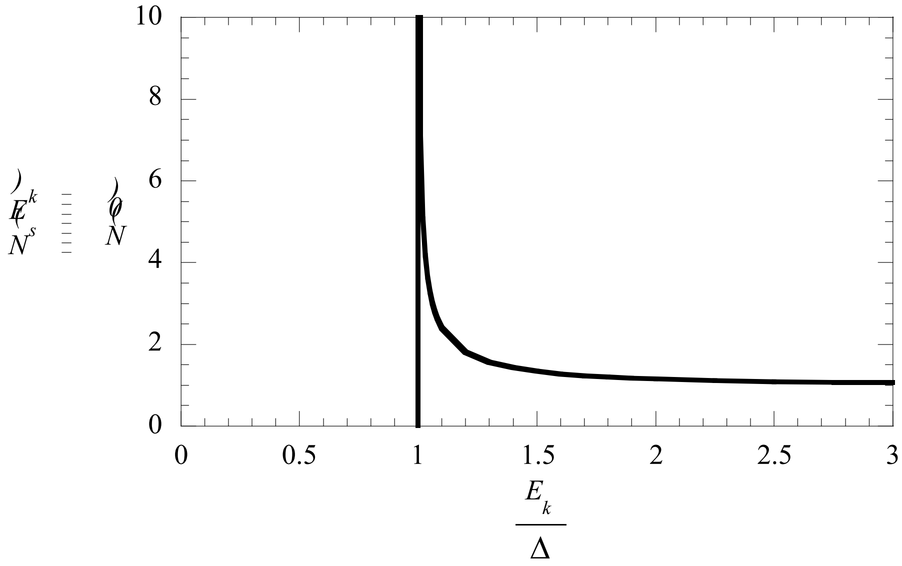

Figure 2·2 BCS density of states

probability of a state being occupied, as shown in equation 2·11 which at finite temperatures gives:

$$\Delta = V\sum_{\underline{k}} v_{\underline{k}}\sqrt{1-v_{\underline{k}}^2}\left(1-2f_{\underline{k}}\right) \tag{2·14}$$

where $f_{\underline{k}}$ is the Fermi function.

As equation 2·9 shows, Δ is the minimum energy a quasiparticle must have before it can enter the superconductor. Andreev, in 1964, proposed a way that an electron with energy near the Fermi level could enter the superconductor. An electron in the superconductor is retroreflected at the interface as a hole and a Cooper pair is carried away in the superconductor, as shown in figure 2·3. This is one way in which superconductivity can extend into a normal metal in contact with a superconductor as the incoming electron and the retroreflected hole will have a strong phase

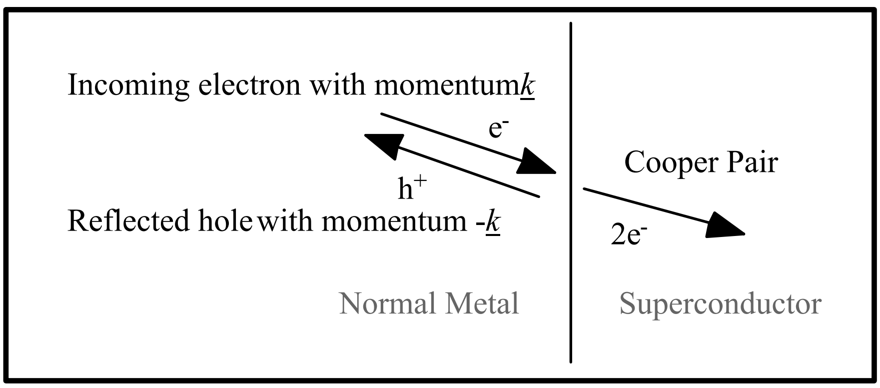

Figure 2·3 Andreev reflection of an electron at a superconductor/normal metal interface.

relationship.

BCS theory describes the superconducting properties of many superconductors. The exceptions include the heavy fermion materials, such as $CeCu_2Si_2$ and UPt_3, the ruthenates and the high T_c superconductors. The heavy fermion materials are so called because the conduction electrons behave as if their mass was many times larger than that of electrons in free space. In both the heavy fermion superconductors and the superconducting oxides of ruthenium, such as Sr_2RuO_4, the Cooper pairs appear to be formed from two electrons with the same spin. This triplet state alters the superconducting properties, most especially the response to a magnetic field [Knigavo 1998, Machida 1998, Belitz 1999].

In the case of high T_c superconductors, which include the cuprates $YBa_2Cu_3O_{7-\delta}$ and $Tl_2Ba_2CaCu_2O_8$ and the organic Cs_3C_{60}, the problem is that the T_c is too high for the simple model of lattice deformation to explain. The BCS coupling parameter NV is limited by the structure of the lattice and this in turn was thought to limit T_c to a maximum of about 30 K. A T_c above 30 K would require that the lattice be deformed by the conduction electrons to such an extent that it would spontaneously transform into a more stable form, with a lower NV. This would be analogous to the transformation of iron from face centred cubic to body centred cubic on cooling. This has lead to suggestions that high temperature superconductivity involves a different mechanism, such as the formation of a Cooper pair by a spin rather than phonon mediated attraction. At present the most widely accepted explanation for the cuprate superconductors is a modified BCS theory where the superconducting wavefunction is d-wave rather than s-wave. In a d-wave superconductor the sign and magnitude of the superconducting wavefunction varies with the crystalographic direction, along certain of which the wavefunction goes to zero.

The Proximity Effect

At a good electrical interface, where the interfacial resistance is low, between a superconductor and another conductor there is a region over which the properties of the two 'blur' into one another. Cooper pairs 'leak' into the non-superconducting conductor effectively creating a superconducting order parameter. This reduces the number of Cooper pairs in the superconductor near the boundary and suppresses T_c in this region, shown schematically in figure 2·4. This effect can be seen in a

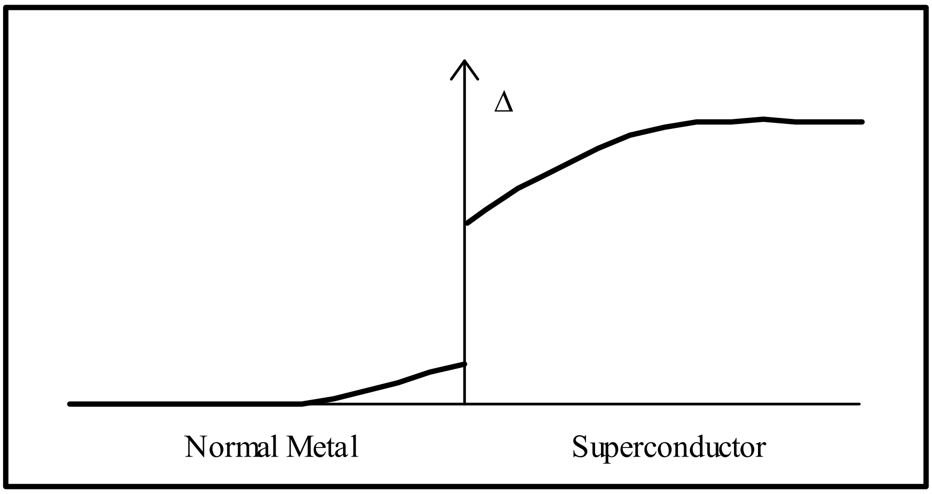

Figure 2·4 Schematic of the superconducting gap function (Δ) at the interface between a superconductor and a normal metal.

sufficiently thin film bilayer of two superconductors. The bilayer will have a T_c that is intermediate between the transition temperatures of the two constituents. A superconducting/non-magnetic insulator bilayer has properties that are almost identical to the bulk superconductor [de Gennes 1964].

The mean free path of the electrons in the normal metal (l_N) determines the form of the coherence length in the normal metal, giving two limits which are often important in modelling the proximity effect. The following equations apply for a superconducting/normal metal boundary with negligible electron-electron interactions in the normal metal, in no applied magnetic field. In the clean limit, where l_N is longer than the coherence length in the normal metal (ξ_N), there is an exponential decay in the number of Cooper pairs over a characteristic penetration depth (ξ_N) given by:

$$\xi_S = \frac{\hbar v_{F_S}}{\pi \Delta_0} \tag{2·15}$$

$$\xi_N = \frac{\hbar v_{F_N}}{2\pi k_B T} \tag{2·16}$$

where: v_{F_S}, v_{F_N} is the Fermi velocity in the relevant conductor.

Δ_0 is the superconducting gap at T = 0 K.

In the dirty limit, where $l_N < \xi_N$, the Cooper pairs diffuse into the normal metal and the coherence length in the normal metal is a function of the mean free path.

$$\xi_N = \left(\frac{\hbar D}{2\pi k_B T}\right)^{\frac{1}{2}} = \left(\frac{\hbar v_{F_N} l_N}{6\pi k_B T}\right)^{\frac{1}{2}} \qquad (2\cdot17)$$

where D is the diffusion constant, $D = \frac{1}{3} v_{F_N} l_N$.

The dirty limit is often easier to model as the exact properties of the interface, the reflection and transmission coefficients, are less important as the motion of electrons are described by simple diffusion equations.

The T_c of a superconducting/normal metal (S/N) bilayer depends upon both the thickness of the superconductor and the normal metal and the interface between them. A thicker normal metal layer reduces the T_c of the bilayer until a certain critical thickness when the T_c reaches a limit. This limit depends upon the thickness of the superconducting layer and the bilayer may not become superconducting if the S layer is thin enough. This observation led Cooper to introduce an effective pairing potential $\left([N(0)V]_{eff}\right)$ which is simply the spatial average of the pairing potentials on both sides of the interface [Cooper 1961]. This new pairing potential can then be used in the BCS equations to obtain the properties of the bilayer. Assuming for simplicity that the BCS coupling coefficient in the normal metal $[N(0)V]_N = 0$, then:

$$[N(0)V]_{eff} = \frac{d_S [N(0)V]_S}{d_S + d_N} \qquad (2\cdot18)$$

where d_S and d_N are the thickness of the superconducting and normal layers.

However this model is only valid if d_S and d_N are much less than the respective coherence lengths, ξ_S and ξ_N.

The proximity effect, was also modelled by de Gennes and Werthamer [Werthamer 1963, de Gennes 1964, Parks 1967 Chapter 17]. This analysis was based on generalising Gor'kov's treatment of superconductivity using Green's functions with a position dependent electron-electron interaction and consequently a spatial variation in the superconducting energy gap $\Delta(r)$ [Gor'kov 1958]. The model uses the limit where both the superconducting and normal layers are much thicker than the respective coherence lengths. It assumes a specular interface between the layers and that the only difference between the superconductor and the normal metal is the BCS electron-electron interaction potential (V), which is a uniform constant throughout the material. The de Gennes–Werthamer analysis then gives three linked equations for an implicit solution to the transition temperature of a superconductor / normal metal sandwich [Hauser 1965]:

$$\begin{aligned}
\ln\left(\frac{T_{cS}}{T_c}\right) &= \Psi\left(\frac{1}{2}+\frac{\xi_S^2 k_S^2}{2}\right)-\Psi\left(\frac{1}{2}\right)\\
\ln\left(\frac{T_{cN}}{T_c}\right) &= \Psi\left(\frac{1}{2}-\frac{\xi_N^2 k_N^2}{2}\right)-\Psi\left(\frac{1}{2}\right)\\
N_S\xi_S^2 k_S \tan\left(k_S d_S\right) &= N_N\xi_N^2 k_N \tanh\left(k_N d_N\right)
\end{aligned} \tag{2·19}$$

where: ξ is the effective coherence length defined as $\left(\frac{\pi\hbar k_B\sigma}{6T_c e^2\gamma}\right)^{\frac{1}{2}}$.

Ψ is the digamma function.

σ is the low temperature conductivity.

γ is the coefficient of the normal electronic specific heat.

N is the density of states at the Fermi surface, assumed proportional to γ.

d is the layer thickness.

$_S$ and $_N$ indices are the superconducting and normal state, respectively.

The parameter k_n^{-1} gives a measure of the depth of the penetration of the superconducting pairs into the normal metal as the gap function is:

$$\Delta\left(\underline{x}\right) = \begin{cases} e^{\pm ik_S x} & 0 < x \le d_S \\ e^{\pm k_N x} & -d_N \le x < 0 \end{cases} \tag{2·20}$$

assuming that x>0 in the superconductor and x<0 in the normal metal.

The Usadel equations are a generalisation of BCS theory allowing the inclusion of pair breaking and non-equilibrium effects [Usadel 1970]. The differential equations describe the diffusion of electrons through a metal, and so are only valid in the dirty limit, in terms of a complex function $\theta\left(\underline{r},E\right)$. $\underline{r}$ is the position vector, E is an energy variable that describes the electron states – in the diffusive state the electrons cannot be described by $\underline{k}$-vectors – and $0<\left|\theta\right|<\frac{\pi}{2}$ with $\theta = 0$ corresponding to the normal state. The Usadel equations used to solve $\theta\left(\underline{x},E\right)$, the one dimensional case, are:

$$\frac{\hbar D}{2}\frac{\partial^2\theta}{\partial x^2}+iE\sin\theta-\left[\frac{\hbar}{\tau_f}+\frac{\hbar D}{2}\left(\frac{\partial\varphi}{\partial x}-\frac{2e}{\hbar}A_x\right)^2\right]\cos\theta\sin\theta-\Delta(x)\cos\theta=0 \qquad (2\cdot21)$$

$$\Delta(x)=nV_{eff}\int_0^{\hbar\omega_D}\tanh\left(\frac{E}{2k_BT}\right)\mathrm{Im}[\sin\theta]\,\mathrm{d}E \qquad (2\cdot22)$$

where: $D=\frac{\sigma}{ne^2}$ is the diffusivity constant.

n is the density of states.

σ is the normal state conductivity.

τ_f is the spin-flip time.

φ is the superconducting phase.

$\underline{A}$ is the magnetic vector potential.

Δ is the superconducting order parameter.

V_{eff} is the BCS-like interaction potential.

$\hbar\omega_D$ is the Debye energy.

T is the temperature.

Im[*f(x)*] takes the imaginary part of *f(x)*.

Equation 2·21 has four parts, the first describes the diffusion of electrons while the other three describe the pairing of electrons to form the superfluid condensate. The excitation energy term (*iE*) tends to make $\theta=0$ and so make the sample normal, the third term describes pair breaking through spin-flip scattering, currents and magnetic fields while the fourth is the superconducting pairing term. In the case where $\frac{\partial^2\theta}{\partial x^2}=0$ with no pair breaking the Usadel equations simply gives the BCS gap equation.

The Usadel equations can easily be extended to describe many systems. Impurities increase the diffusivity constant, though this only results in a suppression of Δ if $\frac{\partial^2\theta}{\partial x^2}\neq 0$. Magnetic impurities can be described through the spin-flip time and the proximity effect can be modelled after taking into account that conservation of spectral current at an interface requires that:

$$\sigma_l \frac{\partial \theta_l}{\partial x} = \sigma_r \frac{\partial \theta_r}{\partial x} = \frac{G_{\text{int}}}{A} \sin(\theta_l - \theta_r) \tag{2·23}$$

where: $\frac{G_{\text{int}}}{A}$ is the electrical conductance per unit area of the interface.

$_l$ and $_r$ index the two sides of the interface.

This gives a linked set of equations that can be either solved analytically, where the geometry is simple, or numerically to give the T_c of a superconductor/normal metal heterostructure in the dirty limit [Martinis 2000].

The Josephson Effect

In 1962, Josephson predicted that the supercurrent flowing between two superconductors separated by a thin tunnel barrier, such as a thin oxide film, would depend upon the sine of the difference in the phase of the superconducting wavefunction. This effect is also observed when two superconducting layers are separated by a normal metal, or a region with a lower superconducting gap parameter, as there is a similar exponential decay due to the proximity effect.

If the two superconductors are close enough together that the exponential tails of the superconducting wavefunction in the weak link overlap, a supercurrent can flow between the superconductors, producing a Josephson junction. A Josephson junction shows several unusual characteristics. The application of a potential difference across the junction causes an oscillating supercurrent with a frequency dependent on the magnitude of the potential difference. This frequency is typically in the GHz range and so a Josephson junction can be strongly affected by irradiation with microwaves. The microwaves generate a normal current across the junction by exciting quasiparticles to tunnel between the superconducting regions. At certain frequencies this normal current phase locks with the Josephson supercurrent, shifting the energy of the superconducting gap. As the frequency of the supercurrent is proportional to the voltage this gives rise to Shapiro steps, displacements in the measured current vs. voltage data, which can be used to prove the existence of a Josephson junction [Shapiro 1963].

Non-Equilibrium Superconductivity

The properties of superconductors driven out of equilibrium have been extensively studied, both as a means of providing deeper understanding of the phenomenon of superconductivity and to produce superconducting devices [see Mannhart 1996 for a review of high-T_c transistors]. Electron or phonon injection, microwave irradiation and electric or magnetic fields have all been used to control superconductivity. While an extensive review of non-equilibrium superconductivity is beyond the scope of this work, devices based on the injection of excess quasiparticles are considered. In these devices current is injected into the superconductor to locally increase the population of quasiparticles and so suppress T_c, as in the controllable weak link (CLINK) and the quasiparticle injection tunnelling effect (QUITERON) [Wong 1976, Chang 1978, Faris 1983, Hunt 1985, Kobayashi 1989]. The excess of quasiparticles suppresses the superconductivity by directly altering the gap function, as given by equation 2·14. This can be described in terms of a local change in the temperature, the T^* model, or a local change in the chemical potential, the μ^* model. The μ^* model is more applicable in cases where the quasiparticle thermalise with low temperature phonons more rapidly than they recombine into pairs and the escape rate of phonons from the superconductor is large. In this limit the quasiparticle temperature is in the steady state and the excess quasiparticles can be described by the increased chemical potential [Owen 1972]. In the opposite limit, where quasiparticle recombination is more likely than thermalsation and the escape rate of phonons is small there is a 'phonon bottleneck' as the phonon created by the formation a Cooper pair goes on to break another pair. The excess quasiparticles form a steady state distribution which is the same as that given by equilibrium at the higher temperature T^* [Parker 1975].

The non-equilibrium quasiparticles rapidly relax and recombine into Cooper pairs, restoring the equilibrium quasiparticle population once the injection current is removed. This gives a switching time in the order of tens of picoseconds, depending on the type of superconductor used. However if a 'phonon bottleneck' forms the effective quasiparticle relaxation time appears to be considerably longer and this becomes more likely if large injection currents are used. The creation of local hot spots can increase both the current and voltage gain, but only at the expense of a longer switching time. In general the current gain $\left(G = \frac{\Delta I_c}{I_{inj}}\right)$ is on the order of ten for conventional BCS superconductors while cuprate superconductors generally show a gain that is an order of magnitude less, given switching times on the order of 0.1 ns [Arie 1997-I]. Devices manufactured from conventional BCS superconductors tend to show current gain an order of magnitude larger than that seen in devices manufactured from cuprate superconductors, probably due to the more complex interfacial engineering [Schneider 1997].

Care must also be taken in manufacturing the device. Interfacial resistance can lead to additional localised heating, further processing required to deposit the injection contacts may damage the superconducting film (oxygen depletion on the surface of a cuprate superconductor is a classic example of this) and current addition must be taken into account. The total current carried by the superconductor will be the sum of both the supercurrent and the injected current. The results can be strongly altered by changing the injection geometry [Arie 1997-I].

BASIC MAGNETIC THEORY

Magnetic Materials

Magnetic properties arise from the overlap of the electron orbitals of adjacent atoms, this is why the interatomic spacing is important in determining the magnetic nature of a material. This can be seen in iron, cubic close packed iron (austenite) is not magnetic while body centred cubic iron (ferrite) is ferromagnetic. In a ferromagnetic material the overlap is such that the energy is lowered if the electron spins are parallel. This is normally described as an interaction energy that decreases the energy of one spin band with respect to the other, giving an excess of one spin direction and a spontaneous magnetisation. Antiferromagnetic materials have a minimum energy state where adjacent spins are antiparallel. Heating a magnetic material will destroy this spontaneous magnetisation as the entropic gain from randomised spins exceeds the exchange interaction. In this state the material becomes paramagnetic and the individual spins will only weakly align with an applied magnetic field. The temperature below which a material becomes ferromagnetic is known as the Curie temperature (T_C) and the temperature below which a material becomes antiferromagnetic is known as the Néel temperature (T_N).

The magnetic interaction extends beyond the range of the interatomic spacing as the magnetic moment polarises the conduction electrons in the region around the magnetic atom, the RKKY interaction. The RKKY interaction has a phase term in addition to decaying with distance, encouraging parallel or antiparallel alignment of the local moments. Some magnetic materials have no possible configuration by which every atom is in the minimum energy state with respect to all its neighbours, this is known as frustration. An example of this is a dilute magnetic alloy, such as a few percent of iron in gold, the random spacing of magnetic atoms leads to frustration and the formation of a spin glass. In a spin glass there is local alignment of spins, as given by the exchange interaction, but there is no long range magnetic order.

There is also an additional reduction in energy when the individual spins align with the local magnetic field, up to a limit where all of the individual spins are aligned with the field, the saturation magnetisation ($\underline{M_S}$). This is true for both ferromagnets and antiferromagnets, though a much higher field is required to align the spins in an antiferromagnet as the energy gain from alignment must overcome the exchange

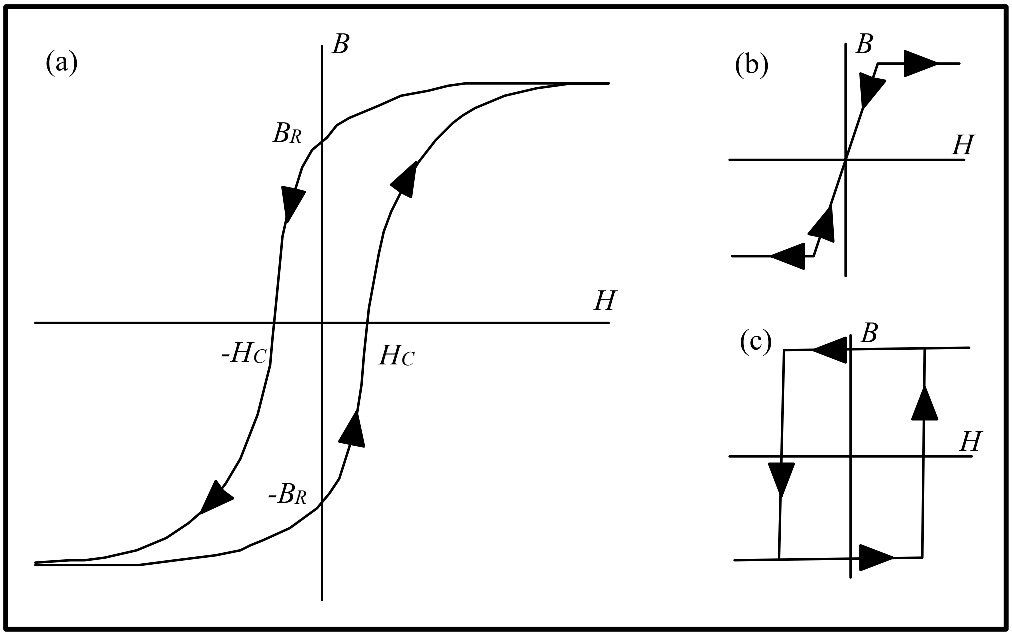

Figure 2·5 (a) Form of a magnetic hysteresis loop, applied magnetic field vs. magnetic flux in the sample, showing the coercive field and the remnence.
(b) Hysteresis loop for an ideally soft ferromagnet.
(c) Hysteresis loop for an ideally hard ferromagnet with very square loop.

interaction. The exchange interaction must also be considered in a ferromagnet, as it depends upon the overlap of electron orbitals it also depends upon the direction relative to the crystalline structure. This is modelled as the magnetocrystalline anisotropy energy and the directions in the crystalline structure along which this energy is a minimum are called the easy directions while the maximum energy is along the hard directions. The hard directions act as an energy barrier to reversing the direction of the magnetisation and so are the cause of magnetic hysteresis. A certain applied field is required to rotate the magnetisation through the hard direction, overcoming the energy barrier. Reducing the applied magnetic field to zero leaves a remnant magnetic field, also called the remanence ($\underline{B}_R$), and the applied magnetic field at which the magnetisation goes to zero is known as the coercive field ($\underline{H}_C$). Hysteresis will occur if the change in the magnetic field is reversed at any point, it is not necessary to go to saturation. A soft magnetic material is one in which the coercive field is very low; a hard material has a large coercive field. A magnetic material has a square loop if the remanence is large.

The bulk shape of the ferromagnet also has an effect on the response to applied magnetic field, the shape anisotropy. Magnetic poles form at both sides of the ferromagnet, with the magnetic field flowing from the north poles to the south. This generates a demagnetising field ($\underline{H}_D$) in the ferromagnet, still flowing from north to south and so antiparallel to the magnetisation ($\underline{M}$), that depends on the strength of the magnetisation and how close the poles are to each other, $\underline{H}_D = N_D \underline{M}$. N_D is the demagnetising factor, which only depends upon the sample geometry. It can only be

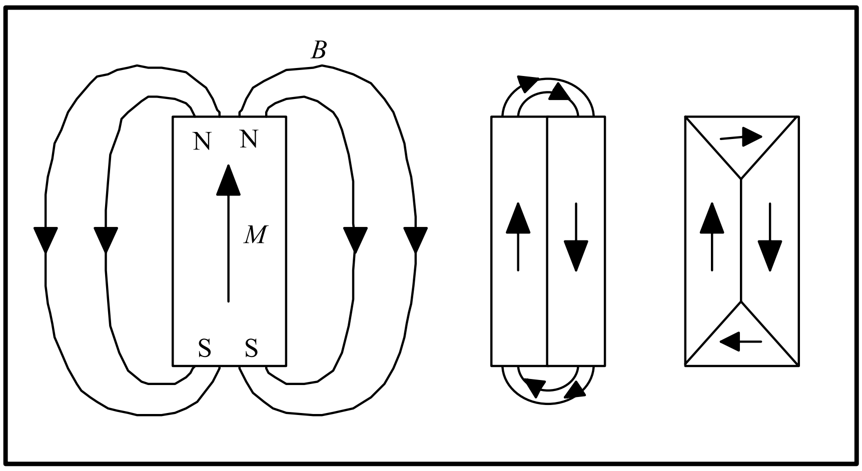

Figure 2·6 Reduction in magnetic flux by the formation of domains.

calculated for ellipsoids, and is $^1/_3$ for a sphere, but has a maximum of one, where the magnetisation is perpendicular to an infinite lamella, and a minimum of zero, magnetisation parallel to an infinite rod. The shape anisotropy is also important in the critical field of a superconductor, in the Meissner state flux is forced to flow around the superconductor and the flux lines bunch at the edges. This effectively increases the applied field and regions of the superconductor will become normal at applied fields below the superconducting critical field, forming the intermediate state.

Although a sample may be below the Curie temperature it may still appear to be unmagnetised due to of the formation of magnetic domains. Domains, see figure 2·6, form in order to reduce the magnetic field outside the material. The external magnetic field has an energy that is given by:

$$\frac{1}{2}\iiint \underline{B}.\underline{H}\,\mathrm{d}\tau = \frac{1}{2}\iiint \mu_0\mu_r H^2\,\mathrm{d}\tau \qquad (2{\cdot}24)$$

where: $\underline{H}$ is the magnetic field strength.
$\underline{B}$ is the magnetic flux density and is equal to $\mu_0\mu_r\underline{H}$.
μ_0 is the permeability of free space, 1.257 x 10^{-6}H/m.
μ_r is the relative permeability of any other material.
the integral is applied over all space.

The easy directions in each domain need not be at 180º to each other as any easy direction is available. The external magnetic flux can go to zero below T_C if closure domains form. The formation of domains 'costs' energy in the creation of a domain wall, a region where the magnetisation rotates between the two easy directions that make up the two domains. This is a 180º domain wall if the magnetisation directions are at 180º to each other. If the sample is small enough then domains will not form as the energy gain from forming domains is not sufficient to balance the cost of forming the domain walls required. An external magnetic field causes those domains with a magnetisation closest to the direction of the field grow at the expense of less favourable domains. If the applied field is sufficiently strong the direction of magnetisation in a domain may rotate to align with it, away from the easy direction.

The size and nature of a domain wall depends upon the exchange interaction and the anisotropy energy, both magnetocrystalline and shape. The energy cost of the wall comes from the exchange energy for non-parallel spins and the energy cost of having spins in non-easy directions. The width of the wall depends on a balance between the cost in exchange energy for non-parallel spins, which favours a wide wall with adjacent spins almost parallel, and the magnetocrystalline anisotropy energy, which favours a narrow wall. The wall width can be obtained by minimising the wall energy per unit area (E_{wall}) with respect to the wall width (l_{wall}), in the case of a 180º domain wall this is approximated by:

$$E_{wall} = \frac{\mu_0 I \underline{m}^2 \pi^2}{l_{wall} a} + K_1 l_{wall} \tag{2·25}$$

$$l_{wall} = \sqrt{\frac{\mu_0 I \underline{m}^2 \pi^2}{K_1 a}} \tag{2·26}$$

where: $\underline{m}$ is the magnetic moment per atom.
I is the exchange interaction between nearest neighbours.
a is the lattice parameter.
K_1 is the first anisotropy constant.

For bulk nickel, which has a very low anisotropy, this calculation gives a domain wall energy of 10^{-3} J/m^2 and a domain wall width of 100 nm. Bulk cobalt, which has a strong uniaxial anisotropy, has a domain wall energy of 8×10^{-3} J/m^2 and a domain wall width of 15 nm.

The shape of the ferromagnet can have an influence on the domain structure. The energy of the demagnetising field must also be considered, especially in the case of thin films. In general the magnetisation will lie in the plane of the film, though certain materials, such as TbFe, have very high magnetocrystalline anisotropy and so the magnetisation can be perpendicular to the thin film surface despite the very large demagnetising field this magnetisation direction gives. These materials have been exploited as magnetic storage materials, giving a higher storage density as each bit would require a smaller area. Equally, despite the strong uniaxial magnetocrystalline anisotropy, closure domains can form at the edge of a cobalt thin film [Craik 1965].

Magnetoresistance

Most metals show increased resistance as a magnetic field is applied. This is simply understood in terms of the Hall effect. As the magnetic field is applied the Lorentz force pushes the moving electrons to one side of the metal, effectively reducing the area of the conductor and so increasing the resistance. This effect is usually very small, a fraction of a percent. A larger magnetoresistance, anisotropic magnetoresistance or AMR, can be observed in ferromagnetic materials, as the magnetic field couples with the electron's spin and orbit angular momentum. Depending upon the relative orientation of the current flow, magnetic field and crystallographic directions this can be either positive or negative but in any case will only be a few percent. AMR is so small because the only effect of the applied field is to rotate the internal magnetisation of the ferromagnetic material. It also decreases with increasing temperature as thermal activation acts to balance out the populations of the spin bands eventually going to zero at T_C [Moodera 1995].

Far larger values of magnetoresistance can be observed. Alternating layers of ferromagnetic and normal metals on an insulating substrate can show giant magnetoresistance (GMR) with a change in resistance of up to 2.2 times the resistance at zero applied field. Comparatively long-range interactions, on the scale of several nanometers, between the ferromagnetic layers can lead to antiparallel magnetisation when the normal metal thickness is correct. The resistance of the multilayer, with antiparallel magnetisation in adjacent ferromagnetic layers at zero field, drops when an applied field causes parallel magnetisation, a result of the spinor transformation which projects one spin state onto another. There is interest in devices in which the ferromagnetic layers are separated by insulating layers, a ferromagnetic tunnel junction. The magnetoresistance of this structure may be lower than that in classic GMR but the higher resistance gives a larger voltage signal. The largest values of magnetoresistance have been measured in the colossal magnetoresistive materials (CMR). Materials based on doped $RMnO_3$, where R is a transition metal, undergo a transition from a high temperature insulating state to a low temperature metallic state, an applied magnetic field will increase the transition temperature. Thus an applied field can reduce the resistivity to less than a thousandth of the zero field value. These materials have limited practical application at present as the switching field is comparatively large, on the order of a Tesla while GMR requires milliTesla, and temperature stability must be maintained. At present the exact mechanism of the magnetoresistance is unclear and there is interest in the grain boundaries as they show a resistance change at a lower switching field.

Spin–Polarised Tunnelling

The study of the interrelation between the spin and charge of the electron began with the realisation that ferromagnetism arises from an imbalance in the number of spin up and spin down electrons. It was then suggested that electrical conduction in a ferromagnet can be modelled by two distinct 'spin channels', one consisting of electrons with spin parallel to the magnetisation and the other with spins antiparallel [Mott 1936]. The channels remain relatively independent as although spin-flip processes between channels are possible they occur on a time scale that is long compared to those of other processes, the spin diffusion length is much longer than the mean free path. Early experiments with europium chalcogenides [Esaki 1967, Thompson 1971] showed that the resistance dropped as an applied field changed them from an antiferromagnetic to a ferromagnetic state, an effect put down to 'spin-ordering' where the resistance of a single 'spin channel' falls while the other stays the same. Europium chalcogenides, and other materials that similarly underwent 'spin-ordering', could thus be used as 'spin-filters', only allowing electrons with the correct type of spin to pass through them. These materials were used in attempts to determine the imbalance of spin in a ferromagnetic metal.

None of these early tunnelling experiments were as definitive as the work of Tedrow and Meservey in the 1970s [Meservey 1970, Tedrow 1971, Tedrow 1973, Meservey 1976, Meservey 1994]. In these experiments electrons tunnelled from a ferromagnetic metal into a superconducting Al film, through an Al_2O_3 barrier, in a strong applied magnetic field (H). In addition to magnetising the ferromagnet the magnetic field splits the quasiparticle energy states (Zeeman splitting), decreasing the energy of quasiparticles with spin parallel to the applied field by $\mu_B H$ and increasing the energy of quasiparticles with antiparallel by the same amount, where μ_B is the Bohr magneton. If the electrons do not change spin in the tunnelling barrier then the tunnelling current will depend upon the number of filled states in the ferromagnet and the number of empty states in the superconductor. When the applied voltage across the tunnel junction lies between $\Delta - \mu_B H$ and $\Delta + \mu_B H$ the tunnelling current will be due to electrons tunnelling from the majority spin band of the ferromagnet, as shown in figure 2·7. In reality there will also be a contribution from the tunnelling of quasiholes from the superconductor into the ferromagnet and from thermal excitations at the Fermi surface, though these contributions should be small they must be taken

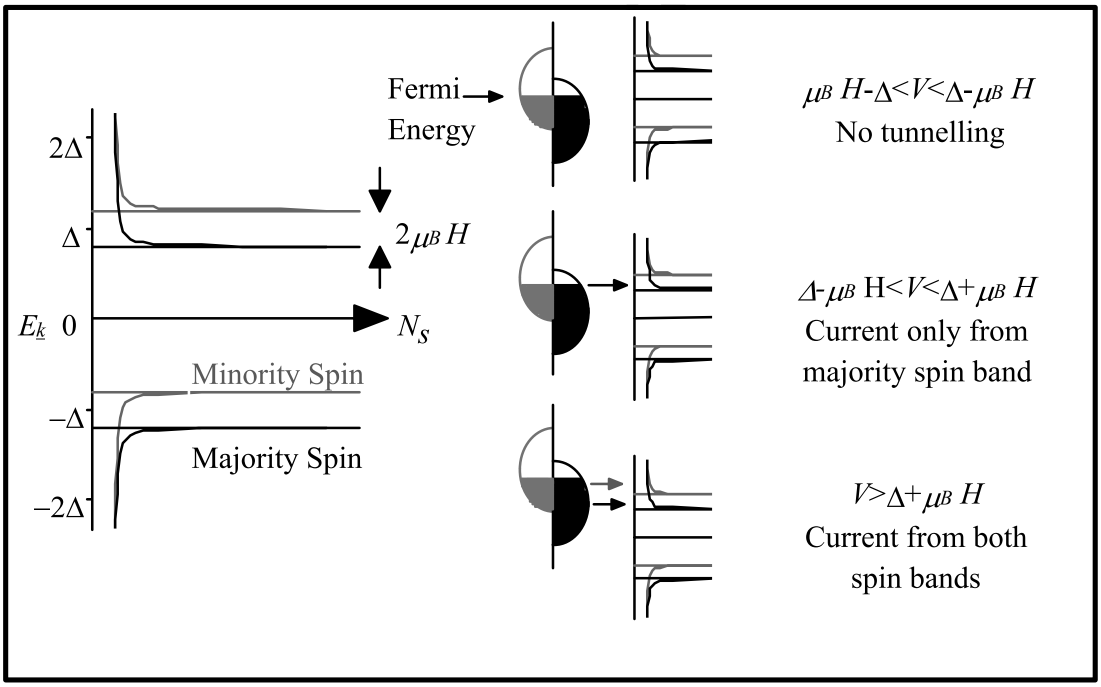

Figure 2·7 Zeeman splitting of the BCS density of states by a strong magnetic field. This allows the two different spin bands to be distinguished, as in the tunnelling experiment illustrated.

into account. Analysis of the peak obtained when the potential difference exceeded $\Delta + \mu_B H$ also gave information on the density of states in the minority spin band. The tunnelling current, as a function of the potential difference across the junction, allowed the calculation of the imbalance in the spin populations of a ferromagnetic metal within 1 meV of the Fermi surface. The imbalance in the spin population is given in terms of the polarisation (P):

$$P = \frac{n_A - n_B}{n_A + n_B} \tag{2·27}$$

where: $n_A n_E$ are the numbers of electrons in the respective spin bands.

The tunnelling experiment can also be used in reverse, if the density of states in the ferromagnet is known then the spin dependent density of states in the superconductor may be mapped [Tedrow 1982].

There was initial confusion concerning the results from these tunnelling experiments as the polarisation was positive, which contradicted the results from field emission experiments. This was explained by Stearns in 1977, who pointed out that the electrons that took place in tunnelling would be the nearly free s-d hybridised electrons. This allowed the data to be fit to known data on the band structure without the need for flexible parameters.

The superconductor-ferromagnet tunnel junctions used by Tedrow and Meservey are limited as they will only give good results if the aluminium film is carefully deposited so as to give a spin relaxation time (τ_s) that is as long as possible and a large gap parameter (Δ). Spin-orbit scattering, which occurs more often from atoms with a high mass, mixes the singlet and triplet states of the Cooper pairs, effectively merging the two spin bands in the superconductor. If $\tau_s \Delta << \hbar$ then there will be so much spin-orbit scattering in the superconductor that the spin-mixing effect gives unobservable Zeeman splitting, merging the spin dependent peaks [Grimaldi 1996, Grimaldi 1997]. Spin mixing can be reduced by coating the aluminium with a 'spin-filter', such as EuS, in which the spin polarisation of tunnelling electrons is high [Moodera 1993].

Further tunnelling experiments were performed using a ferromagnetic metal to detect the spin [Juliere 1975]. Juliere used a Co/Ge/Fe trilayer, the iron had a lower $\underline{H}_C$ than the cobalt and so when the magnetic field direction was reversed the two magnetisations will be antiparallel between $\underline{H}_{C_{\mathrm{Fe}}}$ and $\underline{H}_{C_{\mathrm{Co}}}$. He found that the conductance was 14% higher when the magnetisation of the ferromagnetic metals was parallel compared to when it was antiparallel. There was difficulty in repeating these results, mainly due to an inability to deposit a good quality insulating layer that was thin enough for a measurable tunnelling current. With modern deposition techniques more reliable results can be obtained. A polarisation of 24% has been observed with electrons tunnelling between ferromagnetic films through Al_2O_3 at 4.2 K [Moodera 1995]. However, there is still uncertainty as to what effect, the amorphous Al_2O_3 has on the tunnelling electrons [Zhang 1998]. A ferromagnetic tip can be used in scanning tunnelling microscopy (STM), where the barrier is the more easily understood vacuum [Wolf 1985 Chapter 7]. The signal from such a probe should depend upon the angle between the magnetisation of the sample and the tip, allowing magnetic domains to be mapped [Johnson 1990, Wiesendanger 1990]. The fundamental problem of using a ferromagnetic tip is the difficulty of determining the spin state at the atomic limits of a tunnelling tip [Prinz 1995].

It is possible to draw an analogy between a spin-polarised current passing between two ferromagnetic metals and light passing through crossed polarisers [Datta 1990, Prinz 1995]. Conductivity is highest when the magnetisation of the ferromagnetic metals is parallel and lowest when the magnetisation is antiparallel, in just the same way that the intensity of plane polarised light through a second polariser varies with angle. There is a $\cos^2\left(\frac{\theta}{2}\right)$ dependence between the extremes, as the spin state is projected onto an axis at an angle θ to the initial spin state through the spinor transformation. This has led to the idea of electrical analogues for optical and opto-electronic devices, such as the spin-polarised field-effect transistor. This device uses the electric field created by the gate electrode to control the precession of the spins as they move between the source and the drain in the same way the axis of polarisation of plane polarised light rotates in a birefringent material [Prinz 1995].

Spin Imbalance in a Paramagnetic Metal

In 1976, Aranov suggested that paramagnetic materials would also have an imbalance in spin centred on the point where current from a ferromagnetic metal entered, limited by spin scattering events. He described the imbalance of spin as a flux of magnetisation, with each electron contributing one Bohr magneton. If the Fermi surface of the ferromagnetic metal is entirely within one spin band (the idealised Stoner model transition-metal ferromagnet) then the current is solely carried by electrons of that spin with each electron adding to the total magnetisation. For most real ferromagnetic materials both spin bands are present but with a pronounced imbalance between the two. This reduces the efficiency of injection of magnetisation across the interface by at least the ratio between the difference between the currents from the spin bands and the total current (the sum of both spin band contributions), effectively speaking the polarisation given in equation 2·27. There are also reductions in injection efficiency from spin scattering at any interface.

The spin transport properties of a material were initially studied by exciting a non-equilibrium spin population with microwave radiation in spin-resonance experiments [Dyson 1955, Feher 1955, Johnson 1988]. Conduction spin-electron resonance, CSER, was the first method used. The sample is placed into a microwave cavity in a strong magnetic field. The microwave energy is absorbed as the electrons flip between spin states in the magnetic field. This reduces the quality factor of the microwave cavity, giving a characteristic peak when:

$$\omega_L = \gamma H \tag{2·28}$$

where: ω_L is the Larmor frequency.
γ is the gyromagnetic ratio.
H is the applied magnetic field.

Since the resonance depends upon the spins flipping in unison, the width of the peak gives the spin relaxation time and, knowing the electron diffusion constant, the spin diffusion length can be determined.

An alternative method is transmission spin-electron resonance, TSER, in which two microwave cavities are used with the sample between them. The microwaves induce transverse magnetisation in the sample. This non-equilibrium magnetisation decays to produce radiation in the opposite cavity. When the microwave frequency (ω) equals γH electron spins will precess at the same rate as the rotation of the electromagnetic field, giving a resonance peak. As before, the width of the peak gives a measure of the spin relaxation time, and the signal can be enhanced by coating the sample with a ferromagnetic film [Silsbee 1979]. One problem with both CSER and TSER is that the microwave radiation and kiloGauss magnetic fields drive the system far from equilibrium, making it almost impossible to use on a superconductor or a spin glass [Vier 1983]. In addition, any anisotropy in the relaxation processes broadens the peak, in some cases to the point where it can no longer be observed.

In 1985, M. Johnson and R.H. Silsbee suggested a less invasive method of determining both the spin relaxation time and the spin diffusion length. Since electron-spin resonance (ESR) had indicated that some metals, at low temperature, had a reasonably long spin diffusion length they proposed a simple injector-detector method, see figure 2·8. As the spin-polarised electrons are injected into the paramagnetic metal a non-equilibrium magnetisation builds up, represented by the difference in the population of the spin bands (Δn in figure 2·8). The non-equilibrium magnetisation shifts the chemical potential of the spin bands in the paramagnetic metal away from equilibrium, an effect resulting from the fact that spin and charge are carried by the same particle. The second ferromagnetic film, as the Fermi surface is almost entirely within a single spin band, matches chemical potential with only one spin band of the paramagnetic metal. The open circuit voltage is thus the difference between the chemical potential of the paramagnetic film when the non-equilibrium magnetisation is present and when it is in equilibrium. Essentially current flows to neutralise the spin imbalance just as it would to neutralise a charge imbalance.

The spin diffusion length (δ_s) can be determined from the measured voltage difference between the parallel and antiparallel states [Johnson 1993, Johnson 1994]. The flux of spins into the normal metal, essentially the magnetic current (I_M), will depend upon both the electron current (I_e) and the relative population of the spin bands in the ferromagnet:

$$I_M = \frac{\eta_1 \mu_B I_e}{e} \tag{2·29}$$

where: μ_B is the Bohr magneton.

e is the electronic charge.

η_1 gives the spin imbalance in the current from F_1, $\eta = \frac{J_A - J_B}{J_A + J_B}$.

$J_{A,E}$ are the current densities for each spin band.

In the steady state I_M gives the rate at which spins enter the paramagnet and they are lost at a rate given by the spin relaxation time (T_2). This gives a non-equilibrium magnetisation in the paramagnet $(\tilde{M})$ given by:

$$\tilde{M} = \frac{I_M T_2}{Ad} \tag{2·30}$$

where: Ad is the volume occupied by the non-equilibrium spins.

The voltage signal obtained on switching between the magnetisation states can be related to the non-equilibrium magnetisation through:

$$eV_d = \frac{\eta_2 \mu_B \tilde{M}}{\chi} \tag{2·31}$$

where: χ is the Pauli paramagnetic susceptibility of the paramagnet.

$\frac{\tilde{M}}{\chi}$ can be thought of as the effective magnetic field generated by the non-equilibrium spins. Combining these three equations and assuming a free electron expression for the susceptability:

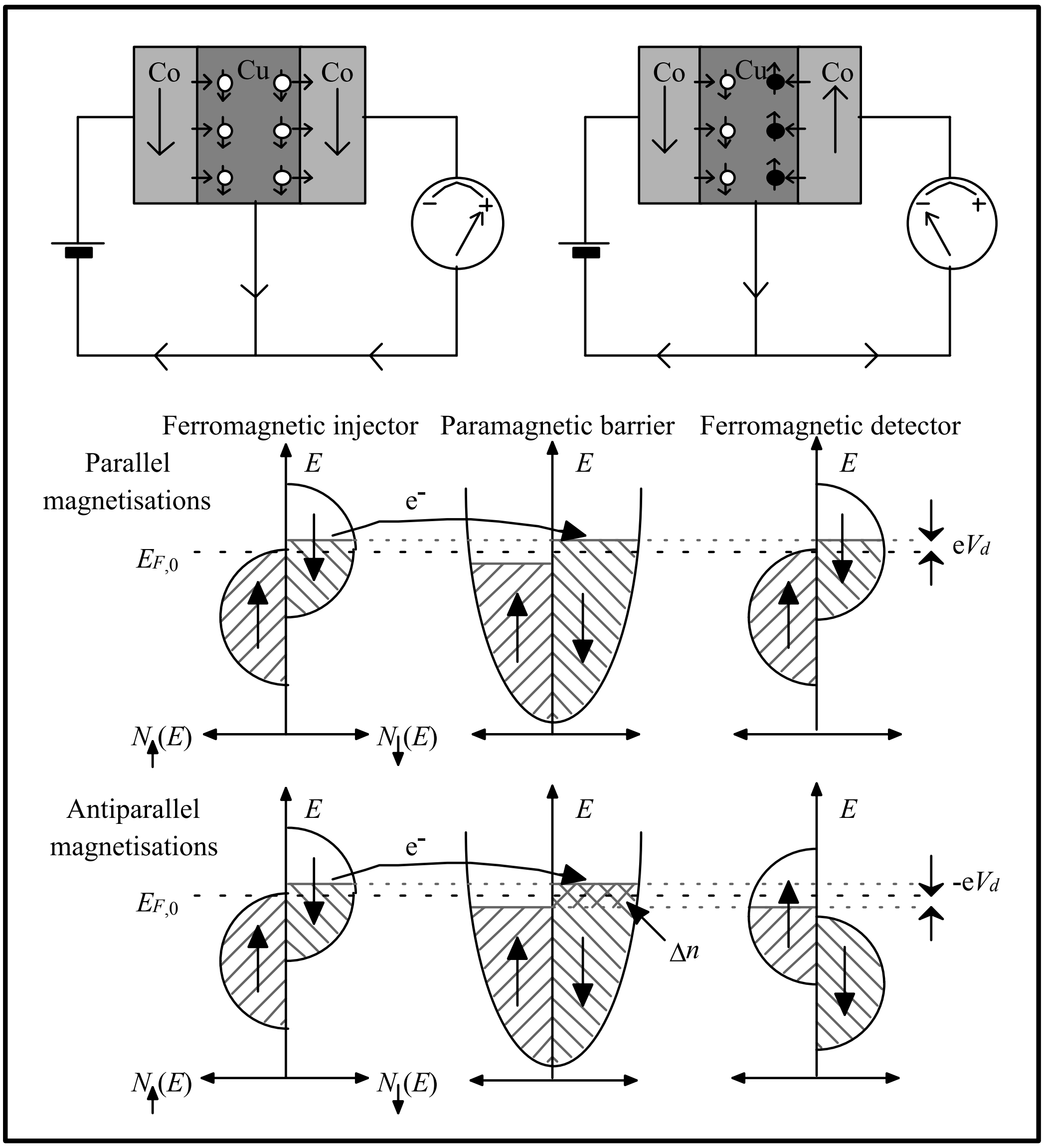

Figure 2·8 Pedagogical model of the three terminal device, including diagrams of the densities of state. Spin accumulation at the paramagnet/detector interface generates a potential difference (V_d). $E_{F,0}$ is the Fermi energy in the paramagnet which is the average of the two spin states while the ferromagnetic detector only samples one spin band in the paramagnet. Δn is the increase in occupation of the spin bands in the paramagnet caused by the current from the ferromagnetic injector. After Johnson 1985 and Prinz 1995.

$$\chi = \mu_B^2 N(E_F) = \frac{3\mu_B^2 n}{2E_F} \tag{2·32}$$

where $N(E_F)$ is the density of states at the Fermi energy (E_F).

n is the density of conduction electrons.

with an Einstein relation for the electrical resistivity (ρ):

$$\rho = \frac{1}{e^2 D N(E_F)} \tag{2·33}$$

where D is the diffusivity constant.

the measured voltage can be related to the injected current. In the case where the thickness of the paramagnet is very much less than δ_s:

$$V_d = \frac{\eta_1 \eta_2}{e^2} \frac{2 T_2 E_F}{3nAd} = \eta_1 \eta_2 \frac{\rho \delta_s^2}{2Ad} \tag{2·34}$$

where $\delta_s = \sqrt{2DT_2}$.

For aluminium at 40 K this calculation gives δ_s = 0.4 mm, while in gold δ_s = (1.5 ± 0.4) μm between 4 and 70 K. This lengths are longer than those derived from measurements in GMR systems, though this may be due to the simplified model used and spins being repolarised by spin-flip interactions at the interface [Zhang 1996, Fert 1997].

The potential difference created at the interface of the ferromagnet and the paramagnet opposes any further increase in the spin imbalance, a 'spin bottleneck'. As the voltage is proportional to the injected current it is normally described as an additional interfacial resistance, resulting from the fact that both spin and charge are carried by the same particle. This resistance will occur in any system where a current flows between two materials with a different resistance in each 'spin channel', for example a 'spin bottleneck' has been measured in magnetic tunnel junctions [Jungwirth 1998]. The direction of the potential difference created by the spin imbalance depends upon the magnetisation state of the ferromagnetic layers so the structure shown in figure 2·8 also has potential as non-volatile computer memory element, storing information in the relative orientation of the second layer. This all metal device, called the bipolar spin transistor, was suggested by Johnson in 1996 though the signal is limited.

An alternative method of measuring the spin relaxation time (T_2) uses the Hanle effect in the spin-injection experiment [Johnson 1988]. Application of a small magnetic field causes the electron spin to precess. As each electron takes a different amount of time, though if it takes longer than T_2 the electron will have lost spin-polarisation through a scattering event, to diffuse to the detector each will have a different spin. If the magnetic field is weak, each electron can only precess through a small angle before relaxation and so contributes coherently to the non-equilibrium magnetisation. As the strength of the magnetic field increases the scatter in the spin increases and the open circuit voltage falls. When the field equals $(\gamma T_2)^{-1}$, where γ is the spin gyromagnetic ratio, the magnetisation is diminished to about half the zero field value. The half-width in field at half maximum of the bell-shaped curve centred at zero field gives T_2.

The magnetic field used in the spin injection experiment is much smaller than that used in ESR (milliGauss rather than kiloGauss), allowing the measurements to be made in systems much closer to equilibrium. A further advantage of this method is that the signal is inversely proportional to the thickness of the sample [Johnson 1993] allowing the use of very small samples. The signal can be further enhanced by using a paramagnetic material with a small atomic number as this reduces the probability of spin-orbit scattering which in turn extends the spin relaxation time [Johnson 1994]. Spin-flip interactions at the ferromagnetic-paramagnetic interface will also repolarise the spins as the interfacial scattering is dependent upon the spin, the scattering can be enhanced by interdiffusion and roughness at the interface [Zhang 1996].

The ability of a ferromagnet to create a spin imbalance in a paramagnetic metal also extends to other materials, often giving a more pronounced effect [Gregg 1997]. Spin injection into a semiconductor offers the potential for numerous devices, for example a GMR structure between two Schottky barriers where changing the magnetic configuration changes the energy relaxation scattering length and to the fraction of the emitter current that arrives at the collector. The spin diffusion length in a semiconductor can be long, with a spin scattering time of approximately 5×10^{-8} s [Dzhioev 1997]. Some of these heterostructures have the potential to show power gain, which is not possible in the all metal bipolar spin transistor. The spin polarised injection current emitter (SPICE) injects a spin polarised current into a bipolar transistor structure with the addition of a ferromagnetic layer between the collector and the base. This device has the potential to realise a performance combining magnetic sensitivity with the high current gain of a conventional bipolar transistor. A hybrid superconductor/semiconductor structure has been predicted to be sensitive to the spin polarisation of the current flowing through it [Žutić 1999-II]. The transparency of the superconductor/semiconductor interface increases in the presence of spin polarisation and the Andreev reflection amplitude gives a measure of the spin polarisation magnitude, independent of the potential strength and the Fermi velocity in the superconductor.

Chapter Three

COEXISTENCE OF SUPERCONDUCTIVITY AND MAGNETISM

There is no such thing as a solid object.

All matter consists of bundles of pure energy called ch'i, the life force, and shih, the motion force.

All energy is controlled by adherence to classical patterns.

The Three Laws of Taoist science

Superconducting and magnetic order tend to be mutually exclusive as they involve different ordering of the electrons in the material, consequently the two can have a considerable effect on each other. First the effect of magnetic impurities on the properties of a superconductor and the theories used to model these effects are discussed. This is followed by a discussion of the proximity effect in ferromagnetic materials and the electrical and magnetic properties of superconductor/magnetic material multilayers, both ferromagnetic or antiferromagnetic and conducting or insulating. A simplified model for determining the superconducting transition temperature of a superconductor/ferromagnet multilayer is given. Next we consider active superconductor/ferromagnet devices where the spin polarised current from the ferromagnet is used to suppress the critical current of the device. Finally the properties of systems in which both ferromagnetic and superconducting order can occur, the magnetic superconductors are discussed, and the devices based on active control of the ferromagnetic exchange interaction in the superconductor that they have inspired.

Magnetic Impurities in Superconductors

In 1956, Ginzburg studied the suppression of superconductivity in ferromagnetic materials. Assuming that the magnetic induction ($\underline{B}$) was large compared to the superconducting critical field ($\underline{H}_c$) the coexistence of superconductivity and ferromagnetism in a material is only possible in exceptional cases, such as thin films where the magnetic induction is suppressed or when the magnetisation is in the opposite direction to the applied field. Superconducting electrons and magnetic moments can also interact through the exchange interaction [Matthias 1958]. The tendency to align the spins of the electrons, which can be described by an exchange field ($\underline{h}$), opposes the formation of the Cooper pairs. This suppression of Cooper pairs is known as the paramagnetic effect. In addition the exchange scattering of electrons from the localised moments, which are present at all temperatures, also has a detrimental effect on singlet pairing [Abrikosov 1960].

Abrikosov and Gor'kov modelled the effect of dilute magnetic atoms in a dirty superconductor, in the absence of any magnetic interactions other than scattering from the individual moments. The magnetic impurities break the time-reversal symmetry of the Cooper pairs, i.e. the symmetry with respect to changing the sign of the momenta and spins of the conduction electron, separating the two spin states by some typical energy (2α). The rapid scattering between momentum states in the dirty limit tends to average out the depairing energy over a time scale given by the time required for the relative phase of the two time-reversed electrons to be randomised. This time was linked to the typical energy difference by de Gennes who equated 2α with $\frac{\hbar}{\tau_K}$ as, over a time τ_K, this produces a phase shift on the order of unity [de Gennes 1963]. The critical pair breaking strength $\alpha_c(T)$, the value of α for which T_c is the given temperature, can be linked to the temperature-dependent coherence length (ξ) through the diffusion constant (D):

$$\xi^2(T) = \frac{D\hbar}{2\alpha_c(T)} = D\tau_{K_c}(T) \qquad (3\cdot1)$$

This coherence length can be applied to the linearized Ginzburg-Landau equation, equation 2·5, all the way down to absolute zero, in the dirty limit.

Beyond acting as a depairing mechanism, and so giving a rapid decrease in T_c as the concentration of magnetic impurities increases, magnetic impurities can also give rise to gapless superconductivity [Parks 1967 Chapter 18]. This state occurs in many superconductors in the presence of a strong perturbation, such a thin film in a parallel magnetic field or near an interface with a normal metal in the dirty limit. The creation of sub-gap energy states does not destroy the superconductivity, reflecting that superconductivity arises from the electron pairs, but does change the properties of the material. For example in a gapless superconductor the specific heat behaves linearly with temperature at low temperatures rather than the exponential form given by BCS theory. All of these states can be described in terms of some critical pair breaking strength $\alpha_c(T)$.

The Superconducting Proximity Effect in Ferromagnets

As shown above the pair-breaking effects in a ferromagnetic material are much stronger than those in a normal metal. When placed in contact with a thick magnetic layer the transition temperature of the superconductor decreases many times more rapidly, as the thickness of the superconductor is decreased, than with an adjacent normal metal layer [Hauser 1966]. Andreev reflection from a ferromagnet into a superconductor is strongly suppressed due to the spin polarisation of the conduction electrons in the ferromagnet [Upadhyay 1998]. Depending upon the strength of the exchange interaction relative to the Fermi energy, the conductance can either increase or decrease as the superconductor becomes normal [de Jong 1995]. Andreev reflection creates a hole with the opposite spin and momentum states to the incoming electron so the probability of an electron entering a superconductor via Andreev reflection depends upon the availability of states for that hole. Thus Andreev reflection depends upon the electronic density of states for the minority spin, which can be essentially zero in half-metallic ferromagnets such as CrO_4 and $La_{1-x}Ba_xMnO_3$. Andreev reflection can be used to determine the interfacial transparency and the spin polarisation of the direct, rather than tunnelling, current [Soulen 1998]. Even if electrons do enter the superconductor through Andreev reflection this will create a spin imbalance in the ferromagnet and may give rise to additional interfacial resistance, reducing the interface transparency, if a 'spin bottleneck forms' [Jedema 1999-II].

The superconducting order parameter extends into the ferromagnetic layer and will suppress the long range component of the ferromagnetic exchange interaction. If the layer is thin enough then ferromagnetism will be completely suppressed and it will become paramagnetic, though a paramagnetic layer will also form if there is any interdiffusion at the interface between the superconductor and the ferromagnet [Strunk 1994, Mühge 1997]. In this paramagnetic case the nature of the multilayer can be described by a combination of the de Gennes-Werthamer theory of the proximity effect combined with the Abrikosov-Gorkov model for pair breaking by independent moments [Hauser 1966, Entin-Wohlman 1975]. When the long range ferromagnetic order comes into existence, when the layer becomes thick enough, this model no longer fits the data. Increasing the thickness of the ferromagnetic layer still further continues to suppress T_c, up to the limit of approximately five times the superconducting coherence length in the ferromagnet. The superconducting wavefunction has such a low magnitude after passing through that much ferromagnet that T_c is essentially stable for further increase in ferromagnet thickness. Equally the exchange field of the ferromagnet will only extend for a limited distance into the superconductor. For Nb/Co heterostructures a magnetic penetration depth of 35-40 nm in niobium has been inferred while 0.6 nm of cobalt, the thickness at which the cobalt becomes ferromagnetic, is sufficient to isolate two 30 nm thick niobium layers [Lee 2000].

If the ferromagnetic layer is insulating rather than conducting the affect on the superconductor is similar to that of a low level of contamination with magnetic impurity atoms, this can be contrasted with a non-magnetic insulator which has little effect on the properties of a superconductor [DeWeert 1989]. The scattering of quasiparticles from the spin-polarised wall causes resonant pair breaking and the formation of states within a single spin band of the superconducting gap. The addition of a ferromagnet insulator can increase the superconducting critical field, parallel to the layers, in a ferromagnetic insulator/superconductor multilayer. The ferromagnetic insulator carries most of the flux and, as the superconducting wavefunction is zero in an insulator, this prevents the flux from interacting with the Cooper pairs [Chien 1997]. If the ferromagnetic layer is very thin then the suppression of superconductivity may be less than that given by an antiferromagnetic layer. The Cooper pairs reentering the superconductor will be virtually unchanged in phase, giving minimal change in the superconducting properties.

Further interest in superconductor/ferromagnet heterostructures was sparked when a nonmonotonic dependence of T_c on the iron thickness was reported for V/Fe superlattices with a fixed vanadium thickness, in addition to the step in T_c at the paramagnetic/ferromagnetic transition [Wong 1986]. This was also found in other superconductor/ferromagnet multilayers and was initially thought to be the result of π-phase coupling between the superconducting layers. The superconducting wave function still extends into the ferromagnetic material through the proximity effect however the exchange field alters the phase as the Cooper pairs pass through it [Demler 1997]. The decaying oscillation in the superconducting wavefunction in a ferromagnet can be used to explain the nonmonotonic behaviour of T_c with the ferromagnet thickness. If a local maxima in the superconducting wavefunction from one superconducting layer is in the same position in the ferromagnet as a local minima from the other layer then the Josephson coupling is a maximum when the phase difference between the superconducting layers is π rather than zero [Chien 1997].

The discovery of nonmonotonic behaviour in F/S/F trilayers called the π-phase interpretation into question [Mühge 1997, Lazar 2000-I]. As there is only a single superconducting layer there is no possibility of Josephson coupling. Instead it is explained in terms of the wavefunction reflected from the far side of the ferromagnet, which has been phase shifted by the exchange interaction [Tagirov 1999]. There is quantum interference between this wavefunction and the superconducting wavefunction incident on the superconducting/ferromagnet interface. As the phase shift in the reflected wavefunction depends upon the thickness of the ferromagnetic layer this leads to the oscillating and reentrant behaviour of T_c. It has also been suggested that spin-flip scattering is the dominent pair-breaking process rather than the exchange field [Vélez 1999].

There has been recent interest in superconducting/ferromagnet heterostructures formed from a cuprate superconductor such as $YBa_2Cu_3O_{7-\delta}$ and a colossal magnetoresistive material such as $La_{0.67}Sr_{0.33}MnO_3$. In addition to showing interesting properties these materials are both based on the perovskite structure and so epitxial growth on a suitable substrate is possible [Kasai 1990]. Even very thin layers, down to 2 nm, can show superconductivity or CMR behaviour respectively [Jakob 1995]. However there is the problem of interdiffusion between perovskites, as seen between $YBa_2Cu_3O_{7-\delta}$ and $LaAlO_3$ where a thin interfacial transition layer of $Ba_3Al_2O_6$ was observed and between $YBa_2Cu_3O_{7-\delta}$ and $La_{0.7}Ca_{0.3}MnO_3$ where the superconductor absorbed oxygen from the CMR material [Guo 1995, Bari 1997]. This creates an interfacial region that is neither ferromagnetic nor superconducting, changing the properties of the multilayers [Kasai 1992, Stadler 2000].

An atomically flat interface with little strain is desirable to maximise the superconducting properties of a superconducting/ferromagnet heterostructure [Sá de Melo 1997]. If the interface is rough then there will be demagnetising fields that will suppress the superconductivity even further. Again increased spin-orbit scattering in the multilayer will reduce any effect a ferromagnetic layer has on a superconductor, making the two spin bands increasingly equivalent as the spin-orbit scattering time increases [Demler 1997].

There have been reports of a long superconducting coherence length, the anomalous proximity effect, in superconductor/ferromagnet structures. The resistance of a nickel track is changed by up to 1% on cooling below T_c and H_c of a tin island deposited on the track, the resistance can either increase or decrease depending upon the distance between the island and the measured region [Petrashov 1994]. Conventionally the superconductor can not be the cause of the change because the distance between the island and the measured region is more than thirty times the length scale over which the superconducting pair correlation should be destroyed by the exchange interaction (L_c):

$$L_c = \frac{\hbar v_F}{I} = \frac{\hbar v_F}{k_B T_C} \tag{3·2}$$

where: v_F is the Fermi velocity.

I is the energy of the exchange parameter.

T_C is the Curie temperature of the ferromagnet.

Similar changes were also observed in cobalt wires with aluminium islands, in coupling between tin contacts across a 40 nm nickel wire and in tunnelling between $YBa_2Cu_3O_{7-\delta}$ layers across a very thick, 500 nm, $La_{0.7}Ba_{0.3}MnO_3$ barrier [Kasai 1990, Giroud 1998-II, Lawrence 1999]. In the case of the nickel bridge the resistance only increases when an oxide layer forms at the Sn/Ni interface and the coherence length shows a temperature dependence that is not predicted by theory. However in other experiments 80 nm of $La_{0.7}Ca_{0.3}MnO_3$ was sufficient to prevent coupling between $YBa_2Cu_3O_{7-\delta}$ layers [Bari 1997].

Modelling Superconductor/Ferromagnet Multilayers

The critical temperature and critical field of a superconductor/ferromagnet multilayer have been modelled by numerous authors. The model of Radović et al. has very few free parameters and, despite the somewhat unrealistic assumptions in the model, produces results giving a reasonable fit to the data for strong and weak ferromagnets [Radović 1988, Verbank 1994, Mercaldo 1999-II]. The model is based upon the quasiclassical equations for Gorkov's Green functions, assuming both the superconductor and ferromagnet are in the dirty limit. The normal excitations are described by $F(\underline{r},\omega)$ and close to T_c this is given by:

$$-\frac{D}{2}\left(\nabla+\frac{2\pi i}{\Phi_0}\underline{A}\right)^2 F(\underline{r},\omega)=\frac{\Delta(\underline{r})}{\hbar}-\omega F(\underline{r},\omega) \tag{3·3}$$

where: $\Delta(\underline{r})$ is the pair potential.

D is the diffusion coefficient.

$\hbar\omega=\pi k_B T(2n+1)$ with $n\in Z^+$.

$\underline{A}$ is the magnetic vector potential.

Φ_0 is the flux quantum.

This should be completed by the self consistency condition relating $\Delta(\underline{r})$ to F:

$$\Delta(\underline{r})\frac{T_{c_0}}{T}=2\pi k_B T\sum_{\omega}\left[\frac{\Delta(\underline{r})}{\hbar\omega}-F\right] \tag{3·4}$$

where: T_{c_0} is the bulk critical temperature, i.e. T_{c_S} or T_{c_F}.

Employing the ansatz:

$$F=\frac{\Delta}{\hbar\omega+2\pi k_B T_{c_0}\rho(t)} \tag{3·5}$$

where: $\rho(t)$ is the pair-breaking parameter.

t is the reduced temperature with $t=\frac{T}{T_{c_S}}$.

This allows equation 3·3, in the superconductor, to be reduced to:

$$\left(\nabla+\frac{2\pi i}{\Phi_0}\underline{A}\right)^2 F_S=-k_S^2F_S \tag{3·6}$$

where: $k_S^2=\frac{2\rho(t)}{\xi_S^2}$.

$\xi_S=\sqrt{\frac{\hbar D_S}{2\pi k_B T_{c_S}}}$.

This is formally equivalent to the linearized first Ginzburg-Landau equation, equation 2·5, and the Ginzburg-Landau coherence length is related to ξ_S by:

$$\xi_{GL}(t)=\frac{\pi\xi_S}{2\sqrt{1-t}}. \tag{3·7}$$

The self consistency equation, equation 3·4, can then be transformed to link the pair-breaking potential to the reduced temperature:

$$\ln t = \Psi\left(\frac{1}{2}\right) - \mathrm{Re}\left[\Psi\left(\frac{1}{2} + \frac{\rho}{t}\right)\right] \tag{3·8}$$

where: Ψ is the digamma function.

$\mathrm{Re}[f(x)]$ takes the real part of $f(x)$.

In a superconductor/normal metal system the pair-breaking potential is real, in superconductor/ferromagnet system it is complex because of the exchange field. This is reflected in the oscillations in the superconducting wavefunction as it decays in the ferromagnet, as opposed to the simple exponential decay in a normal metal [Demler 1997]. Additional pair-breaking mechanisms, such as Pauli paramagnetism or spin-orbit scattering, are neglected but could be included as they are additive.

The ferromagnet is dominated by the polarisation of the conduction electrons by the exchange field, represented by the exchange energy (I_0). Equation 3·3 holds with $\hbar\omega \to \hbar\omega + iI_0$ and, assuming $T_{c_F} = 0$ and so $\frac{\rho}{t} = -\frac{1}{2}$, it can be rewritten in the ferromagnet as:

$$\left(\nabla + \frac{2\pi i}{\Phi_0}\underline{A}\right)^2 F_F = k_F^2 F_F \tag{3·9}$$

where: $k_F^2 = \frac{2(\pi k_B T + iI_0)}{\hbar D_F} \xrightarrow[I_0 >> k_B T_{cS}]{} \left(\frac{2(1+i)}{\xi_F}\right)^2$.

$$\xi_F = \sqrt{\frac{4\hbar D_F}{|I_0|}}.$$

ξ_F is the characteristic decay length of the quasiparticles in the ferromagnet and is temperature independent, given $I_0 >> k_B T_c$. The fact that ferromagnetic layers are far more effective at decoupling superconducting layers than a normal metal can be seen as ξ_F is far shorter than $\xi_N = \sqrt{\frac{\hbar D_N}{2\pi k_B T}}$ with $T_{c_N} = 0$ and $D_F = D_N$.

It is possible, using the above equations, to determine the critical temperature of a superconductor/ferromagnet multilayer in the case where the superconducting layers are strongly decoupled and thin enough that they will not contain a flux vortex. This reduces the problem to that of a thin superconducting layer embedded in a ferromagnet. The pair-breaking potential, as a function of the reduced critical temperature of the bilayer $\left(t = \dfrac{T_c}{T_{c_S}}\right)$ with T_{c_S} the transition temperature of the bulk superconductor, is given by:

$$\rho(t) = \frac{2\phi^2 \xi_S^2}{d_S^2} \tag{3·10}$$

where: d_S is the thickness of the superconductor.

$$\phi \tan\phi = (1+i)\frac{d_S}{\xi_S \varepsilon}.$$

$$\varepsilon = \frac{\xi_F}{\eta \xi_S}.$$

η characterises the S/F interface, given by the generalised de Gennes-Werthamer boundary condition:

$$\frac{\mathrm{d}}{\mathrm{d}x}\ln F_S = \eta \frac{\mathrm{d}}{\mathrm{d}x}\ln F_F . \tag{3·11}$$

In the dirty limit with a specular interface η is given by the ratio of the normal state conductivities, $\eta = \dfrac{\sigma_F}{\sigma_S}$.

The assumption that the generalised de Gennes-Werthamer boundary condition, which implies a high quantum mechanical transparency, can be applied directly to the problem of superconductor/ferromagnet structures is one of the main weaknesses of this model. Fitting experimental results to the model gives values of η that are at least one order of magnitude lower than the ratio of the normal state resistivities [Koorevaar 1994, Stunk 1995, Jiang 1996, Mühge 1997]. While this is partially due to the non-perfect nature of the interface giving rise to non-specular scattering, there is also the problem of spin accumulation at the interfaces. As with a ferromagnet/normal metal interface there will be an imbalance in the spin populations at the ferromagnet/superconductor interface that creates a potential difference opposing the flow of electrons across the interface [Hass 1994]. This additional interfacial resistance must be taken into account when modelling a superconductor/ferromagnet structure [Aarts 1997, Fal'ko 1999, Golubov 1999]. This gives a discontinuity in F at the interface and the following boundary equation [Lazar 2000]:

$$-D_F\left(\underline{n}_F \cdot \nabla F_F\right) = \frac{v_F T_I}{2}\left(F_S - F_F\right) \tag{3·12}$$

where: $\underline{n}_F$ is the unit vector perpendicular to the interface.

v_F is the Fermi velocity in the ferromagnet.

T_I is the interface transparency parameter given by $T_I = \int_0^1 \frac{tT(t)}{1-T(t)}\mathrm{d}t$.

T(t) is the angle-dependent quantum mechanical transmission coefficient.

t is the cosine of the angle between the interface normal and the trajectory of the transmitted electron.

Solutions involving a more accurate boundary condition unfortunately require additional parameters to obtain a solution [Tagirov 1998].

The spin-orbit scattering of superconducting electrons decreases the effect of the magnetic exchange field on superconductivity as it scatters electrons between the two spin states, mixing the singlet and triplet states of the Cooper pairs [Grimaldi 1997-I]. The effect of the exchange interaction would only be completely suppressed in the extreme dirty limit, where the electronic mean free path is on the order of the interatomic distance. Although the analogy is not complete, the behaviour in an applied magnetic field is different, the behaviour of the exchange interaction in a dirty superconductor corresponds to the behaviour of a superconductor containing magnetic impurities. The effective exchange scattering time (τ_m) is then given by:

$$\tau_m^{-1} = \sum_q \frac{2l\arctan(ql)\,h_q h_{-q}}{ql - \arctan(ql)} \tag{3·13}$$

where: l is the electron mean free path.

q is the wave vector of the magnetic field produced by the non-uniform magnetic structure.

h is the exchange field.

Antiferromagnetic materials have a reduced effect on superconductivity as both the magnetic induction and the exchange field average out to practically zero on the length scale of the superconducting coherence length (ξ). There is still the effect of exchange scattering though this is also reduced, as equation 3·13 shows. The effective exchange scattering time due to an antiferromagnet, where $\underline{q}$ is approximately equal to the atomic spacing, is far less than that due to a ferromagnet, where $\underline{q}$ is approximately equal to the domain spacing. The coexistence of superconductivity and band antiferromagnetism in layer contacts has been modelled [Krivoruchko 1993].

Despite the antagonistic nature of ferromagnetic and superconducting order it is theoretically possible for ferromagnetic layers to couple across a superconducting layer, as in a GMR structure, and for superconducting layers to couple across a ferromagnetic layer via Andreev reflection [Sá de Melo 1997, Kadigrobov 1999-I]. In order for the ferromagnetic layers to couple both above and below T_c the superconductor must have a high T_c and short coherence length much shorter than the thickness of the superconducting layer while the superconductor must be thin enough for magnetic coupling, at most a few nanometers. Equally the metallic ferromagnet can not give rise to a large pair-breaking effect. Attempts to observe coupling in Fe_4N/NbN multilayers were unsuccessful, though it may occur in $La_{1-x}Ba_xMnO_3/YBa_2Cu_3O_{7-\delta}$ heterostructures [Mattson 1997, Przysłupski 1999]. The analysis also indicates that the effect of roughness at the superconductor/ferromagnet interface on T_c is negligible provided that the length scale of the roughness is much less than the coherence length. The interfacial roughness can have a strong effect on any magnetic coupling as the coupling must be averaged over thickness fluctuations and lateral fluctuations break the translational invariance and so conservation of momentum parallel to the interface. By analogy, the problem of interfacial roughness must also be considered in the proximity effect as the coherence length in a ferromagnet tends to be very short, making the interfacial roughness more significant.

Spin-Polarised Quasiparticles in a Superconductor

Electron spin resonance is not possible in bulky superconductors due to the limited penetration and spatially inhomogeneous magnetic field [Aronov 1976]. This is unfortunate as the spin transport properties, especially in cuprate superconductors, offer a probe of any spin-charge separation in the superconductor, the nature of quasiparticles and anisotropic properties. This leads to the modification of the spin-injection experiment, where the spin transport properties of a superconductor can be investigated by injecting spin-polarised quasiparticles from the ferromagnet [Johnson 1994]. It was also hoped that using spin-polarised quasiparticles could improve the gain of various superconducting devices without increasing the switching time. As in other conductors the spin diffusion length in a superconductor was expected to be much longer than the mean free path of the quasiparticles and the excess spin would have to relax before the quasiparticles could recombine to form Cooper pairs. Thus a small current of injected spin polarised quasiparticle would give rise to the same non-equilibrium quasiparticle population as a larger current injected through a normal metal injector, giving less heating for the same change in the critical current. Equally the spin-polarised electrons could be viewed as a flux of magnetisation as well as charge, potentially giving the paramagnetic effect in the superconductor.

Initial experiments, in both conventional and cuprate superconductors, used the spin-injection geometry. The spin-polarised current is generated in the first ferromagnetic film, flows through the superconductor. The spin-polarised current is detected by measuring the potential difference between a second ferromagnetic film and an adjacent paramagnetic film [Hass 1994, Johnson 1994 and Johnson 1995]. This is the superconducting equivalent of the bipolar spin transistor. As before the potential difference should change with the angle of magnetisation between the two ferromagnetic films. As a magnetic field is swept across the device from saturation through zero field and the coercive field (H_C) to saturation the magnetisation direction reverses. While the magnetisation changes, near H_C, the magnetisation of the two films will be essentially randomised and so there will be no overall spin-polarisation of the injected current. This reduces the measured voltage, to zero if there is no spin imbalance in the superconductor, and this signal implies that the spin-polarised quasiparticles are transmitted through the superconductor. Any asymmetry in the deposition of the two detectors will lead to a voltage offset so care must be taken when determining the magnitude of the signal [Johnson 1995]. As one would expect any voltage offset is effectively reduced to zero below T_c.

The voltage signal is much smaller below T_c, in general by an order of magnitude [Hass 1994, Johnson 1994 and Johnson 1995]. The signal usually has a larger full width at half maximum (FWHM), though it can normally be detected with a SQUID. The signal also decays quite rapidly as the temperature is reduced while in the superconducting regime. This reflects the fact that the spin diffusion length (δ_s) seems to be far shorter below T_c. At 10 K $\delta_s = 0.8$ μm in niobium while when superconducting the characteristic length for spin diffusion ($\lambda_{s,0}$) is only 2 nm, which is shorter than the quasiparticle diffusion length. In a kinetic picture, this suggests that the spin equilibration time is much shorter than the charge imbalance relaxation time.

A layer of gold is normally deposited as a barrier between the ferromagnetic material and the superconductor, in the case of oxide materials an oxide insulator may be used so as to maintain epitaxial growth. This barrier layer prevents magnetic atoms diffusing into the superconductor as they would act as spin scattering sites, dramatically reducing both $\lambda_{s,0}$ and T_c in the superconductor. In the case of oxide superconductors the barrier also reduces the diffusion of oxygen into the ferromagnet. If a ferromagnetic metal, such as permalloy, is deposited directly on $YBa_2Cu_3O_{7-\delta}$ an intermediate 'spin-glass' phase is observed with a much lower magnetisation than the ferromagnetic film [Rubinstein 1993]. This is either caused by partial oxidation of the permalloy or by a non-uniform distribution of oxygen in the surface layers of the YBCO. As the spin diffusion length in gold is reasonably long, on the order of a micron, the film should have little effect though there will be an exponential decay in the magnitude of the spin imbalance as the thickness of the gold layer is increased [Johnson 1993, Lee 1999].

A device has been proposed that combines both the suppression of critical current by injection of spin-polarised quasiparticles and the change in the current voltage characteristics with the change of the magnetisation state of a pair of ferromagnetic layers. The conductance of a ferromagnet/superconductor/ferromagnet double tunnel junction as a function of the applied voltage depends upon both the voltage and applied magnetic field [Takahashi 1999]. It has been theorised that, at a critical voltage inversely proportional to the spin polarisation of the tunnelling current, the injection of spin polarised quasiparticles would completely suppress the superconductivity. As the critical voltage depends upon the spin imbalance in the superconductor it would depend upon the relative magnetisation state of the ferromagnetic layers. This means that the tunnelling magnetoresistance of the device would be strongly dependent upon the bias voltage.

Suppression of Critical Current by Injection of Spin-Polarised Quasiparticles

The use of spin-polarised quasiparticles in devices has focused on the cuprate superconductors, where the lower charge carrier density, and the possibility that spin plays a role in forming the superconducting condensate, may make the effect of spin-polarised injection far more obvious. Equally devices using the cuprate superconductors tend to have a gain that is at least an order of magnitude lower that that found in devices using standard BCS superconductors, so any way of increasing the gain is of interest. A variety of injection geometries have been used, with the most popular being direct injection into the superconductor through a finger [Chrisey 1997, Dong 1997, Soulen 1997, Lee 1999]. One disadvantage of this configuration is that the injected current is added to the supercurrent and gives the appearance of a lower supercurrent than is actually the case. The ferromagnetic film can also be deposited as a base layer with the superconducting track on top, the spin-polarised current then 'shorts' through the superconductor [Vas'ko 1997, Yeh 1999-II]. A disadvantage of this technique is the uncertainty as to how much of the spin-polarised current flows through the superconductor.

Initially a ferromagnetic metal, permalloy, was used as the source of the spin-polarised current with a paramagnetic gold injector as a control [Chrisey 1997]. Permalloy was chosen as it exhibits quite a high, 45%, degree of spin polarisation. As usual there is a gold barrier between the permalloy and the superconductor. Injection through permalloy in the best sample gave a significantly larger reduction in the critical current, a current gain of about 7, while injection through the gold, considering current summation, gave a current gain of approximately 1. The gain being the change in the critical current divided by the injected current $\left(\frac{\Delta I_c}{I_{inj}}\right)$. Other samples showed a smaller difference [Soulen 1997].

If one assumes a large phonon escape rate, so that when the quasiparticles recombine the phonon produced does not go on to break a Cooper pair and a spin relaxation time longer than the quasiparticle recombination time, then this result can be explained in terms of a 'spin bottleneck'. The presence of the non-equilibrium quasiparticles disrupts the superconducting order parameter via the electronic degrees of freedom and any heating effect, leading to a reduced critical current. To recombine to form a

Cooper pair the two quasiparticles must have opposite spin, thus one of them must have undergone some sort of spin-flip event. If such events are infrequent the non-equilibrium population of spin-polarised quasiparticles will persist for a longer period, and so have a greater effect on the gap parameter, than if they were not spin-polarised. An alternative, and not so useful, possibility is that the 'spin bottleneck' is a potential barrier to further quasiparticle injection. The injected quasiparticle would then have a higher energy and the superconductor would be at a higher temperature than it would be if the quasiparticles were not spin-polarised. This heat would have to diffuse away and so switching times would be increased in any device.

Other work used a material with colossal magnetoresistance, CMR, such as $La_{0.67}Sr_{0.33}MnO_3$, as it is believed that the spin-polarisation in such materials is very close to unity. As the structure of the cuprate superconductors is very similar to that of the manganate CMR materials, both are based on the perovskite structure, it should also be possible to deposit them epitaxially on each other. In order to improve the crystal structure of the second deposited phase, to act as a diffusion barrier and to limit the proximity effect between the ferromagnetic film and the superconductor, an insulating layer is deposited between the two. This does mean that additional heating occurs but this is claimed to be a small effect and a thicker barrier reduces the gain [Dong 1997, Vas'ko 1997]. If heating from the barrier were the cause of the reduction in the critical current a thicker barrier would generate more heat and so give a larger gain.

Much larger gains have been reported through CMR materials, a gain of approximately one compared to a gain of approximately 0.04 through gold [Vas'ko 1997]. Gold however has a radically different density of carriers, resistivity and interfacial barrier to a manganate CMR material and there was no insulating barrier between the gold and the superconductor. A better comparison may by found by using $LaNiO_3$ as the control injector, though it is interesting to note that the superconducting film deposited on the $LaNiO_3$ had a significantly lower critical current [Dong 1997]. The spin-polarised injector gave a gain of 3.2 for a 8 nm thick insulating barrier, increasing to 9.3 for a 16nm barrier and falling rapidly for barriers thickner than 20 nm, while the control injector gave a gain of less than 0.3 [Dong 1998]. The largest reported gain for a spin-polarised injector is 35 though a significant portion of the effect could well be due to heat as there is a critical current gain of 6 when the current is passed through the CMR material without being injected into the superconductor [Soulen 1997, Koller 1998, Stroud 1998]. Pulsed currents have been used to minimise the Joule heating of the superconductor [Yeh 1999-II].

The Theory of Spin-Polarised Quasiparticles

The current injected into the superconductor from the ferromagnet can be considered in terms of a spin injection current and a quasiparticle charge current, as opposed to that carried by the superconducting condensate [Zhao 1995]. As the spin in a singlet superconductor is a good quantum number, and is conserved, spin can diffuse independently of the charge [Senthil 1998]. The injected spin will not be equal to the injected current as there will be some minority spins injected, the fraction of the total current injected as quasiparticle spin can be approximated by the difference in the spin populations divided by the sum. The injected quasiparticle charge must be modified by the fact that, with a probability depending upon the energy of the quasiparticle, it can have an electron-like or a hole-like character. The additional injected charge will be carried by the superconducting condensate.

The injected spin-polarised current can be detected with a second ferromagnetic film. The voltage when the magnetisations of the ferromagnetic films are parallel (V_1) and when they are antiparallel (V_2) can give the spin and charge relaxation times in the superconductor. As in the bipolar spin transistor, the difference between V_1 and V_2 is proportional to the injected quasiparticle spin, the spin relaxation time (τ_s) and the difference in the density of states of the detector's spin bands relative to the sum. The sum of V_1 and V_2 depends upon the injected quasiparticle charge and the charge relaxation time (τ_q). When the quasiparticles enter the superconductor they are distributed between the gap energy (Δ) and the injection energy (eV_{inj}), the energy range over which there are filled states in the injector and available states in the superconductor. Electrons may enter the superconducting condensate directly through Andreev reflection but, as discussed above, the probability is reduced for ferromagnetic injectors. Inelastic scattering cools the quasiparticle distribution towards equilibrium with a characteristic time (τ_E) that is on the order of 0.1 ns [Arie 1997-I]. This also gives a certain degree of charge relaxation, as the lowest energy states are near the Fermi level where the electron-like or hole-like nature is less clear. Additional charge relaxation occurs either when quasiparticles recombine to form Cooper pairs or are cross-branch scattered, changing from being electron-like to hole-like or vice versa. This can occur due to inelastic electron-phonon scattering or by impurity elastic scattering in the presence of anisotropy in the superconducting gap and cooling has little effect on these processes. As spin can relax without branch crossing or recombination, the initial cooling can have a strong effect on the spin relaxation time.

The two major spin relaxation processes are magnetic impurity scattering, where the quasiparticle spin couples with the spin of the magnetic atom, and spin-orbit scattering, this originates from spin-orbit coupling to impurities or strong electric fields near the boundaries of the film. The probability of spin-orbit scattering is proportional to the mass of the impurity atom. The change in the spin relaxation time on the transition from the normal to the superconducting state depends upon the scattering mechanism. For elastic magnetic impurity scattering, if spin relaxation takes more time than the cooling process, τ_s initially increases below T_c and then decays exponentially with temperature. However if the spin imbalance relaxes faster than the temperature imbalance, τ_s increases and saturates as the temperature is reduced below T_c. For elastic spin-orbit scattering τ_s increases below T_c. Considering the results of the spin-injection experiment into niobium, where the spin diffusion length fell as the temperature drops, this suggests that the niobium was contaminated with magnetic impurity atoms [Johnson 1995]. It also suggests that the spin relaxation time, in that system, is longer than the cooling time. In part, this is confirmed by a measured spin relaxation time (T_2) of 0.6 ns in normal state niobium at 10 K.

Care must be taken when modelling the transport of spin-polarised quasiparticles into a cuprate superconductor due to the d-wave symmetry of the superconducting wave function. The sign change in the superconducting wavefunction can make the electrical properties of ferromagnet/d-wave superconductor interfaces significantly different to those of ferromagnet/s-wave superconductor interfaces. Features present in the s-wave case may be absent in the d-wave case, for example the decrease in the differential conductance when the electrical potential energy across the superconductor/ferromagnet interface is equal to the gap energy, or vice versa

[Zhu 1999]. Interfacial scattering can lead to a maximum in the conductance at finite bias and under certain circumstances, for certain directions relative to the superconducting wavefunction, Andreev bound states can occur that strongly suppress the injection of magnetisation into the superconductor [Merrill 1999, Zhu 1999-II].

It is possible that there is spin-charge separation within the superconductor [Si 1997]. For a steady superconducting state $\mu_s + e\Phi$ must be a constant, where μ_s is the chemical potential of the superconductor and Φ is the electrostatic potential, otherwise the Cooper pairs will accelerate until it is constant. Thus the quasiparticles, in a fully gapped superconductor in three dimensions, should be neutral, spin ½ particles due to perfect screening of charge and the Meissner effect. Therefore charge and spin transport are separated as the charge current is carried by the condensate within a penetration length of the surface while the spin current is carried by quasiparticles in the bulk. It may be possible to check this experimentally using the spin injection experiment to determine the temperature dependence of the spin diffusion length in the superconductor. If τ_s does not show the same linear temperature dependence as the electrical resistivity then spin-charge separation is likely.

Magnetic Superconductors

Although BCS superconductivity and magnetism are antagonistic types of electron ordering there are certain ternary compounds, such as $ErRh_4B_4$ and $HoMo_6S_8$, that show both states [Bulaevskiĭ 1985]. These materials have a superconducting transition temperature (T_c) that is significantly higher than the magnetic transition temperature (T_M) and all of them are type II. They initially become superconducting at the upper superconducting critical temperature $\left(T_{c_U}\right)$ and on further cooling begin to show magnetic order at T_M. In materials, such as $ErRh_4B_4$ and $HoMo_6S_8$, that show long-range ferromagnetic ordering there is a lower superconducting critical temperature $\left(T_{c_L}\right)$ below which the ferromagnetic exchange interaction completely suppresses superconductivity. Below T_M, to the limit of T_{c_L} where there is ferromagnetic ordering, these materials show both gap-less superconductivity and magnetic order, the coexistence state. There may even be a transition from type II behaviour near T_{c_U} to type I behaviour near T_M. External perturbations can strongly affect magnetic superconductors, spin diffusion will suppress the superconductivity and an increasing magnetic field can cause a transition from an antiferromagnetic to a ferromagnetic state [Dupont 1983, Hampshire 1998].

Antiferromagnetic ordering has significantly less effect on a superconductor than ferromagnetic ordering. In the clean limit the decrease in the superconducting gap parameter relative to the initial value $\left(\frac{\delta\Delta}{\Delta_0}\right)$, assuming $h >> \Delta_0$, is given by:

$$\frac{\delta\Delta}{\Delta_0} \approx \frac{h}{v_F G} \ln \frac{h}{\Delta_0} \tag{3·14}$$

where: h is the exchange field in energy terms.

v_F is the Fermi velocity.

$^G/_2$ is the antiferromagnetic wave-vector.

However even non-magnetic impurities can increase the depairing effect of the exchange field, which is reflected in the decrease in the superconducting gap parameter relative to the initial value in the dirty limit:

$$\frac{\delta\Delta}{\Delta_0} \approx \frac{h^2}{\Delta_0 v_F G} \approx \frac{T_N}{T_c} \tag{3·15}$$

where T_N is the Néel temperature.

Superconductivity actively suppresses the ferromagnetism in magnetic superconductors, reducing the Curie temperature (T_C), as the Meissner currents shield the long range part of the dipole-dipole interaction between the localised moments. This can be clearly seen in aluminium with a submonolayer coating of gadolinium where there is a localised RKKY spin polarisation in the normal state that vanishes below T_c with the long range spin susceptibility [Tkaczyk 1988]. The transition between ferromagnetic and paramagnetic ordering can be suppressed by a platinum layer due to the high spin-orbit scattering in a layer with a high atomic mass [Tkaczyk 1992-I]. This encourages the formation of a non-uniform magnetic structure known as the cryptoferromagnetic state [Anderson 1959], at the extreme this gives antiferromagnetic ordering. The magnetic structure was predicted, modelling the exchange interaction in an isotropic material, to be a simple helix [Bulaevskiĭ 1979]. However any magnetic anisotropy transforms the helix into a one-dimensional domain-like structure [Fulde 1964].

Matthias proposed in 1960 that superconductivity could persist below T_{c_L} in the region of a magnetic domain wall even when the superconductivity is suppressed inside the domain. In the centre of a domain wall the local magnetisation is very small and so Cooper pairs can form. As the width of the wall is smaller than the superconducting coherence length, the type of the wall is irrelevant. Magnetic scattering on localised moments will narrow the region will narrow the region of existence for localised superconductivity. The domain structure may become energetically unfavourable, especially if the ferromagnetism is weak or in an applied field, and transform into a superconducting vortex state. This model was used to explain the combination of superconducting and ferromagnetic properties observed in dilute solid solutions of rare earth elements, especially gadolinium, in metallic superconductors.

Superconductivity at domain walls has been used to explain the anomalous resistivity behaviour below T_{c_L} in $ErRh_4B_4$ and $HoMo_6S_8$ [Tachiki 1979, Kulić 1981]. Close to zero temperature, when in the non-superconducting ferromagnetic state, the resistivity (ρ) of $ErRh_4B_4$ is about 40% of the value just above T_{c_U} while the application of a magnetic field over 5 kOe restores the resistivity to the higher value [Fertig 1977]. A similar effect is also seen in $HoMo_6S_8$, though it is smaller with $\rho(T < T_{c_L}) \approx 0.9\rho(T > T_{c_U})$ and the normal resistivity is restored when $H > 0.7$ kOe.

The Cryptoferromagnetic Phase

Superconductivity can persist within the domain wall of a ferromagnetic superconductor as the local magnetisation, which must be averaged over the length scale of the Cooper pair which is effectively the coherence length (ξ), is low. This concept was extended to superconductor/ferromagnet bilayers by Buzdin and Bulaevskiĭ in 1988. They theorised that a ferromagnetic layer on a superconductor would spontaneously form a domain structure on the length scale of ξ when it became thin enough. The energy cost of forming the large number of domain walls would be compensated by the increased superconducting gap energy. Vanadium, which shows evidence of surface ferromagnetism [Rau 1986], may well show this sort of domain structure when it becomes superconducting.

Buzdin and Bulaevskiĭ noted that the details of the transition between the normal ferromagnetic state and the fine domain structure would depend upon many system parameters: film homogeneity, the details of the superconductor/ferromagnet interface, the density of electronic states in both films and many others. They calculated the maximum thickness of the ferromagnetic layer for the formation of the domain structure to be energetically favourable based upon the following simplifying assumptions. They assumed the simplest possible model with a perfect interface, a coherent modulation of the ferromagnetic order over the entire thickness of the ferromagnet, short electronic mean free paths (the dirty state), a ferromagnetic easy direction parallel to the interface, that the ferromagnet thickness (d_F) was less than ξ and the transition into the fine domain structure takes place close to T_c. In this case the transition to the fine domain structure occurs when:

$$\frac{T_C h}{T_c^2}\frac{d_F}{l_F}\sqrt{\frac{d_F}{\xi}} < 1 \qquad (3\cdot16)$$

where: T_C is the Curie temperature,

$T_C \approx \frac{h^2}{\varepsilon_F}$ for a ferromagnet with RKKY interaction.

h is the exchange field, measured as a temperature.

l_F is the electronic mean free path in the ferromagnet.

ε_F is the Fermi energy in the ferromagnet, measured as a temperature.

For a bilayer with $T_C \gtrsim T_c$, $h \approx 100$ K, $l_F \approx 1$ nm, $\xi \approx 100$ nm then the ferromagnetic layer must be thinner than 1 nm.

The concept of superconductivity persisting in regions of low magnetisation, and providing the energy to form such regions, was used to explain some unusual measurements in epitaxial Fe/Nb bilayers [Mühge 1998]. The bilayers showed a decrease in the effective saturation magnetisation (M_{eff}) on cooling below T_c, measured by means of ferromagnetic resonance at 9.4 GHz, for iron layers thinner than 1.6 nm. This decrease was confirmed with a SQUID magnetometer and could not be explained in terms of the demagnetising field of the superconductor as the two resonances (H_0^u and H_0^a) had a different temperature dependence. In addition to this effect a sharp decrease in the T_c of the bilayer was measured at the same iron thickness at which M_{eff} no longer showed a decrease on cooling below T_c.

The reduction in M_{eff} was interpreted as the formation of cryptoferromagnetism, a spatial modulation of the ferromagnetic order due to a modification of the RKKY interaction in the superconducting state. The iron layer was approximately an order of magnitude thicker than the maximum possible to form this state using the Buzdin-Bulaevskiĭ model, 0.7 to 2.7 nm while $d_{F_{crit}} \sim 0.1$ nm. The Buzdin-Bulaevskiĭ model is a highly idealised model and in a real system a slight angular modulation of the ferromagnetic order near the interface is possible, which gives a larger thickness limit for the ferromagnetic layer before the cryptoferromagnetic phase becomes energetically unfavourable. The transition between the cryptoferromagnetic phase and the ferromagnetic phase with increasing iron layer thickness also explains the step in T_c as the cryptoferromagnetic phase would not be expected to strongly suppress the superconductivity.

The modulation in the ferromagnetic order will also disappear if there is a thick paramagnetic region between the ferromagnet and the superconductor, possibly caused by interdiffusion at the interface, as the Cooper pairs must penetrate the ferromagnet strongly to alter the RKKY interaction. These trends are observed in the epitaxial Fe/Nb bilayers. The suppression in M_{eff} would also have a component due to the local demagnetisation fields at monolayer steps in the Nb/Fe interface rotating the magnetisation out of the plane of the film. This effect would have the same dependence on layer thickness as the cryptoferromagnetic phase and it is impossible to distinguish which effect is more important in producing the suppression of M_{eff}.

The magnetisation of the ferromagnetic layer can also have a more direct effect on the superconducting properties of the heterostructure. Measurements of $YBa_2Cu_3O_{7-\delta}/(BiDy)_3(FeGa)_5O_{12}$ heterostructures show a reduction in T_c of up to 9 K on poling the BiDy-IG garnet with 0.5 T [Mou 1998]. The remnant magnetisation of the BiDy-IG garnet is perpendicular to the surface of the film and, equivalently to Clinton's superconducting valve, the magnetic field suppresses T_c [Clinton 1997, Clinton 1998]. Clinton's superconducting switch has a perpendicular ferromagnetic film deposited on a superconducting track, with an insulating layer separating them. When the magnetisation of the ferromagnet is parallel to the track there is a fringing magnetic field intersecting the superconductor, locally suppressing superconductivity. An applied magnetic field rotates the magnetisation in the plane of the film, giving a minimum field in the superconductor when the magnetisation is perpendicular to the track. As the T_c of the device depends upon the magnetic history it can be used for memory applications. The region of suppressed superconductivity can be sufficiently narrow for Josephson coupling, giving a magnetically switchable Josephson junction [Clinton 1999]. The device was modified so as to require a uniaxial switching field by using two independent ferromagnetic layers with different coercive fields, replacing the single ferromagnetic layer with something similar to Juliere's tunnelling structure [Juliere 1975, Clinton 2000].

Controlling the Exchange Interaction in the Superconductor

Theoretical superconductor/ferromagnet heterostructure devices have been proposed that take advantage of the ability to form Cooper pairs in regions where the local exchange field ($\underline{h}$) is short range and weak [Oh 1997, Tagirov 1999]. Both of these devices use two ferromagnetic layers than can either have parallel or antiparallel magnetisation depending upon the applied magnetic field and the magnetic history. The pair-breaking potential created in the superconductor by a ferromagnetic layer has a spatially varying phase. The second ferromagnetic layer will create either constructive or destructive interference with the pair-breaking effect of the first layer, changing the T_c of the device. The relative magnetisation state giving a higher T_c will depend upon the design of the device, both physical and electronic structure will have an effect. As the T_c, and so the I_c, of the device depends upon the applied field and the magnetic history these devices could act as superconducting memory elements or low field switches.

One way of accomplishing this is based upon the GMR structure [Oh 1997]. Two ferromagnetic layers separated by a normal metal spacer are deposited on the superconductor. The thickness of the normal metal spacer is chosen such that, in zero applied field, the magnetisations are antiparallel. Changing the magnetisation state of the two ferromagnetic layers changes the details of the decay and phase shift of the Cooper pairs as they travel through the ferromagnetic layers and so the superconducting properties of the device. In this device the magnetisation state giving a higher T_c depends upon the details of the superconducting wavefunction in the ferromagnetic layers, the state that gives a longer coherence length in the ferromagnet corresponds to a smaller exchange field ($\underline{h}$) in the superconductor and so a higher T_c. The device was described using the Usadel equations with the inclusion of the exchange interaction. The device requires a good quality interface, a low spin-orbit scattering rate, a low ferromagnetic exchange energy and a long coherence length in the ferromagnetic layers to maximise the change in the T_c.

An alternative device structure sandwiches the superconducting layer between ferromagnetic layers, with the magnetisation of one of the ferromagnetic layers pinned by an insulating antiferromagnetic layer [Tagirov 1999]. The application of a small magnetic field rotates the magnetisation of the free ferromagnetic layer while a much higher field is required to change the magnetisation of the pinned layer. The proximity effect in this device can be described by linearised equations for Usadel's anomalous Greens functions, derived from the linear Gor'kov equation for the order parameter near T_c. The change in the T_c of the device, in both relative magnetisations, is described in terms of a pair-breaking parameter R'' with T_c in the parallel magnetisation state being suppressed to zero while the device is can still superconduct, though at a suppressed T_c, in the antiparallel magnetisation state. Care must be taken with the design of the device, if R'' is too high then the device will not superconduct in either magnetisation state. As always when considering the effect of a ferromagnetic material a high spin-orbit scattering rate will suppress any difference between the magnetisation states.

A similar dependence on the magnetic state of the system can also be observed when current is injected through a superconductor between two ferromagnetic point contacts [Deutscher 2000]. If the separation of the point contacts is less than the coherence length in the superconductor then, when in the antiparallel magnetisation state, one quasiparticle from each ferromagnet can combine to form a Cooper pair as they have opposite spins. This allows Andreev coupling between the point contacts when in the antiparallel magnetisation state and not when in the parallel state, altering the conductivity. This idea can also be applied to superconductivity within a 180º domain wall, where the antiparallel domains would take the place of the two ferromagnetic point contacts.

Chapter Four

EXPERIMENTAL METHODS

If you're studying Natural Science,
I suggest that you wear an appliance.
You strap it on thus,
Then hop on a bus,
And you'll find you get masses of clients

I'm Sorry I Haven't A Clue

In this chapter we discuss the fabrication and methods of measurement of the devices. To avoid failure many parameters must be controlled and monitored during fabrication and measurement. The first part of this chapter describes the deposition of the heterostructures and the fabrication of the deposited thin film into devices. We begin with a discussion of the choice and preparation of substrate and the ultra high vacuum system used for deposition of the thin film heterostructures. The films were patterned using standard photolithography and both local and non-local ion milling. Appendix B lists the wafers.

The second part of the chapter discusses the electrical and magnetic measurement of the as-deposited films and the patterned devices. The magnetic hysteresis loops were measured with magnetometers, at various temperatures, while the domain structure was imaged with Lorentz microscopy. The electrical properties of the devices were measured with a custom built cryogenic probe and electronics while the data was stored and processed with a custom written LabVIEW™ program. Electrical properties can be measured as a function of temperature, down to 4.2 K, magnetic fields, up to 47 mT, and with the application of microwave radiation.

Film Deposition

Before depositing the superconducting film a suitable substrate must be chosen. A number of factors should be taken into consideration for any given experiment, such as lattice matching to the film, thermal conductivity, acoustic matching, the possibility of interdiffusion between the substrate and the film, durability, availability and cost [Kaplan 1979, Guo 1995]. The electrical, magnetic and optical properties of the substrate are also important, in order to minimise the effect of the substrate on the devices almost all substrates are non-magnetic insulators. The optical properties are of concern during photolithography, discussed below. In the majority of the work we used r-plane sapphire substrates as it was easily available, robust and commonly used in our laboratory. Sapphire also has excellent lattice matching with niobium, reducing the strain in the deposited film, especially when depositing an epitaxial film [Huang 1991]. We have also used oxidised silicon as the remaining silicon beneath the oxide coating blocks the transmission of light, though it was less robust than sapphire.

The r-plane sapphire was cut down, from a 50 mm x 50 mm x 0.5 mm wafer into 10 mm x 5 mm x 0.5 mm substrates suitable for two 4.5 mm x 4.5 mm device patterns, using a diamond coated dicing saw. The two devices, protected by a thick layer of photoresist, could also be separated using the dicing saw after patterning. Before depositing the film the substrate was carefully cleaned in a clean room, which was also used for subsequent patterning. The substrate was cleaned ultrasonically in chloroform and acetone for ten minutes in each, to remove grease and dust respectively, with the excess solvent blown off using an airgun. If solvent dries on the substrate then drying marks form, which can be extremely difficult to remove. To prevent this the substrate was airbrushed with isopropanol, which has a very low vapour pressure. The substrate was then placed into a chip carrier to protect it from contamination before deposition.

The metallic heterostructures were deposited on the substrate using DC magnetron sputtering. A schematic of the sputtering system, the Cambridge Device Materials 'Mark VII', is shown in figure 4·1. The system was pumped down to ultra high vacuum (UHV) with a turbomolecular pump that was backed with an Edwards 18 rotary pump, the same pump was used to rough the chamber to approximately 10^{-2} mbar. The chamber was pumped down for at least 18 hours to a pressure below 10^{-7} mbar. A bake-out tape was used to heat the walls of the chamber and encourage any contaminants to desorb. The inner chamber (insulated by vacuum from the outer wall when the chamber was pumped down) was cooled by a liquid nitrogen jacket in order to trap oxygen and water contaminants before deposition, reducing the partial pressure of oxygen and water below 10^{-10} mbar and 10^{-8} mbar respectively. In order to control the flow of gas through the system during deposition a gas reservoir and needle valve were used. The system has been fully described by Blamire *et al* in 1998.

The plasma generated by the high potential difference was localised around the target as the electrons follow the magnetic field lines, preventing the plasma from touching the substrate and increasing the deposition rate. A continuous flow of argon gas, with purity greater than 99.999%, was used during deposition. The target was presputtered for 10 minutes before deposition. The presputtering stage cleans the surface of the target of oxides and other contaminants, a lower pressure was used because the plasma then covers and consequently cleans a larger area of the target. The additional

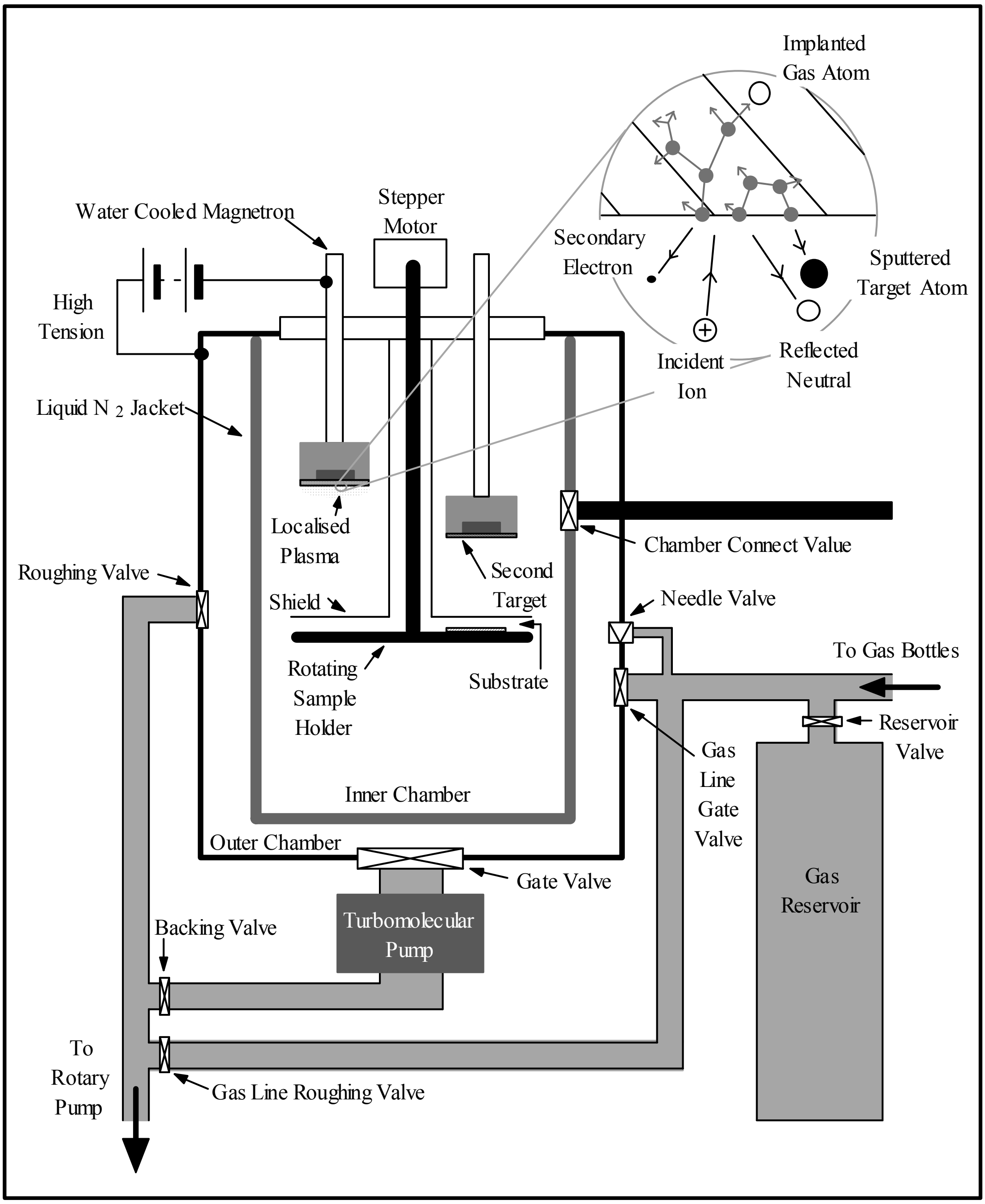

Figure 4·1 Schematic of the Mark VII sputtering system with the possible processes involved in sputtering inset.

care was required in depositing superconducting niobium as none of the oxides of niobium superconduct in liquid helium. The different metallic layers in the heterostructures were deposited without breaking the vacuum so as to prevent the formation of contaminated interfacial layers. This means that the superconducting niobium was almost certainly contaminated with magnetic impurities, the concentration of these impurities can be measured in normal metals by means of the

Kondo effect, discussed below. Deposition was static, where the sample remains stationary under the target, or rotating, where the stepper motor rotates the sample holder during deposition giving the same coating on each sample but taking a longer time and giving the same layer thickness. The deposition parameters of individual elements are given in table 4·1. Please note that, as it was co-deposited with the cobalt to give a multilayer, the pressure given for copper deposition was not optimised to give close to neutral stress in the film.

	Power (W)	Argon gas pressure (Pa)	Deposition rate (nm / min)	Substrate – target distance (mm)
Al presputter	25	0.50		
Al rotating	25	0.67	1.7 ± 0.4	42
Co presputter	30	0.65		
Co static	30	1.00	10.4 ± 3.1	69
Cu presputter	7.5	0.55		
Cu static	5	1.00	21.2 ± 1.0	53
Nb presputter	60	0.75		
Nb static	50	1.20	16.4 ± 5.5	53

Table 4·1 Deposition parameters for the metals used in the heterostructures, deposited in the Mark VII sputtering system.

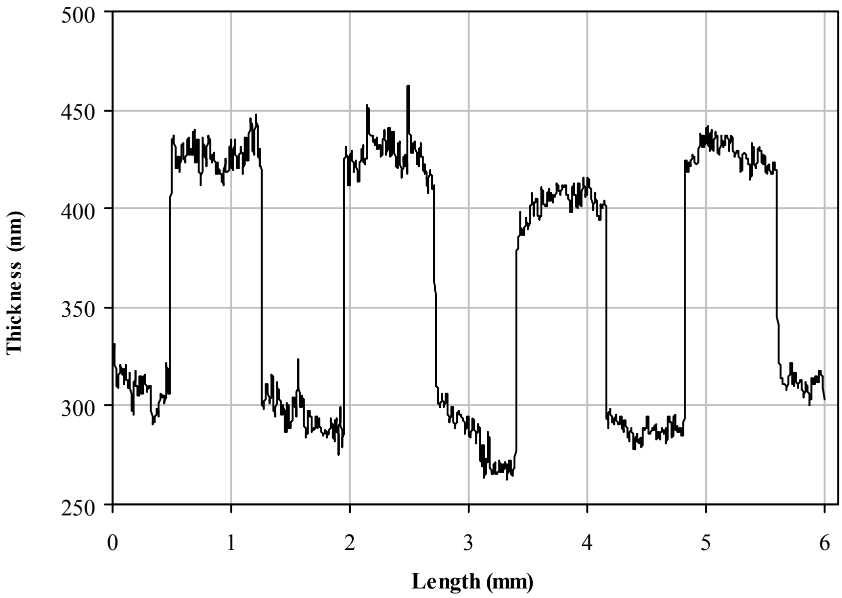

Figure 4·2 Profilometer data from a (116 ± 15) nm thick Nb/Co bilayer patterned into stripes.

The thickness of the sample was determined using a profilometer, a Taylor-Hobson Talysurf 6 with a 120 mm traverse. A glass substrate was patterned with approximately one millimetre wide photoresist strips, separated by about a millimetre. On soaking in acetone the metal deposited on the photoresist lifts off and the steps are measured with the profilometer. The profilometer measures the deflection of a diamond stylus with a piezoelectric chip and the film thickness at that point was given by the step in the signal. As shown in figure 4·2 there is considerable noise in the measurement so the film thickness was determined from an average of at least twenty-five of these measurements. The noise in the signal is actually smaller than the noise in the film thickness, in the data shown in figure 4·2 the noise within an individual stripe is approximately 10 nm while the noise in the thickness measurement is 15 nm. Given that much of the instrumental noise should be removed by averaging there is a significant variation in the film thickness across the chip. The film thickness could also be measured with an atomic force microscope (AFM) which uses a laser beam to measure the deflection of a tip. As the deflection is caused by interatomic forces this gives a measure of the distance between the tip and the surface of the chip. Unfortunately only a limited area of the chip could be measured without manual adjustments and so variations in thickness across the whole chip are not observed. The AFM measurement gave a 5 nm variation in the film thickness, though some component of this variation must be due to instrumental broadening.

The Kondo Effect

The concentration of magnetic impurities in the sputtered films can be estimated from the Kondo effect. The Kondo effect represents the contribution to the resistance due to the scattering of conduction electrons from the local moments of the isolated magnetic impurities. As with all magnetic phenomena there is a characteristic temperature, in this case known as the Kondo temperature (T_K), which can be used to determine the level of impurities in the sample. One of the easiest ways to observe the Kondo effect is in resistance vs. temperature measurements at low temperatures. The contribution to the resistivity due to the Kondo effect increases with decreasing temperature giving rise to a minima in the resistance at a temperature above absolute zero, as in figure 4·3a. Applebaum and Kondo gave an expression for the resistivity (ρ) at temperatures very much less than T_K:

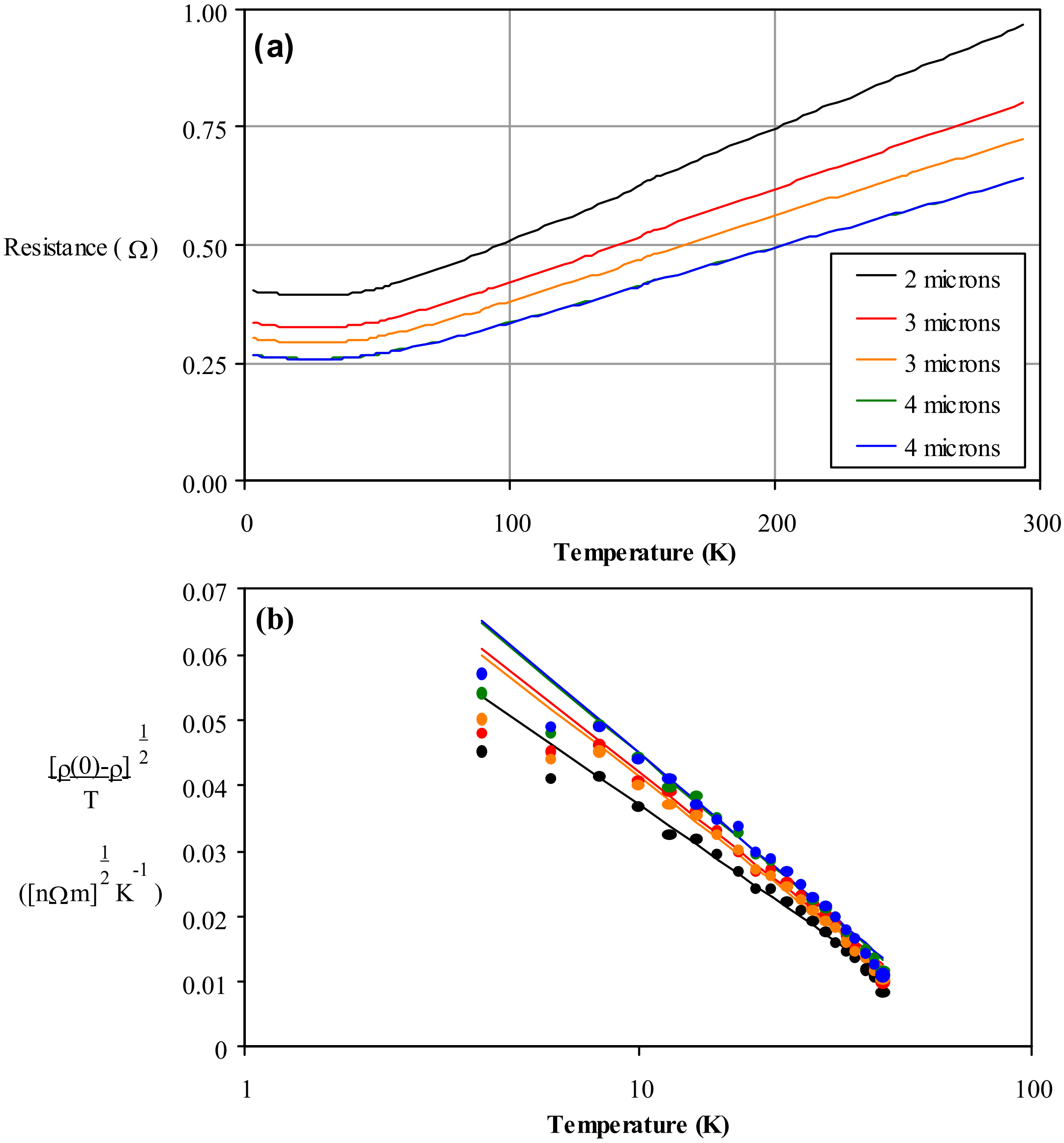

Figure 4·3 Electrical characterisation of a (127 ± 6) nm thick copper film patterned into 10 μm long track with the various widths given in the legend. Part a shows the resistance vs. temperature measurement for the tracks and part b shows the plot derived from equation 4·1 to give the Kondo temperature T_K.

$$\rho = \rho(0)\left\{\cos^2(\delta_v) - \frac{16}{3}\cos(2\delta_v)\left(\frac{T}{T_K}\right)^2 \ln\left(\frac{T}{T_K}\right)^2\right\} \qquad (4\cdot1)$$

where: $\rho(0)$ is the resistivity at zero Kelvin.

δ_v is the phase shift for potential scattering.

Thus a plot of $\frac{\sqrt{\rho \log \rho}}{T}$ against $\log[T]$ should be linear and intercept the temperature axis at T_K, as shown in figure 4·3b. At the lowest temperatures this equation fails to describe the data but does allow an estimate of T_K to be made. For the copper deposited in the Mark VII deposition system this gives $T_K = (77.1 \pm 0.5)$ K which indicates that the copper was contaminated with approximately 0.05% iron [Loram 1970]. As the deposition rate and power used in depositing both the copper and the niobium were similar one would expect a similar proportion of magnetic contaminants in the niobium.

Patterning the Device

The deposited heterostructure was patterned into the initial device structure, which are shown schematically in figure 4·4, using standard photolithographic techniques. The pattern was transferred from a chromium on fused silica photomask to a polymer film, which allows replication of the pattern in the underlying film. In this case, the polymer film was a novolac resin (AZ5214 photoresist) containing a base insoluble sensitiser, an inhibitor, which prevents the resin dissolving in the alkaline developer.

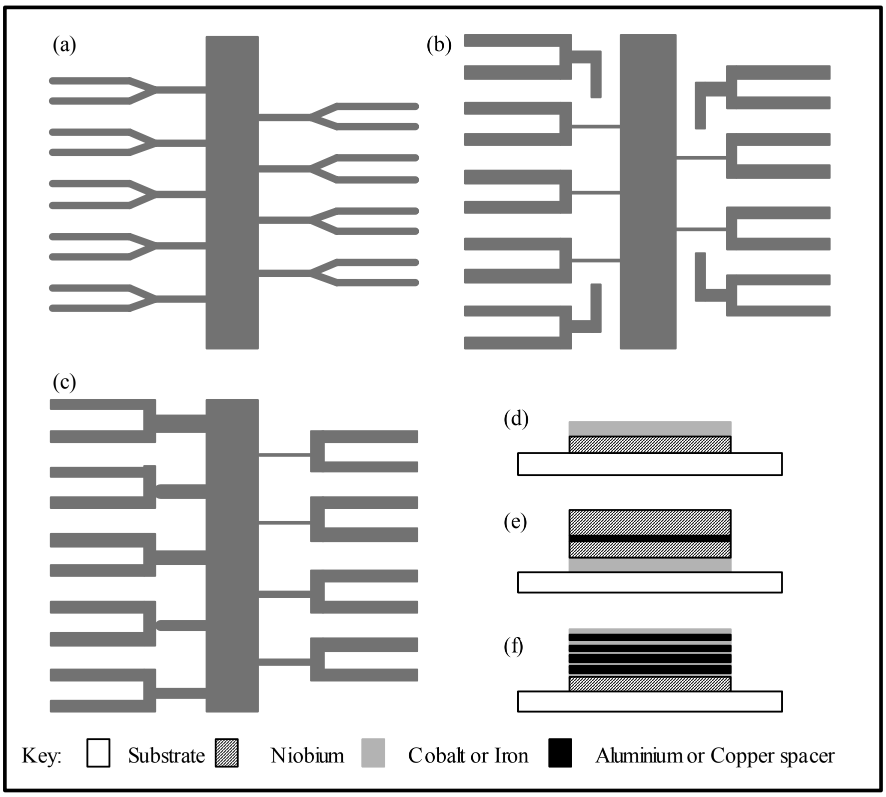

Figure 4·4 Plan and profile schematics of the device patterns showing the patterns for the various track widths and multilayer structures.

On exposure to ultra-violet light, UV, the inhibitor becomes an acid and the resin can be developed. If the exposed photoresist was heated it undergoes an acid catalysed reaction, becoming cross-linked and insoluble. The photomask can be reproduced as either a positive or a negative image of the pattern of the mask, see figure 4·5, which can itself be either a positive or negative image of the device structure.

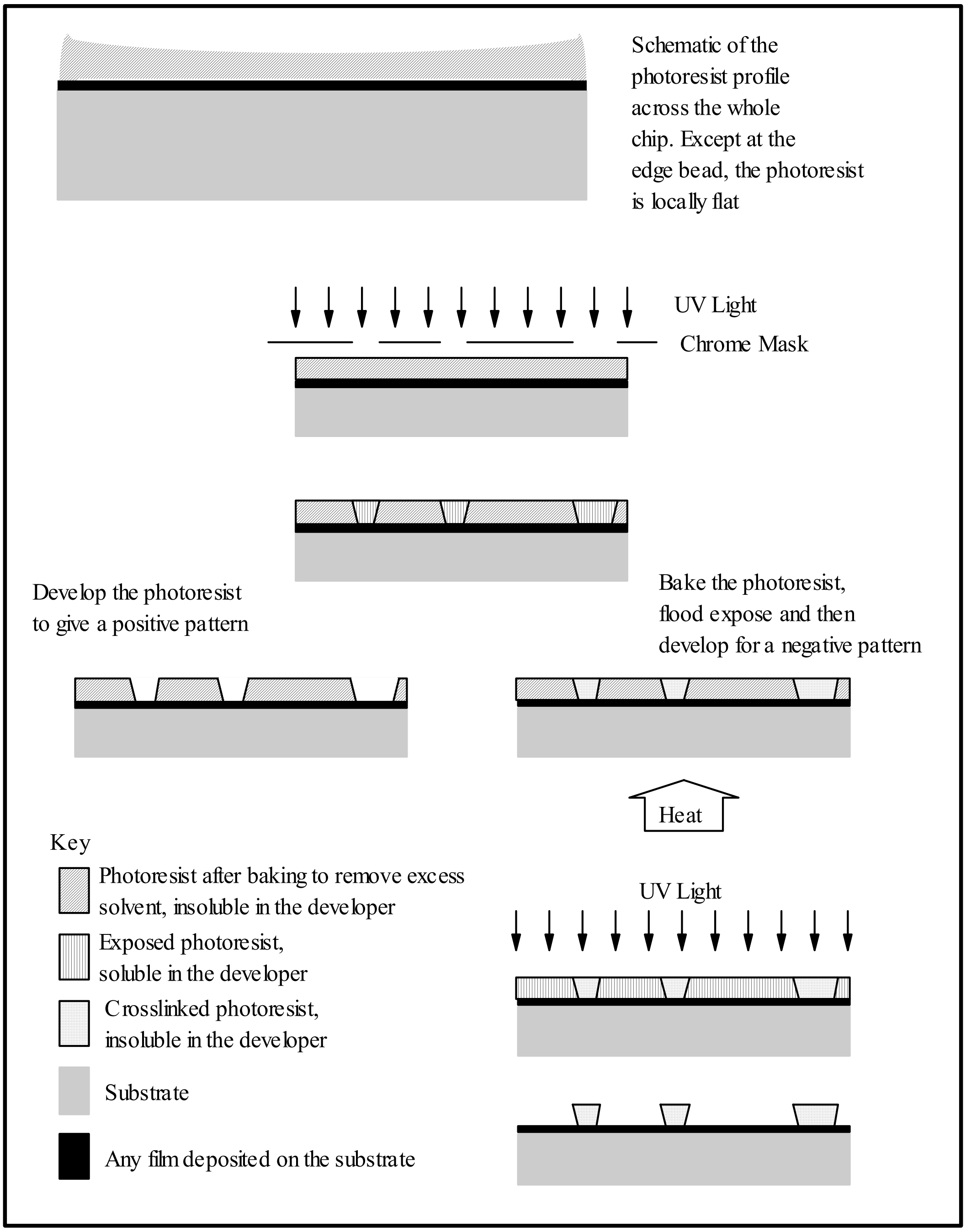

Figure 4·5 Schematic of the photoresist profile, showing the edge bead and the processing route giving a positive or negative reproduction of the pattern in the chrome mask into the photoresist and so into the device structure.

Two alternative methods were used to create the initial pattern, in both cases positive processing was used. The AZ5214 photoresist was spun on to the chip at 6,000 rpm for 30 seconds and baked for 1 minute at 100°C. This gave a central region that was flat to within a few hundred nanometres, however surface tension effects cause resist to build up at the edge of the chip, see figure 4·5. This edge bead was removed using a Canon projection photolithography system and a suitable mask. After a three minute exposure the edge bead was dissolved away in a solution of 4 parts AZ developer to 1 part water (4:1 solution) in about thirty seconds. The excess developer was removed with distilled water and the chip dried with an air gun. Any resist on the bottom of the chip was then removed by rubbing the chip against an acetone soaked cloth. Acetone was drawn up between the tweezers and the chip and, if done before the edge bead was removed, would damage the photoresist.

The pattern can then be transferred into the photoresist using a Karl Suss mask alignment lithography microscope. This machine placed the mask in very close proximity to the chip, rather than projecting the pattern onto the chip using the 1 to 1 optics in the Canon projection photolithography system. The resolution obtained allowed one micron tracks to be patterned. After an eight second exposure the chip was developed in 2:3 solution for ten to fifteen seconds. Once the pattern was clear the chip was immediately washed in distilled water to stop further development and then dried with an airgun. If the tracks were not fully resolved then a few seconds of additional developing was used in an attempt to resolve them. If the tracks were overdeveloped then the resist was stripped off with acetone, either using an airbrush or an ultrasound bath for a few minutes, and the lithography process repeated.

The initial device pattern could be formed using a negative mask to give a negative pattern on the substrate. The film was deposited on this substrate and, after deposition, the chip was placed in acetone in an ultrasonic bath. Pulsed ultrasound shook the metal deposited on the photoresist free of the chip as the photoresist dissolved. If the substrate-film adhesion was poor, the whole film could de-adhere from the chip. This process had the advantage of simplicity but the edges of the device tended to be rough due to a combination of the lift-off processing (the positive resist route was used so the film was continuous) and the difficulty in determining when developing was complete, given a transparent substrate and a nearly transparent photoresist. The removal of the edge bead also gave a ring of metal around the devices which had to be removed with a diamond stylus if it shorted the contact pads. If a reflective substrate was used, the development of the photoresist can be observed in the change of the interference fringes caused by the phase difference in the light reflected from the chip/photoresist and photoresist/developer interfaces. If the negative photoresist process was used then the resist profile causes discontinuities in the deposited film and so a cleaner lift off. However the process involves more steps and risked reduction in the width of narrow tracks due to the resist profile, occasionally to the point where these tracks did not exist.

The device can also be fabricated after the film has been deposited. A positive pattern was created in photoresist deposited on the film and the excess metal film was then removed by ion milling by a broad beam argon ion milling system, in the 'New OAR' system shown in figure 4·6. The ion beam was generated by a Kaufmann ion source, preventing damage to the chip by the plasma, and the Ar^+ ions are accelerated to 50 keV. A few percent of oxygen was included in the argon gas as this encourages the initial stages of milling. The ion beam then sputters away the surface of the chip. This is a purely physical process, the rate at which surface particles are lost depends upon the momentum transfer, which in turn depends upon the mass of the surface particle compared to the Ar^+ ion, and the bonding at the surface. The carbon based photoresist should mill away more slowly than the film and so, for film thicknesses less than a micron, the film was milled through before the protective photoresist layer was milled away. The remaining photoresist was then cleaned away with acetone in an ultrasonic bath. This process improved the definition at the edges of the device pattern but it required an additional processing step and the ion milling heated the sample and may have caused additional interfacial diffusion within the heterostructure. The device structure could then be modified using a focused ion beam instrument (FIB) and reactive ion etching (RIE). The 'New OAR' also had the capability to deposit aluminium, gold, silver and superconducting niobium by means of magnetron sputtering.

Modifying the Device Pattern

The focused ion beam instrument (FIB) has become a valuable tool for microelectronics fabrication, combining in-situ high resolution imaging and the ability to modify fine features on a sample. Huge commercial effort has been saved in the

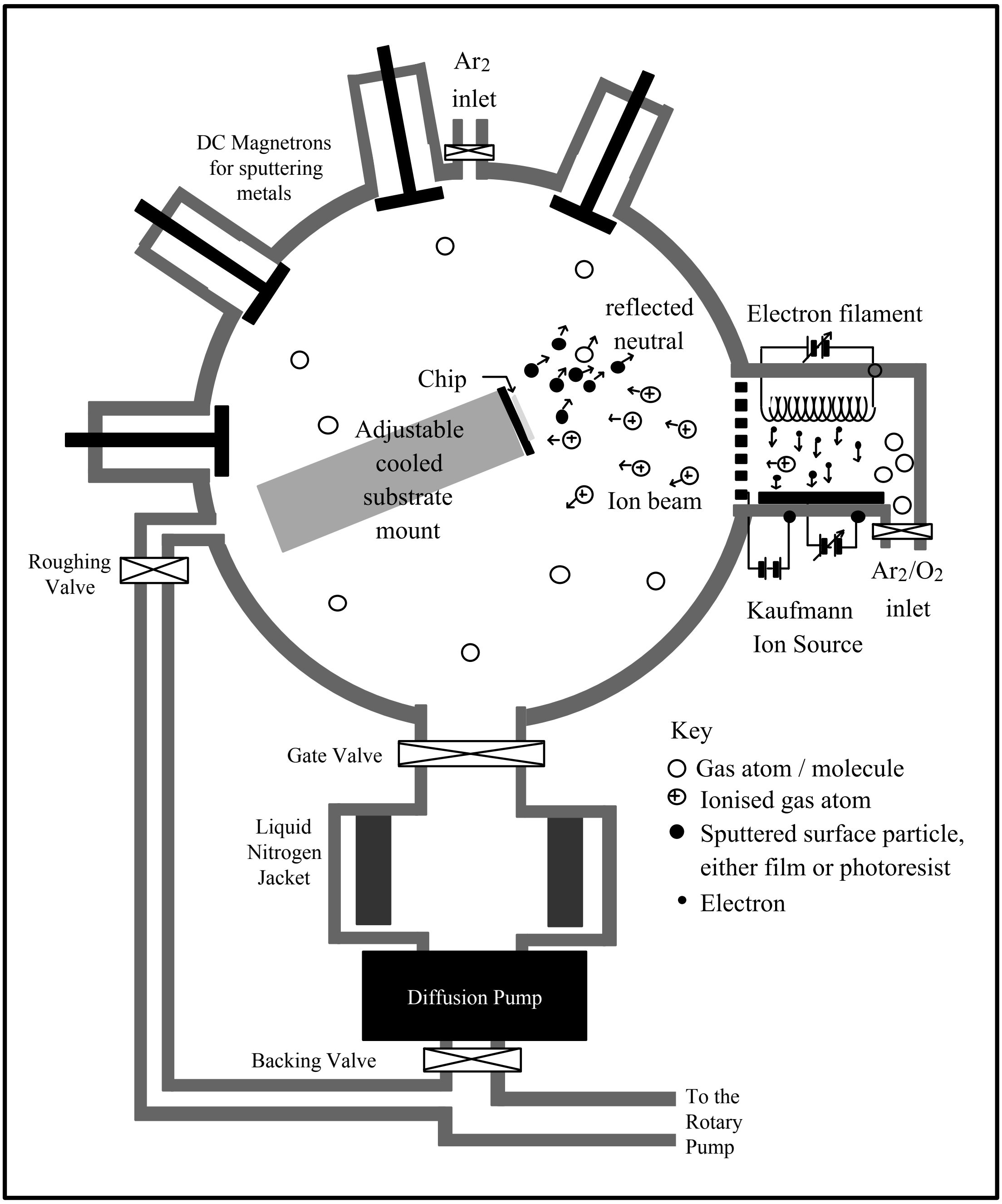

Figure 4·6 Schematic of the New OAR vacuum system, containing four DC magnetrons to deposit metals and a Kaufmann ion source that produced an ion beam that will ablate the surface of the chip.

semiconductor industry through rapid inspection and modification of the faulty circuits that arise from manufacturing flaws. FIB instruments have been used to prepare samples for use in transmission electron microscopy, fabricate microsurgery tools and coupled arrays of Josephson junctions [Altmann 1999, Vasile 1999, Moseley 2000]. A brief description of the use and limitations of a FIB was given

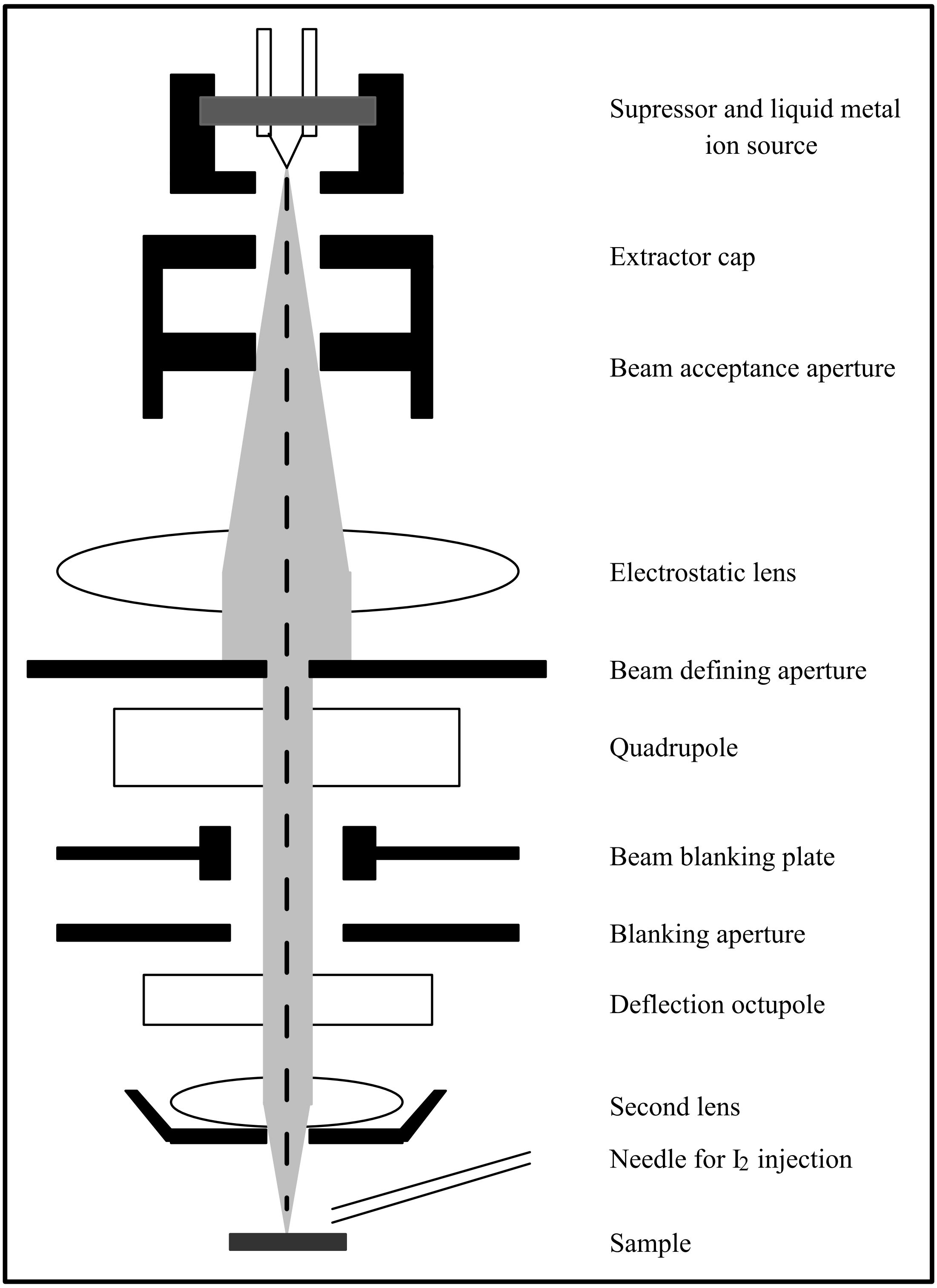

Figure 4·7 Schematic of the main column of the focused ion beam (FIB) system. The vacuum system, power supply and electronics are not shown.

below, a detailed description of the theory and operation of a FIB can be found elsewhere [Young 1993, FEI 1996].

The FIB produces a beam of gallium ions that are focused on the sample, the focusing column is shown schematically in figure 4·7. The column must be under a high vacuum (below 7.5×10^{-5} Pa) to prevent the distortion of the beam by atmospheric gas molecules. A strong electric field was applied to the liquid gallium at the top of the column extracting the positively charged ions, feedback was used to maintain this current at 2.2 μA. The ions were then focused into a beam and a point on the surface of the sample by electrostatic lenses. A steering quadrupole and an octupole stigmator/deflector allowed the beam to be traversed over the sample (though it can also be moved physically) and helped to correct any focusing aberration. The beam passed through a small aperture into the sample chamber, which was at a base pressure of less than 5×10^{-4} Pa, and the ions milled away the surface of the sample, in effect a localised version of the Ar^{+} milling in the 'New OAR' described above. The secondary electrons and ions produced by the milling process are collected, as in a scanning electron microscope, and used to image the surface of the sample as the ion beam was scanned across the surface. Care was taken as the ion beam milled away some of the surface atoms even while being used for imaging. The ion beam could be deflected into a Faraday cup, allowing the beam current to be measured in addition to protecting the sample.

The diameter of the beam on the surface of the sample depended upon the beam voltage, the beam current (effectively a measure of the rate at which ions strike the surface) and the working distance. The column was operated at 30 kV and the working distance could be varied between 15 and 75 mm depending upon the sample and the holder it was mounted on. The beam current was determined by the size of the variable aperture and could be varied automatically between 1 and 1,000 pA, though in this work an 11 pA beam was used. The chromatic aberration in the ion beam, caused by the spread in the ion energies of approximately 5 eV, caused the beam to spread with increasing aperture size so there was a compromise between the milling rate and the definition of the milled region. The milling rate can be enhanced by the injection of iodine gas into the sample chamber as the iodine reacts with the sputtered particles, preventing deposition back onto the sample surface, providing a degree of chemical selectivity and improving the aspect ratio of the cut. The aspect ratio is defined as the ratio of the depth of the cut to its width, a deeper cut would wider at the surface if the aspect ratio is constant. A high aspect ratio means a small width for the depth. In this work the cut width was approximately 20 nm.

The material properties of the sample are also important. Just as with Ar^+ ion milling atoms with a mass similar to that of the milling ion and weak bonds will have a higher sputtering rate. Aluminium was often used as an etch stop, for the same reason it is used as shielding in sputter deposition systems – the milling rate is very low compared to that of other metals. The stray field from a ferromagnetic material will distort both the ion beam and the secondary electrons used to image the sample surface. This magnetic contrast made focusing difficult and, combined with the beam distortion, the width of the cut in a ferromagnet tends to be larger than in a non-magnetic material. The ion beam can also alter the properties of the remaining material in the sample. Some proportion of the gallium in the ion beam was implanted into the surface of the sample, the depth depending upon the atomic mass and structure of the material though normally approximately 10 nm. There was also a degree of lateral spread, though this was smaller, and so a few nanometers into the wall of a cut was also contaminated. These additional impurity atoms reduce the order parameter and so the transition temperature of a superconductor. The ion beam also locally heated the sample and could, for example, locally modify the magnetisation of a ferromagnetic film.

In this work the FIB was used in two ways, see Chapter 6 for a full discussion. Open boxes were cut into the sides of the track in order to create a local constriction in the track. The open boxes consisted of four straight lines giving the perimeter of a rectangle which was sufficient to prevent current flow without significantly altering the magnetic structure of the cobalt layer, see figure 6·13. The magnetic flux across the cut spreads slightly above and below the plane of the cobalt layer but, as the width of the cut was of the same order of magnitude as the thickness of the cobalt layer, this was only a very minor effect. The superconducting niobium exceeded its current carrying capacity in the local constriction, so the measured critical current was the critical current of the constriction. Thus by altering the length and separation of the isolation cuts local effects could be determined. The FIB was also used to thin the superconducting layer without changing the width of the track. As discussed above the top few nanometres of the niobium are then contaminated with gallium. To avoid this reactive ion etching could be used on a Nb/Al/Nb/Al structure. The top

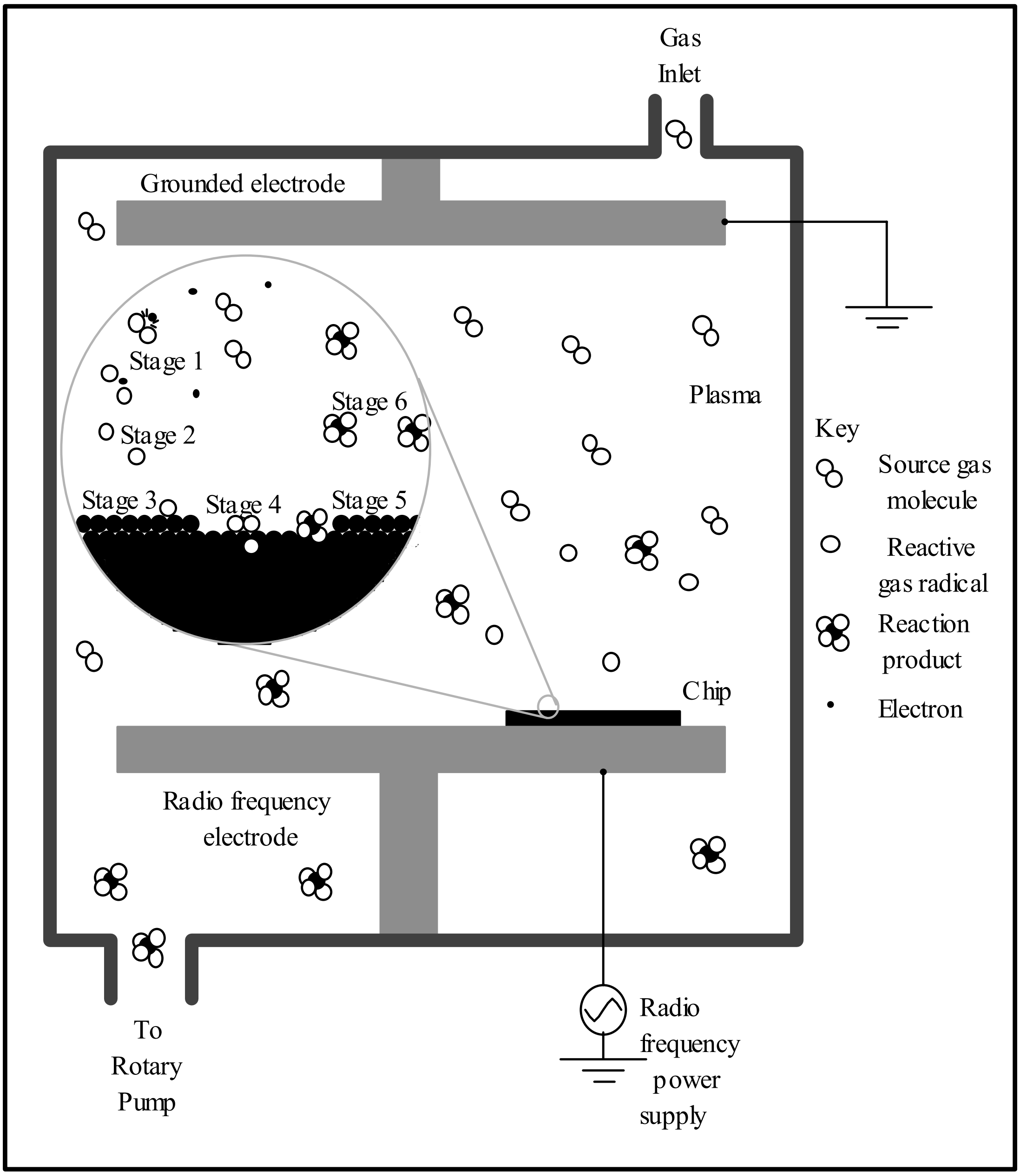

Figure 4·8 Schematic of the reactive ion etching (RIE) system and inset, the etching process.

aluminium layer was removed with the focused ion beam in the required areas and the chip was then placed in the reactive ion etching system (RIE), shown in figure 4·8. The RIE provides a chemically selective anisotropic etch, removing the exposed niobium but not removing any aluminium. Reactive radical species are formed in the plasma, stage 1, and diffuse towards the chip, stage 2. The radicals are adsorbed onto the surface, stage 3, where they react with surface atoms, stage 4. The product species then desorb from the surface, stage 5, and diffuse into the gas, stage 6. Initially oxygen plasma was used to remove any organic material left on the surface.

The niobium forms niobium chloride in the $SiCl_4$ plasma and a CF_4 plasma was used to mop-up any remaining chloride radicals and prevent the formation of threads of niobium chloride running through the film, known as niobium worm. The film was quenched in water and examined under the microscope. The smooth aluminium layer should be clearly visible and if not the etch can be repeated.

Gold can be sputter deposited onto the contact pads after the device has been cleaned and patterned. A chip carrier with copper tracks linked to a standard male 'D' electrical connector was used to connect the chip to the electrical measurement equipment. The device was linked to the chip carrier by aluminium wire-bonds, which are ultrasonically welded to the contact pads and the copper tracks on the carrier. Metallic devices generally do not require gold deposited, though if the substrate-film adhesion was poor then gold can be useful.

X-Ray Analysis of the Unpatterned Films

Analysis of the X-ray diffraction data from the heterostructures can give information on the texture and crystallite size of the metallic films. The texture of the film can be determined by comparing the intensity of the diffraction peaks given by the sample with the intensity obtained from a standard sample. The lattice planes giving peaks with increased intensity are more strongly aligned with the X-rays in all the crystallites rather than being randomly aligned.

There are many contributions to the width of the X-ray diffraction peak [Peiser 1955 Chapter 17]. The experimental broadening of the diffraction peak can be derived from the finite size of the X-ray source, the collimating system and specimen, which gives an angular spread in the X-ray beam striking the sample. There will also be broadening due to the energy spread in the incident X-ray beam. Equally the measuring device has a finite size, depending upon the compromise between the measurement time and the peak sharpness. The broadening in the X-ray diffraction peak intrinsic to the sample itself was due to the crystallite size and any stress within the film.

In a perfect crystal a diffraction peak only occurs when the Bragg condition, equation 4·2, is met as this is the only case where the diffracted waves interfere constructively. If the crystal has a finite size then a small deviation from the Bragg condition will only cause the scattered waves to be slightly out of phase and so they will not cancel out completely. The effect of a small deviation from the Bragg condition can be determined using calculus to give Von Laue's expression for the integral breadth of the diffraction peak, equation 4·3.

$$\lambda = 2d\sin\theta \tag{4·2}$$

$$B = \frac{K\lambda}{t\cos\theta} + b \tag{4·3}$$

where: λ is the wavelength of the X-rays.

d is the separation of the lattice plains.

θ is the angle between the incident X-ray beam and the diffracted beam.

B is the measured breadth of the diffraction peak.

K is the Scherrer constant.

t is the linear dimension of the crystallite.

b represents the instrumental broadening.

The Scherrer constant depends upon the exact shape of the crystallites and is usually taken as 1.08. This value gives an error less than 8%, usually smaller than the other contributions to the error.

Stress in the polycrystalline film bends, shears, stretches or compresses the lattice planes, changing the lattice spacing in the crystallites. It is possible to distinguish between the crystallite size and the strain in the film, given enough diffraction peaks, due to the different angular dependence of the two effects. A plot of $\beta\cos\theta$ against $\frac{\sin\theta}{E_{hkl}}$, where $\beta = \frac{t}{K}$ and E_{hkl} is the Young's modulus for the [hkl] direction, will give a straight line with the intercept giving the effect of crystallite size and the slope giving the isotropic strain. The instrumental broadening can be obtained from a measurement of a sample of the material with large, stress free crystallites. In the absence of data from multiple peaks it was not possible to separate the effect of crystallite size and strain but it was still possible to compare peaks to look for systematic changes. After subtracting instrumental broadening, an estimate for the minimum crystallite size was obtained by assuming there was no stress in the film and using equation 4·3. It was possible to estimate the width of the peak in two ways, either by determining the full width of the peak at half the maximum intensity of the peak (FWHM), after subtracting the background intensity, or by determining the integral breadth (IB). The integral breadth was determined by calculating the area of the peak and dividing it by the peak height. Both methods have their advantages and should give the same answer.

The crystallite size could also be approximated using electrical measurements. The mean free path of electrons in a metal is limited to the mean spacing of defects in the film, which can be assumed to be the crystallite size if this is smaller than the film thickness. The resistivity of a metal is due to the linear combination of the resistivity due to phonon scattering ($\rho_{thermal}$) and that due to scattering from defects, impurities and surfaces, the residual resistivity ($\rho_{residual}$). The electronic mean free path gives the distance between electron scattering events and so is inversely proportional to the residual resistivity, which can be determined from the residual resistance ratio (RRR):

$$\begin{aligned} RRR &= \frac{R_{300\mathrm{K}}}{R_{T\to 0}} = \frac{\rho_{thermal}(300\mathrm{K}) + \rho_{residual}}{\rho_{residual}} \\ \Rightarrow \rho_{residual} &= \frac{\rho_{bulk}(300\mathrm{K}) - RRR.\rho_{bulk}(T\to 0)}{RRR-1} \end{aligned} \tag{4·5}$$

The phonon scattering was determined using the bulk resistivity (ρ_b) as the residual resistivity can be assumed to be the minimum possible. This also reduces any error in the calculation as it removes the cumulative errors from the cross-sectional area and length of the track. The resistivity-mean free path product is given by:

$$\rho\, l = \frac{12\pi^3\hbar}{e^2 S_F} \tag{4·6}$$

where: S_F is the area of the Fermi surface.
l is the electronic mean free path.
e is the electronic charge.

As the area of the Fermi surface was a material property the resistivity-mean free path product was expected to be a constant for a metal, independent of the extrinsic defect structure. Combining equations 4·5 and 4·6 gives the mean free path and so an estimate for the crystallite size, assuming the crystallites are smaller than the film thickness.

Magnetic Properties of the Cobalt Layer

The magnetic hysteresis loop of the cobalt layer was determined using a vibrating sample magnetometer (VSM) at room temperature and a superconducting quantum interference device (SQUID) magnetometer at cryogenic temperatures. Both devices measure the distortion in the applied magnetic field caused by the ferromagnetic material and, by comparing this with the distortion produced by a known calibration sample, determine the magnetisation-volume product of the ferromagnet at that field. The VSM, shown schematically in figure 4·9, measured the voltage signals induced in a pair of sensor coils as the sample vibrated past the measurement coils. A lock-in amplifier was used as it only amplifies the component of the signal in phase with the vibration of the sample and the difference in the signal from the coils was used as it was independent of any external magnetic field. The SQUID magnetometer measured the voltage signal caused by the flux in the SQUID as the sample was swept from below to above it. The SQUID magnetometer used a continuous flow cryostat to cool the sample over a range down to liquid helium temperatures but the sample space and method of mounting the sample limited the measurement configuration to that where the magnetic field was parallel to the magnetic film.

The domain structure of the ferromagnetic layer could be imaged using Lorentz microscopy, a variant of transmission electron microscopy (TEM). Conventional

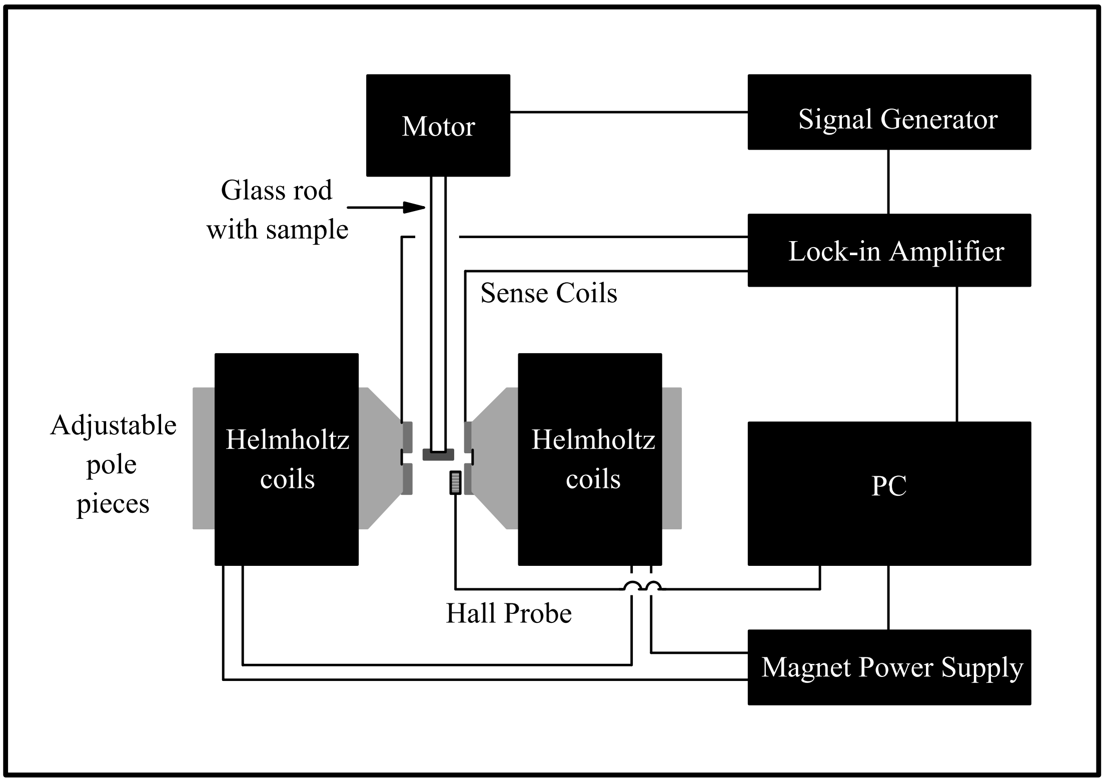

Figure 4·9 Schematic of a vibrating sample magnetometer (VSM) used to obtain room temperature magnetic hysteresis loops.

TEM is similar to X-ray microscopy in that the diffraction pattern from the atoms in the sample was measured, however in TEM a beam of high energy electrons is diffracted rather than high energy photons. The very short wavelength of the electrons and the very thin films used in TEM allows many diffraction maxima to be sampled at the same time and so the detail of the film can be imaged. Unfortunately a very thin film must be used as the exponential decay length of electrons in a material was on the order of a few tens of nanometres. While this thickness can be achieved by thinning samples with a FIB in this work the thin film was deposited on a rock salt substrate which was then dissolved away. Lorentz microscopy exploits the fact that the magnetic field produced by the exchange field within a ferromagnet produces a Lorentz force on the electron beam. While this has no effect on the focused TEM

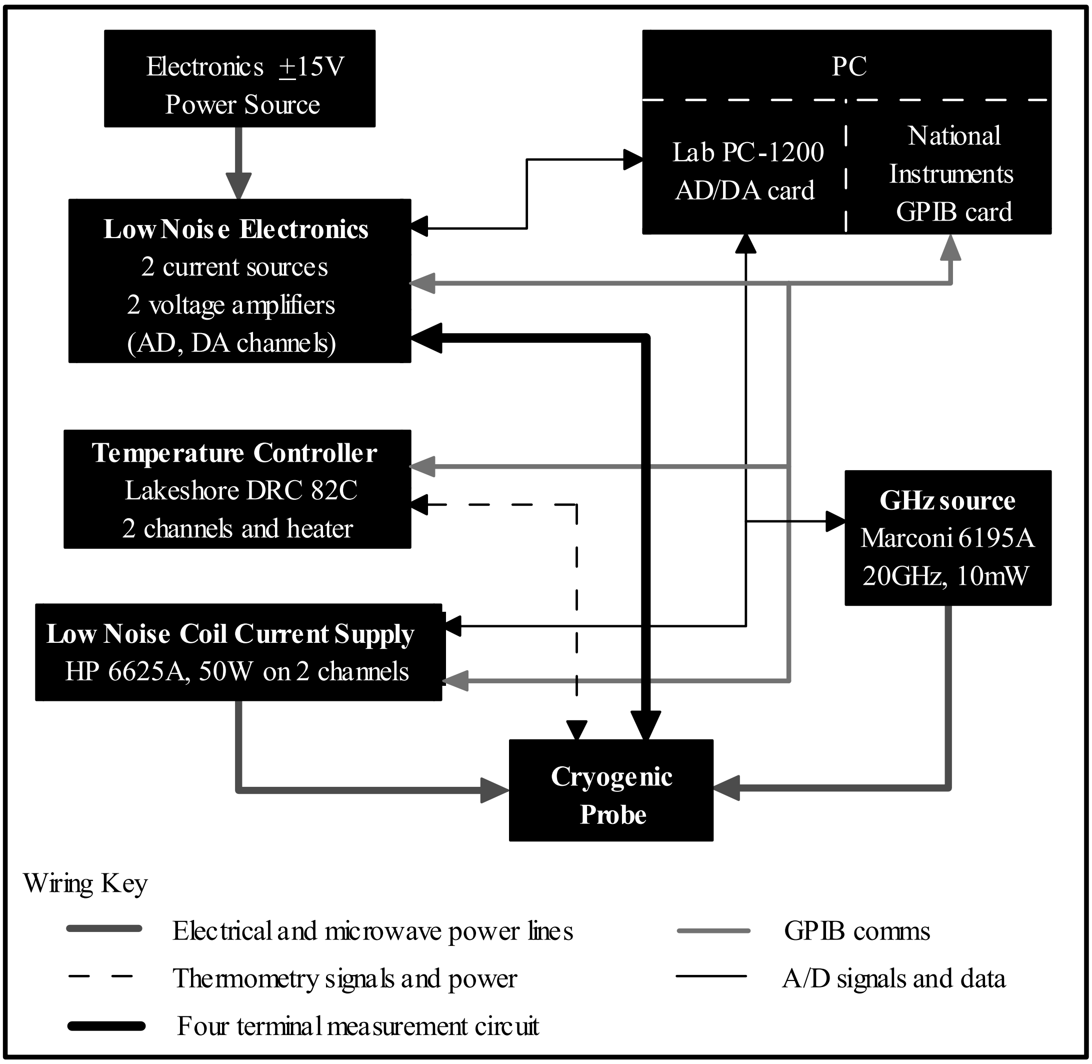

Figure 4·10 Schematic of the devices rig used to measure the electronic properties of the devices in a range of conditions, including varying temperature, magnetic field, and microwave radiation.

image shifting the image slightly out of focus allowed the domain walls, where the direction of the exchange field was rapidly changing, to be imaged. This allowed the plane of the magnetisation and the domain size to be determined. Unfortunately a patterned film was too fragile to mount, even if a sample deposited on rock salt could be successfully patterned, and so only the properties of a continuous film can be determined.

Electrical Properties of the Heterostructure Device

The electrical properties of the devices were measured using a cryogenic dip probe allowing measurements up to 50 mA and 15 V over a temperature range from 300 to 4.2 K, magnetic fields between ±470 Oe in liquid helium and the application of microwave radiation. The devices rig, shown schematically in figure 4·10, was designed and constructed by Dr. W. Booji and Dr. G. Burnell. The rig uses a LabVIEW™ program written by Dr. Burnell to control the magnet power supply while acquiring and processing the data. The amplitude and frequency of the sinusoidal current source are manually controlled between zero and five in the 1 μA, 10 μA, 100 μA, 1 mA and 10 mA ranges. The voltage amplifications given by the low noise electronics are x1, x10, x100, x1,000 and x10,000 and the current and voltage signal are digitised with a 16 bit card before being converted into a current-voltage data file.

The cryogenic probe, shown in figure 4·11, was built by Dr. W. Booji and was designed to be lowered into a dewar of liquid helium. The chip was bonded to a small chip holder with contacts made using ultrasonically bonded thirty micron diameter aluminium wires. The holder was then plugged into a standard 'D' socket and rested on a copper block. Up to nineteen signal lines were fed up into the room temperature end of the probe before being filtered, a current and voltage path was selected with the matrix board and the signal was sent on to the low noise electronics. The probe contained two pairs of Helmholtz coils, allowing the application of a magnetic field along the axis of the probe (x-coils) and perpendicular to the chip (z-coils). There was also a microwave wave-guide and dipole antenna. A semiconductor thermometer and a 25 W heater are embedded in the copper block. External stray fields were minimised with a high permeability μ-metal shield, which reduced the external field to 320 nT at room temperature.

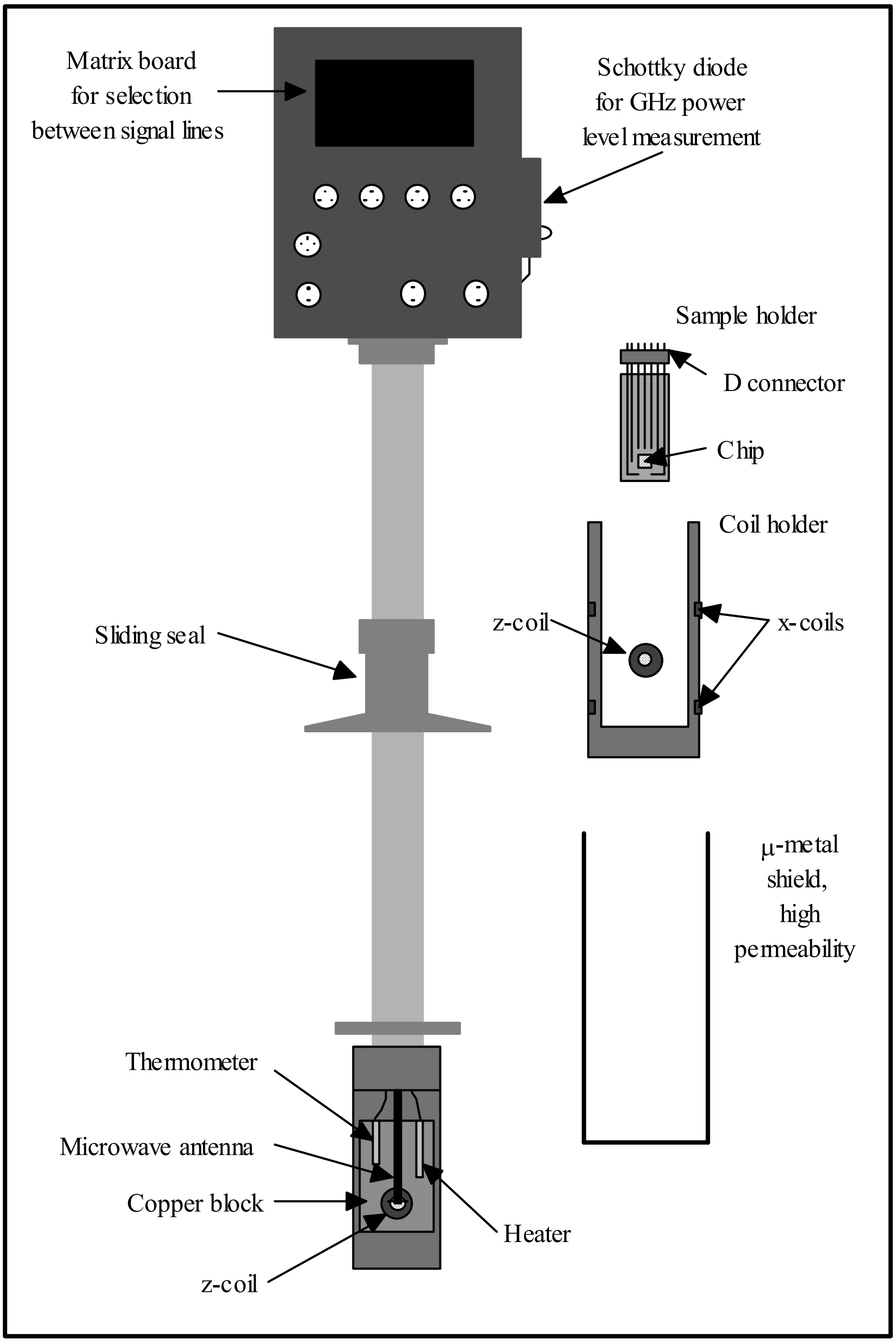

Figure 4·11 Schematic, and partial cut-away, of the cryogenic dip probe.

The critical current was extracted from the current-voltage data files by means of defining a voltage criterion, as shown in figure 4·12. The voltage criterion could be set manually but was more normally calculated as three times the noise in a current-voltage data file in which the applied current was just below the critical current. As there can be no potential difference within a uniform superconductor we can assume that the voltage limit established gives a measure of the noise in the system, normally on the order of 1 μV though this does depend upon the background noise in the electrical supply. The critical current was taken as the current for which the voltage generated by the increasing current, in the appropriate direction, exceeds the criterion. As figure 4·12 shows, it was sometimes possible to extract two critical currents from the current-voltage data, the low voltage criterion and the high voltage criterion. As a convention the positive direction of current flow was parallel to the positive magnetic field and antiparallel to the negative magnetic field. The forward critical current $\left(I_{c_f}\right)$ is the critical current for positive current. The reverse critical current $\left(I_{c_r}\right)$ is the critical current for current flowing in the negative direction. In order to display the data from both current directions I_{c_r} is shown as negative in plots of critical current vs. applied magnetic field, thus in the first and third quadrants the current is parallel to the applied magnetic field.

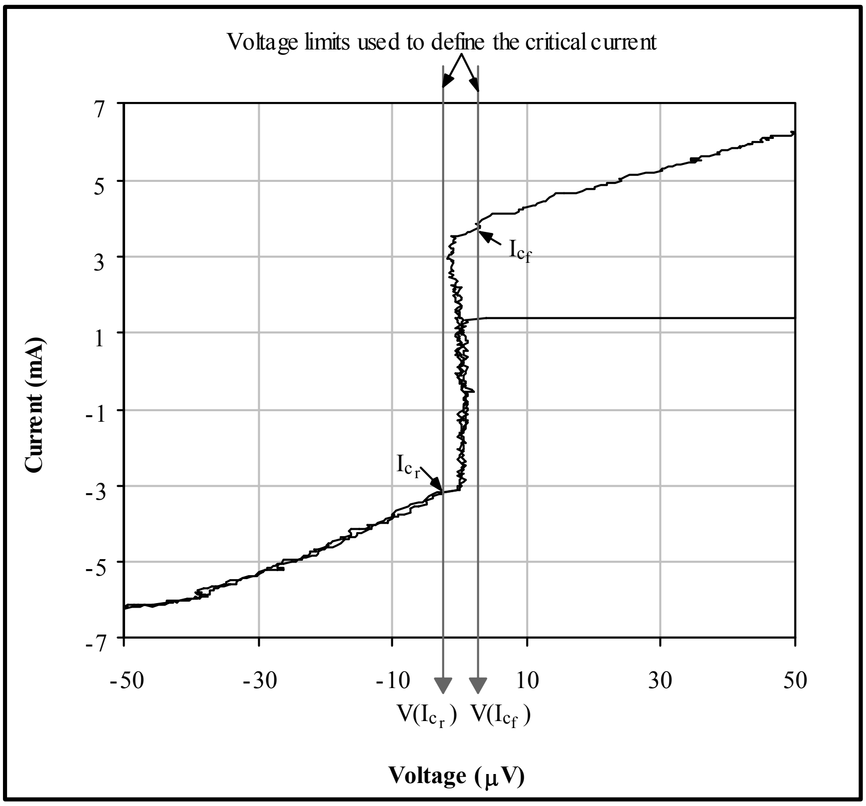

Figure 4·12 Current voltage characteristic for a 2 μm by 10 μm track in a bilayer consisting of (46 ± 16) nm of niobium and (52 ± 16) nm of cobalt. This measurement was made at zero applied field and in liquid helium at 4.2 K.

This method of determining the critical current has the advantage of speed as it takes two measurements with each cycle, however there is the potential for misleading data due to the affects of flux flow resistivity. If some component of the flux vortices within the superconductor is perpendicular to the current flow then it will experience a Lorentz force, perpendicular to both current and field. If this force causes the flux vortex to move then this generates a potential difference which opposes current flow, in effect a resistance even though the material is still superconducting. The motion of the vortices is opposed by pinning forces, potential wells in which the energy of the vortex is reduced due to some defect in the superconductor. These pinning sites are, unless manufactured artificially, randomly spaced and possess random potential. As the vortices are either moving or else no longer exist when the current exceeds the critical current there is no certainty that the pinning potential will be the same for each measurement of the critical current. However a field of 1000Oe, which is equivalent to forty eight flux vortices per square micron, there will only be 1·45 vortices in a one micron wide by thirty nanometre thick track. Given the natural variations in track width and layer thickness there will be a much higher density of possible pinning sites and so the variation in pinning potential will simply add to the noise in the critical current vs. magnetic field data rather than give a systematic difference between the two current directions.

Chapter Five

CHARACTERISATION OF NIOBIUM/COBALT BILAYERS

Error can point the way to truth, while empty-headedness can only lead to more empty-headedness or to a career in politics.

Li Kao, Late Sui Dynasty, c. 600 AD

In this chapter we discuss the effect of applying a magnetic field, parallel to the current flow, on the superconducting properties of niobium/cobalt bilayers. We observe that the critical current as a function of the applied magnetic field is strongly dependent on the magnetic history of the bilayer, as shown in figure 5·1a. Rather than simply observing the expected monotonic decrease in the critical current with increasing applied field we see instead that the critical current tends to a maximum at a small field in the direction opposite to that used to pole the bilayer. For the same value of the applied magnetic field the critical current can differ by almost an order of magnitude, depending on the magnetic history of the track.

The critical current vs. applied magnetic field data for the Nb/Co bilayers can be characterised by a combination of components. Each is discussed separately. An idealised version of each behaviour is shown in figures 5·1b to 5·1e. Figure 5·1b shows the 'double peak' behaviour, an increase in the critical current of several hundred percent that occurs when the magnetisation of the cobalt layer is close to zero, around the coercive field (H_C). The critical current can be suppressed near to H_C, as shown in figure 5·1c. The suppression normally occurs at the same magnetic field as the 'double peak' structure creating structure within the peak, see figure 5·22a for a striking example of this behaviour. There is the expected monotonic suppression of the critical current with applied field, though the maximum critical current may be offset from zero applied field, as shown in figure 5·1d. The critical current can switch between two critical current states, depending upon the magnetic history, as shown in figure 5·1e. The data shown in figure 5·1a does not show this hysteretic switching between two critical current states but does show a mixture of the other three behaviours.

In order to provide a basis of comparison for the niobium/cobalt bilayers, the chapter begins with a discussion of the observed behaviour of niobium films, slightly contaminated with magnetic impurities. A discussion of the structure of the cobalt layer follows because any difference in the behaviour of the niobium films and the bilayers must be the result of the interaction of the superconducting niobium layer with the ferromagnetic cobalt layer. Next the bilayers and the individual components of the critical current vs. magnetic field behaviour shown in figure 5·1 are considered. Reproducibility of the measurement data is discussed before concluding with an analysis of the special case of hysteretic switching, figure 5·1e. Systematic changes, for example, layer thickness or track width are discussed in Chapter 6 and supplementary data is provided in Appendix B.

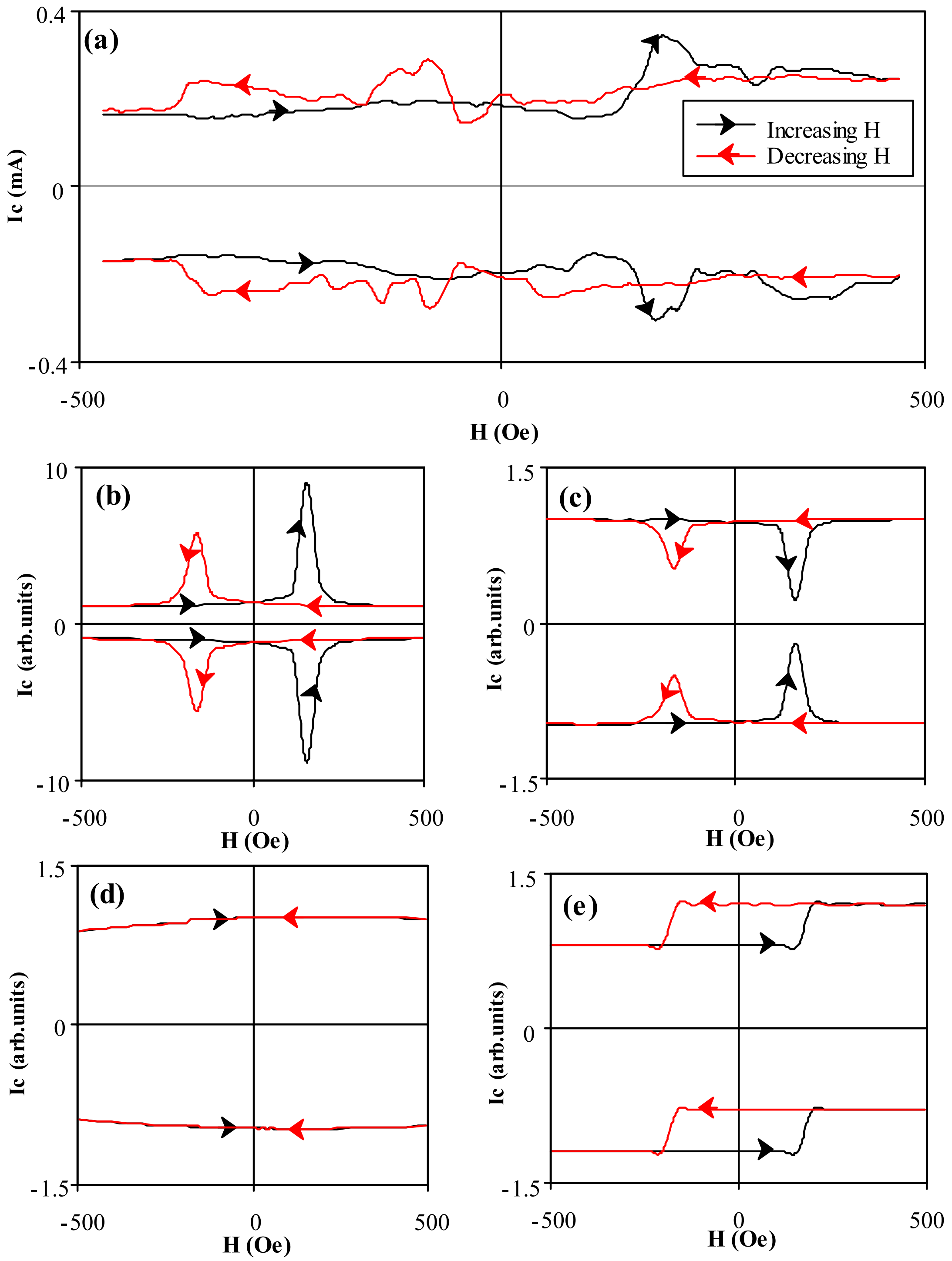

Figure 5·1 (a) Critical current vs. magnetic field measurements for a 10 μm by 1 μm track in a Nb/Co bilayer with (27 ± 9) nm of niobium.

(b) to (e) Freehand sketches of the individual components of the critical current vs. magnetic field behaviour which, when combined, give (a).

Unless otherwise stated the magnetic field is applied parallel to the direction of current flow, in an atmospheric pressure liquid helium bath at 4.2 K and the cobalt layer in the niobium/cobalt bilayers is (52 ± 16) nm thick.

MEASUREMENT OF A NIOBIUM FILM

In order to discuss the behaviour of the niobium/cobalt bilayers it is useful to consider the behaviour of a niobium film measured using the same experimental method. This provides a baseline with which to compare the experimental data from the niobium/cobalt bilayers. In order to ensure that the composition and structure of the niobium films was as similar as possible to the niobium layer in a bilayer the niobium was deposited in the same system, normally during the same deposition run, as the bilayers. Inevitably this means the niobium will be contaminated with magnetic impurities, and this must be taken into account when analysing the data. In chapter 4 we showed, using the Kondo effect, that a copper film was contaminated with approximately 0.05% of ferromagnetic impurities. Although the exact concentration of impurity atoms will vary with the deposition parameters they are sufficiently similar that one can expect a similar concentration of impurities in the niobium film. As discussed in Chapter 3 magnetic impurities reduce the superconducting transition temperature.

Critical current vs. applied field for a niobium film

A magnetic field reduces the transition temperature of a BCS superconductor and so suppresses the critical current, discussed in Chapter 2. The absolute limit for the critical current in any superconductor is given when the self-field generated by the current flow exceeds the critical field for the superconductor, however far lower current densities may require a potential difference. Niobium is a type II superconductor and so, when the local magnetic field exceeds the lower critical field $\left(H_{c_1}\right)$, it contains flux vortices. In a type II superconductor that contains flux vortices the critical current is the current at which flux vortices begin to move. Current flow generates a Lorentz force on the component of the flux vortices perpendicular to the current and the motion of vortices induces a potential difference. If the superconductor contains a volume where the superconducting gap parameter is suppressed compared to the surrounding region (due to a magnetic impurity or void, for example) and if the normal core of the vortex coincides with this place then the energy of the superconductor is lowered. This gives rise to a pinning potential which must be overcome by the combination of the Lorentz energy induced by the current flow and the thermal energy before the vortex will start to move. The pinning potential is limited to the bulk gap parameter – the suppressed superconducting gap parameter can go no lower than zero – which is also a function of temperature and field. Thus, for a type II superconductor containing flux vortices, the critical current is a complex function of the applied field and the temperature.

It is possible to make some generalisations about the change in the critical current in niobium with applied field. At low applied fields the vortices tend to be located on pinning sites. Thus the limiting factor for the critical current will be the flux vortex on the weakest pinning site and a small increase in the magnetic field gives rise to a significant suppression in the critical current. At high magnetic fields the flux vortices are close enough to influence each other and so form a lattice. The lattice of vortices moves as a whole and consequently is limited by the strongest pinning potential. Thus the reduction in the critical current with increasing magnetic field is reduced at higher fields, appearing similar to a logarithmic dependence of the critical current on applied field. As the magnetic field is increased there is an initial rapid decline in the critical current, gradually levelling out until it reaches zero at H_{c_2}. Behaviour similar to this can be seen when the magnetic field is applied perpendicular to the niobium/cobalt bilayer, this is discussed in Chapter 6.

Niobium is an isotropic superconductor, so the superconducting critical field has no dependence on the orientation of the magnetic field relative to the crystallographic axes. However the applied magnetic field is not the same as the local field experienced by the superconducting film due to the shape anisotropy of the sample, as discussed in Chapter 2. Thus the superconducting critical field parallel to the plane of the film $\left(H_{c_{//}}\right)$ is many times larger than the critical field perpendicular to the plane $\left(H_{c_{\perp}}\right)$. When the current is parallel to the magnetic flux there is no Lorentz force on the vortices, the force-free configuration. In the force-free configuration the critical current vs. applied field behaviour is difficult to predict as the system becomes very sensitive to small variations in the orientation of the flux vortex relative to the local current flow. Figure 5·2 shows the critical current vs. applied field data for four niobium tracks that are within at most 10º, and probably within 5º, of the force-free configuration.

The niobium films discussed in this work did not always show the expected monotonic suppression of the critical current with increasing field, though figure 5·2b shows that this behaviour does sometimes occur. Linear extrapolation of this data to

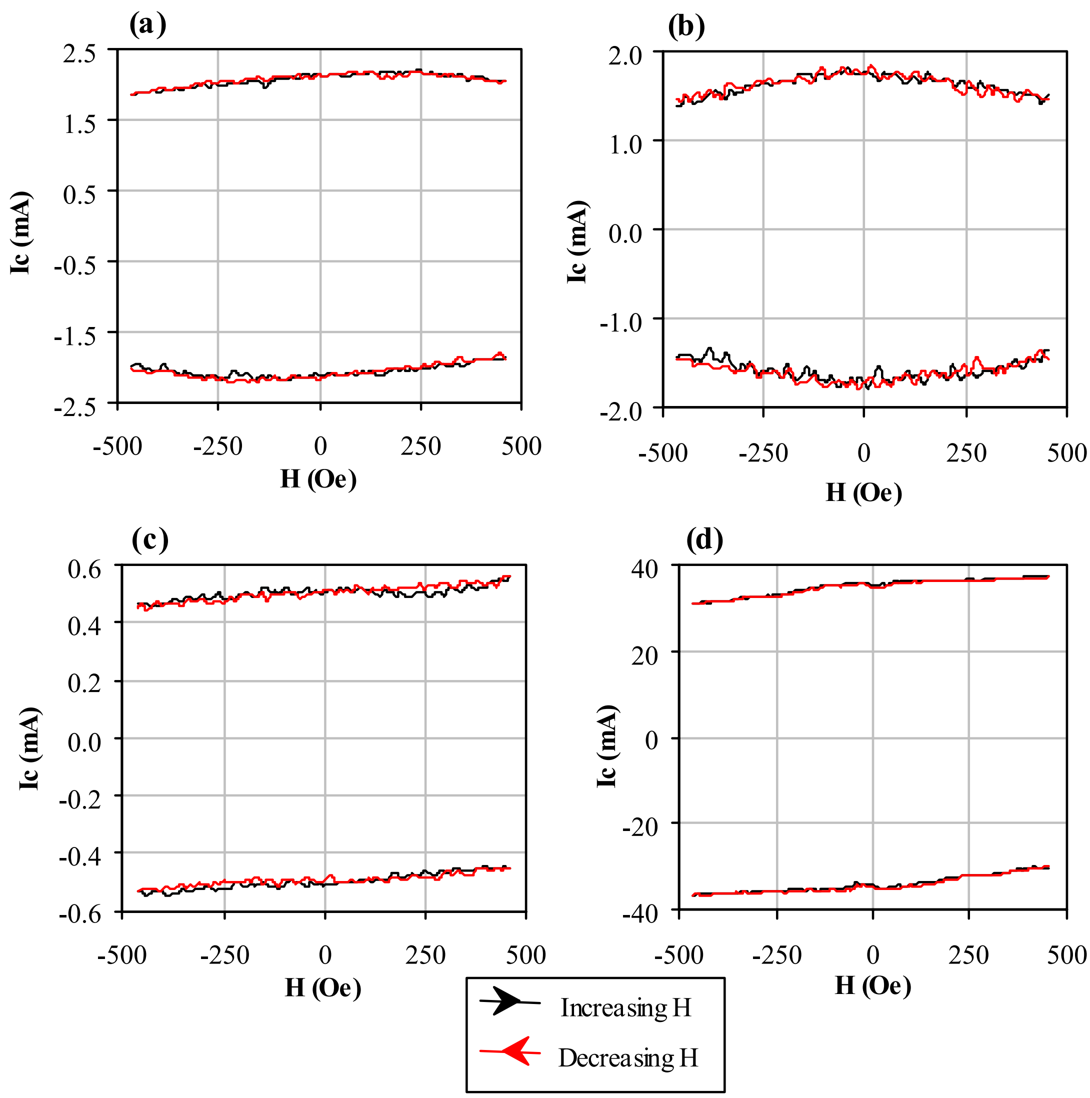

Figure 5·2 (a) to (c) show critical current vs. magnetic field data for three 10 μm by 1 μm tracks in a (18 ± 5) nm thick niobium film at 4.2 K. The film had a T_c of (7.1 ± 0.01) K. All three tracks underwent the same processing.

(d) shows critical current vs. magnetic field data for a 10 μm by 1 μm track in a (87 ± 12) nm thick niobium film at 4.2 K. The film had a T_c of (9.22 ± 0.05) K.

zero critical current gives an upper critical field $\left(H_{c_2}\right)$ at 4.2 K of (2.8 ± 0.1) kOe. Given that the decrease in critical current will be monotonic this is the maximum upper critical field. This value for H_{c_2} can be extrapolated down to the value at absolute zero using the experimental observation that the critical field is proportional to $1-\left(\frac{T}{T_c}\right)^2$, where T_c is the superconducting transition temperature and $\frac{T}{T_c}$ is the reduced temperature. This gives $H_{c_2} = (4.32 \pm 0.17)$ kOe which can be compared with the upper critical field of bulk pure niobium, 4.05 kOe, though anisotropy must also be taken into account [Kaye 1995]. The sample has a transition temperature of 7.1 K compared with the value for bult pure niobium ,9.25 K, which suggests that the niobium contains magnetic impurities. Also this value for H_{c_2} will be less than $H_{c_{//}}$, which in turn will be four thirds of the value for a spherical bulk sample, as it is impossible to perfectly align the track with the magnetic field. There will always be some component of field perpendicular to the film. In these circumstances the angular dependence of the critical field for a very thin film is given by:

$$\left|\frac{H_c(\theta)\sin\theta}{H_{c_\perp}}\right| + \left(\frac{H_c(\theta)\cos\theta}{H_{c_{//}}}\right)^2 = 1 \qquad (5{\cdot}1)$$

The angle between the direction of current flow (θ) and the magnetic field will be no more than 10º at most and probably less that 5º, thus the component of the field perpendicular to the plane of the film will be small. However as $H_{c_\perp}$ is considerably lower than $H_{c_{//}}$ even a small value of θ can give a significant reduction in H_c [Harper 1968].

Self field and asymmetry

Instead of monotonic suppression of the critical current with increasing field we observe that at some magnetic fields the magnitude of the forward critical current $\left(I_{c_f}\right)$ differs in the magnitude from the reverse critical current $\left(I_{c_r}\right)$. As discussed in Chapter 4, the current is parallel to the direction of positive magnetic field for I_{c_f} while they are antiparallel for I_{c_r}, where I_{c_r} is shown as negative in plots of critical current vs. applied magnetic field. Thus the current and magnetic field are parallel in the first and third quadrants of a plot of critical current vs. applied magnetic field and antiparallel in the second and fourth. The total critical current (I_{c_t}) is the sum of I_{c_f} and I_{c_r}. In figure 5·2c we see almost no change in the total critical current but the difference between I_{c_f} and I_{c_r} is proportional to the applied field. Figures 5·2a and 5·2d show behaviour that is intermediate between that shown in figures 5·2b and 5·2c.

There are few phenomena where the orientation of the magnetic field relative to the current, rather than just the magnitude of the component of the magnetic field in the direction of the current, is important. For the niobium film the most probable effect is the interaction between the externally applied magnetic field and the magnetic field generated by the current flowing through the track, shown schematically in figure 5·3. The strength of this self-field can be calculated using the Biot-Savart Law, which gives the magnetic field ($\underline{B}$) produced by a current element:

$$\mathrm{d}\underline{B} = \frac{\mu_0}{4\pi} I \frac{\mathrm{d}\underline{s} \wedge \underline{r}}{r^3} \qquad (5{\cdot}2)$$

where: μ_0 is the permeability of free space.

I is the current flowing through the element.

$\mathrm{d}\underline{s}$ is the small displacement along current path.

$\underline{r}$ links the current vector to the point where the field is measured.

The Biot-Savart Law can be solved for the current flowing through a rectangular

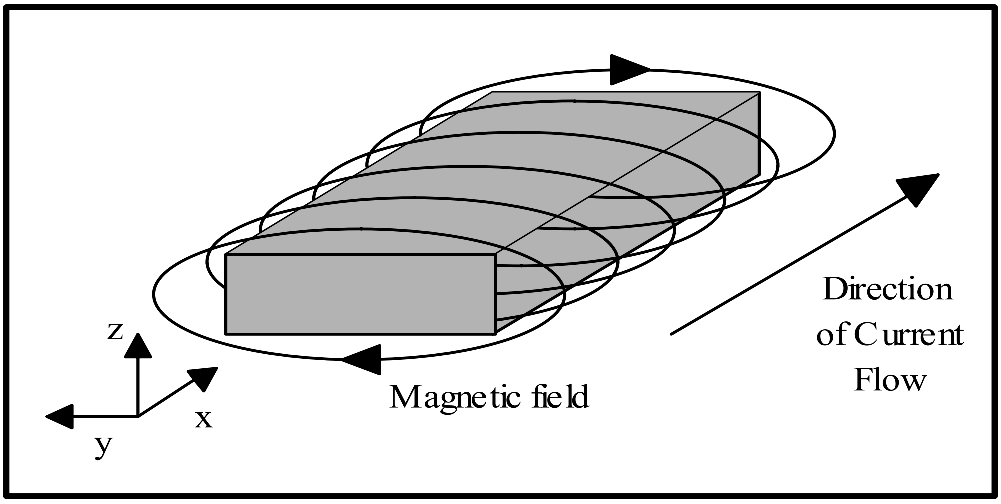

Figure 5·3 Schematic of the magnetic field created by the current flowing through the track. When the bilayer is superconducting the current will only flow through the niobium and the generated field will cut through the cobalt layer. There will also be the external magnetic field.

track. The current flowing through the track in the x-direction is modelled by using the current density and integrating across the cross-sectional area, the y- and z-directions in figure 5·3. The magnetic field generated by each cross-section is then summed along the length of the track. The resulting analytical equation gives real solutions, despite being complex, which can be calculated using a suitable program such as Mathmatica™:

$$\underline{B} = \iiint \frac{\mu_0}{4\pi} i\,\mathrm{d}y\mathrm{d}z \frac{\begin{pmatrix}\mathrm{d}x\\0\\0\end{pmatrix}\wedge\begin{pmatrix}x\\y\\z\end{pmatrix}}{\left(x^2+y^2+z^2\right)^{\frac{3}{2}}} = \iiint \frac{\mu_0}{4\pi} i \begin{pmatrix}0\\-z\\y\end{pmatrix}\left(x^2+y^2+z^2\right)^{-\frac{3}{2}}\mathrm{d}x\mathrm{d}y\mathrm{d}z \quad (5\cdot3)$$

$$\begin{aligned}
\underline{B}_y &= \iiint -\frac{\mu_0 i}{4\pi} z\left(x^2+y^2+z^2\right)^{-\frac{3}{2}}\mathrm{d}x\mathrm{d}y\mathrm{d}z \\
&= \frac{\mu_0 i}{4\pi}\iint\left[\left(x^2+y^2+z^2\right)^{-\frac{1}{2}}\right]_z \mathrm{d}x\mathrm{d}y \\
&= \frac{\mu_0 i}{4\pi}\int\left[\left[\ln\left|y+\sqrt{x^2+y^2+z^2}\right|\right]_z\right]_y \mathrm{d}x \\
&= \frac{\mu_0 i}{4\pi}\left[\left[\left[\begin{gathered} -x + z\arctan\left(\frac{x}{z}\right) \\ + y\ln\left|x+\sqrt{x^2+y^2+z^2}\right| + x\ln\left|y+\sqrt{x^2+y^2+z^2}\right| \\ + \frac{jz}{2}\ln\left(\frac{4j\sqrt{x^2+y^2+z^2}}{2yz\left(x+jz\right)} + \frac{2\left(y^2z+z^3-jxz^2\right)}{y^2z^2\left(x-jx\right)}\right) \\ - \frac{jz}{2}\ln\left(\frac{4j\sqrt{x^2+y^2+z^2}}{2yz\left(x-jz\right)} + \frac{2\left(y^2z+z^3+jxz^2\right)}{y^2z^2\left(x+jx\right)}\right)\end{gathered}\right]_z\right]_y\right]_x
\end{aligned} \quad (5\cdot4)$$

where: i is the current density flowing through the track.

j is the square root of minus one.

$\underline{B}_y$ is the magnetic field in the y-direction.

$[f(x)]_x = f($ upper limit for $x) - f($ lower limit for $x)$.

For a 10 µm by 1 µm by 25 nm niobium track the self-field a nanometer above the centre of the largest face of the track is on the order of ten thousand Oersted per Amp. As shown in figure 5·5 a current of 1 mA gives a self-field of -67 Oe. Using Ampère's law with the contour set at a constant distance of 1 nm from the surface of the conductor gives a self-field of -61 Oe and does not allow for changes in the width of the track.

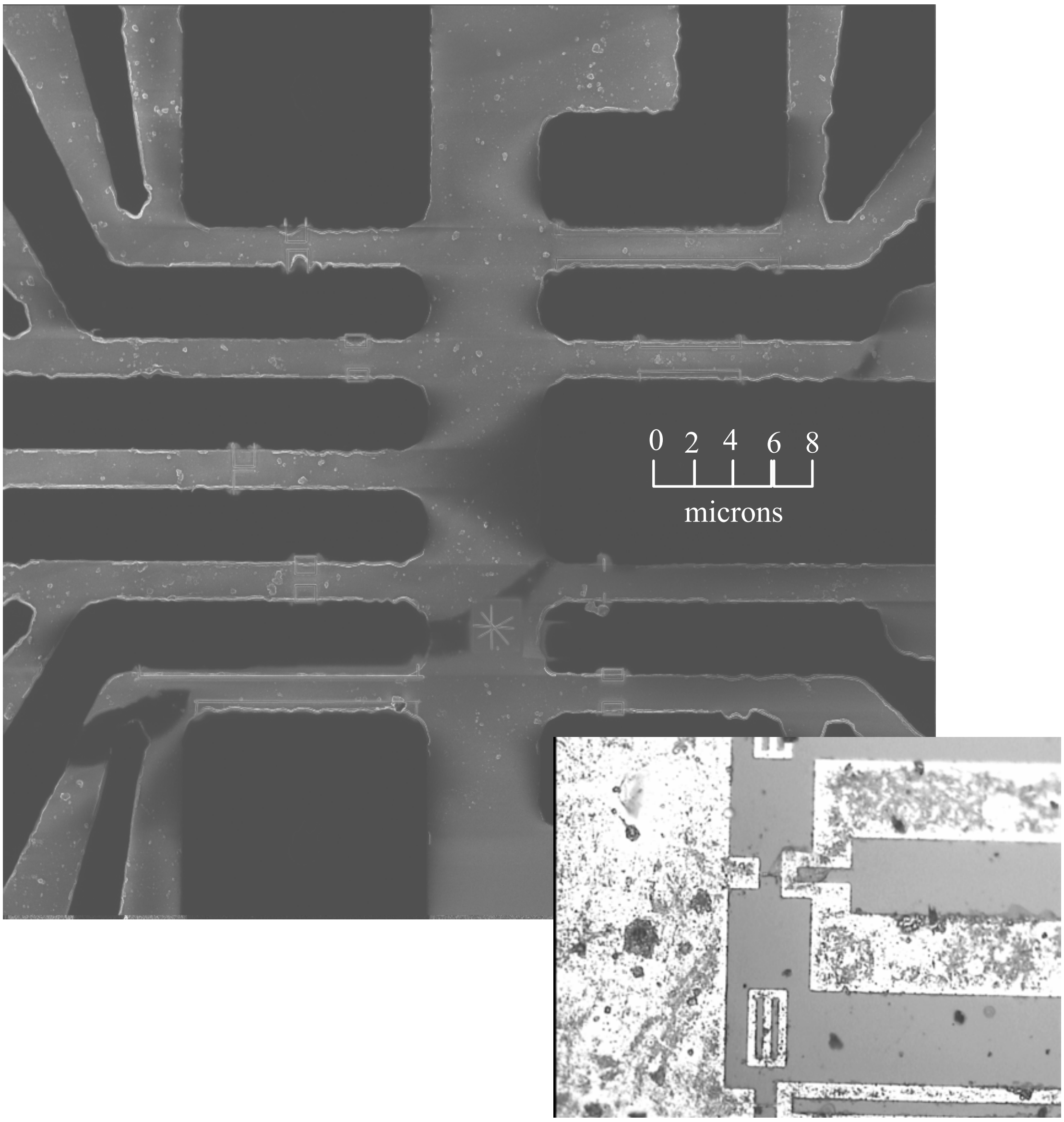

Figure 5·4 FIB image of a niobium/cobalt bilayer with nominally 2 micron wide tracks. Note that many of the dark patches that appear to break the tracks are the result of magnetic contrast. The stray magnetic field from the cobalt layer bends the secondary electrons used to image the surface away from the detector. The track has been patterned with constrictions using the FIB, the effect of patterning is discussed in Chapter 6.

The insert is an optical micrograph of two one micron wide track indicating the patterning for this structure.

The self-field generated by the current flow is symmetrical around the track, as shown in figure 5·3, and so at first could not be the source of the field dependent offset in the critical current as the change in the local magnetic field would also be symmetrical. This fails to take into account the limitations of the processing methods used to create the tracks. There will be some error in the original chrome on fused silica masks, and transferring this pattern into photoresist and then into the bilayer, as discussed in Chapter 4, will add still further errors. Examination of the tracks in the focused ion beam milling system (FIB) shows that the width of the track can vary by several tenths of a micron along the length of the track, see figure 5·4. In general these flaws in the patterning reduce the width of the track so the measured critical current (which is determined by the first region of the track require a potential difference to drive a current) is that of the region where the track is most severely distorted. These

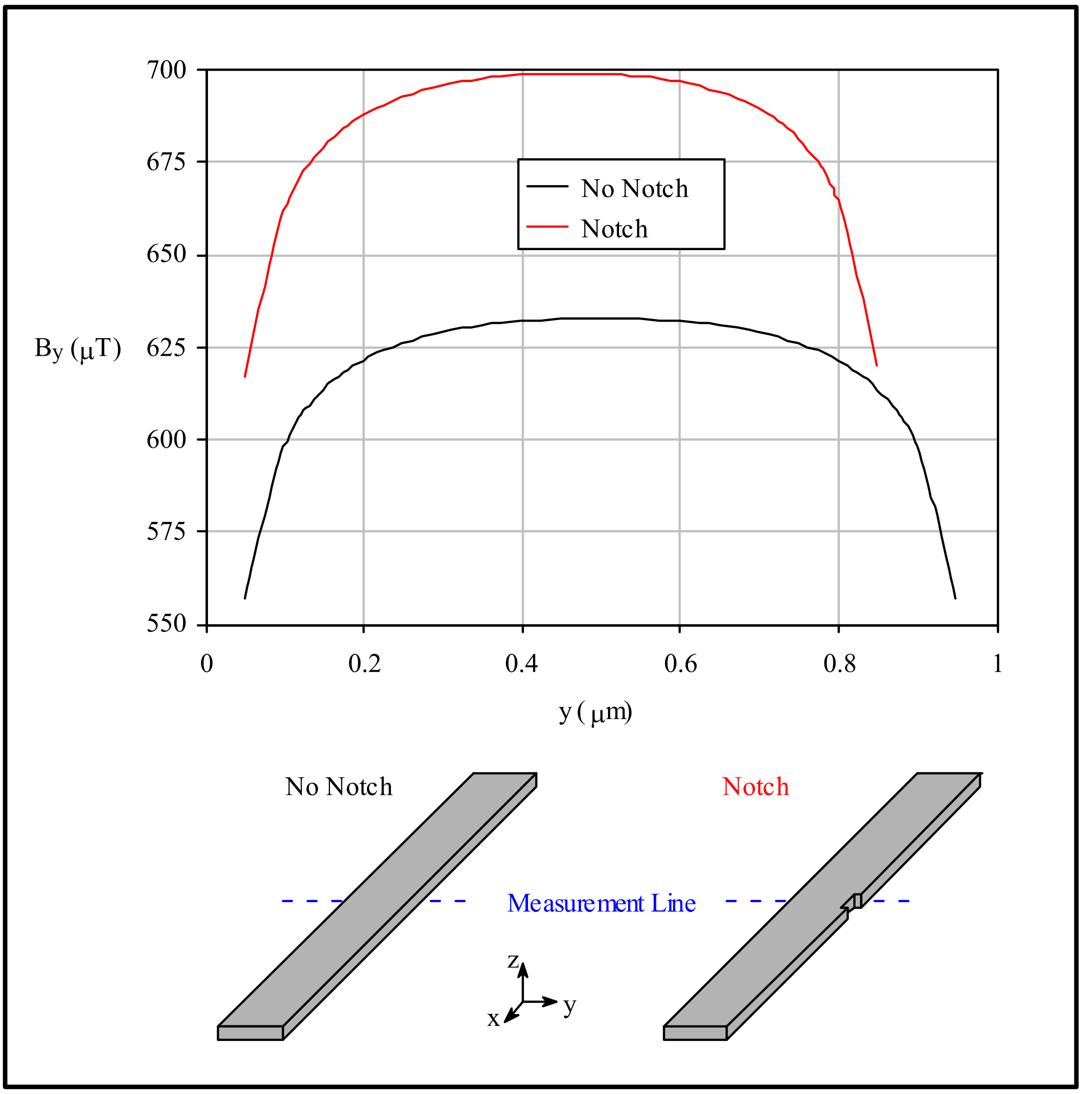

Figure 5·5 Biot-Savart Law calculation for the magnetic field along the central measurement line shown, 1 nm above the upper surface of a 10 μm by 1 μm by 25 nm conductor carrying 1 mA. This is compared with the field above a similar conductor with a 1 μm by 0.1 μm notch in the track.

distortions in the track break the symmetry of the self-field and allow for the field dependent offset in the critical current. As shown in figure 5·5 thinning the track by 10% increases the local field in the y-direction by 11% and will give rise to a self-field in the x-direction as the current flows in the y-direction in order to enter or leave the constriction. Equally, variations in the thickness will give rise to additional self-field in the z-direction. While the local field seems small for the magnitude of the offset in the maximum critical current from zero field, a small local field could have a significant affect on the local pinning of vortices. The local field also accounts for the difference in the magnitude of the offset observed in the three tracks shown in figure 5·2 as the variations in the cross-section of the track will be random. The importance of the geometry of the device can also be seen in other experimental work [Johnson 1995, Arie 1997-I].

Crystallite size

The mean free path of a material gives a measure of the spacing between flaws in the lattice, such as impurity atoms, dislocations or grain boundaries. If the density of impurities is low then the mean free path can be assumed to be the crystallite size, the

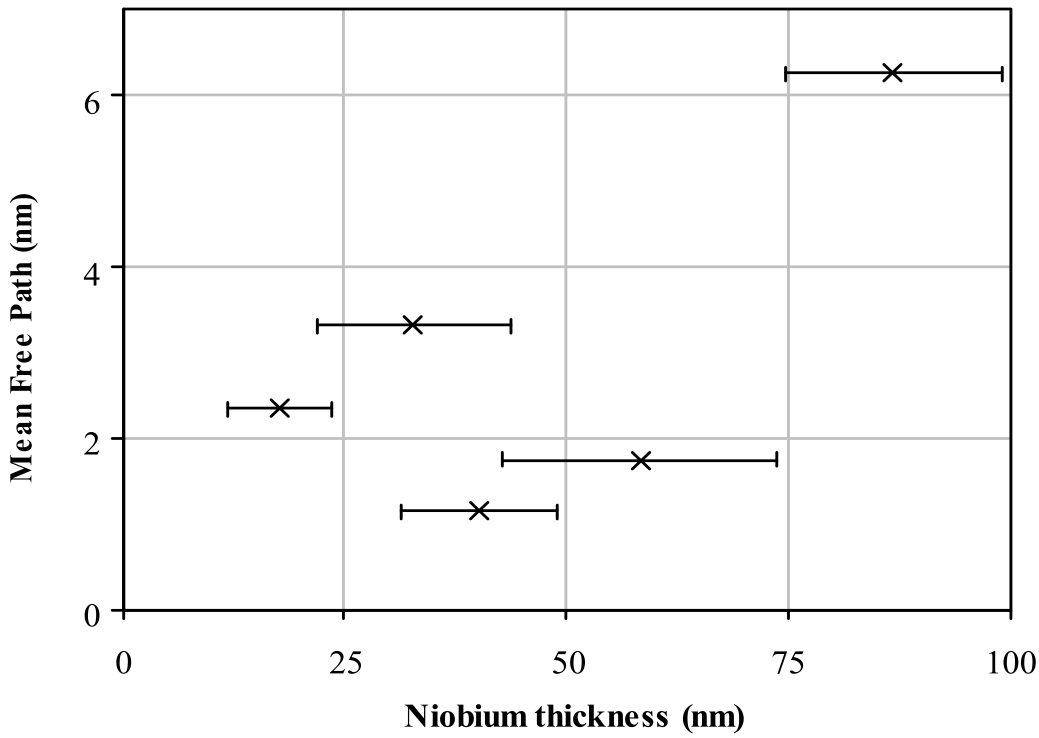

Figure 5·6 Mean free path vs. thickness for various niobium films. The mean free path was calculated from the residual resistance ratio.

mean free path thus provides a minimum crystallite size. In order to calculate the mean free path we have used the analysis given in Chapter 4, taking the mean free path resistivity product to be 460 nΩm.nm and the resistivity of bulk niobium at 300 K to be 139.5 nΩm [Huang 1991, Burnell 1998]. As shown in figure 5·6 the mean free path increases with increasing niobium thickness, reflecting the improving quality of the film. It is, however, unlikely that the crystallites are as small as given by the mean free path. There are magnetic impurities in the niobium, as shown by the Kondo effect in copper discussed in Chapter 4, and it is possible to deposit epitaxial niobium on sapphire at approximately one third the deposition rate used [Burnell 1998].

Magnetic Structure of the Cobalt Layer

Any change in the critical current other than a decreasing critical current with increasing magnetic field must be explained in terms the magnetic structure of the cobalt layer. The magnetisation of the cobalt will reverse at the coercive field and domains will nucleate and change in size as the magnetic field is swept between saturation states. Although cobalt has a strong uniaxial anisotropy it is possible for the domains to extend over many crystallites as the domain wall bends as it moves between crystallites and the magnetisation rotates in the grain boundaries, as shown in figure 5·7. This gives a range of domain sizes and can gives rise to points where two or more domain walls come together. The domain structure of an unpatterned Nb/Co bilayer were imaged using Lorentz microscopy. The cobalt layer showed a web of domain walls that meandered through the film and often merged. The average domain size was on the order of a few microns. Lorentz microscopy also showed that the magnetisation of the cobalt layer lay within the plane of the film, which one would expect given the influence of the shape anisotropy on a growing thin film. This is confirmed by the X-ray diffraction peaks as the (0004) peak has far more intensity than the $(11\bar{2}0)$ peak even though the two would have very similar intensities in bulk cobalt. Thus the cobalt crystallites show preferential c-axis alignment. It should also be noted that the domain structure in a patterned film is more complex than that observed in an 'infinite' film [Craik 1965, Chikazumi 1997]. Even when the cobalt is saturated, domains with opposite magnetisation can be pinned at the discontinuity created by the edge of the track, reducing the stray field and giving rise to 'spike'

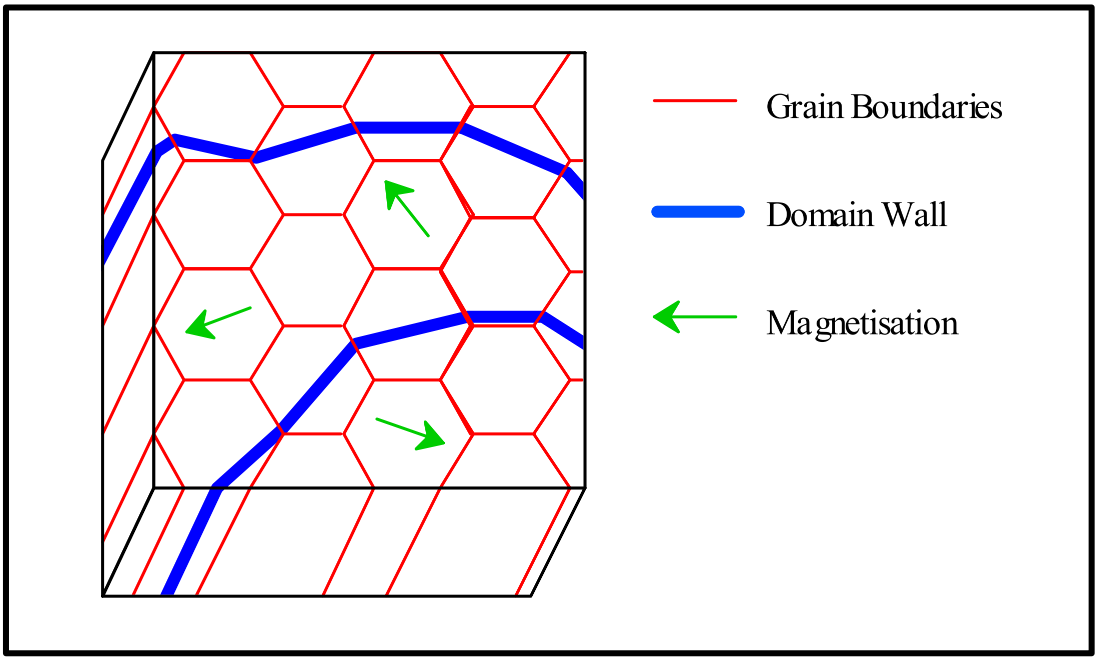

Figure 5·7 Schematic representation of domain walls in polycrystalline cobalt.

domains. Thus the domain walls tend to zig-zag rather than be straight during domain growth when the magnetisation is reversed.

Crystallite size

The X-ray diffraction data can also be used to give the crystallite size by using the peak width, as discussed in chapter 4. We used copper K_α radiation with a wavelength (λ) of 0.154056 nm and assumed that the crystallites in the bulk cobalt sample are sufficiently large, equiaxed and stress-free that the width of the bulk cobalt peak can be taken as instrumental broadening. As the (0004) peak, shown in figure 5·8, is the only peak with sufficient intensity for the width to be determined with any degree of accuracy it is not possible to separate the components of the peak width due to the stress from those due to the crystallite size. We can be certain that there is tensile stress in the cobalt as a sufficiently thick cobalt film deposited on photoresist for lift-off pulls the photoresist away from the sapphire substrate. This is also reflected in the displacement of the (0004) peak compared to that in the bulk cobalt. The tendency of the film to curl up suggests that there is tensile strain in the film. This means that the crystallite sizes given in table 5·1 [page 102] can be taken as the lower limit of the crystallite size. The full width at half maximum gives a crystallite size of (56 ± 4) nm for all three thicknesses of cobalt films. The integral breadth gives a slightly larger crystallite size though this could be due to the slight

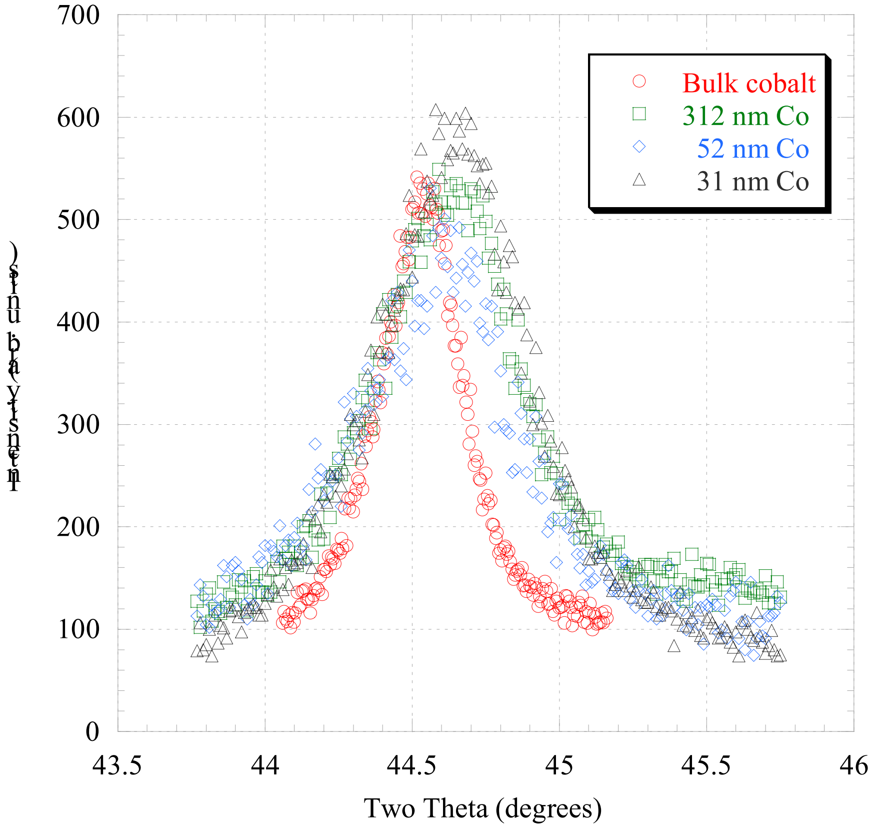

Figure 5·8 (0004) X-ray peak for various thicknesses of cobalt films.

asymmetry of the X-ray diffraction peaks. As, in the case of the thickest cobalt film, this value for the crystallite size is smaller than the film thickness it is likely that this is a true measure of the crystallite size, taking into account that there is a stress term that has not been removed.

	Peak Position (2θ°)	Full Width at Half Maximum (FWHM°)	Crystallite size using FWHM (nm)	Integral Breadth (IB°)	Crystallite size using IB (nm)
Bulk cobalt	44.54	0.30		0.37	
312 nm of Co	44.66	0.54	56 ± 4		
52 nm of Co	44.63	0.53	57 ± 4	0.55	73 ± 5
31 nm of Co	44.66	0.55	54 ± 5		

Table 5·1 (0004) cobalt X ray peak analysis giving the crystallite size for various thicknesses of cobalt films.

The minimum crystallite size can also be determined from the mean free path. The mean free path in a (52 ± 16) nm thick cobalt film is (7.88 ± 0.02) nm, given the residual resistance ratio of (1.794 ± 0.005). This calculation takes the resistivity of cobalt at 300K to be 66 nΩm and the mean free path resistivity product to be the same as that for copper, 660 nΩm.nm [Kaye 1995]. This assumption can be made as the area of the Fermi surface in both metals is very similar. Again the mean free path is very short, almost an order of magnitude smaller than that given by the width of the X-ray diffraction peak, which can be attributed to the impurities in the system. As the mean free path in both the cobalt and the niobium layers are similar, we can assume that the magnetic impurities are due to iron sputtered from the stainless steel chamber and so that the impurity levels are actually higher than those measured by the Kondo effect, as discussed in Chapter 4. The stainless steel will also be a source of carbon and chromium impurities not detected by the Kondo effect.

THE 'DOUBLE PEAK' STRUCTURE

The most interesting behaviour shown by niobium/cobalt bilayers is the 'double peak' structure in the critical current vs. applied field data, as illustrated in figure 5·1b. After saturating the cobalt layer the critical current of the bilayer shows a maximum at a small magnetic field applied antiparallel to the saturating field rather than at zero field. The critical current shows a hysteretic dependence on the magnetic field history of the bilayer. In Chapter 6 we see that the increase in the critical current is a reflection of an increase in the superconducting critical temperature, though there are other possible sources for an increase in critical current. This behaviour is of interest as it offers the possibility of switching the bilayer between the superconducting and normal states with the application of a few hundred Oersted of magnetic field. This effect could be used to manufacture a uniaxial low field superconducting switch or transistor. There are several effects that, given the right conditions, could give rise to the 'double peak' structure in the critical current vs. applied magnetic field response of niobium/cobalt bilayers. The most probable are the motion of flux vortices, the stray field from the cobalt layer and an imbalance in the energy of the spin populations in the niobium created by the exchange interaction in the adjacent cobalt layer.

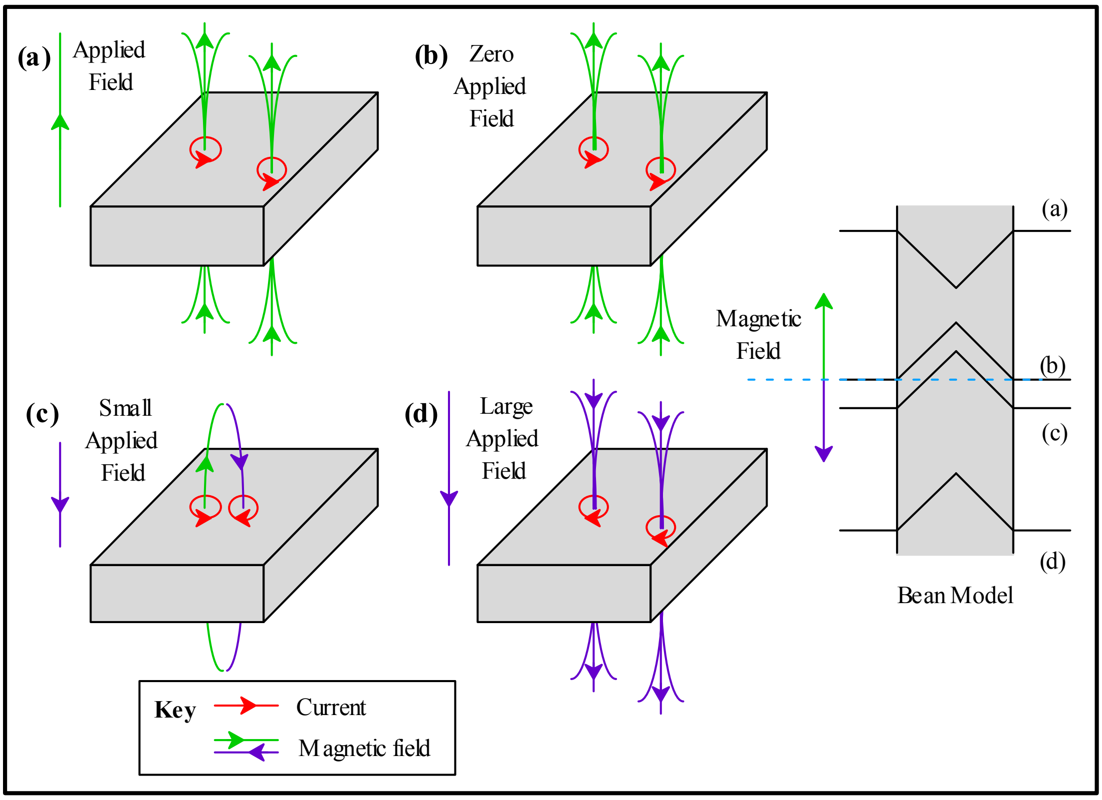

Figure 5·9 Change in the flux vortex pattern in a superconductor as the magnetic field is reversed with the equivalent Bean model prediction for the total flux in the superconductor at each applied field.

Flux vortices

The critical current is strongly dependent upon the number of flux vortices in the superconductor. Vortices only enter the type II superconductor when the lower critical field $\left(H_{c_1}\right)$ is exceeded, but once the vortices are in the superconductor they tend to persist below H_{c_1} on the pinning sites. Thus after applying the magnetic field the critical current does not go back to the original, vortex free value. In order to remove the vortices the sample must be heated above the superconducting transition temperature and cooled again in magnetic field below H_{c_1}. Reversing the magnetic field causes flux vortices with the opposite field direction (anti-vortices) to form at the edge of the superconductor and move towards the centre. When an anti-vortex encounters a vortex the two combine and mutually annihilate, which reduces the amount of flux in the superconductor. Thus the magnetic flux goes to a minimum, and so the critical current goes to a maximum, at a small applied field in the opposite direction. This is illustrated in figure 5·9. The magnetic flux density in an isotropic type II superconducting slab was modelled by C.P. Bean in 1962. In the Bean model the critical current density (J_c) is assumed to be constant and the pinning potential to be sufficiently strong to minimise mutual annihilation, thus the flux density profile is a straight line with a gradient proportional to J_c. Figure 5·9 shows the flux density in the superconductor given by the Bean model as it is initially filled with vortices, figure 5·9a, and then the field is reversed.

As the maximum critical current occurs at a small magnetic field applied antiparallel to the saturating field rather than at zero, flux vortices can give rise to a 'double peak' structure in the critical current vs. applied field data. There are three main objections to this mechanism as the source of the 'double peak' structure we observe in the critical current with applied field measurement of the niobium/cobalt bilayers.

Firstly the 'double peak' structure is absent, to the limit of the noise in the signal, in the critical current vs. applied field measurements of the niobium film, as shown in figure 5·2. Although the cobalt layer increases the local magnetic field, as shown below, and probably increases the number of pinning sites, and the pinning potential at those sites, one would still expect to see some evidence of the 'double peak' structure in the niobium film.

Second, the critical current of the Nb/Co bilayer when it is first cooled, i.e. before any magnetic field is applied, is less than the maximum measured critical current. In the absence of any magnetic field the critical current should be a maximum, by the flux vortex model, as there are no flux vortices. The stray field from the cobalt layer could exceed $\underline{H}_{c_1}$ though this is unlikely as the cobalt layer has not been poled and so the stray field should be close to a minimum. For bulk niobium $\underline{H}_{c_1}$ is equal to 1.73 kOe which, as is shown below, is larger than the stray field at the track even when the cobalt layer is fully poled [Kaye 1995]. The magnetic impurities in the niobium layer will reduce $\underline{H}_{c_1}$ compared to the bulk value but this does strongly suggest that there are no vortices in the as cooled sample.

Finally the geometry of the sample limits the number of flux vortices in the sample. The magnetic field was applied parallel to the length of the track, thus the flux vortices must lie in a cross-sectional area of approximately 1 μm by 50 nm. This can be contrasted with the size of the normal core of a flux vortex in niobium and with the spacing of vortices in an applied field of 500 Oe. The radius of the flux vortex is given by the penetration depth, the shortest possible distance over which the superconducting wavefunction can significantly change, and the flux spacing can be approximated as the flux density inside and outside the superconductor must be the same. The penetration depth (λ) in niobium is 52 nm so the niobium layer is thinner than the penetration depth in most cases. Assuming a triangular lattice of flux vortices, the spacing between vortices (a_0) is given by:

$$a_0^2 = \frac{2\varphi_0}{\sqrt{3}B} \tag{5·5}$$

where: φ_0 is the flux quantum.
B is the applied field.

When the applied field is 600 Oe the vortex spacing is 200 nm, limiting the number of vortices in the track to five at most. It is also likely that the vortices were trapped at the edge of the track as the variations in track width create a strong pinning sites. If a component of the magnetic field was not parallel to the track then there could have been a significantly larger number of vortices. This component will tend to be even smaller than that in the case of a niobium film as the magnetic field will tend to be concentrated parallel to the cobalt layer due to the large permeability of cobalt relative to free space. The evidence strongly suggests that flux vortices are not responsible for the 'double peak' structure in the critical current vs. applied field measurements of the Nb/Co bilayers.

Stray magnetic field

The second mechanism by which the 'double peak' structure might be obtained is stray magnetic flux from the edges of the cobalt layer. Below the Curie temperature there is a spontaneous bulk magnetisation within a ferromagnet. Unless closure domains form there will be an external field around the ferromagnet that must be added to the applied magnetic field in order to obtain the local magnetic field. Thus it is possible for the local magnetic field to be significantly stronger than the applied field. As the local magnetic field is dependent upon the magnetisation, which is hysteretic, the suppression of the superconducting critical current may not follow the expected monotonic decrease from zero magnetic field. The stray field from the cobalt layer must be considered in two parts, the field due to the cobalt layer of the

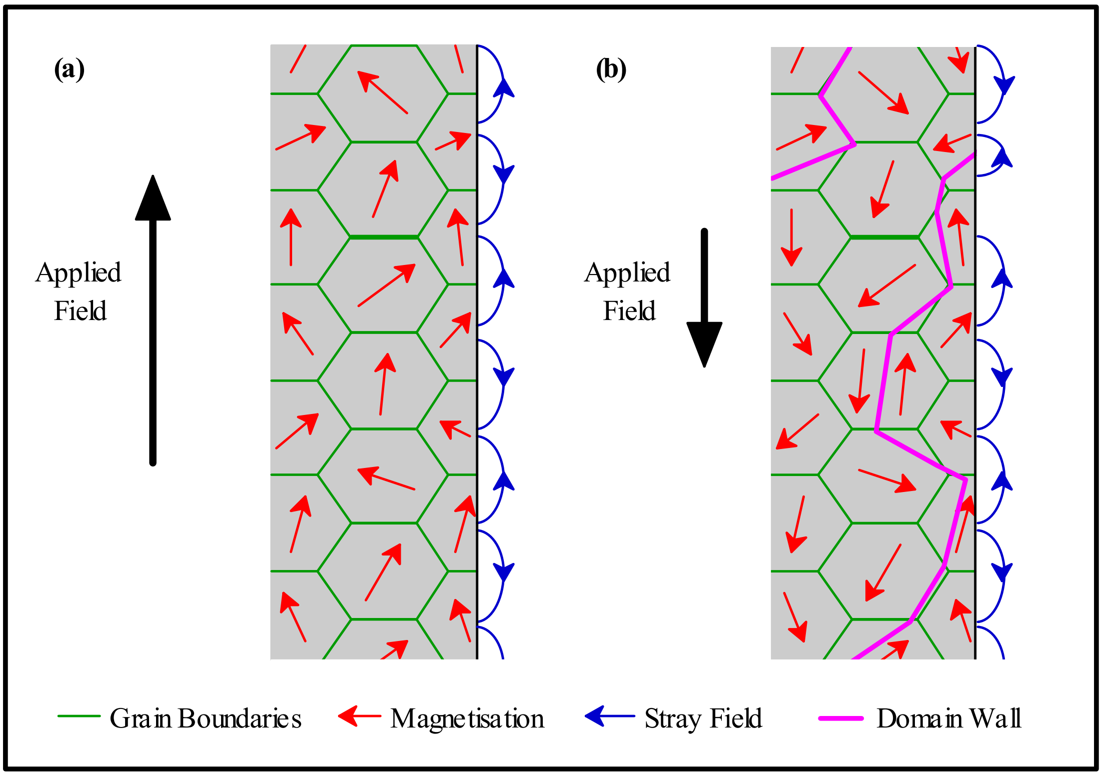

Figure 5·10 Plan view schematic of the change in the magnetisation and so the stray magnetic field between (a) saturation and (b) H_c.

track itself and that due to the cobalt layer of the electrical connections from the track to contact pads. The stray field from the upper and lower faces of the cobalt layer, i.e. vertically through the niobium/cobalt interface, will be very small as the magnetisation is confined within the plane of the film, as is shown by the X-ray analysis given above.

The stray field from the cobalt layer of the track itself will have a very strong effect on the niobium layer due to the close proximity to the region of the niobium being measured. However, as shown in figure 5·10, this stray field is not expected to change significantly with the applied field. The strong uniaxial magnetocrystalline anisotropy in cobalt means that the magnetisation in each crystallite is fixed along a single axis at the magnetic field strengths used in these measurements. Thus, in most crystallites, changing the domain simply reverses the magnetisation and so reverses the direction of the stray field without changing the magnitude. The only exception to this occurs in those crystallites where the domain wall reaches the edge of the track, then there would be a small amount of additional stray field. This will give a reduction in the critical current at the coercive field, though only slightly smaller than

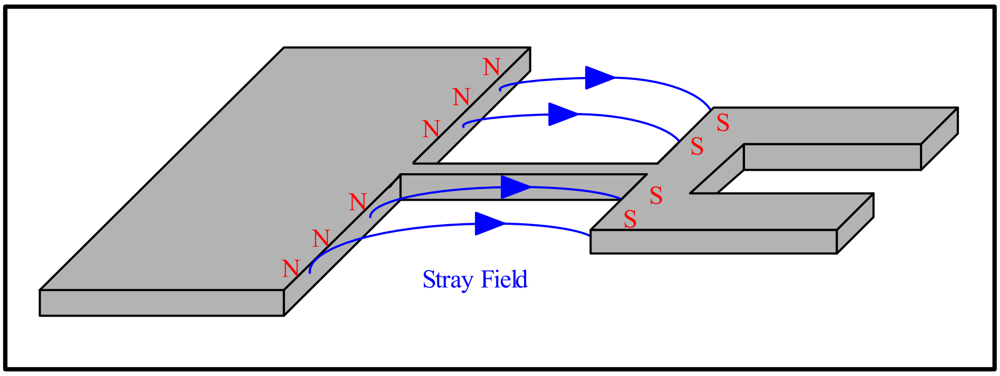

Figure 5·11 Schematic of the stray field between the electrical connections to the track when the cobalt is saturated.

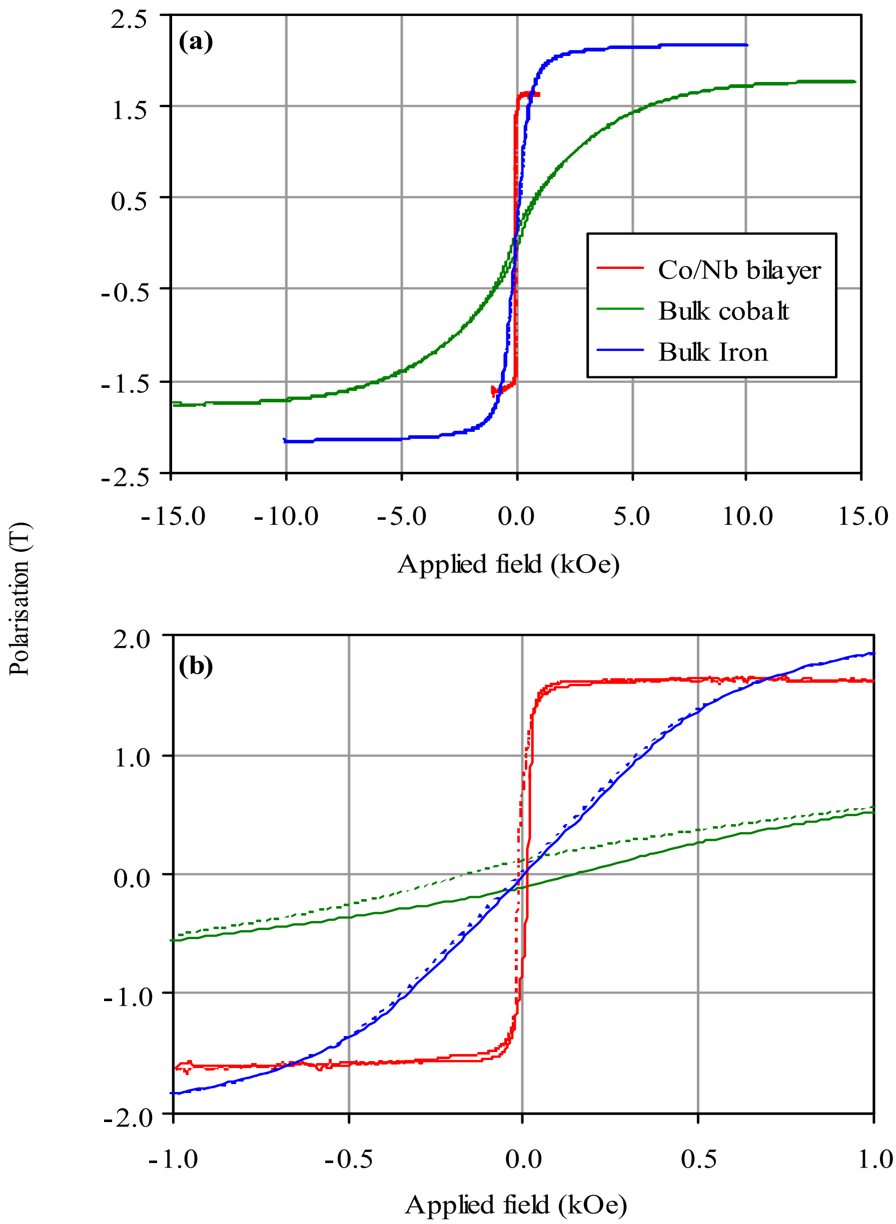

Figure 5·12 Polarisation vs. applied field loops for a niobium/cobalt bilayer, bulk cobalt and bulk iron at room temperature. (b) shows the low applied field detail of (a).

the critical current when the cobalt layer is saturated. Thus the stray field from the cobalt layer of the track could not give rise to the 'double peak' structure but may cause some of the structure observed within the peak, the component of the critical current vs. applied field behaviour shown in figure 5·1c.

An additional source of stray magnetic field comes from regions of the bilayer that are patterned to act as electrical connections to the track, see figures 5·4 and 5·11. This effect could give rise to the 'double peak' structure as the stray field will be a maximum when the cobalt is saturated and a minimum at the coercive field. At the coercive field the domain structure in the connections will cause the field to form loops near the edge, similar to the pattern shown in figure 5·10, rather than crossing

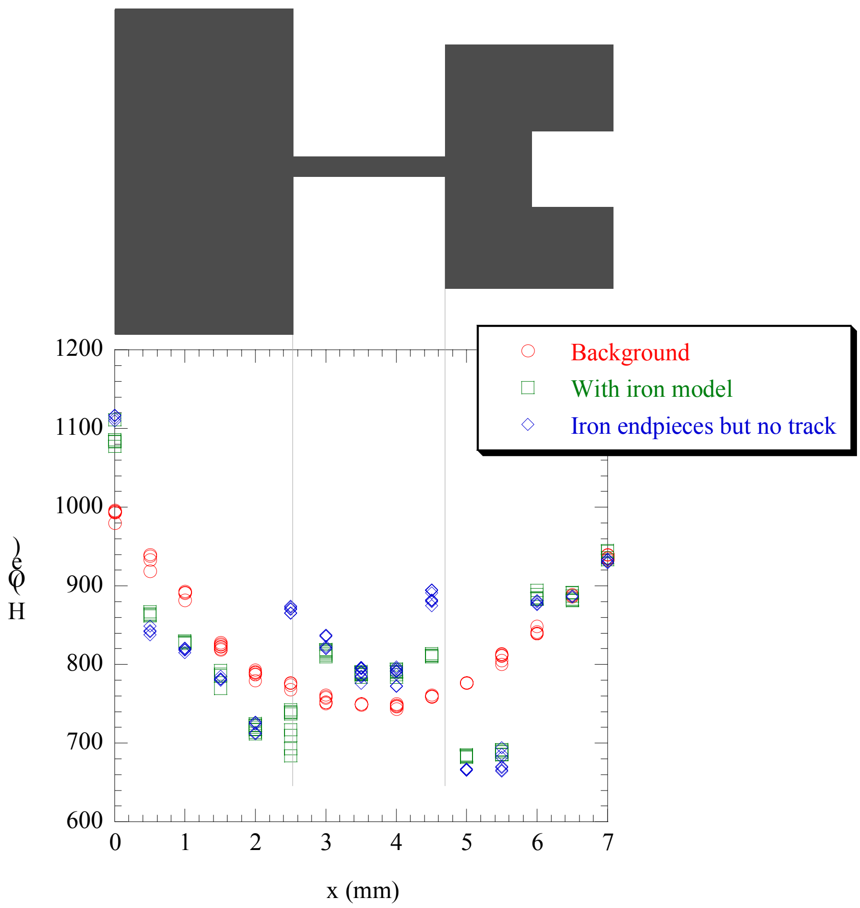

Figure 5·13 Determination of the change in the magnetic field caused by the ferromagnetic layer. A one micron wide track with suitable end pieces was scaled by 2100:1 as an iron model and the magnetic field was measured along the centre line at room temperature.

the air gap and cutting the track. In order to determine the magnitude of the local magnetic field we have made a scale model of the closest potion of the electrical connectors to the track. However, as figure 5·12 shows, an extremely high magnetic field, in excess of 10 kOe, is required to saturate a sample of bulk cobalt. This field strength can not easily be obtained so we have used iron to make the model as bulk iron has the same room temperature polarisation as the cobalt/niobium bilayer in an applied magnetic field of approximately 700 Oe, which is easily obtained with a pair of permanent magnets [Meservey 1994].

The magnetic field strength was measured using a Hall probe placed adjacent to the iron. As the Hall probe is wider than the niobium layer, as scaled up relative to the ferromagnet layer, we have used a slightly larger applied field strength to compensate for the averaging across the Hall probe. As expected the magnetic flux tends to flow through the iron, thus the local magnetic field depends upon the presence of the track between the portion of the electrical connections shown in figure 5·13. If the track is present the local magnetic field is approximately 60 Oe stronger than that generated by the magnets, while if the track is absent the increase in field strength is approximately 125 Oe. Thus we can estimate the maximum size of the peaks that the stray field using the data for a niobium film given in figure 5·2. Taking the reduction in the critical current with applied field to be linear over the relevant range of applied field gives a reduction of 0.36% in the critical current per Oersted. Given the form of the critical current with applied magnetic field, discussed above, this is probably a reasonable estimate of the reduction in the critical current. Taking the maximum possible change in the magnetic field the local magnetic field goes from 625 Oe at saturation (500 Oe of applied field plus 125 Oe of stray field) to zero field close to the coercive field. This model gives a peak critical current that is 1.3 times the critical current when the cobalt layer is saturated. The more reasonable assumption that the maximum stray field is only 60 Oe gives a peak critical current that is 1.25 times the critical current when the cobalt layer is saturated. As figure 5·14 shows, critical current vs. applied field measurements give ‘double peak’ structures that show significantly larger changes in the magnitude of the critical current. See figure 5·12 for a comparable M(H) loop. This strongly suggests that while the stray field contributes to the ‘double peak’ structure there must be another mechanism contributing to the change in the critical current.

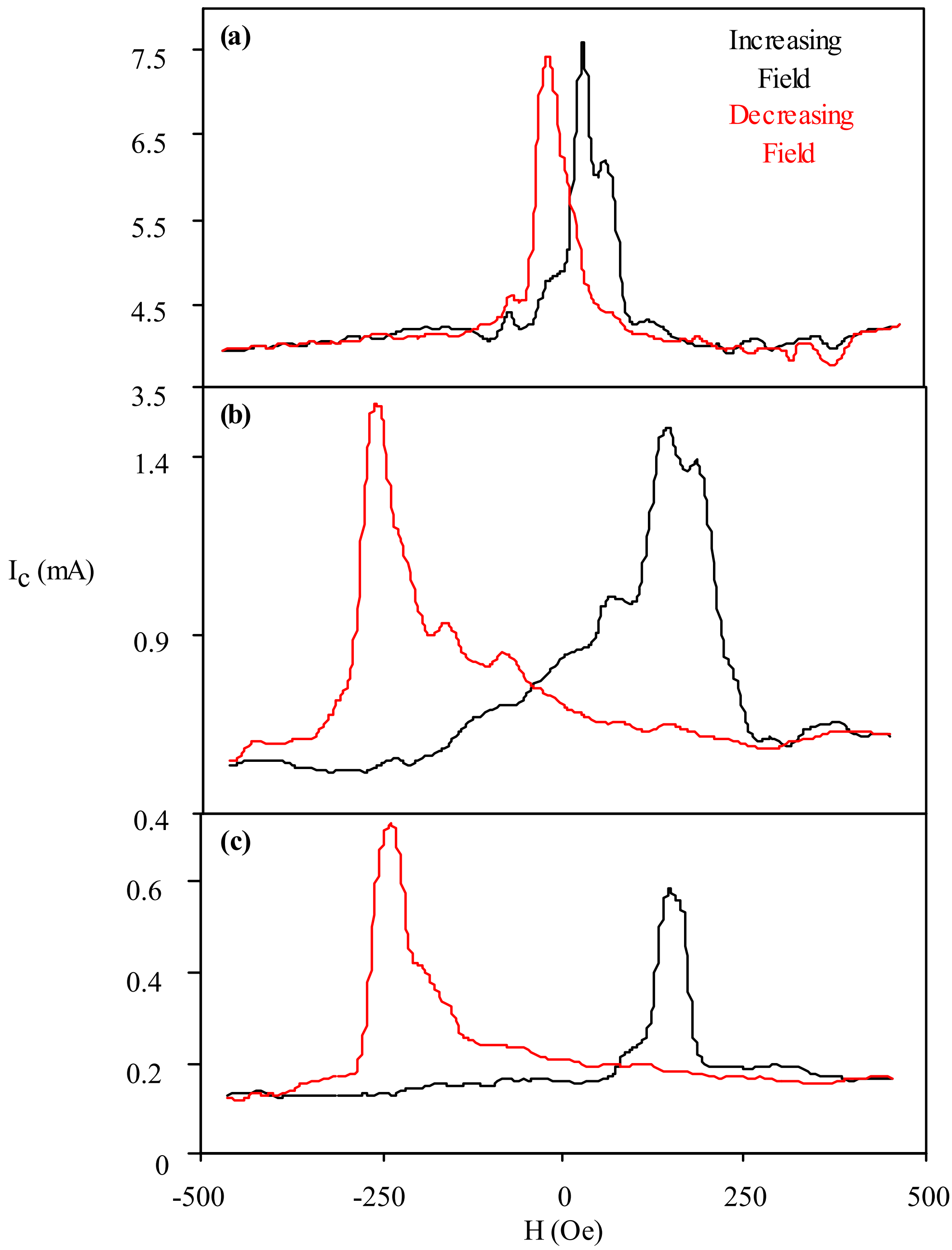

Figure 5·14 Forward critical current vs. magnetic field measurements at 4.2 K for a 10 μm by 1 μm track in a Nb/Co bilayer with:

a) (58 ± 16) nm of niobium.

b) (32 ± 11) nm of niobium.

c) (24 ± 8) nm of niobium.

Additionally, the stray field in a thin film is likely to be smaller than that given by a bulk sample, even though the shape anisotropy and polarisation are the same. As shown in figure 5·15, closure domains can form at the edge of a thin film even if there

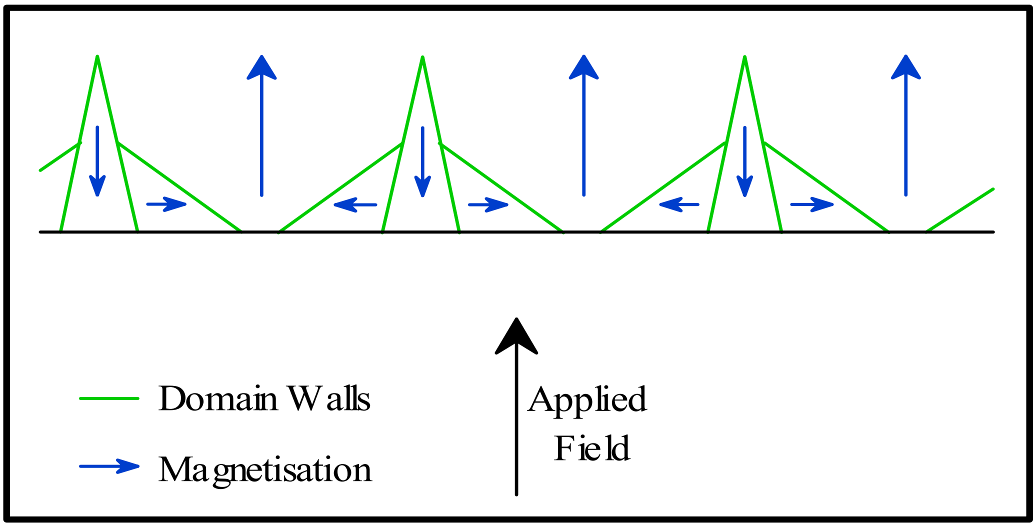

Figure 5·15 Plan view schematic of 'spike' domains at the edge of a thin film of a ferromagnet with a strong uniaxial magnetocrystalline anisotropy, after Craik 1965. These domains will form at the edge of the electrical connections to the track.

is a strong uniaxial magnetocrystalline anisotropy. This is due to the small number of atoms in a thin film, thus there is a reduced long range interaction which is the basis of the magnetocrystalline anisotropy. The pinned domains also provide an explanation for the offset of the monotonic decrease in the critical current vs. magnetic field measurements, as shown in figure 5·1d. As these domains are pinned in place the stray field they generate will be constant and so shift the zero applied field behaviour to some small finite field, giving a constant offset in the critical current vs. magnetic field measurements.

One final mechanism by which the stray field could increase the critical current near the coercive field relative to the high field value is by the formation of strong pinning sites [Muirhead 2001]. Given that cobalt only has a single magnetic easy axis the direction of the magnetisation on one side of a domain wall must be antiparallel to that on the other side, unless the domain wall runs along a magnetically disordered region such as a grain boundary. In either case there may be some component of the magnetisation perpendicular to the domain wall and this could lead to stray magnetic field cutting the superconducting layer and creating a strong pinning site for flux vortices, see figure 5·16.

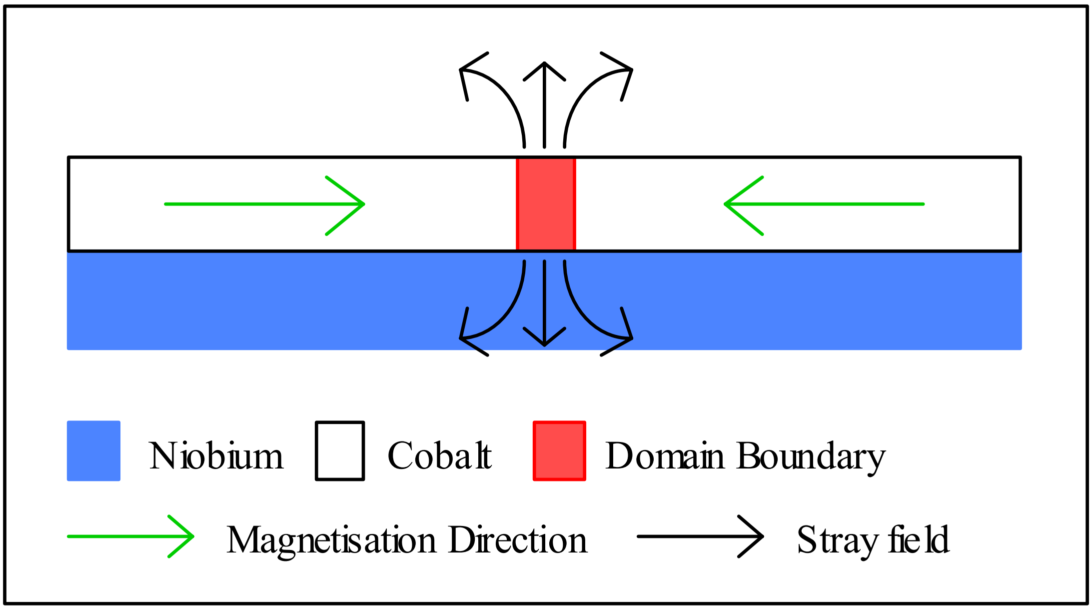

Figure 5·16 Schematic of the stray field at the domain wall between two antiparallel domains.

Domain walls form in order to minimise the energy of the system. Although it costs energy to create the domain wall, 0·01 Jm^{-2} in the case of bulk cobalt, this energy is compensated for by the reduction in the energy of the external magnetic field. Thus if the domain wall were to cut through a grain and, in so doing, create a significant magnetic field then the domain wall would move to prevent this even at the cost of creating more domain wall. In theory it should be possible to determine the maximum possible field, given that the system seeks a state of minimum energy and the average grain size in the cobalt is known. However this calculation would be very difficult to quantify as the amount of additional domain wall required would vary with grain size and shape, film thickness, domain wall type and numerous other factors. Taking all this into account it is not possible to dismiss this mechanism but it does seem that significant pinning sites would be rare. The stray field and the low magnitude can be seen in the care required to decorate domain walls with magnetic powder for imaging.

A stronger reason for rejecting this mechanism as the source of the double peak structure can be found in the critical current vs. applied magnetic field curves taken using the high voltage criterion. In this case the measured critical current is the current at which the track as a whole ceases to be superconducting, thus the resistance of the track is the normal state resistance. In this case the motion of the flux vortices is irrelevant and so the stray field could not be a cause of the double peak structure, see figures 5·19 and 5·20.

Ferromagnetic exchange interaction

The third possibility for the 'double peak' structure involves the exchange interaction extending into the niobium from the cobalt layer. There are several ways of visualising this phenomenon though they are, as is often the case in magnetism, very similar. The proximity effect creates an interfacial region where the electrical properties of the two conductors 'blur' together, giving a region with intermediate properties. Thus, despite the strong pair-breaking effects within a ferromagnet, superconductivity will exist within the ferromagnet layer of a ferromagnet/superconductor bilayer, though the superconductivity decays within a few nanometers from the interface. Equally the exchange interaction in the ferromagnet, as reflected by the energy separation between the two spin states, will extend into the superconductor reducing the gap parameter, as shown in figure 5·17. Thus the shift in the energy level of the two quasiparticle states reduces the energy gap and so the number of Cooper pairs. This separation decays exponentially through the superconductor, which is reflected in the change in the transition temperature of a superconductor/ferromagnet multilayer with the thickness of the superconducting layer, as discussed in Chapter 3. The shift in the band structure has a sign as well as a magnitude, depending upon the magnetisation of the ferromagnetic domain. Thus, as with the ferromagnetic superconductors discussed in chapter 3, the exchange interaction from an antiparallel ferromagnetic region will counteract the effect of the

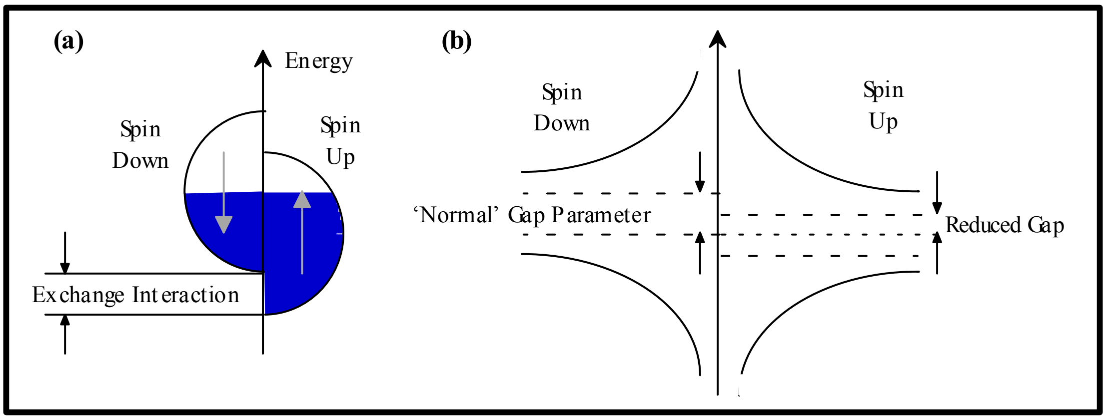

Figure 5·17 (a) Schematic of the band structure of a ferromagnet.
(b) Schematic of the band structure of a superconductor near the interface of a S/F bilayer.

original ferromagnetic layer. Beneath a 180° domain wall in a superconductor/ferromagnet bilayer there will be a region where the reduction in the superconducting gap parameter is smaller than in a similar region under a single domain. This gives rise to channels through the superconducting layer with a slightly higher T_c, as shown in figure 5·18.

One can also consider the effect in terms of a single Cooper pair. The exchange interaction shifts the energy of one spin with respect to the other, reducing the energy gap. However if the Cooper pair extends over two antiparallel domains then the two electrons will both be changed by the same amount and the gap will remain the same. The T_c in that region is not suppressed and so is higher than the T_c of the rest of the bilayer. Alternatively one can consider that there is an imbalance in the spin population in the superconductor at the S/F interface. The spin imbalance diffuses into the superconductor and is renewed at the interface as quasiparticles and Cooper

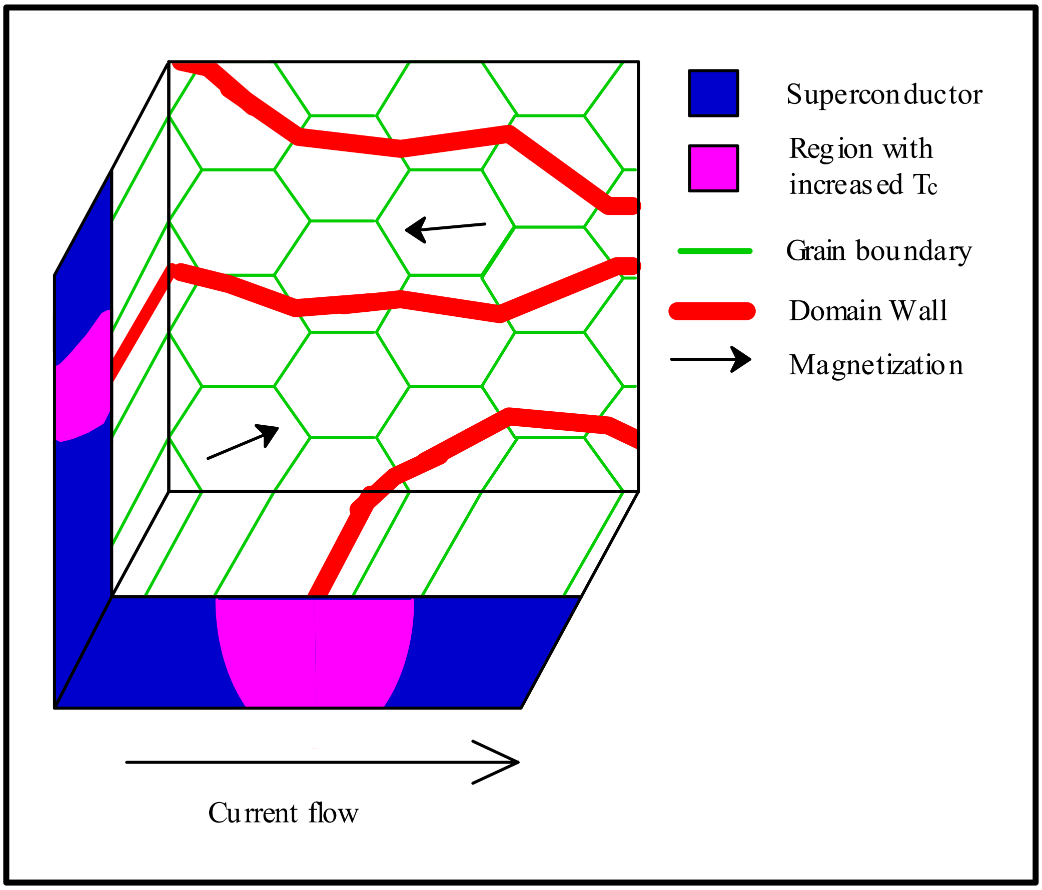

Figure 5·18 Schematic of a portion of the S/F bilayer near H_c, showing the grain boundaries and domain walls in the cobalt layer and the regions with increased transition temperature beneath the domain walls.

pairs enter the ferromagnet, a steady state condition. The sign of the spin imbalance depends upon the direction of the magnetisation in the ferromagnet and so the excess spin from two antiparallel domains will cancel out. Even if the domains are not antiparallel the antiparallel components will cancel out. In all three cases there is a web of regions with a slightly higher T_c through which additional critical current can flow. The three models suggest different length scales, for example the coherence

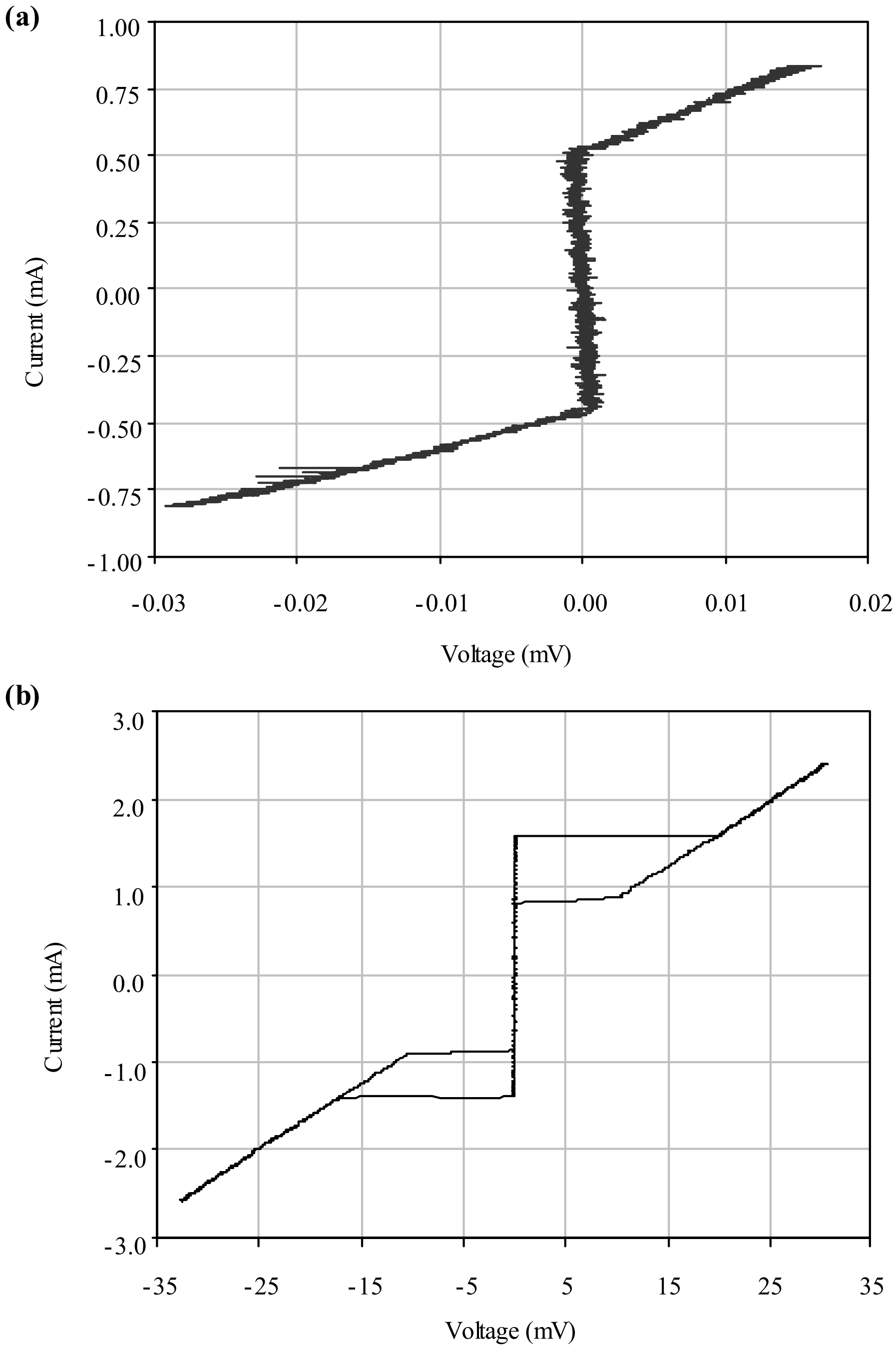

Figure 5·19 Current-voltage characteristic for a 10 μm by 1 μm track in a Nb/Co bilayer with (34 ± 10) nm of niobium at 4.2 K and zero applied field.

length or the spin diffusion length in the superconductor, but all three give an increase in the critical current at the coercive field of the bilayer and so could give rise to the 'double peak' structure.

Voltage criteria

As shown in figure 5·19 it is possible to isolate two critical currents in the current-voltage characteristic of the bilayer. The current at which the first region of the track develops a potential difference across it [normally due to flux flow resistivity], figure 5·19a, and the current at which the whole track is no longer superconducting, figure 5·19b. They can be identified as the low voltage criterion and the high voltage criterion. In general the critical current of the whole track tends to follow the low voltage criterion critical current though the features are smaller, as shown in figure 5·20. The reduction in feature size can be easily understood in terms of the exchange interaction as the regions with increased T_c meander across the track, an increase across a short region is more probable than an increase across a longer region. The stray field from the electrical connections will not be uniform across the track and this could also be used to explain the variation in feature size.

The high voltage criterion is of interest as it means the structures have slightly more

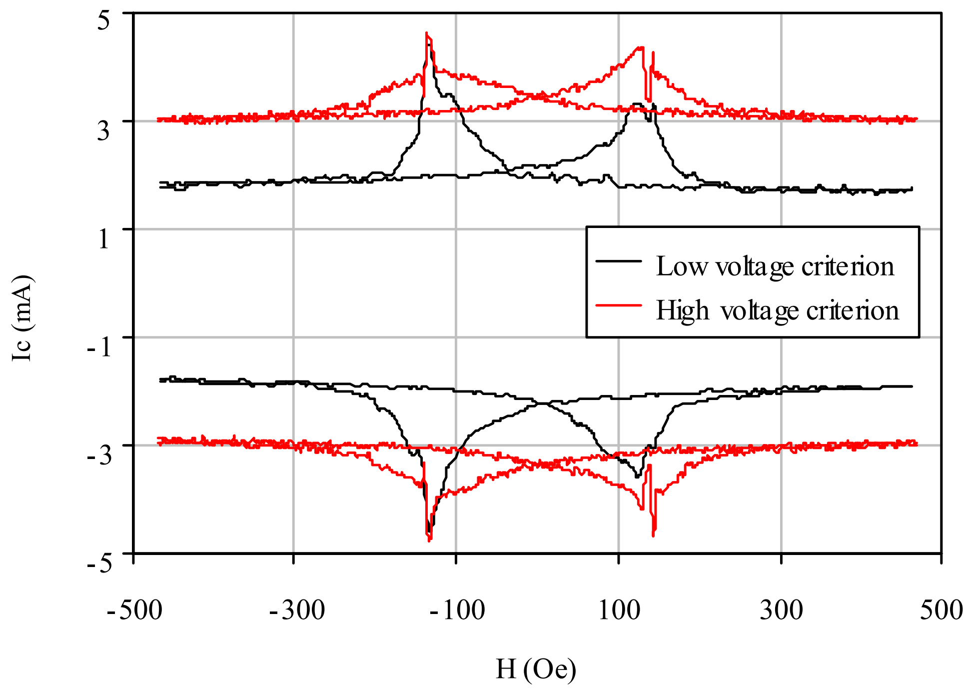

Figure 5·20 Critical current vs. magnetic field measurements for a 10 μm by 1 μm track in a Nb/Co bilayer with (41 ± 14) nm of niobium at 4.2 K.

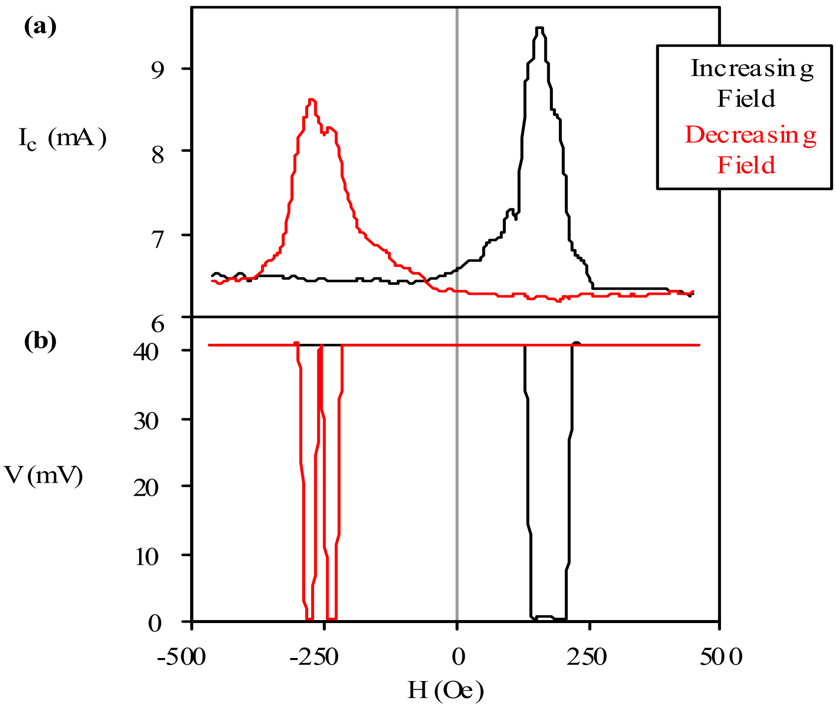

Figure 5·21 Data from a 10 µm by 1 µm track in a Nb/Co bilayer with (63 ± 18) nm of niobium, at 4.2 K. (a) shows the change in the critical current of the whole track and (b) shows the change in the voltage signal when 8 mA is passed through the track.

potential as devices. Figure 5·21 illustrates that the high voltage criterion gives a much stronger voltage signal when the bilayer is used as a superconducting switch. Rather than being limited to a few tens of microvolts, at the low voltage criterion, it is possible to get switching voltages on the order of tens of millivolts. The main limitation is the limited range of currents for which switching will occur. The switching voltage obtained depends on the thickness of the niobium layer and the track width. These parameters are limited by the need for a niobium layer thick enough to still be superconducting at the operating temperature and a track wide enough for multiple domains to easily form. Multiple domains are required for the double peak structure to be observed as the exchange interaction seems to be the only way to gain a significant change in the critical current.

Reproducibility and Barkhousen Noise

The stability of the electrical properties of the bilayers is of key importance, if the critical current vs. magnetic field data changes on repeated measurement then the utility of the bilayers for devices is compromised. Figure 5·22 shows repeated measurements of four different tracks with the data files superimposed upon each other for comparison. The features remain fundamentally the same though there is, naturally, some electrical noise in the system. The electrical noise can be determined from multiple measurements at a constant magnetic field and is most easily seen at high magnetic field where there is no difference between the data from increasing and decreasing magnetic field. Of more interest is the noise within the hysteretic region of the data, which is of far larger magnitude. This noise can be divided into two components, where the field at which a feature occurs has changed slightly and where the magnitude of the feature has changed. These affects can be explained in terms of the Barkhausen effect [Chikazumi 1997].

Barkhousen discovered that a change in the magnetisation of a ferromagnetic material occurs in many small discontinuous steps, as the domain wall moves between pinning sites. Thus the domain structure depends critically upon the initial state, a chaotic system. As there is a dynamic interaction between the local magnetic field and the pinning forces the domain will not repeat itself exactly with each sweep of the magnetic field. The position of the domain walls and any stray field between the domains will not be the same just because the magnetic field history is the same. This explains why the features can be offset on repeated sweeps of the magnetic field.

The Barkhousen effect can also provide an explanation for the structure within the hysteretic regions. Whether the change in the critical current is due to the reduced exchange interaction at domain walls or due to the stray field from the cobalt layer interacting with the niobium it is critically dependent upon the domain structure within the cobalt. As Barkhousen showed, this domain structure is a dynamic thing changing with each step in the magnetic field before the measurement of the critical current is made. Thus there may be domain configurations for which there is no domain wall across the track and so there is no increase in the critical current, alternatively the configuration of the domains could cause a large amount of stray flux to intersect the niobium. In both cases this would lead to the sudden reductions in the critical current seen in figure 5·22a.

The sharp transitions in the critical current increase the weight of evidence pointing towards the exchange interaction explanation for the double peak structure. To give rise to the change in the critical current shown in figure 5·22a by the stray field mechanism the local magnetisation of the electrical contacts must have gone from close to minimum to maximum and back to minimum again over a range of approximately twenty Oersted. Given the inverse square behaviour of magnetic field

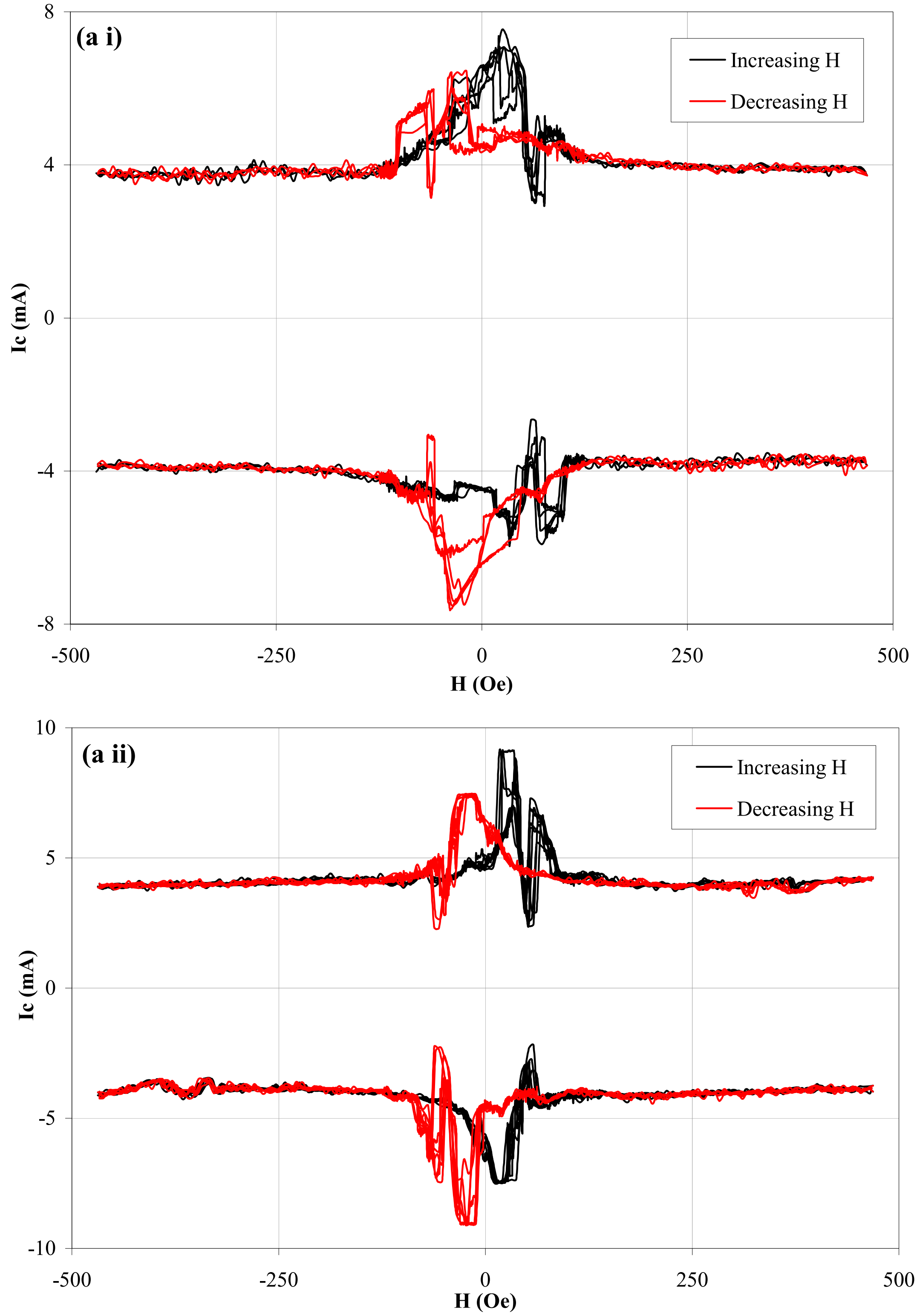

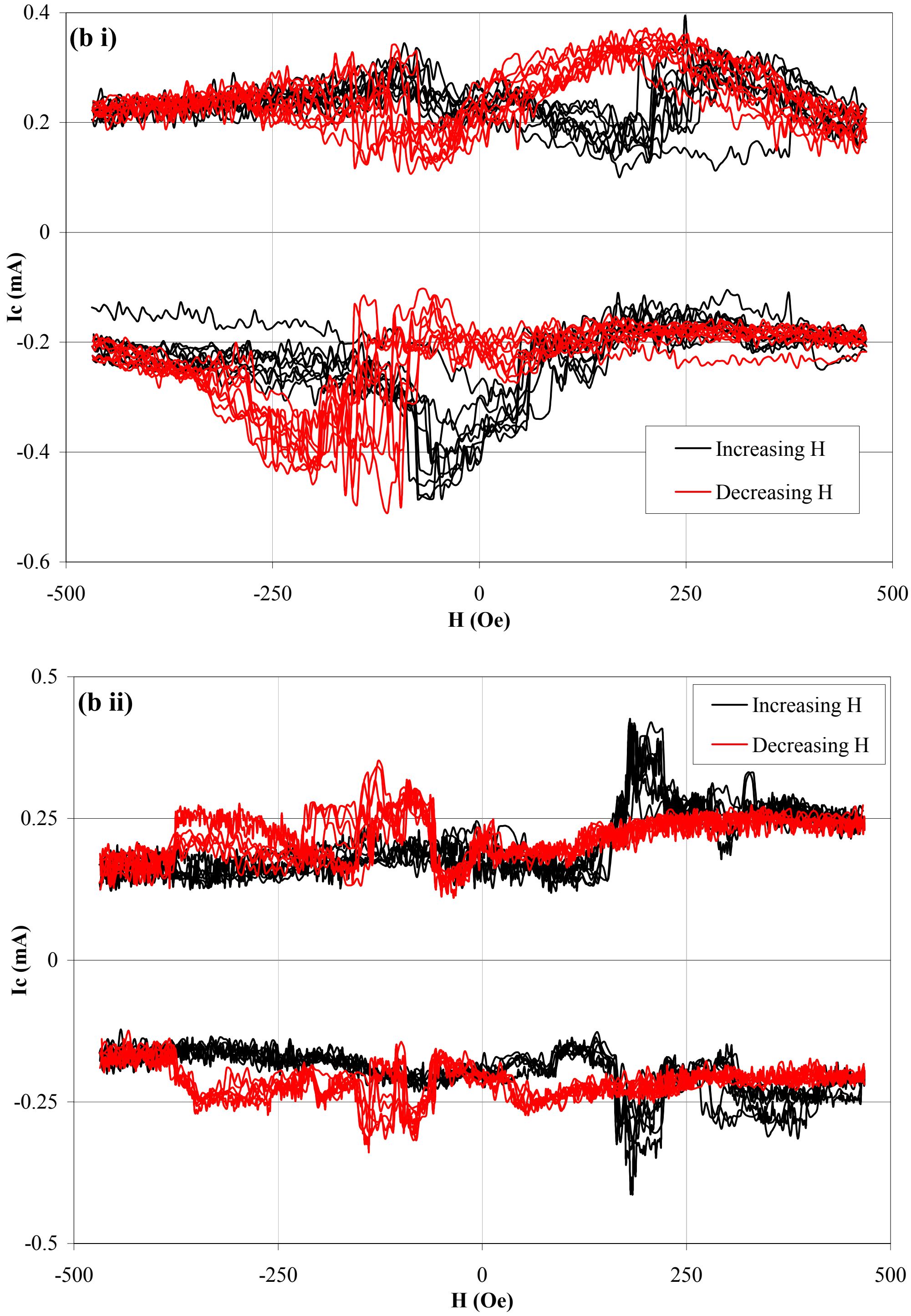

Figure 5·22 Repeated critical current vs. magnetic field measurements for a 10 μm by 1 μm track in a Nb/Co bilayer with (a) (49 ± 16) nm of niobium or (b) (27 ± 9) nm of niobium. Multiple measurements are shown to give a measure of both the noise in the signal and the reproducibility. Two tracks are shown for each bilayer, each of which has undergone identical processing.

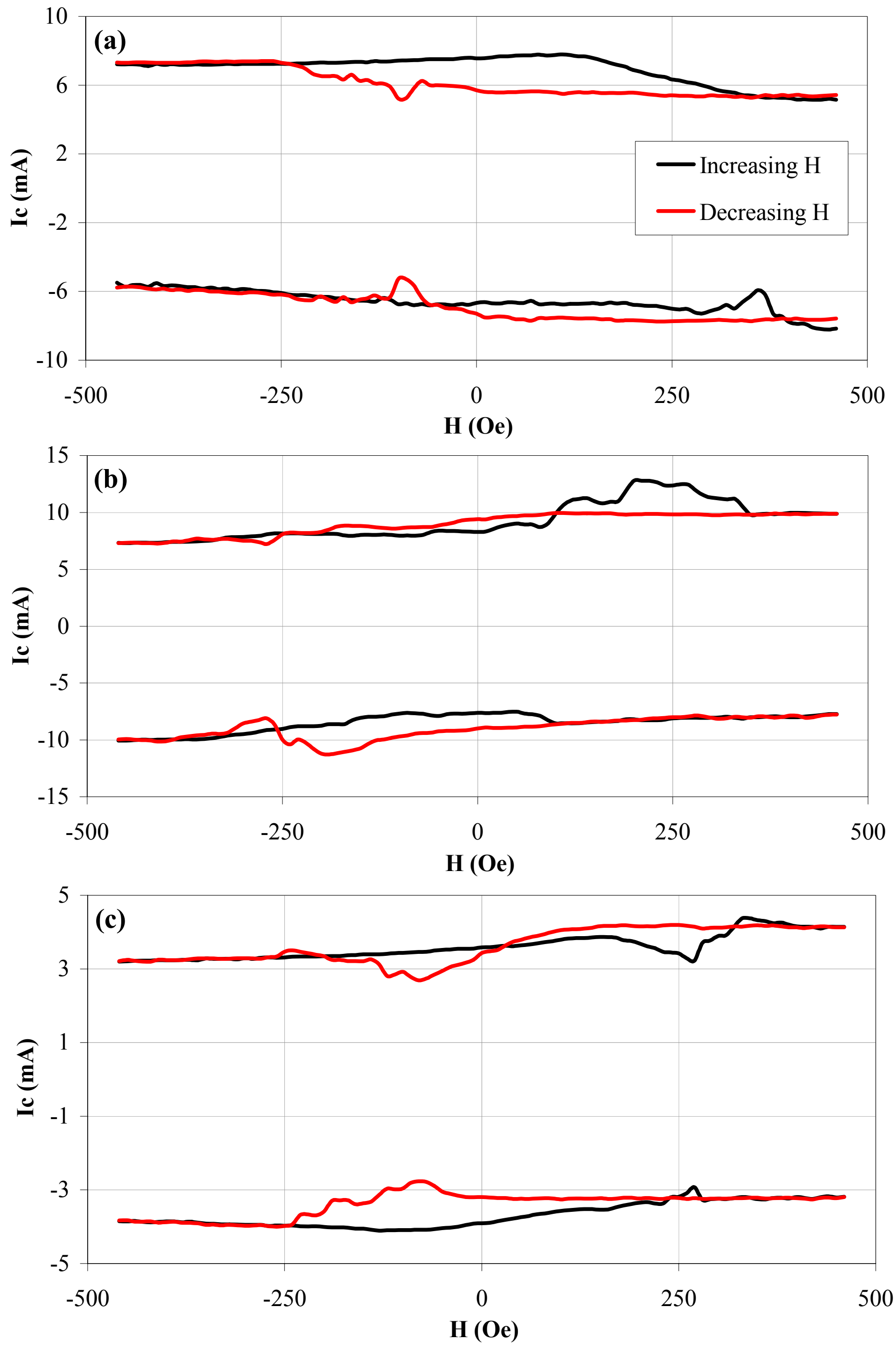

Figure 5·23 Critical current of the entire track vs. magnetic field measurements for a 10 μm by 2 μm track in a Nb/Co bilayer with a) (46 ± 15) nm of niobium, b) (32 ± 11) nm of niobium, or c) (16 ± 5) nm of niobium.

strength with distance for a point half a micron from the edge of the electrical contacts, 90% of the stray field is due to the cobalt layer within three microns of the track. However as the magnetisation reverses the new domains grow from the 'spike' domains at the edge of the bilayer. This gives rise to the characteristic zig-zag edge of the growing domains. As the domain grows in to the electrical connections from the edges it is difficult to imagine how a four micron wide region could temporarily form unless the domain walls were moving perpendicular to the magnetic field. The web of domain walls that form near the coercive field and carry the additional critical current by the exchange interaction mechanism will be very sensitive to a small change in the magnetic field. Thus there is the potential for the very sharp changes in the critical current as the domain wall must bridge the first area to develop a potential difference due to excess current for there to be any increase in the critical current. The additional suppression of the critical current beyond that at saturation can be explained by the pinned domains at the edge of the track which could provide a limited pathway for additional critical current at saturation but become blocked as the domain walls move.

Hysteretic Switching in the Critical Current

As shown in figure 5·23 some tracks show hysteretic switching between two critical current states. Though there is no change in the total critical current there is displacement such that the forward critical current $\left(I_{c_f}\right)$ is greater than the reverse critical current $\left(I_{c_r}\right)$ in one saturation state while $I_{c_f} < I_{c_r}$ when the magnetisation is reversed. This effect has also been observed in experiments where the applied magnetic field is perpendicular, though still in the plane of the film, to the direction of current flow, as shown in figure 5·24 [Callegaro 2000]. In this set of experiments there was clear switching between critical current states at the coercive field of the permalloy bridge, as measured with a Kerr magneto-optical hysteresis loop tracer, very similar to the idealised behaviour shown in figure 5·1e. The authors attempted to explain this behaviour in terms of the fringing field from the permalloy layer, in a manner similar to the superconducting valve [Clinton 1997]. However, as the authors observed, this explanation has drawbacks as the fringing field is limited to a few 10^5 Am^{-1} and a homogeneous field of this intensity has no significant effect on the transport properties of niobium [Quateman 1986]. Equally the fringing fields could not account for the increase in one of the critical currents.

We propose an alternative mechanism for the switching between current state that could, given certain underlying assumptions, account for the observed behaviour. Firstly we note that the interface between the niobium and the permalloy will not be

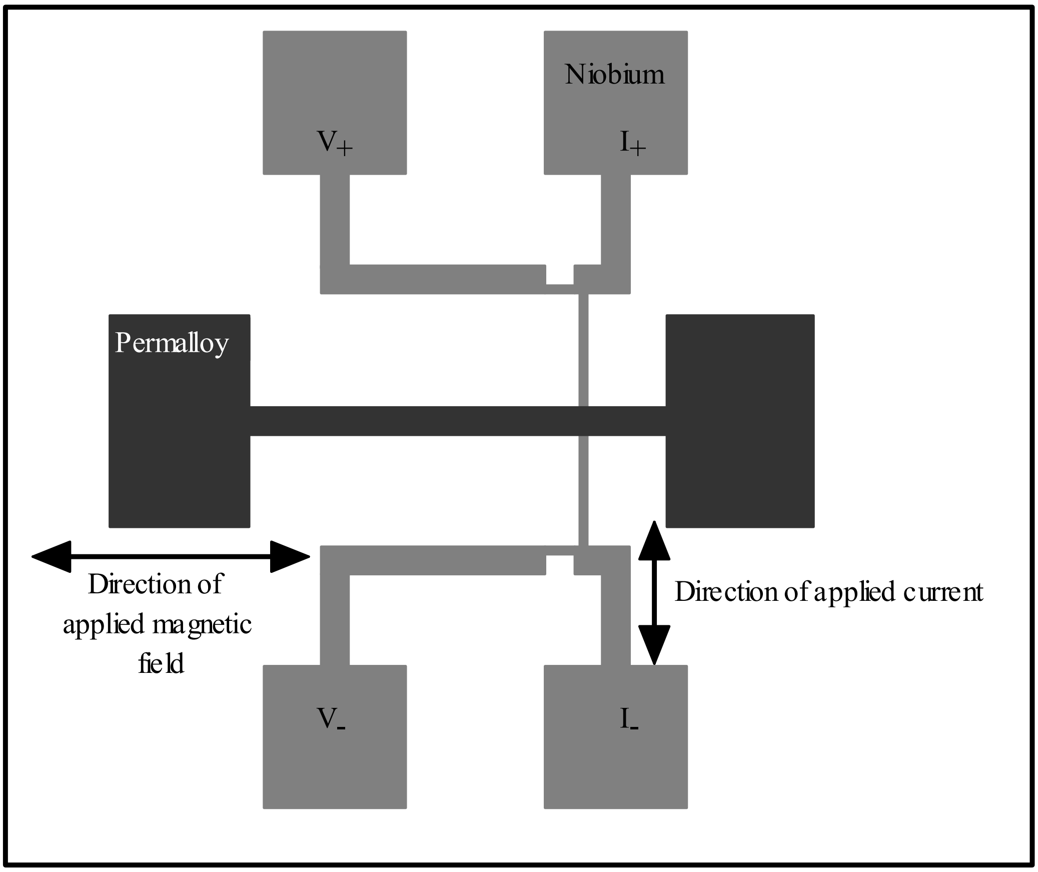

Figure 5·24 Schematic representation of the sample configuration (not to scale) used by Callegaro *et al*. for measuring critical current as a function of applied magnetic field. The electrical contact pads on the Permalloy bridge were not used in these experiments [after Callegaro 2000].

atomically smooth. This allows for the possibility of magnetic field loops through the niobium between regions in the permalloy which would suppress the critical current of the niobium [Mühge 1998]. The magnetic field would be generated by dipoles and so decay rapidly, as the inverse cube, with distance but the field will be approximately equal to the polarisation at the interface between the niobium and the permalloy, which is on the order of one Tesla. The current flowing through the niobium also generates a magnetic field, the self-field discussed above, which will either oppose or add to the magnetic field created by the interfacial roughness, as shown in figure 5·25. The self-field will be on the order of a thousand Oersted per Amp, the track used by Callegaro *et al* has a cross-sectional area of 5 μm by 100 nm and is 100 μm long. This gives a self-field of approximately 100 Oe at the mean critical current of 10 mA. If this model is correct then the difference in the forward (or equally in the reverse) critical current is equal to the difference in critical currents when the local field is

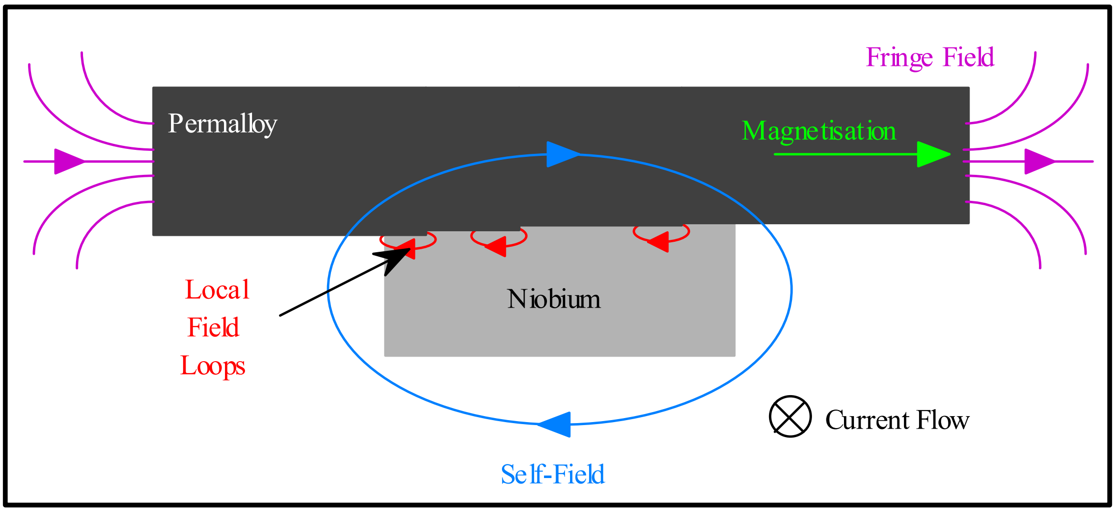

Figure 5·25 Schematic representation of the magnetic fields created by the magnetisation of the permalloy bridge and the current flowing through the niobium.

opposed by the self-field and the critical current, when the self-field adds to the local field. Given a quasi-linear dependence of the critical current on the applied field this gives a change of 1.1 mA in 100 Oe which can be extrapolated to given a superconducting critical field of only 900 Oe. This value for H_{c_2} neglects the effect of the flux vortices, which will be far closer to the expected flux vortex behaviour given the sample geometry and so will increase H_{c_2} considerably. It also ignores the local field loops, this magnetic field would have to be added to the critical field and so would increase it to a more reasonable value. Equally the above rough calculation does not take into account the decay of the magnetic field with distance from the S/F interface resulting in the superconducting wave function changing through the depth of the niobium, increasing with distance from the interface. Despite the fact that the self-field seems too weak to give the measured magnitude of switching this effect does give an explanation for the switching between the critical current states. The suppression of the critical current depends upon whether the magnetisation and the self-field, which in turn depends upon the direction of current flow, are parallel or antiparallel. Thus the model reflects the odd symmetry observed in the critical current vs. magnetic field data and a small change in the local magnetic field may have a significant effect on the pinning of flux vortices.

This model for hysteretic switching between critical current states can also be applied to the niobium/cobalt bilayers giving the critical current vs. magnetic field data shown in figure 5·23. It may seem that the fact that the magnetic field is applied in the direction of the current makes this interaction between the self-field and the magnetisation impossible. However the strong uniaxial magnetocrystalline anisotropy of cobalt means that the magnetisation is not necessarily in the same direction as the applied magnetic field. There will be a random distribution in the directions of the local field loops. For those tracks where there is an imbalance in the directions of the local field loops favouring one direction perpendicular to the track, but in the plane of the film, an interaction between the local field loops and the self-field becomes possible. Thus we can explain any hysteretic switching in the critical current in terms of local field loops that are not in the direction of the current flow interacting with the self-field of the current flowing through the niobium.

The interaction between local field loops and the self-field can also explain the asymmetry in the two critical currents (I_{c_f} and I_{c_r}), as shown in figure 5·22. This effect occurs near the coercive field in most measurements. In some cases this asymmetry can be ascribed to two competing effects, as in figure 5·23b which can be understood in terms of the sum of a double peak structure and hysteretic switching. In other cases, see figure 5·22a for two examples of this, this is not possible and another explanation for the effect must be found. We again consider the interaction between the self-field generated by the current and the local magnetisation of the cobalt as the critical current vs. applied magnetic field loop shows odd symmetry, the magnitude of the critical current depends upon whether the current is parallel or antiparallel to the magnetic field. As calculated above the self-field will be on the order of 100 Oe, though this will be close to 90° away from the applied magnetic field. However the magnetisation of the individual domains will not align perfectly with the axis of the magnetic field due to the strong magnetocrystalline anisotropy and so there will be some component of the self-field in the direction of the magnetisation. Close to the coercive field this component of the self-field will be sufficient to influence the domain structure, effectively switching it between two configurations as the direction of the applied current is reversed. As the critical current depends on the domain configuration we see two different critical currents depending upon whether the current is parallel or antiparallel to the applied magnetic field. At higher applied fields this small contribution from the self-field is dominated by the applied field and so is not seen.

The interaction between the self-field and the magnetisation also affects the dynamic resistance at currents slightly larger than the critical current, see figure 5·26. The

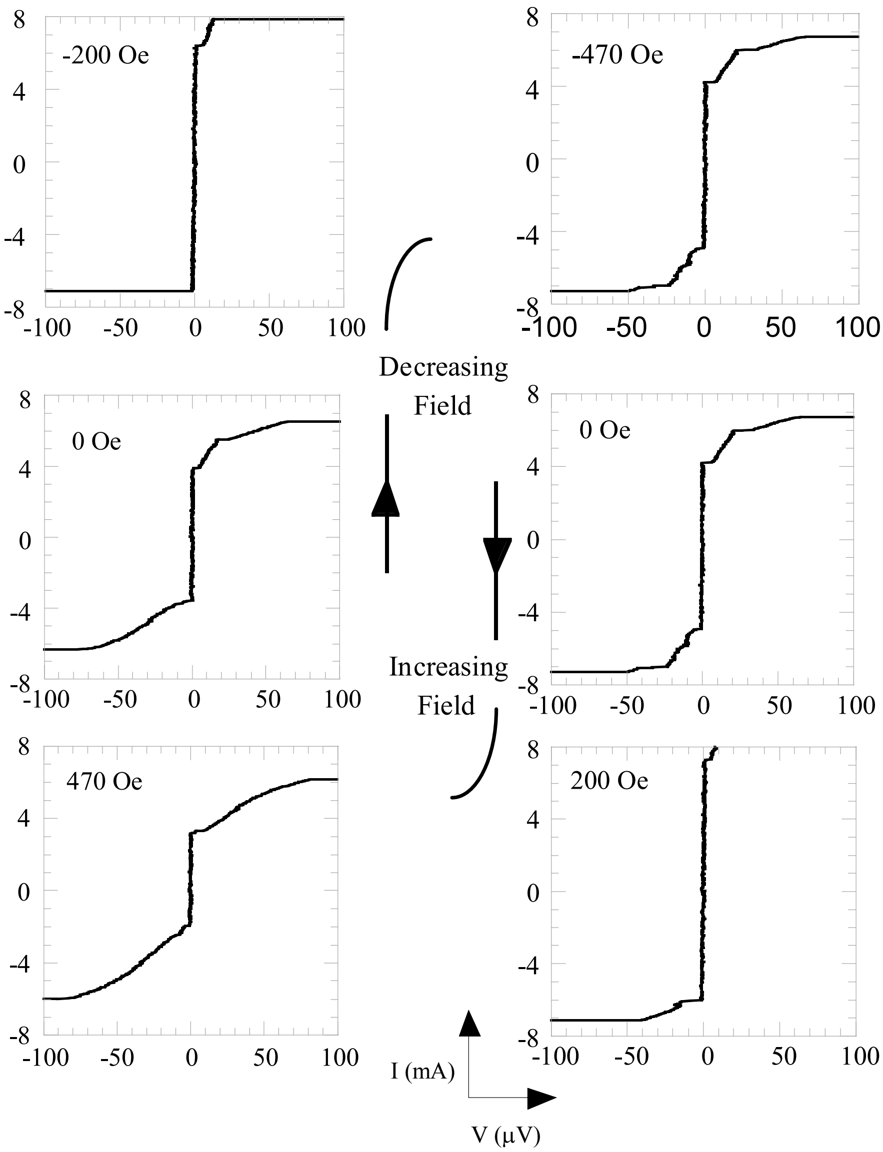

Figure 5·26 Changing current-voltage characteristic of a one micron wide by ten micron long track with magnetic field. The niobium/cobalt bilayer has (66 ± 22) nm of niobium. The current, plotted vertically, is measured in milliamps while the potential difference, plotted horizontally, is measured in microvolts. The magnetic field is increased from saturation at –470 Oe down the right hand column and reduced from saturation at +470 Oe up the left hand side.

dynamic resistance depends upon the proportion of the track which has a potential difference across it due to the combination of the current flowing through it, the magnetic environment and the heat generated by the current flowing through a resistive region of the track. The critical current gives a measure of the first region of the track to have a potential difference across it, either due to flux flow resistivity or the complete supression of superconductivity. The dynamic resistance, before superconductivity is suppressed for the entire track, indicates the current at which other regions of the track require a potential difference. Thus one can expect to see all of the affects discussed above to also be reflected in the dynamic resistance,though the difference on increasing or decreasing is the most obvious and can be explained by the influence of the self-field on the domain structure.

SUMMARY

The electrical properties of the niobium/cobalt bilayers differ both qualitatively and quantitatively from the properties of a niobium film. Most of the differences can be explained in terms of the interaction between the magnetic field generated by the magnetisation of the cobalt layer and the superconducting niobium. This explanation is not sufficient to explain the magnitude of the change in the critical current in the 'double peak' structure. After saturating the cobalt layer the critical current of the bilayer shows a maximum at a small magnetic field applied antiparallel to the saturating field rather than at zero field. The absence of this 'double peak' structure in the critical current vs. applied field data for a niobium film and the measurement geometry imply that the 'double peak' structure is not due to the motion of flux vortices. This suggests that the majority of the 'double peak' structure is caused by the interaction of the exchange interaction in the cobalt with the superconducting niobium. The energy of the spin bands in the superconductor is shifted by the ferromagnetic exchange interaction, extending into the superconductor by means of the proximity effect, which reduces the superconducting gap parameter. Beneath a 180° domain wall, which would form at the coercive field, the suppression of the gap parameter is reduced as the exchange interaction from two domains with antiparallel magnetisation cancels out. This gives a web of channels with a slightly higher T_c at the coercive field and so the 'double peak' structure. The critical current vs. applied field behaviour of the bilayers is reproducible to the limits of electrical and

Barkhousen noise. Barkhousen noise is the result of the discontinuous motion of domain walls through the cobalt layer.

Chapter Six

SYSTEMATIC CHANGES

Proof, n. *Evidence having a shade more of*
plausibility than of unlikelihood.
The testimony of two credible
witnesses as opposed to that of one

Ambrose Bierce, The Devil's Dictionary

In Chapter 5 we outlined two mechanisms that give rise to a 'double peak' structure in the critical current vs. applied magnetic field applied parallel to the track measurements in niobium/cobalt bilayers, stray field from the electrical connections and the exchange interaction in the superconductor. In this Chapter we discuss measurements made with systematic changes in the experimental parameters to see if it is possible to clarify the relative importance of the two mechanisms. We begin with those changes that are possible during the measurement of a single bilayer, these include the affects of varying the maximum applied field, field direction and temperature. Although the width and layers of the track are fixed, direct comparison of the data is more reliable, as we have not yet been able to fully control the magnetic structure of the cobalt layer. There is always some risk that a portion of the difference is not due to the systematic changes but is instead due to the subtle variations in the domain structure of the ferromagnetic layer. This is true when either comparing the behaviour of two different bilayers or the behaviour of two tracks in the same bilayer. We continue with discussions of the effect of changing the track width, niobium layer thickness, cobalt layer thickness and replacing the cobalt layer with an iron layer.

Stray magnetic field from the electrical connections to the track will cut the track and reduce the superconducting transition temperature. This in turn gives a reduction in the critical current, though the amount of reduction depends upon the pinning of flux vortices in the superconductor. The stray field depends upon the local magnetisation of the cobalt layer in the electrical connections and the distance from the critical region in the track. The critical region is the first region of the track to be driven normal due to exceeding the critical current density, which in turn depends upon the local temperature and magnetic field. The flux vortices tend to settle at pinning sites, sites where the superconducting gap parameter is lower than that in the surrounding region. The magnetic field required to start the vortex moving depends upon the 'depth' of the energy well of the pinning site, the pinning potential. Thus any change in the critical current due to stray magnetic field will depend upon both the magnitude of the stray field and the pinning potential in the superconductor.

Beneath a 180° domain wall in the ferromagnetic layer, there is a region in the superconducting layer where the exchange interaction is reduced. The exchange interaction in a ferromagnet causes, through the proximity effect, a distortion in the energy of the spin bands in the superconducting layer, which reduces the superconducting gap parameter. A stronger local exchange interaction in the superconductor gives rise to a decreased gap potential and so a smaller transition temperature and critical current density. Thus beneath a domain wall there is a region that can carry additional critical current though this region must bridge the critical region before there is any increase in the measured critical current. The critical region is defined here as the first region of the track to develop a potential difference across it due to the magnitude of the current, either due to flux flow resistivity or else the region becoming normal. The increase in the critical current depends upon the number of 180° domain walls crossing the critical region and the amount of additional critical current the region beneath each domain wall can carry. The amount of critical current carried beneath each domain wall will depend upon the length scale of the exchange interaction in the superconductor. A longer length scale means that the volume with a suppressed exchange interaction will be larger and so the change in the critical current between saturation and the coercive field will be larger.

Another key difference between the two mechanisms is the sensitivity to small changes in the domain structure. The stray field between the electrical contacts is the sum of the stray fields from each crystallite, which in turn depends upon the orientation of the easy axis relative to the film edge, the domain structure and the inverse square of the distance from the critical region. If we assume that there is only one domain wall in the electrical contacts and that it lies down the middle of the track then the stray field is zero. If this domain wall moves perpendicular to the track by half a micron then the local field half a micron from the electrical contacts will change from zero to 68% of the maximum value. This is the maximum possible change in the stray field at this position if the domain wall moves by half a micron. For the same motion the domain wall will move from the critical region in a micron wide track and the critical current will reach to the value it has when the ferromagnetic layer is fully saturated. In a more realistic model of the cobalt layer there are multiple domain walls near the coercive field and domains grow into the ferromagnetic layer from the edge of the track. The difference between the two mechanisms will then be even more distinct as a small change in the position of the domain walls will cause a small change in the stray field. The same small change could easily move the domain wall out of the critical region, giving rise to a significant change in the critical current by the exchange interaction mechanism.

Unless otherwise stated the magnetic field is applied parallel to the direction of current flow, in liquid helium at atmospheric pressure at 4.2 K and the thickness of the cobalt layer in the niobium/cobalt bilayers is (52 ± 16) nm. None of the bilayers, including those with an artificial constriction, give Shapiro steps when exposed to microwave radiation, the bilayers did not behave as Josephson junctions.

Changes in the Measurement Conditions

This section discusses those changes in the experimental conditions that are possible during the measurement of the critical current vs. magnetic field for a single track. These include the maximum strength of the magnetic field, the field direction relative to the current and the temperature. We discuss the change in the maximum applied field, the direction of the applied magnetic field and the temperature. Although this means that some changes, such as the layer thicknesses, are not possible the advantage is that the magnetic structure remains essentially the same between measurements. The pinning forces in the ferromagnetic and superconducting layers will remain the same, as will the location of the critical region, the first region in the superconductor to go normal. This allows for more direct comparison of the effect of changing the measurement conditions than when comparing the behaviour of, for example, bilayers with a different ferromagnetic layer thickness, which are discussed later in the Chapter.

Maximum applied magnetic field

Both mechanisms for the ‘double peak’ structure give the maximum critical current at applied fields close to the coercive field, the minimum local magnetic field and the maximum number of domain walls. Reducing the maximum applied magnetic field means that the magnetisation of the cobalt layer, rather than going to saturation, follows a minor magnetisation hysteresis loop with a correspondingly smaller coercive field and maximum magnetisation. This also reduces the maximum stray field and increases the probability that there will be some domain walls even at the maximum applied field so the change in the critical current will be reduced with the maximum applied magnetic field. These trends are observed in the critical current vs. applied magnetic field data shown in figure 6·1, providing confirmation that the magnetic structure of the cobalt layer is the key to understanding the properties of the

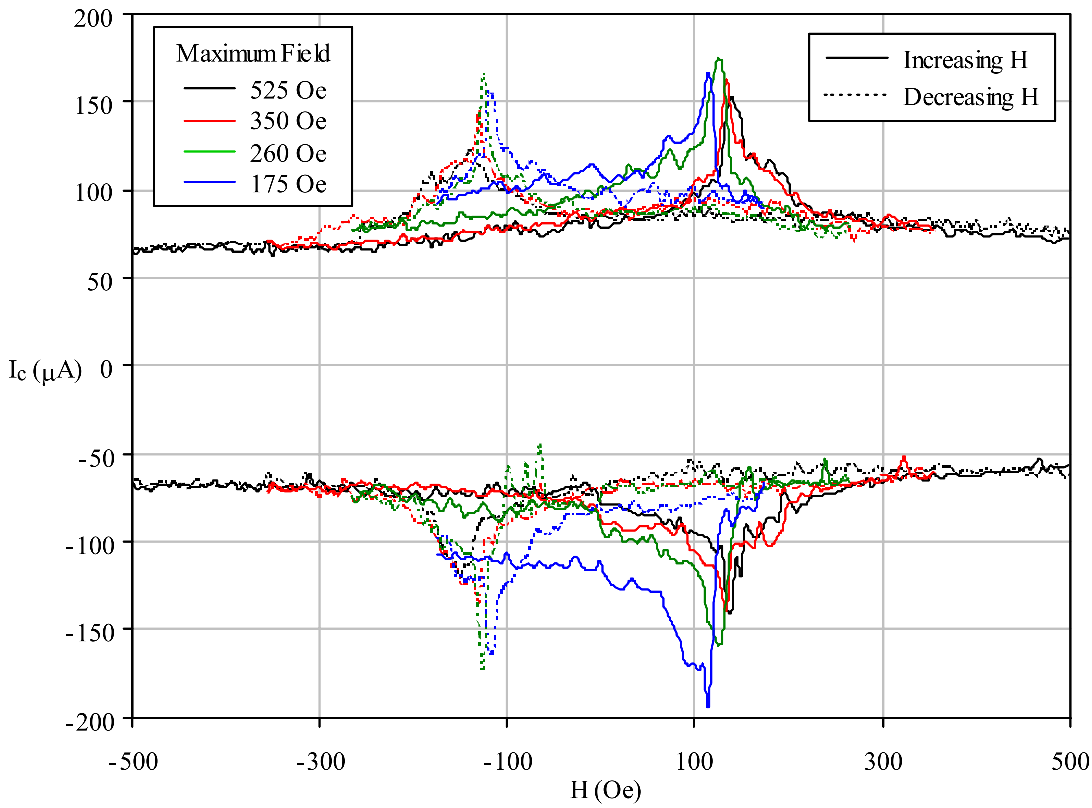

Figure 6·1 Critical current vs. magnetic field measurements for a 10 μm by 1 μm track in a Nb/Co bilayer with (21 ± 7) nm of niobium at 4.2 K. The cobalt layer is not taken to saturation, instead the maximum field, which is applied in both directions, is that given in the legend.

Nb/Co bilayers though it does not help to distinguish between the mechanisms. It is interesting to note the change in the symmetry of peaks as the maximum applied magnetic field is changed. The stray field will be approximately proportional to the magnetisation, the exact value will depend upon the crystallites and the domain structure. For the stray field to give asymmetric peaks the slope of the magnetisation hysteresis loop would be significantly different on either side of the coercive field. This is unlikely so the asymmetry is probably due to the detail of the domain structure.

Magnetic field direction

The magnetic field can be applied in two orthogonal directions to the direction of current flow (the x-direction). The field can be applied perpendicular to the plane of the film (the z-direction) and in the plane of the film but perpendicular to the current flow (the y-direction), as shown in figure 6·2. Applying the magnetic field in the z-direction does not give rise to the 'double peak' structure, in fact there is very little

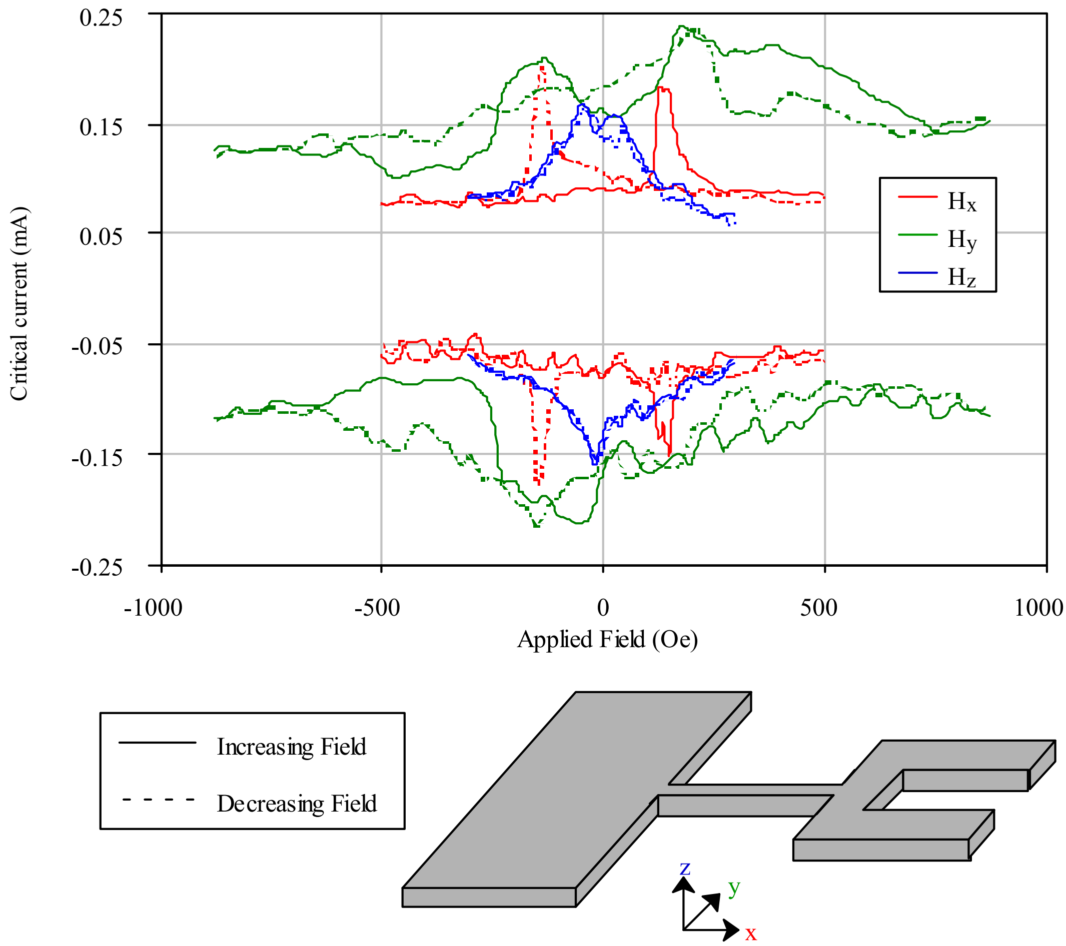

Figure 6·2 Critical current vs. magnetic field measurements for a 10 μm by 1 μm track in a Nb/Co bilayer with (21 ± 7) nm of niobium at 4.2 K. H_x is applied parallel to the track, H_y is in the plane of the film but perpendicular to the track and H_z is perpendicular to the film.

difference between the critical current vs. applied magnetic field curves for increasing and decreasing magnetic field. Rotating the magnetisation of the cobalt layer into the z-direction requires a large amount of energy, and so a high magnetic field. Magnetisation in the z-direction is opposed by both the shape anisotropy, as the free poles at the surface will be very close together, and the magnetocrystalline anisotropy, as the easy direction of the cobalt layer lies in the plane of the film. For an unpatterned 10 mm by 5 mm film at room temperature, an applied field of a few hundred Oersted is sufficient to saturate the cobalt in the plane of the film while a field of 10^4 Oe is not sufficient to saturate the cobalt layer in the z-direction, see figure 6·3. The critical current vs. applied magnetic field in the z-direction roughly follows the typical behaviour of a superconducting track when the critical current is

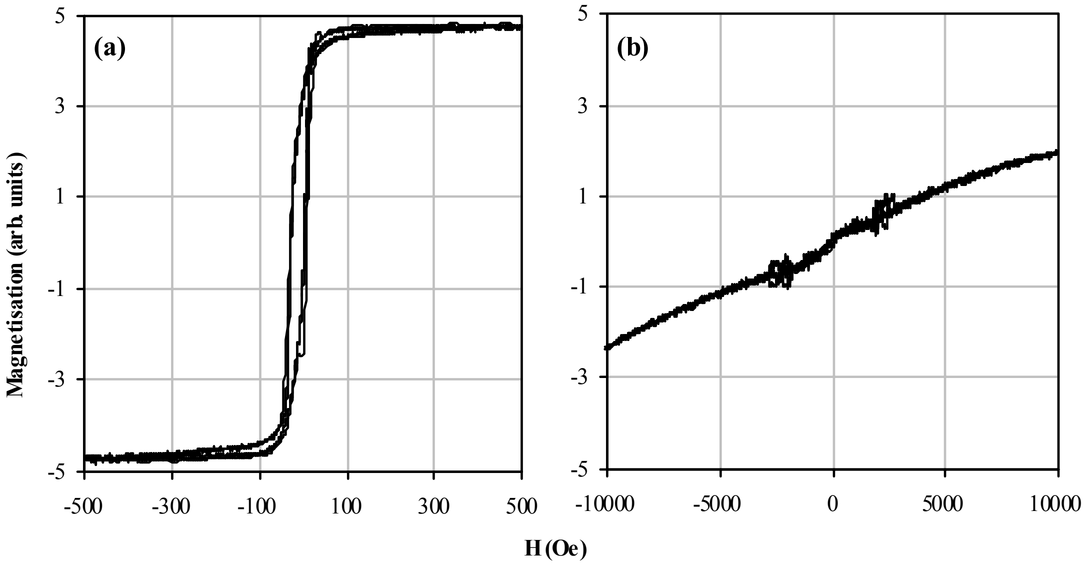

Figure 6·3 Magnetisation hysteresis loops at room temperature for a (52 ± 16) nm thick 10 mm by 5 mm cobalt film with the magnetic field applied:

(a) parallel to the long axis of the film.

(b) perpendicular to the plane of the film.

limited by the motion of flux vortices, as discussed in Chapter 5. As the applied field in the z-direction causes little change in the magnetic structure of the cobalt layer the bilayer behaves as a superconducting film with a suppressed transition temperature and a large number of pinning sites. The small difference between the critical current when increasing and decreasing the magnetic field is probably due to the small component of the magnetic field that is not perpendicular to the plane of the film.

When the magnetic field is applied in the y-direction we observe magnetic hysteresis in the critical current vs. magnetic field measurement. There are two main differences between the critical current vs. magnetic field measurement when the field is applied in the y-direction and when it is applied in the x-direction. The hysteresis extends over a much wider range of magnetic field and the high field critical current, i.e. the critical current at sufficiently large applied fields that there is no hysteresis, is greater when the field is applied in the y-direction. The wider hysteresis reflects that a larger applied magnetic field is required to saturate the cobalt layer. This may be partially due to a change in the shape anisotropy, though this will be a small change as the shape anisotropy is dominated by the component in the z-direction. The magnetic flux tends to flow through the cobalt layer in the electrical connections rather than in the free space between them where the track is. Equally as the features are more widely spaced in the y-direction than in the x-direction, as shown in figure 6·4, any stray field between them will be relatively smaller. This also suggests that the stray field only gives rise to a small component of the hysteretic features in the critical current vs. magnetic field data. Measurement of the magnetic field in the scale model suggests that the reduction in the magnetic field relative to that without the model is approximately 100 Oe. This difference in the magnetic field strength does seem rather small for the difference in the critical current observed in figure 6·2. This will, at least in part, be due to the size of the Hall probe as this averages the magnetic field over an area rather than giving the field at a point. There will also be a contribution from the reduced exchange interaction beneath a domain wall. As the magnetic field is applied across the width of the track the domain walls will also cross the width of the track, linking the spike domains at the edges of the track. The strong magnetocrystalline anisotropy in cobalt means that the domain walls will meander slightly along the length of the track. Thus there can be a path for the additional

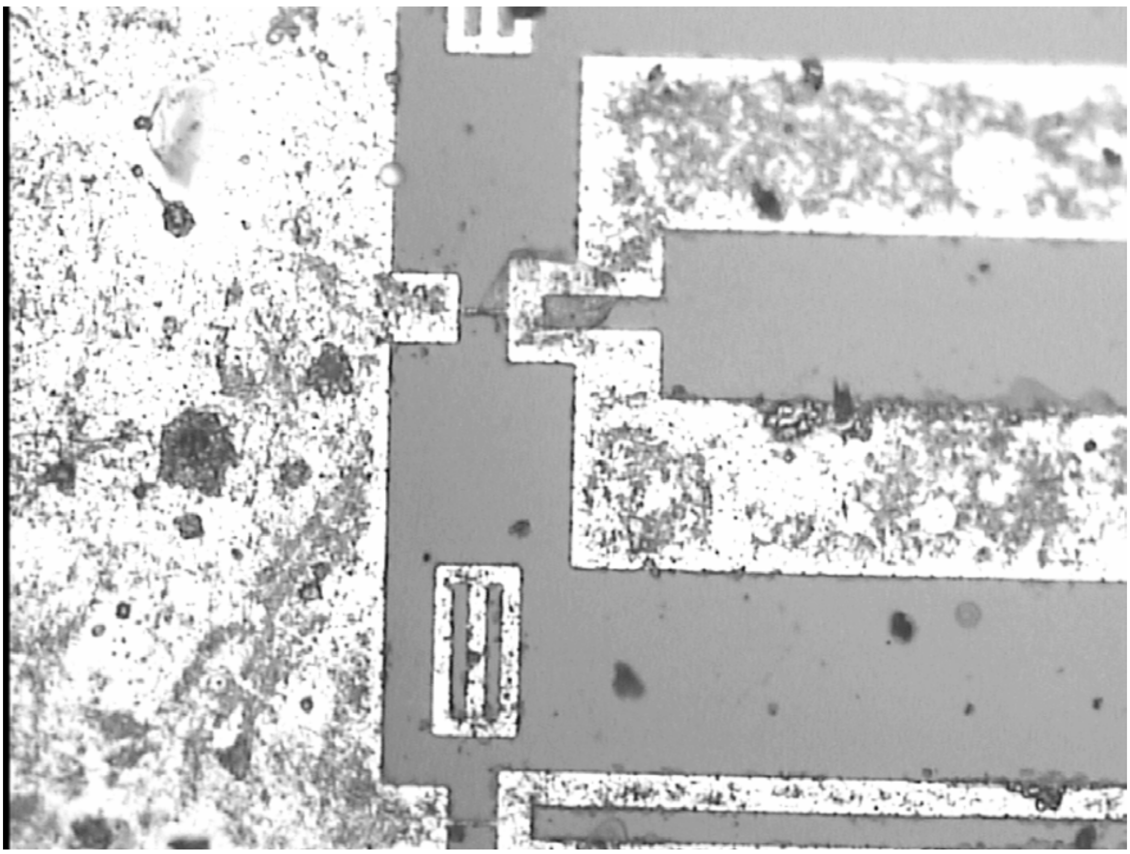

Figure 6·4 Optical micrograph of a one micron wide track and the surrounding patterned Nb/Co bilayer with (21 ± 7) nm of niobium.

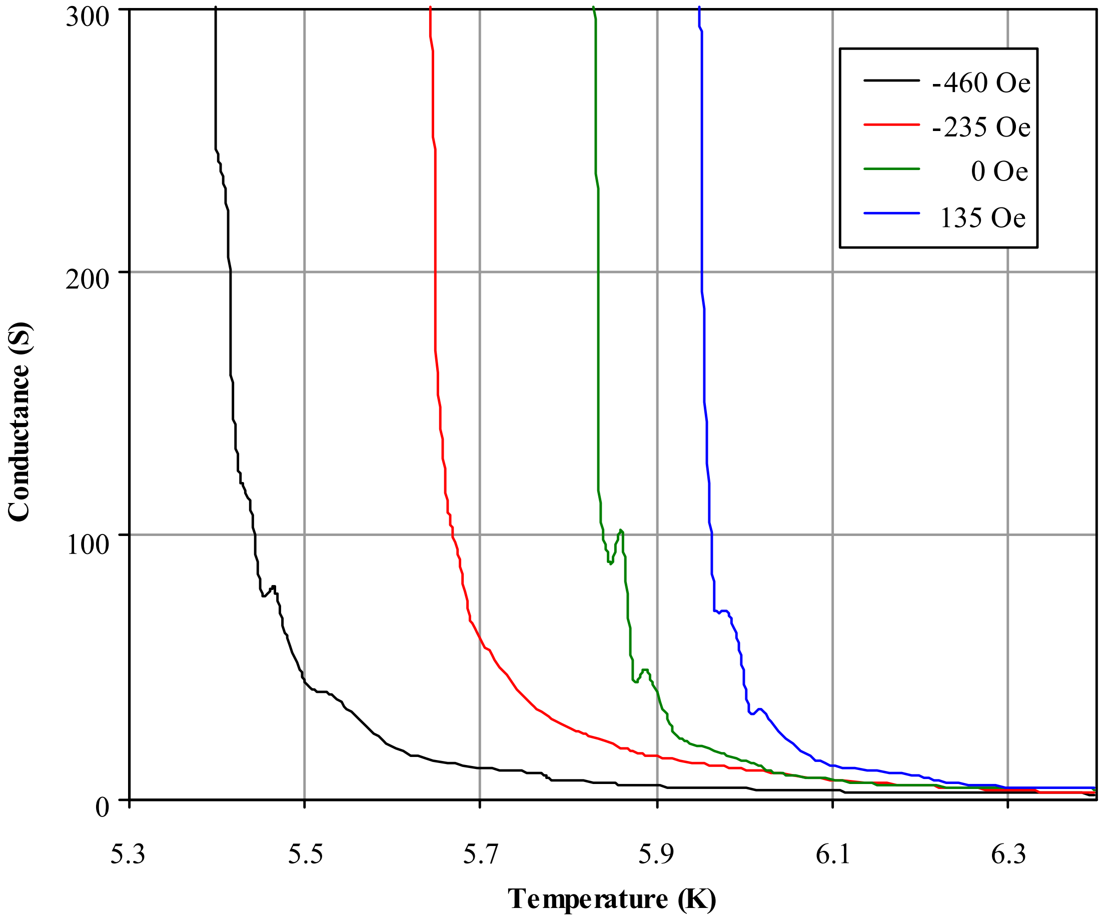

Figure 6.5 Change in conductance at 1μA vs temperature of a 10 μm by 1 μm track in a Nb/Co bilayer with (27 ± 9) nm of niobium with applied magnetic field. The superconducting transition temperature is determined as the temperature at which the conductance goes to infinity. The field was increased from saturation at –460 Oe to saturation at 460 Oe.

critical current along the length of the track. As the local field is significantly smaller than the applied field the domain walls will persist to higher values of applied field than that seen when the field is applied in the x-direction.

Superconducting transition temperature vs. applied magnetic field

The change in the critical current with the applied magnetic field mirrors a change in the superconducting critical transition temperature, as shown in figures 6·5 to 6·7. Unfortunately, due to the experimental set-up, the response of the bilayers to applied magnetic fields above 4.2 K is difficult to measure. Operating the superconducting NbTi coil, which is required to generate a sufficiently strong magnetic field to saturate

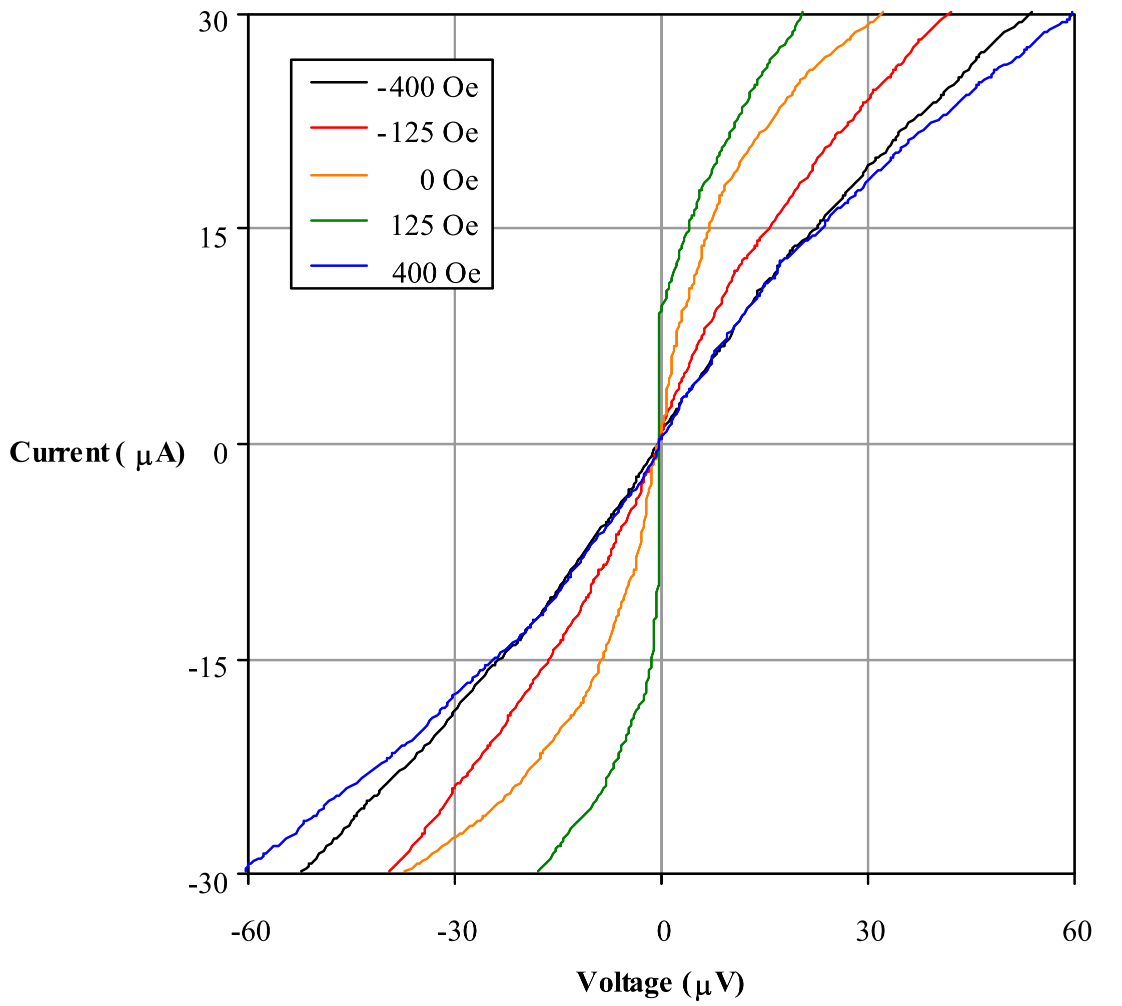

Figure 6·6 IV characteristics of a 10 μm by 1 μm track in a Nb/Co bilayer with (27 ± 9) nm of niobium as a function of applied magnetic field at (6.004 ± 0.003) K. The magnetic field is increased from saturation at -460 Oe to saturation at 460 Oe.

the cobalt layer, when it is not immersed in liquid helium the risk of the generation of a 'hot spot' which causes the NbTi to quench is increased. As the critical current of the bilayer is dependent upon the magnetic history of the cobalt layer the measurement must then be aborted, consequently less data was taken at higher temperatures, see figure 6·10. It can also be difficult to maintain a stable temperature as the current through the system, and so the heat generated, is constantly varying. The superconducting transition temperature changes by at least 0.5 K as the magnetic field is applied to track. This, in turn, means that the application of a few hundred Oersted of magnetic field will cause the transition between the normal and superconducting states when the bilayer is held at a suitable temperature. For this transition the maximum critical current is approximately 20 μA and the maximum

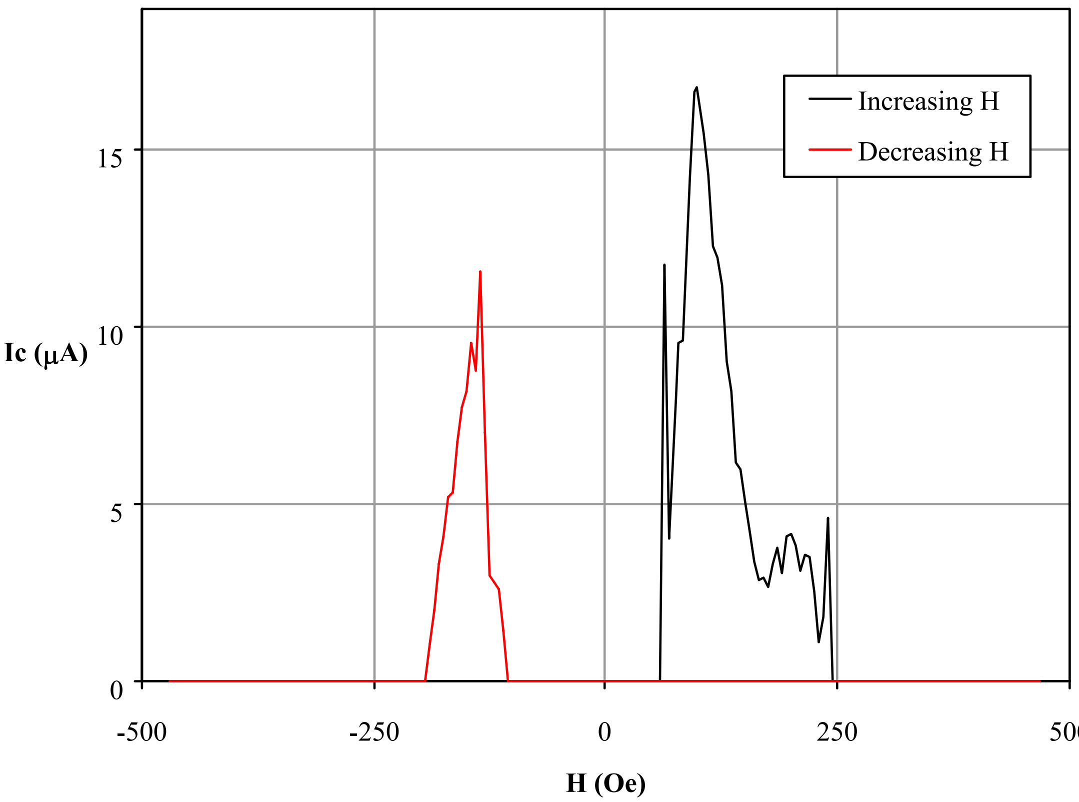

Figure 6·7 Critical current vs. applied magnetic field of a 10 μm by 1 μm track in a Nb/Co bilayer with (27 ± 9) nm of niobium at (6.004 ± 0.003) K. The data has been corrected to eliminate the resistive component caused by the threshold voltage used to determine the critical current.

switching voltage is on the order of 10 μV. While this is signal is sufficient to measure it is still rather small, especially compared to the signal that can be obtained at lower temperatures.

Change in the cobalt structure with temperature

When considering the change in the critical current vs. applied field behaviour of the bilayers it is also necessary to consider what effect the temperature has on the magnetic structure of the cobalt layer. As shown in figure 6·8, an applied field of 500 Oe does not make a 10 mm by 5 mm cobalt film go to saturation when it is cooled below 77 K. The magnetisation hysteresis loop goes round a minor loop which gives rise to a reduced coercive field, as shown in figure 6·9, but an applied magnetic field of 300 Oe is still sufficient to close the hysteresis in the magnetisation loop. If the magnetisation on increasing the field is the same as that when decreasing the field then there will be little difference in the stray field or the number of domain

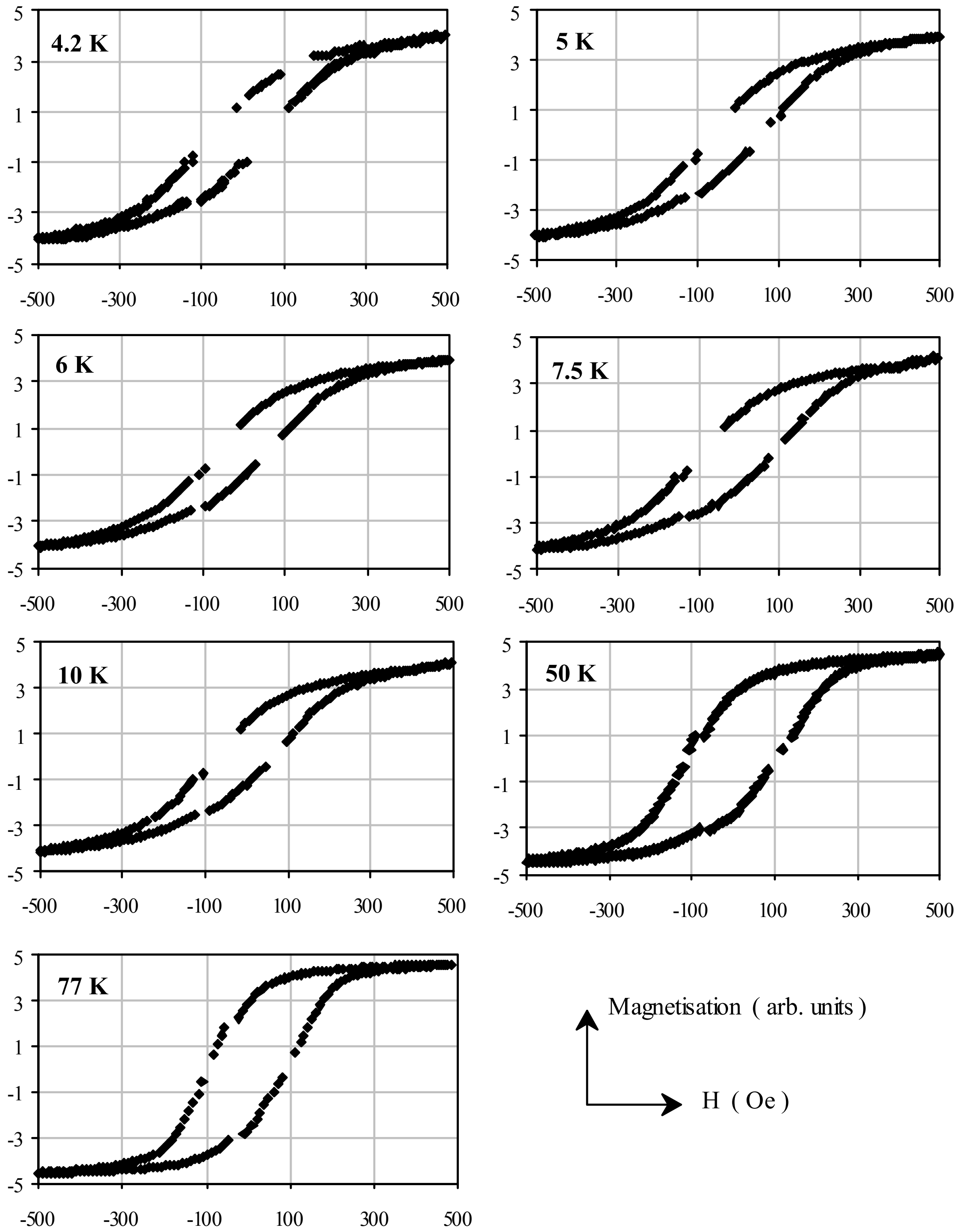

Figure 6·8 Magnetisation hysteresis loops at the temperatures shown for an unpatterned 10 mm by 5 mm Nb/Co bilayer with (27 ± 9) nm of niobium.

walls. As the magnetic field is not sufficient to saturate the cobalt layer there may still be a few domain walls in the cobalt layer. These domain walls could create regions in the superconductor that can carry additional critical current or lead to a slightly reduced stray field. One would expect this effect to be small unless the domain wall happened to bridge the critical region in which case there may be

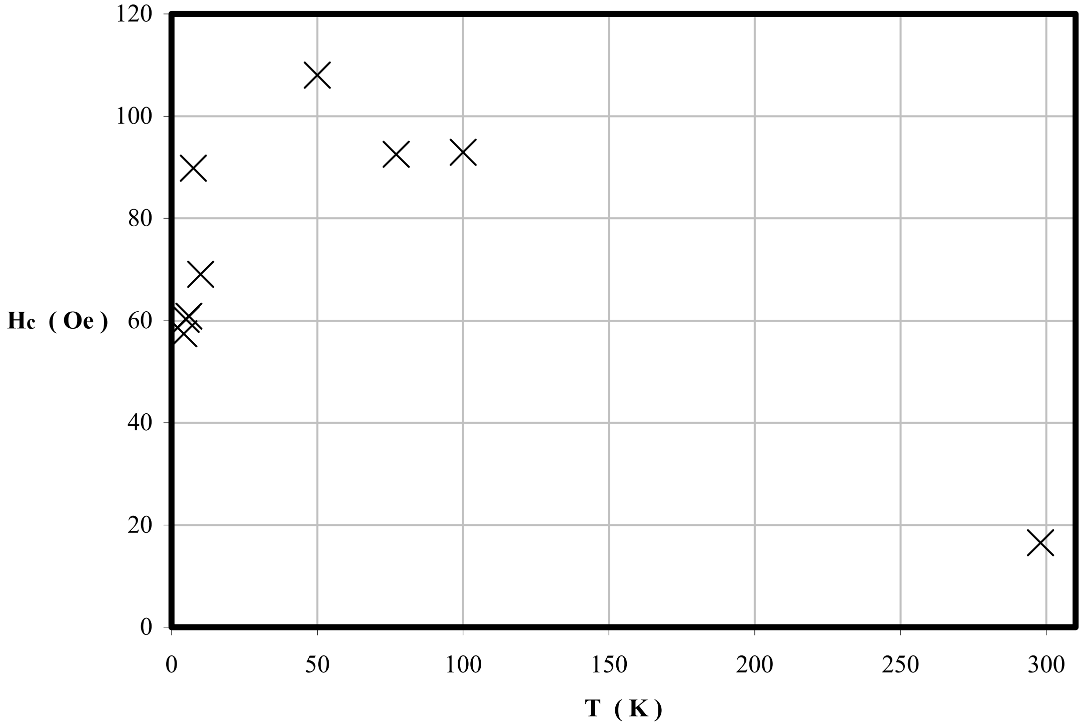

Figure 6·9 Coercive field vs. temperature for an unpatterned 10 mm by 5 mm Nb/Co bilayer with (27 ± 9) nm of niobium.

hysteretic structure at high applied fields. This may be the cause of the hysteresis in the critical current vs. applied field data at 4.2 K in figure 6·10 though, given that the critical current is small, it may also be an artefact of the noise in the system. The coercive field of the cobalt is also sensitive to the temperature of the sample. On cooling the sample there is an initial increase in the coercive field as there is less thermal energy available to overcome the pinning forces on the domain walls so a higher field is required before domains nucleate and grow. For the same reason a higher magnetic field is required to saturate the cobalt layer and eventually the maximum applied field is not sufficient. Again, going round a minor hysteresis loop reduces the coercive field and so there is a reduction in the coercive field of the cobalt layer at low temperatures.

Change in the critical current with temperature

Reducing the temperature of the bilayer increases the critical current of the track, see figure 6·10, increasing both the superconducting gap parameter and reducing the thermal energy available to unpin the flux vortices in the superconducting layer. For data measured at temperatures above 4.2 K the change in the number of measurement points must also be considered. More points taken in the critical current vs. applied field measurement tends to give an increased maximum critical current as there is an increased probability that the true maximum critical current will be measured. Given that fewer points have been taken at higher temperatures, as discussed above, the maximum critical current measured at higher temperature is probably significantly smaller than the true maximum critical current. This will increases the difference between the maximum and high field curves. Interestingly the ratio of the high field critical current to the maximum critical current remains approximately constant at (0.23 ± 0.03) up to 5 K.

The difference between the two critical current vs. temperature curves shown in figure 6·11a can be easily explained in terms of the exchange interaction mechanism. At high applied field the measured transition temperature is that of the track as a whole in that magnetic field but at the coercive field the measured transition temperature is that of the regions beneath the domain walls, where the local exchange interaction is reduced. These two regions will have different transition temperatures and critical fields.

As a test of the stray field model the critical current vs. temperature behaviour of a niobium film in an applied magnetic field was determined. The critical current vs. applied magnetic field behaviour was measured at 4.2 K with a field of -500 Oe to 500 Oe, see figure 5·2b. The critical current vs. temperature behaviour of a 10 μm by 1 μm track in the niobium film was also measured, see figure 6·11b. We assume a linear critical current vs. applied field behaviour and that the upper critical field is proportional to $\left(1-\left(\frac{T}{T_c}\right)^2\right)$, see equations 6·1 below. We also assume that the niobium film has the same high field critical current to the maximum critical current ratio of 5·02 as the Nb/Co bilayer with (27 ± 9) nm of niobium, which is shown in figures 6·10 and 6·11a. We then determine the upper critical field vs. temperature data using the relationship given above and from this we obtain the critical current vs. field data:

$$
\begin{aligned}
H_{c_2}(T) &= H_{c_2}(0)\left[1-\left(\frac{T}{T_c}\right)^2\right]\\
I_c(H) &= I_c(0)\left[1-\frac{H}{H_{c_2}}\right] \qquad (6{\cdot}1)\\
I_c(H,T) &= I_c(0,T)\left[1-\frac{H}{H_{c_2}(0)\left[1-\left(\frac{T}{T_c}\right)^2\right]}\right]
\end{aligned}
$$

As we know the ratio of the critical currents and can extract the upper critical field at absolute zero from the value at 4·2K it is possible to determine the applied magnetic field required to obtain this ratio, 2·25 kOe, and so in turn the curve shown in figure 6·11b

As one would expect, given the calculated value for the maximum magnetic field, the model gives a significantly lower transition temperature at the maximum magnetic field than at zero magnetic field. This model gives a reasonable prediction of the critical current close to 4.2K but then diverges rapidly from the measured data at higher temperatures. In effect the model suggests increasing stray field with decreasing temperature. Although there are a number of assumptions in the model, mainly in the form of the critical current vs. magnetic field, the differences seem too extreme to be simply due to these assumptions. In fact the negative curvature of the critical current vs. magnetic field data for the niobium field would lower the high field transition temperature even further. This suggests that whatever effect causes the difference between the high field and the maximum critical current increases as the temperature is reduced. There will be little if any change in the stray field so this can not provide an explanation for the critical current vs. temperature behaviour at the two applied fields. This behaviour can be explained in terms of the exchange interaction mechanism, the additional critical current will depend upon the decay length of the exchange interaction in the superconductor. A longer decay length gives a smaller critical current in the absence of domain walls as the average exchange interaction in the superconductor will be higher. A longer decay length also increases the volume of the region under the domain wall with a reduced exchange interaction and so increases the critical current at the coercive field. This implies that the decay length

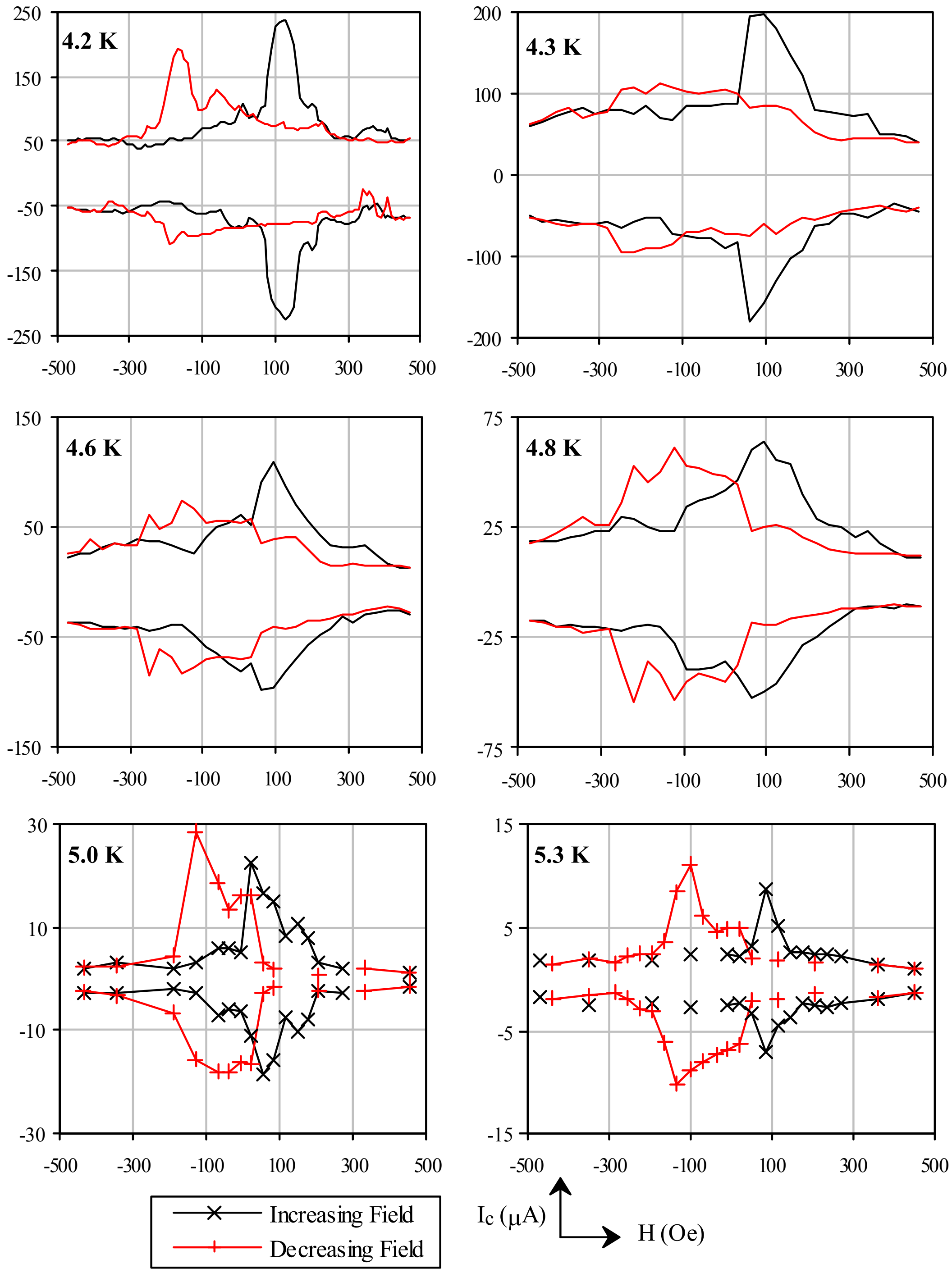

Figure 6·10 Critical current vs. magnetic field measurements for a 10 μm by 1 μm track in a Nb/Co bilayer with (27 ± 9) nm of niobium at various temperatures. The vertical axis gives the measured critical current in microamps and the horizontal axis gives the applied field in Oersted.

increases as the temperature is reduced and so the exchange interaction mechanism probably depends upon the diffusion of quasiparticles through the superconductor. We also see how much the critical current can change on repeated sweeps of the magnetic field, a consequence of the sensitivity of the exchange interaction mechanism to Barkhousen noise.

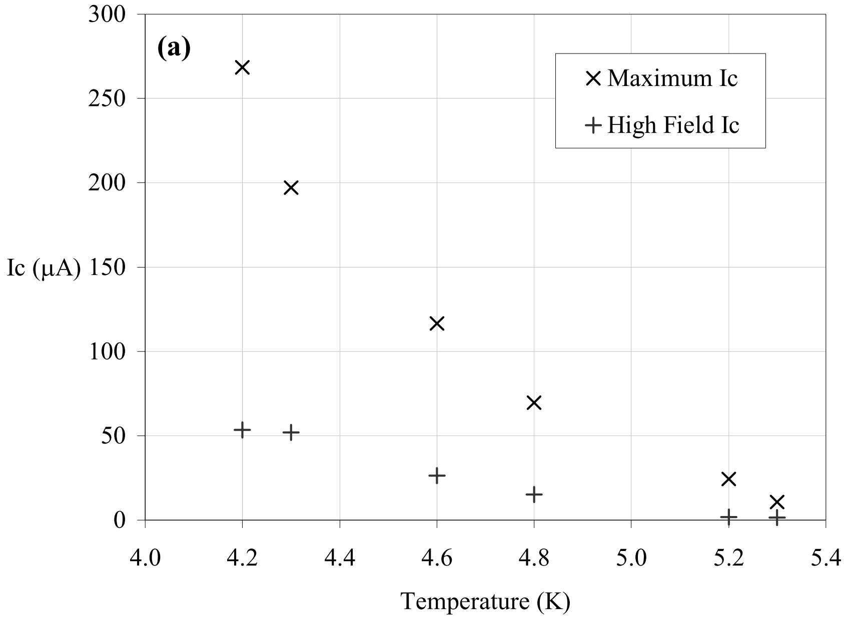

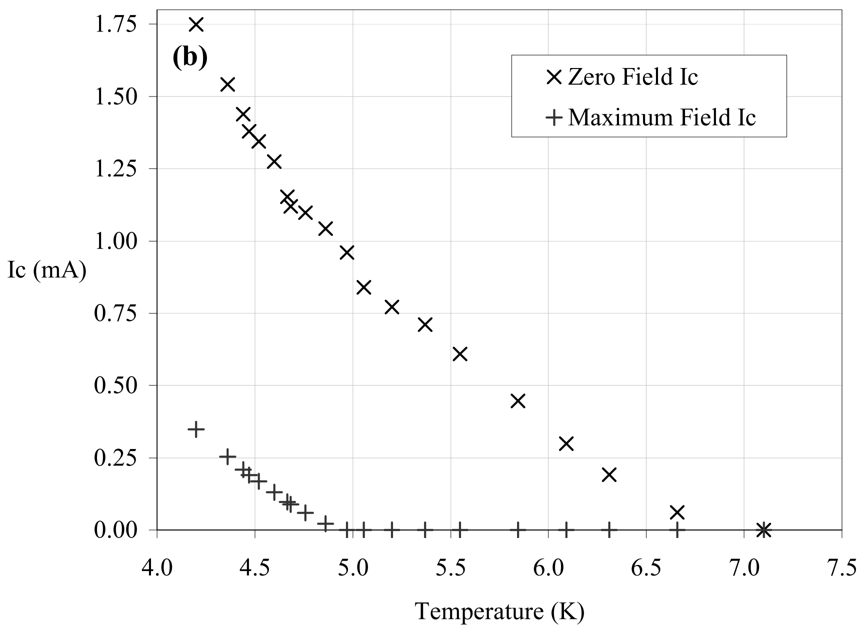

Figure 6·11 (a) Critical current at the coercive field and saturation of the cobalt layer vs. temperature for a 10 μm by 1 μm track in a Nb/Co bilayer with (27 ± 9) nm of niobium.

(b) As deposited critical current vs. temperature for a 10 μm by 1 μm track in a (18 ± 5) nm thick niobium film with the extrapolated high field data also shown.

STRUCTURAL CHANGES

In this section we compare the critical current vs. applied magnetic field behaviour of tracks with different structures. We begin by discussing changes in the width of the track, both the true width of the track and the importance of localising the measurement to a small area of the film. We then discuss changes in the niobium layer thickness and the cobalt layer thickness and conclude by replacing the cobalt with iron.

Track width

The width of the track in the niobium/cobalt bilayer can have a significant effect on both the magnitude and form of the change in critical current with applied magnetic field. Given that the domain size will be unchanged, a wider track would contain more domain walls, giving rise to an increased critical current by the exchange interaction mechanism. The local magnetic field would tend to be slightly stronger in the niobium layer of a wider track due to the change in the shape anisotropy. This change is dependent upon any change in the shape anisotropy and so would be small as the shape anisotropy is dominated by the thickness of the cobalt layer. In both cases the difference between the high field and maximum critical currents would be increased, even if only by a little. Equally in a wider track the effect of stray field at the edge of the track would become less significant and, as discussed in chapter 5, this is one cause of behaviour other than the 'double peak' structure in the critical current vs. applied field measurement. Thus one would expect the 'double peak' structure to be a stronger component of the critical current vs. applied field measurement as the track width increases.

Localising the measurement area

When we compare the critical current vs. applied field measurements for one micron wide tracks with those from two micron wide tracks we see significantly different behaviour, the one micron wide track giving a stronger 'double peak' structure. These differences, which can be seen by comparing figure 6·12b with figure 6·10 or figure 5·14, are not an obvious consequence of either model of the 'double peak' structure. We do find that the behaviour of the critical current vs. applied field measurements with track width is closer to that expected from the models, as given above, if the bilayer is patterned by lift-off rather than by ion milling. As discussed in

Chapter 4 lift-off tends to give a track with a rougher edge than that of a track produced by ion milling, see figures 6·14 and 6·21 for a direct comparison. It seems that the roughness of the edge of the track relative to the track width, rather than the track width, is the important parameter for giving a strong 'double peak' structure. If

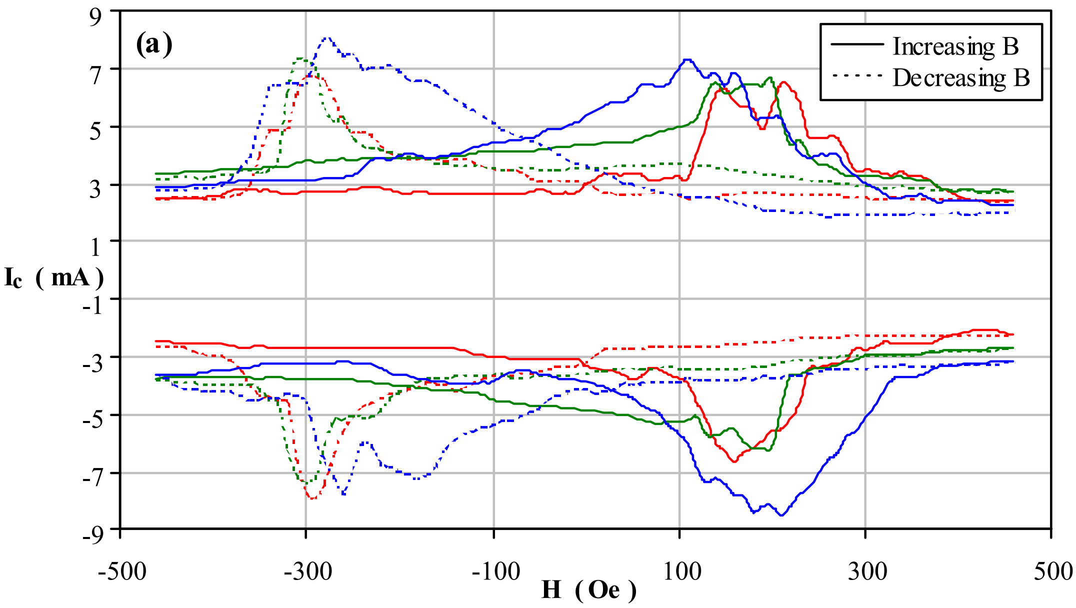

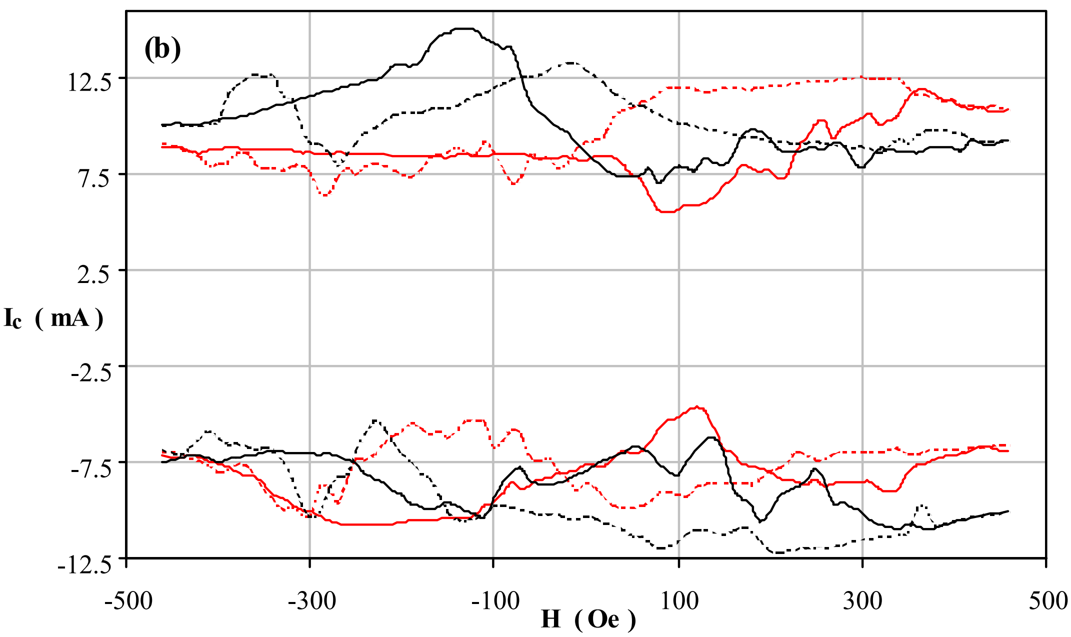

Figure 6·12 Critical current vs. magnetic field measurements for a 10 μm by 2 μm track patterned in a Nb/Co bilayer with (65 ± 22) nm of niobium by ion milling. The three tracks shown in (a) have a 500 nm long and 1 μm wide constriction cut in the track with the FIB while both tracks shown in (b) were as deposited. The pattern used for these measurements is shown in figure 6·13.

we assume that the variation in the track width, effectively the roughness of the edge of the track relative to the track width, is constant across each patterned film then the percentage change in the track width will be larger for a narrower track.

One possible explanation for the difference in the critical current vs. applied field behaviour of the two track widths is that the behaviour varies along the length of the track. Given there was a region of the track that was significantly narrower than the rest then this region would be the first to develop a potential difference across it even at the coercive field. The variations in the track width could create this natural constriction, localising the critical region to a specific short region of the track. In the

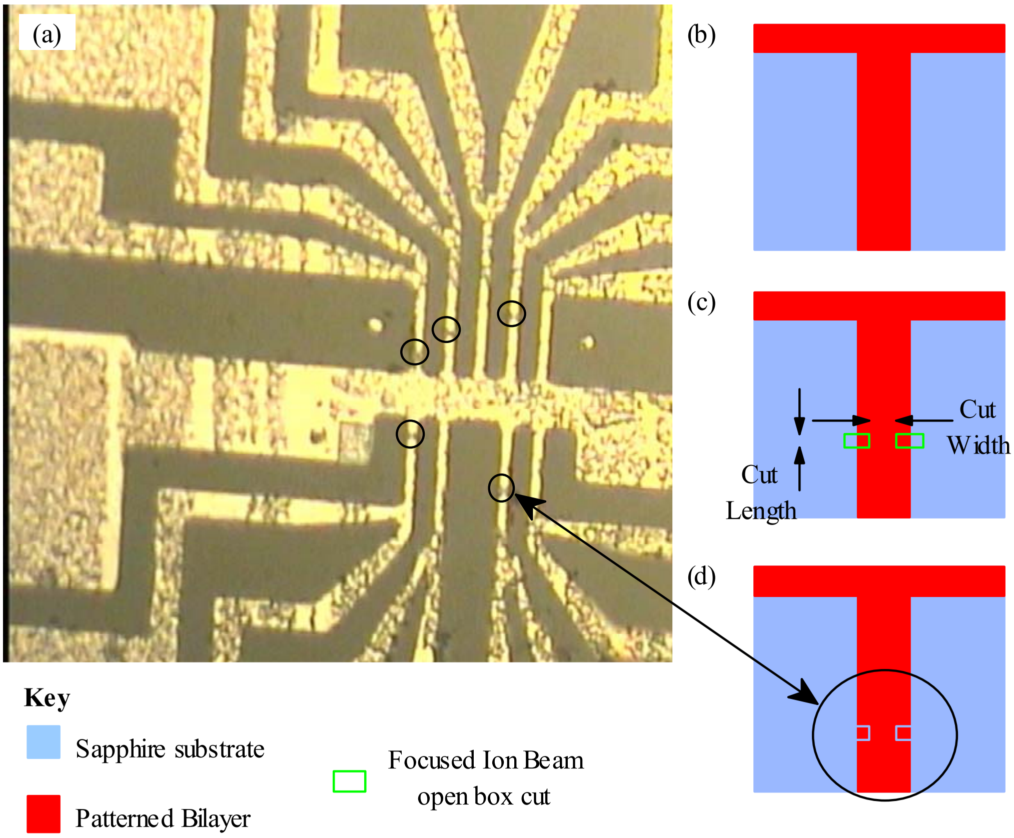

Figure 6·13 a) Optical micrograph of in a Nb/Co bilayer with (65 ± 22) nm of niobium patterned into 10 μm by 2 μm tracks, some of which have been further patterned in the FIB with a 500 nm long and 1 μm wide constriction. The constrictions have been encircled so they can be more easily seen. The surface of the film has deteriorated after approximately a year in the atmosphere.

b to d) Schematic of the patterning process in the FIB showing the uncut in part (b) and the cut track in part (d).

absence of a significant constriction the measured critical current would depend upon the minimum critical current along the whole length of the track rather than just in the constriction. Thus if the critical current vs. applied field behaviour varies along the length of the track then even when the critical current increased in one region to give the 'double peak' structure then it could remain small in another region and so the measured critical current will remain small. Given a range of constrictions along the track with similar critical currents then the stray field or domain walls would cause the critical region to move between constrictions as the magnetic field changes. This would distort the simple 'double peak' structure with other smaller peaks, giving rise to confused critical current vs. applied field behaviour. If the relative change in the track width is small then it is unlikely to give a significant constriction, as in the two micron wide track. In order to test this hypothesis the tracks in the bilayer were further patterned with the focused ion beam (FIB).

The FIB was used to cut a constriction into the two micron wide tracks, as shown in figure 6·13. The first region to go normal, due to the critical current density being exceeded, will lie within the constriction. This mimics the affect of natural variations in the track width. The track was narrowed to one micron in width for a length of half a micron using open boxes in order to minimise any change in the magnetic structure of the cobalt layer. The trench produced by the FIB is only 20 nm wide, less than half the thickness of the cobalt layer. Measurement on a scale model gives an increase in the local magnetic field of only 50 Oe at the niobium layer when the cut is perpendicular to the field and a reduction in the local field of almost 200 Oe when the cut is parallel to the field. Of course this doesn't take the crystallites and domains into account, which would have a significant affect at this length scale but it does imply that any stray field produced by magnetic poles at the free surfaces would not spread out of the cut. Thus one would not expect any significant change to be created in the stray field by introducing the FIB cuts to create the constriction. Any magnetic field that does intersect the niobium within constriction will do so at the side of the track and so would not give rise to the 'double peak' structure, as discussed in chapter 5. This implies that the change in the critical current vs. magnetic field behaviour on creating a constriction, shown in figure 6·12, is purely due to the presence of the constriction in the track rather than any distortion in the local magnetic field caused by variations in the track width. The high field critical current for the tracks without a constriction is also approximately twice that when there is a constriction which also implies that the local magnetic field is not changed by the FIB cuts.

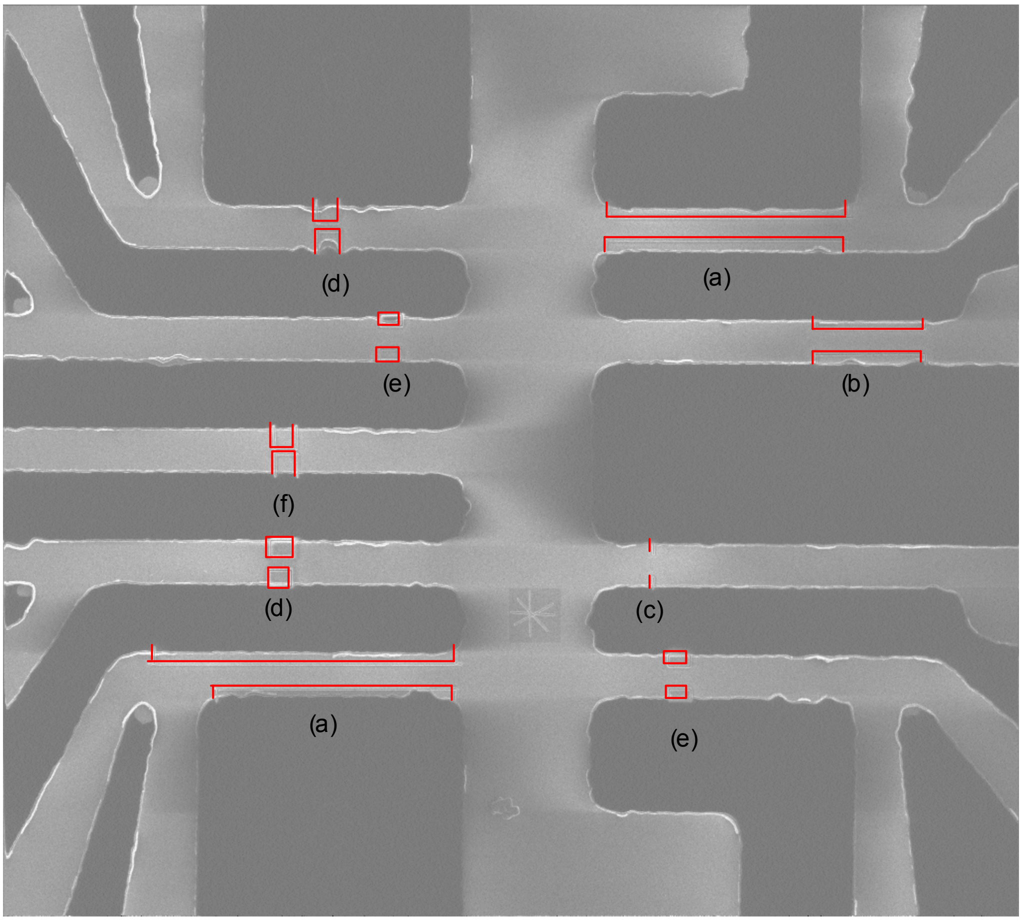

Figure 6·14 Scanning Electron Micrograph of a patterned Nb/Co bilayer with (65 ± 22) nm of niobium showing the additional FIB patterning. The FIB cuts are highlighted in red. Note that most of the contrast within the tracks is the result of magnetic contrast. The stray magnetic field from the cobalt layer bends the secondary electrons used to image the surface away from the detector.

The cuts reduce the track width as follows:

(a) along the whole length to 1 μm wide.
(b) 1 μm wide for 5 μm length.
(c) 1 μm wide for 20 nm length.
(d) 250 nm wide for 1 μm length.
(e) 1 μm wide for 1 μm length.
(f) 100 nm wide for 1 μm length

A possible explanation for the change in the critical current vs. magnetic field behaviour on adding a constriction is that the behaviour observed in the two micron wide track is due to multiple 'double peak' structures at different magnetic fields. The critical current of the track is due to the minimum critical current of each region along the length of the track. The critical current vs. applied field data shown in figure 6·12b appears to be due to two 'double peak' structures. This can be most easily understood in terms of the critical current being reduced from the maximum, either by increased stray field or a decrease in the number of domain walls. At different fields the critical current goes to a minimum in different places, giving rise to two pairs of peaks. The affect of variations in the critical current across the width of the track as well as the length will also be minimised by the constriction as it means that the critical current of a limited volume is measured. Further experiments were performed to test this interpretation. The length and width of the constriction created in the two micron wide tracks was varied between tracks, as shown in figure 6·14, giving the critical current vs. applied field measurements shown in figure 6·15. Simply narrowing the whole track to a width of one micron does not give rise to a strong 'double peak' structure while a shorter constriction does. Different constriction widths and lengths give rise to different peak heights in the 'double peak' structure. The five micron long by one micron wide constriction gives the smallest peaks as well as showing a significant difference in the high field critical current on reversing the magnetic field direction. This difference in the high field critical current, although smaller, can also be seen in the critical current vs. applied field data given by the other constrictions though it is smallest for the one micron by one micron constriction, which also shows the largest peaks.

Given that there are variations in the thickness of the niobium layer in the track one would expect different degrees of change caused by the stray field. A thicker region of niobium will have a higher superconducting transition temperature, figure 6·23 shows that a difference of a single nanometer in the thickness can give a significant change in T_c. These thicker regions will carry a larger proportion of the critical current density, however one would not expect that these regions would switch at different applied fields. Thus the combination of multiple 'double peak' structures with significantly different behaviour at a given magnetic field can not easily be explained using the stray field model.

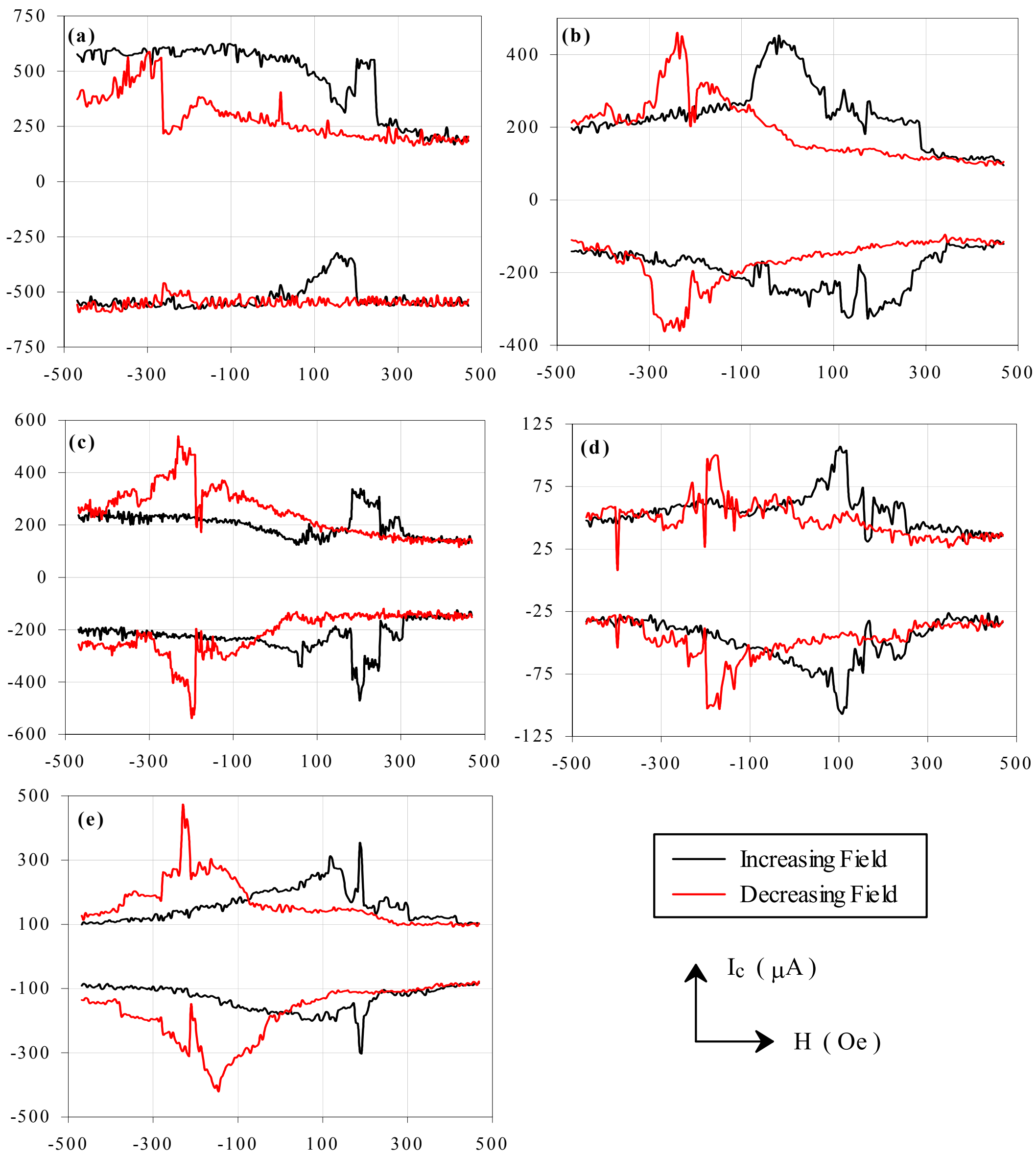

Figure 6·15 Critical current vs. magnetic field measurements for a 10 μm by 2 μm track in a Nb/Co bilayer with (65 ± 22) nm of niobium at 4.2K. The tracks were further patterned with constrictions using the FIB as shown in figure 6·14:

(a) along the whole length to 1 μm wide.
(b) 1 μm wide for 5 μm length.
(c) 1 μm wide for 20 nm length.
(d) 250 nm wide for 1 μm length.
(e) 1 μm wide for 1 μm length.

This behaviour can be explained using the exchange interaction model, where additional critical current is carried by the regions of niobium beneath the 180°

domain walls in the cobalt layer as the exchange interaction goes to a minimum in this region. The peak in the critical current occurs when a domain wall travels across the entire critical region, the critical region being the first to become normal due to excess current, which will lie within the narrowest constriction. A wider track will have a larger number of domains and so it is possible that the domain configuration will be suitable to give an increased critical current at more than one value for applied magnetic field. This would give rise to a critical current vs. applied field that is the sum of more than one 'double peak' structure. In effect there is a network of channels beneath the domain walls through which additional critical current can flow but unless there is a route by which this additional critical current can cross the critical region the total current carrying capacity does not change.

The percolation model

We describe this web of channels carrying additional critical current as the percolation model. An analogy can be drawn with the percolation of critical current between grains in a polycrystalline cuprate superconductor. In a polycrystalline superconductor the grain boundaries can carry a lower critical current density than the material within the crystallite. The critical current density of the grain boundary depends very strongly upon the angle between identical crystal axes in the two crystallites (a) and (b), i.e. the angle between $[100]_a$ and $[100]_b$. The smaller this misorientation angle is the larger the critical current across the grain boundary, with the critical current falling off as the misorientation angle increases. Thus the critical current of the polycrystalline superconductor will be large only if there is some path across it where the critical current only needs to flow through low angle grain boundaries, even if this requires the local current to flow in the opposite direction to the bulk current. The main differences between the case in a polycrystalline superconductor and that due to a web of domain walls is that the grain boundaries act as a limit rather than providing a channel for additional the critical current and the web of domain walls changes with the magnetic field. This is essentially the same model as the 'honeycomb' of superconductivity on domain walls used to explain the combined superconducting and ferromagnetic properties of a dilute solid solution of rare earth elements in superconductors [Matthias 1960]. Percolation of critical current has been extensively studied as it is the key problem in producing long lengths of high-T_c superconducting material [Dimos 1990, Šmilauer 1991, Rutter 2001].

Unfortunately it is not possible to directly apply these models to the web of domain walls as the details of the additional critical current carried in the regions beneath the domain walls are unknown. There are also a number of additional effects to be taken into account, see Chapter 5.

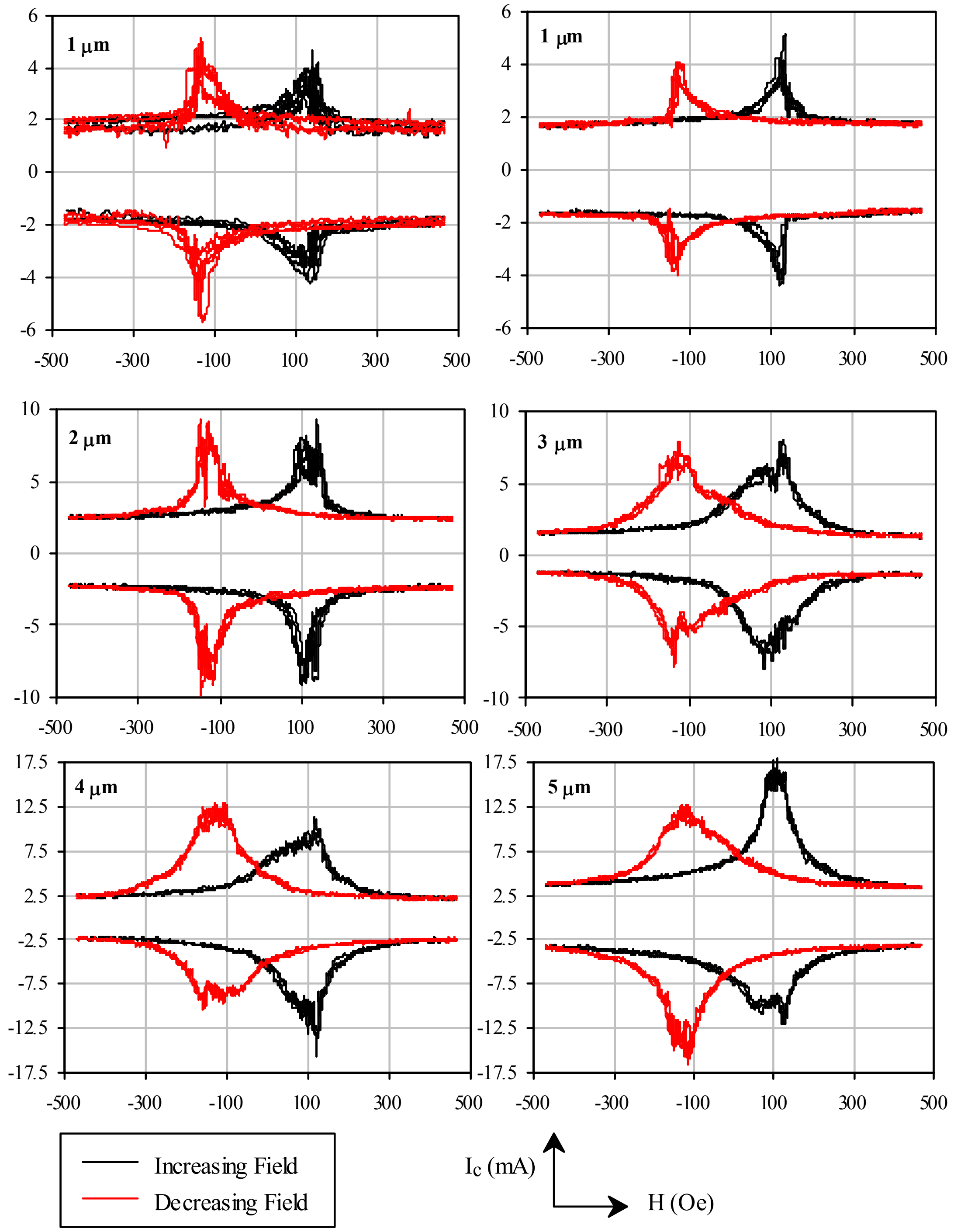

Figure 6·16 Critical current vs. applied field for a 10 μm long track with the width shown in a Nb/Co bilayer with (65 ± 22) nm of niobium patterned by lift-off.

The percolation model provides an interpretation for the results for various lengths of constriction. For an increase in the critical current there must be a percolation path that crosses the critical region. As this is a statistical process a long constriction means that the formation of a channel with additional critical current carrying capacity across the entire length of the critical region is far less probable. Thus the 'double peak' structure becomes a much smaller component of the critical current vs. applied field behaviour.

Changes in track width

As lift-off processing of the bilayer gives rise to 'natural' constrictions in the track that are capable of localising the critical region we have used this method to produce a range of track widths which give the 'double peak' structure without the need for further processing, see figure 6·16. One would expect that the critical current would double when the width of the track was doubled. The change in the shape anisotropy would give a small change in the local field but this would only cause a small change in the scaling of critical current with width. In fact, as shown in figure 6·18, the high

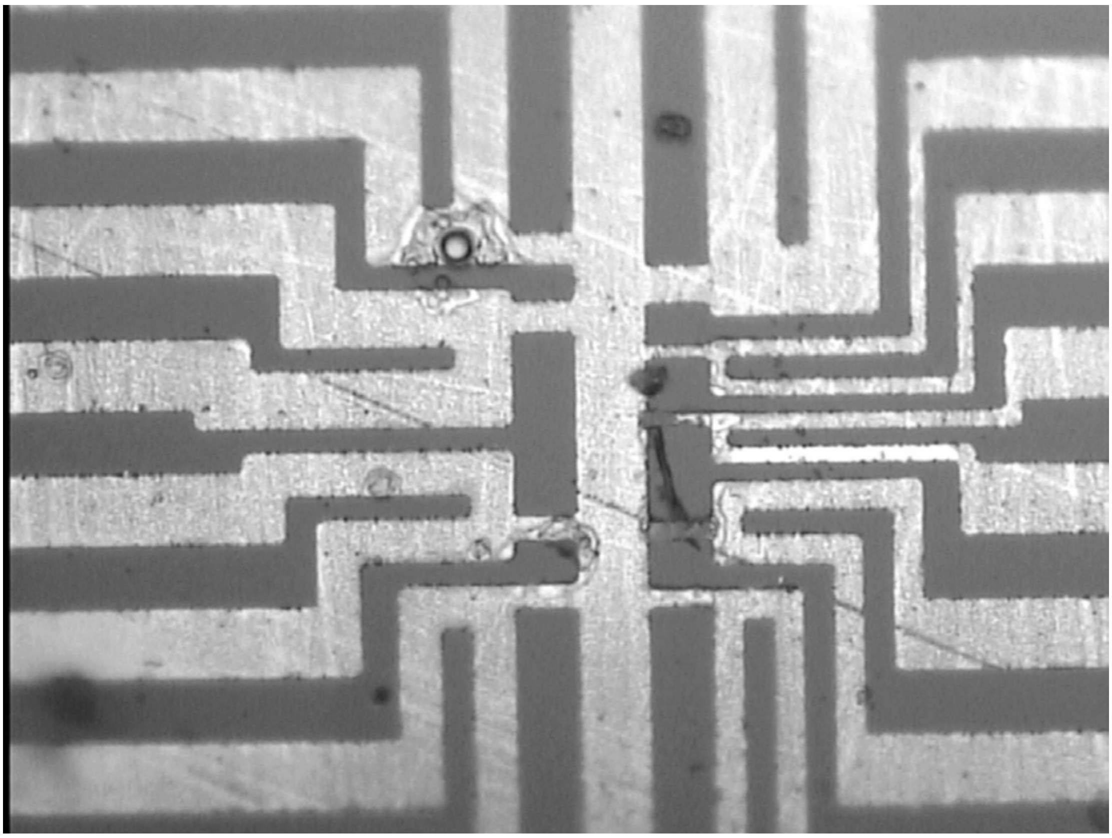

Figure 6·17 Optical micrograph of the patterned Nb/Co bilayer with (52 ± 16) nm of cobalt on (65 ± 22) nm of niobium.

field critical current increases far more slowly with width than one would expect it to, though the maximum critical current does appear to scale as expected. The magnitude of the difference implies that the edge of the track carrying the majority of the critical current in the high field case. This can be understood in terms of the exchange interaction mechanism due to the pinned 'spike' domains at the edge of the track. In a thin film the 'spike' domains tend to persist even when the rest of the film has been saturated and so there are domain walls at the edge of the track even at the high field and so the edge of the track will carry additional critical current. This can also be the case for the maximum critical current, as shown in figure 6·19, though the maximum critical current is also very sensitive to other effects. The number of domain walls in the critical region is very sensitive to the applied field and so may go to a maximum at a magnetic field value that is intermediate between the field values for which the critical current was measured. Equally, as the domain walls meander along the track, there may be a large number of walls, and so a high critical current, in the critical region even if the track is narrow. The stray field at the edge of the track can also act to suppress the critical current in the peak. This can give significant variation from

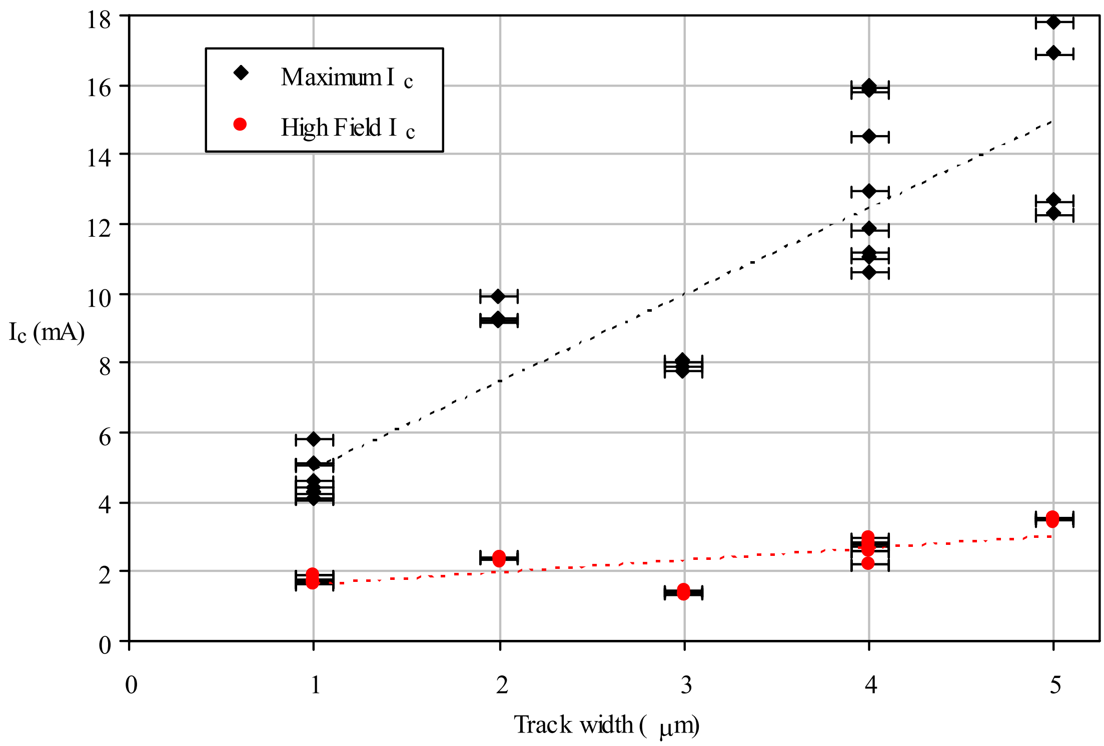

Figure 6·18 Maximum critical current and high field critical current vs. track width for a 10 μm long track in a Nb/Co bilayer with (65 ± 22) nm of niobium patterned by lift-off.

the linear regression shown in figures 6·18 and 6·19.

The width of the peaks in the 'double peak' structure can also provide information. We measure the peak width using the full width at half maximum (FWHM). The stray field mechanism would give the same FWHM regardless of the track width, with small variations for the shape anisotropy, as the critical current depends upon the magnetisation of the cobalt layer. When the magnetisation reaches half the saturation value the stray field will be half the maximum value. Thus the form of the critical current vs. applied field peak will remain the same regardless of the maximum critical current. The exchange interaction mechanism gives a different result. In a wider

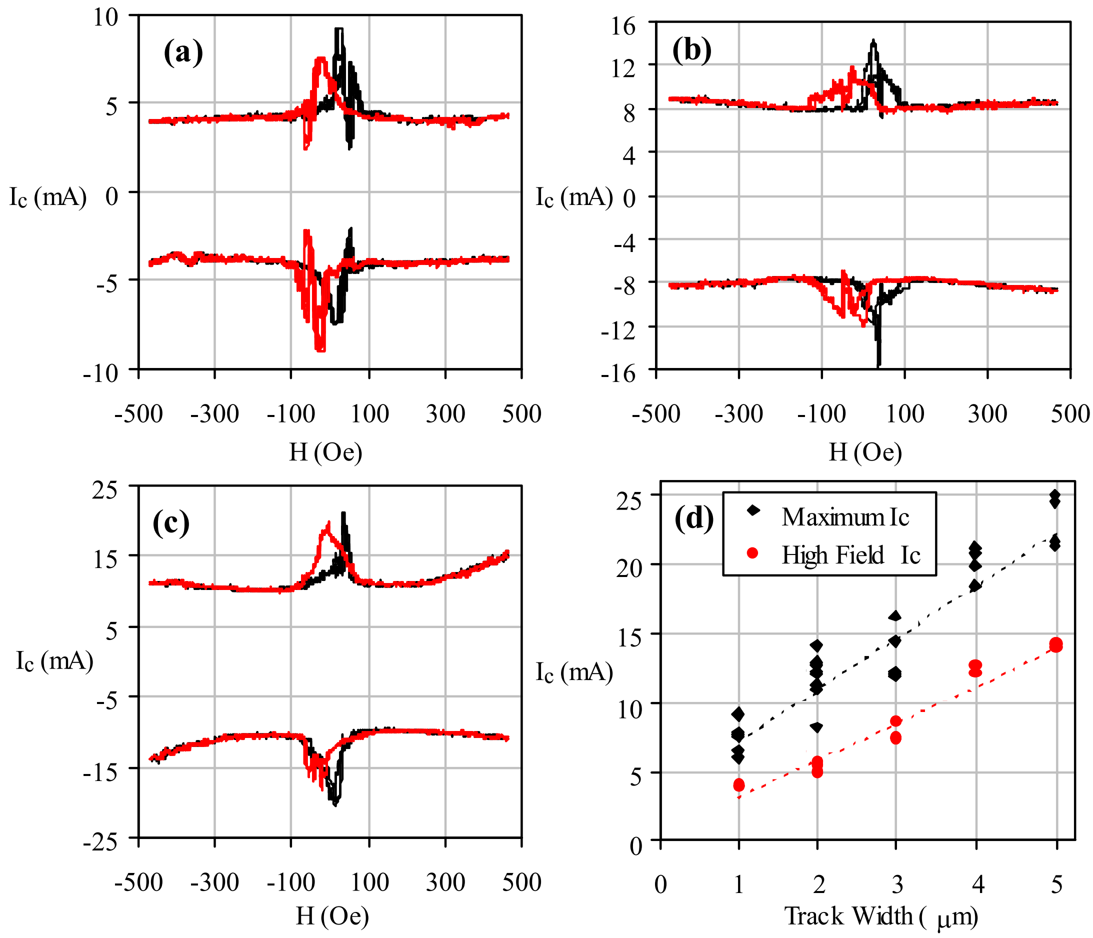

Figure 6·19 Critical current vs. applied field for a 10 μm long track with the width given below in a Nb/Co bilayer with (49 ± 16) nm of niobium patterned by lift-off.

(a) One micron wide track.

(b) Three micron wide track.

(c) Four micron wide track.

(d) Maximum critical current and high field critical current vs. track width.

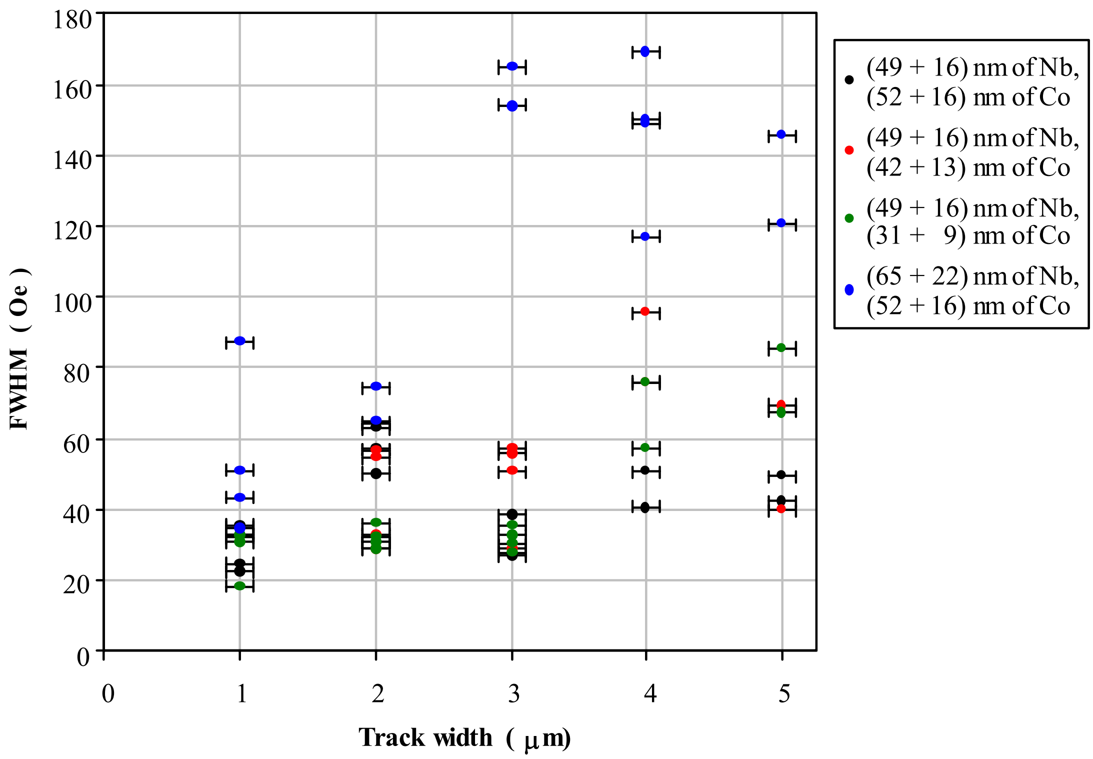

Figure 6·20 Full Width at Half Maximum vs. track width for the total critical current vs. applied field measurements at 4.2 K on Nb/Co bilayers patterned by lift-off with the layer thickness given in the legend.

track the probability of a domain wall in the critical region, at any field, increases, as does the probability that the domain wall will be one that persists to higher magnetic field. Thus the exchange interaction mechanism explains the trend, shown in figure 6·20, for the FWHM to increase with increasing track width.

Thinning the niobium layer

It is possible to introduce a constriction in the superconducting layer without changing the magnetic structure of the cobalt layer by depositing the cobalt layer on the substrate first and then depositing the superconducting niobium on the cobalt to give a Co/Nb bilayer. The niobium can then be selectively thinned with the FIB to give a constriction, as shown in figure 6·21. The thickness of superconducting niobium left after the trench has been cut is less than the total thickness of niobium minus the thickness milled away as the upper surface of the bilayer is contaminated with gallium from the ion beam. The gallium atoms implant to an average depth of 11 nm into the niobium and cause a significant reduction in the order parameter of the surrounding niobium [Moseley 2000]. The niobium layer thicknesses given for figure 6·22 must be modified to take this into account. The room temperature magnetisation hysteresis loop for the unpatterned 10 mm by 5 mm Co/Nb bilayer is very similar to the loops for Nb/Co bilayers. We can assume from this that the structure of the cobalt layer is essentially unchanged by the order of deposition, see figures 6·22e and 6·30. There may be some additional pinning of domain walls in the Co/Nb bilayer as the cobalt no

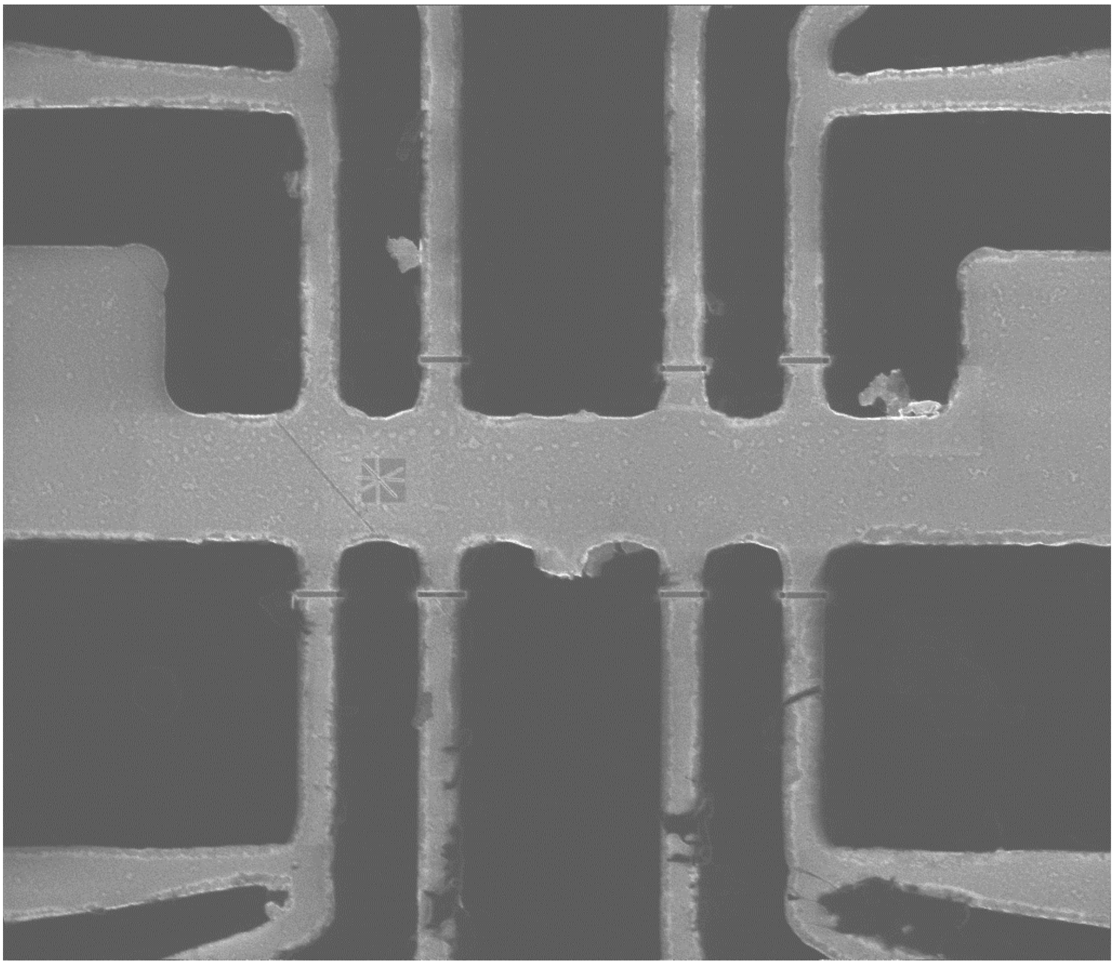

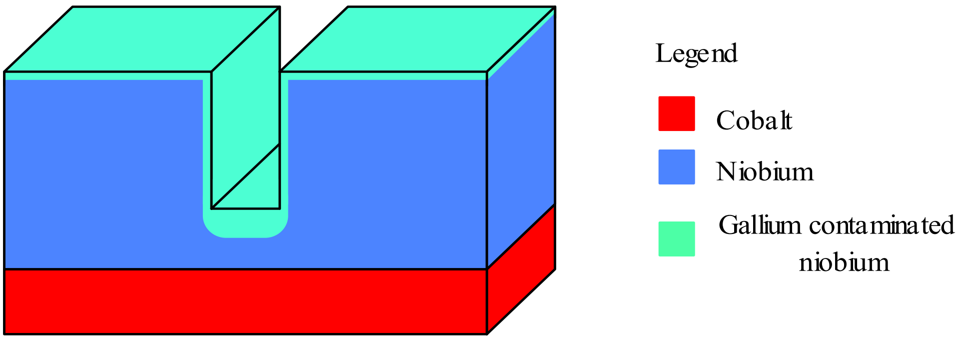

Figure 6·21 Scanning Electron Micrograph of a Co/Nb bilayer with (200 ± 10) nm of niobium on (47 ± 14) nm of cobalt patterned by lift-off, showing the additional FIB patterning. Note that most of the contrast within the tracks is the result of magnetic contrast. A schematic of the trench cut in the track with the FIB is also shown.

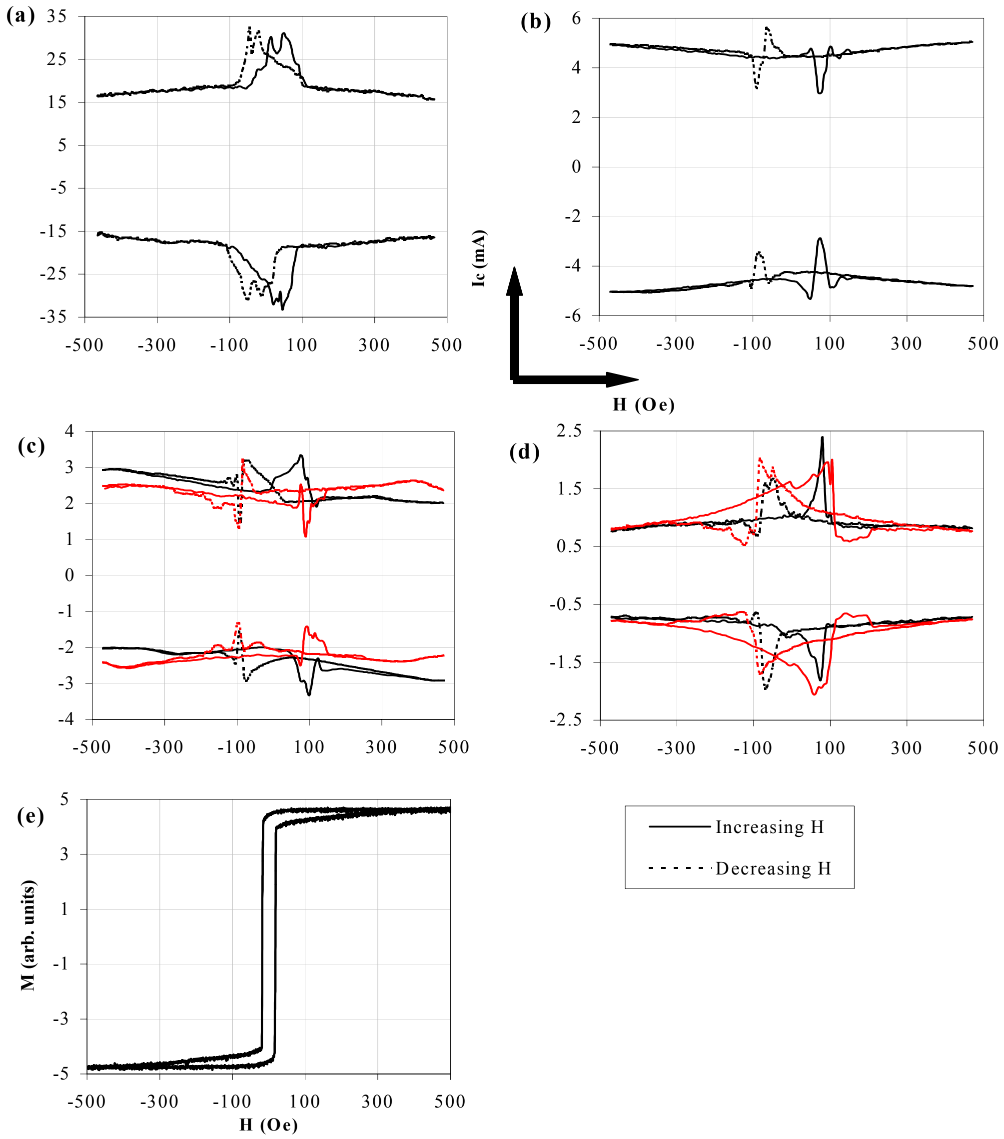

Figure 6·22 Critical current vs. applied magnetic field measurements for 10 μm by 2 μm tracks in niobium on cobalt bilayers with (200 ± 10) nm of niobium and (47 ± 14) nm of cobalt patterned by lift-off. The tracks have had a 500 nm wide trench cut across the track, as shown in figure 6·21, reducing the thickness to:

(a) no trench cut in the niobium.

(b) 50 nm of niobium.

(c) 40 nm of niobium. Note that the response of two tracks is shown.

(d) 30 nm of niobium. Note that the response of two tracks is shown.

Part (e) shows the room temperature magnetisation hysteresis loop of the unpatterned 10 mm by 5 mm Co/Nb bilayer.

longer has a free surface. However the critical current vs. applied field data for the as deposited track, shown in figure 6·22a also suggests that the magnetic structure of the cobalt layer in a Co/Nb bilayer is very similar that in a Nb/Co bilayer.

Forming a constriction in the track by thinning the niobium layer does not give rise to a strengthening of the 'double peak' structure, even when scaled with respect to the high field critical current. This is true regardless of the method used to thin the superconducting layer, either directly using the FIB or by removing the niobium in an area defined by the FIB using reactive ion etching. See Chapter 4 for a discussion of these methods. In fact there appears to be an increase in the suppression of the critical current due to stray field from the side of the track. This can be understood as the supercurrent must be flowing closer to the cobalt layer when there is a constriction where the stray magnetic field is stronger. The change in the peak height as the niobium is thinned does not give any evidence in favour of the exchange interaction model or the stray field model for the 'double peak' structure as the affect of both decreases with distance from the cobalt layer. The fact that this method of forming a constriction increases those components of the critical current vs. applied field behaviour other than the 'double peak' structure makes this method of limited utility.

Changing the niobium layer thickness

The niobium layer thickness has a very strong influence on the critical current vs. applied field behaviour of a Nb/Co bilayer. The exchange interaction in the cobalt extends into the niobium, suppressing the superconducting transition temperature. The exchange interaction in the superconductor decays over a characteristic length scale so that at the interface the superconductivity will be almost, if not completely, suppressed. Thus the superconductor can be visualised as layers of material with the transition temperature increasing with distance from the cobalt layer. If the niobium layer is too thin then the sample will not become superconducting at any temperature or applied magnetic field. Thus a thinner niobium layer should give rise to stronger changes in the critical current with applied field. The suppression of the exchange interaction beneath a domain wall is far more significant, and so far more noticeable in the measurement, when the exchange interaction is strong. The stray field will also be stronger as the current is flowing closer to the cobalt which is the source of the stray field.

Modelling the change in transition temperature

A very small variation in the thickness of the niobium layer can cause significant changes in the superconducting transition temperature of the bilayer, the thickness of the cobalt layer has a much smaller effect, see figures 6·23 and 6·24. Provided that the cobalt layer is thick enough to become ferromagnetic then the exchange interaction will extend into the superconductor from the interface. Bilayers with cobalt layer thickness of (52 ± 16) nm and niobium layer thickness less than 23 nm have a transition temperature below 4.2 K. The curve shown in figure 6·23 is based on the Buzdin-Radović model for an isolated superconducting film between two thick ferromagnetic layers, which was discussed in Chapter 3 [Radović 1988]. This model has been used to analyse the experimental results obtained from S/F multilayers and as the basis for studying the effect of active control of the magnetisation. If the percolation model, which is based upon active control of the exchange interaction in

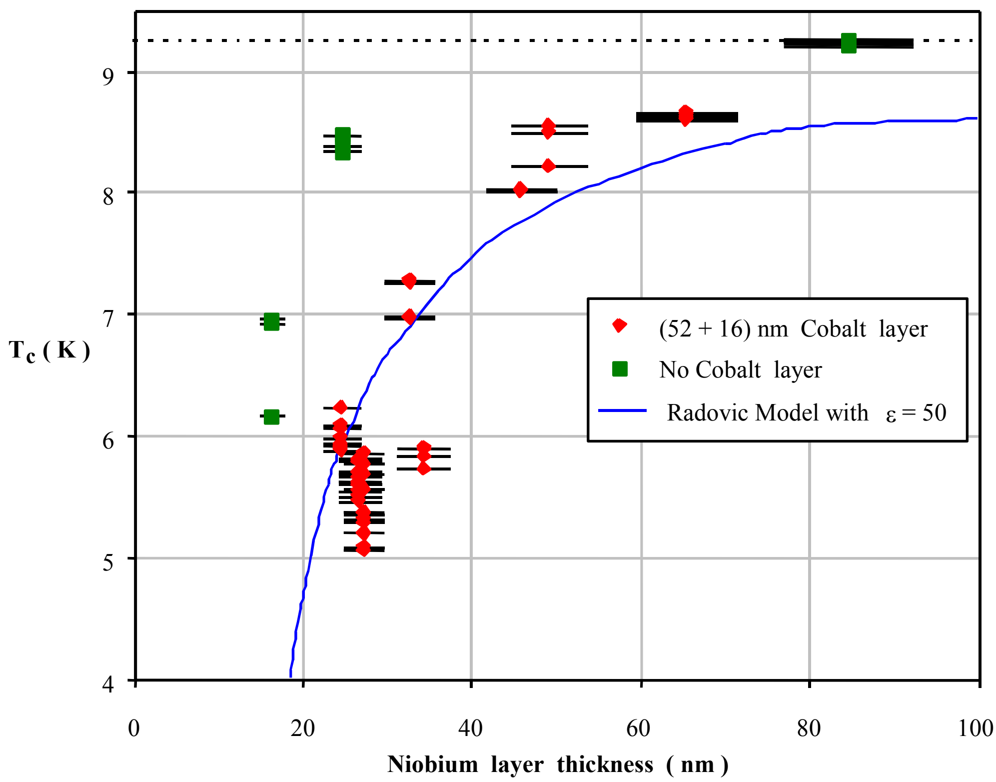

Figure 6·23 Niobium layer thickness vs. superconducting transition temperature for Nb/Co bilayers with the cobalt layer thickness given in no applied magnetic field. The dashed line gives the transition temperature of bulk niobium (9.25 K) while the curve gives the Radović et al. model for a niobium/cobalt multilayer with an interfacial parameter, ε = 50 [Radović 1988].

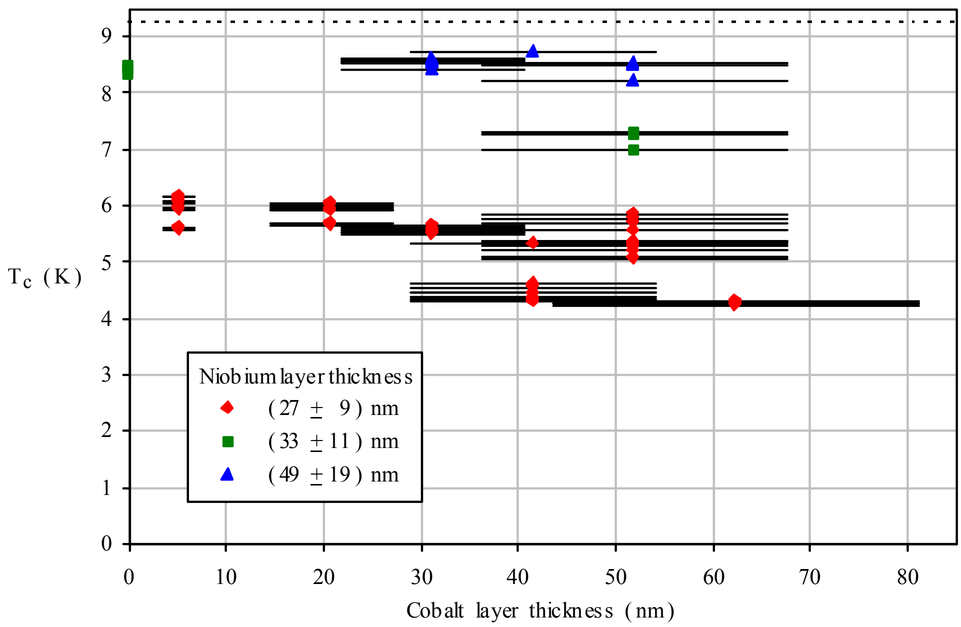

Figure 6·24 Cobalt layer thickness vs. superconducting transition temperature for Nb/Co bilayers with the niobium layer thickness given. The dashed line gives the transition temperature of bulk niobium (9.25 K).

the niobium layer, is accurate then one would expect that the data from the bilayer to fit to the Buzdin-Radović model. The curve shown is that given by $\varepsilon = 50$, which gives a reasonable fit to the data. The value of ε is related to the generalised de Gennes-Werthamer boundary condition, η, by:

$$\varepsilon = \frac{\xi_f}{\eta \xi_s} \qquad (6\cdot1)$$

where: ξ_f is the superconducting coherence length in the ferromagnet.

ξ_s is the superconducting coherence length in the superconductor.

As is normal for real interfaces this gives a value of η is considerably less than that expected for specular scattering, where $\eta = \sigma_f / \sigma_s$ the ratio of the normal state conductivities.

The fit between the Buzdin-Radović model and the data could be improved, though this would increase still further the value for ε used, if approximately 10 nm of the niobium is not superconducting. This seems to be a reasonable assumption from the niobium layer thickness vs. superconducting transition temperature data given by the niobium films, see figure 6·23. This dead layer in the niobium is probably due to poor quality initial growth, though it seems to be rather thick. It is also possible that the 'dead layer' is actually an artefact resulting from the impurities in the niobium layer

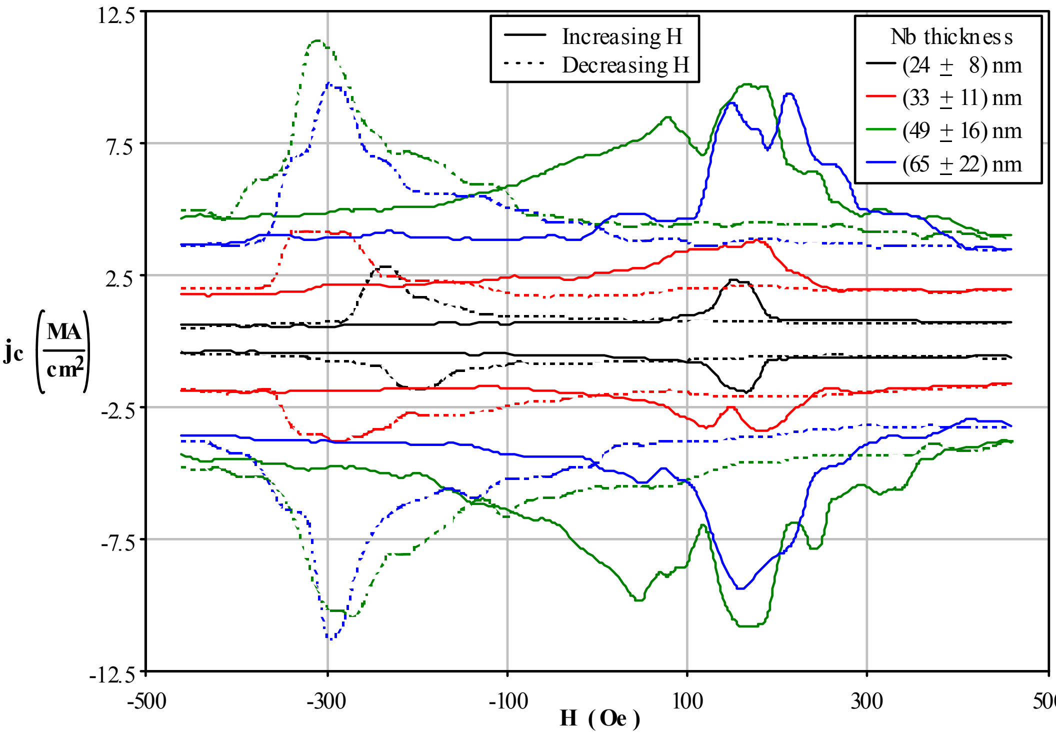

Figure 6·25 Superconducting critical current density vs. magnetic field measurements for a 10 μm by 1 μm track in a Nb/Co bilayer with (52 ± 16) nm of cobalt and the niobium thickness given at 4.2K.

which would reduce the coherence length in the niobium. This would also reduce the value of η for the same value of ε.

Changes in the critical current

The niobium layer thickness also has a strong effect on the critical current density of the bilayer, see figure 6·25. The maximum critical current in the 'double peak' structure also decreases as the niobium layer thickness is reduced and one would expect the high field critical current to decrease more rapidly as the critical current is passing closer to the cobalt layer. The effect of the cobalt layer would decrease with distance for both the stray field and percolation models for the 'double peak' structure. The two models have give different behaviour for the change in the relative peak height with increasing superconducting layer thickness. The stray field mechanism would give the standard inverse square behaviour as the distance from the source of the stray field to the critical region increases. The percolation model gives an exponential behaviour with a length scale given by the characteristic length over which the exchange interaction extends into the superconductor. However, as shown by figures 6·26 and 6·27, this simple behaviour is not observed. This is most probably

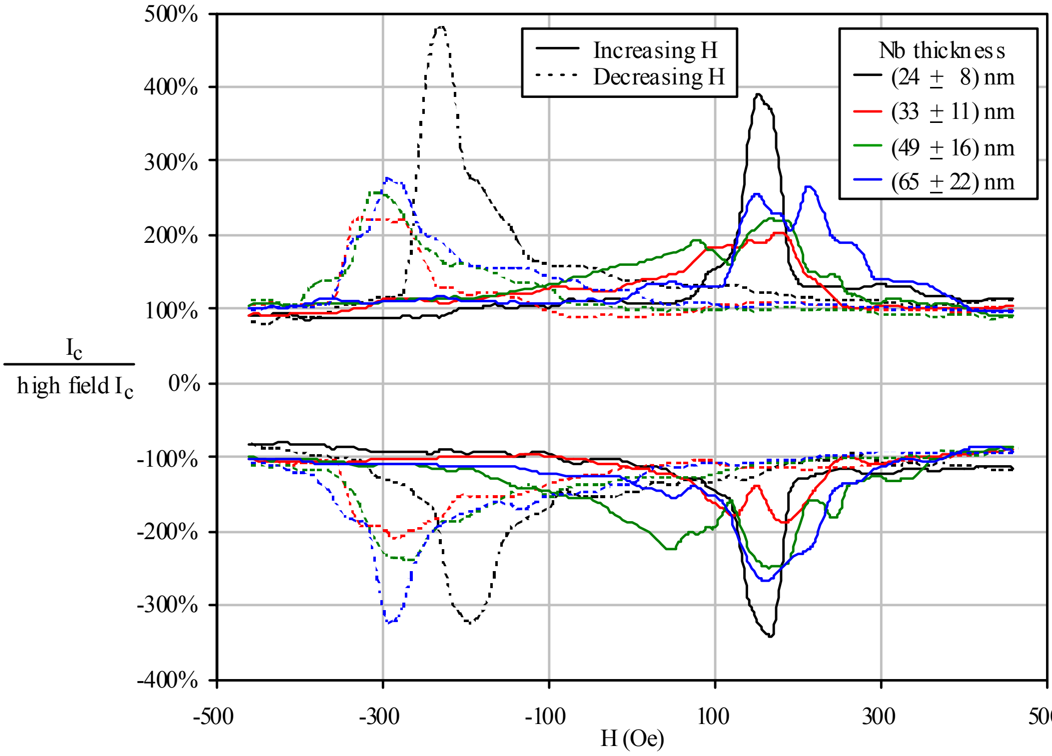

Figure 6·26 Critical current, scaled relative to the mean critical current for magnetic fields greater than 400 Oe, vs. magnetic field measurements for a 10 μm by 1 μm track in a Nb/Co bilayer with (52 ± 16) nm of cobalt and the niobium thickness given at 4.2K.

due to two problems with the experiment. The critical current is measured at certain fixed values of the magnetic field, where the step size is limited by the resolution of the current source for the magnets, for each sweep of the magnetic field between the saturation states. As the discussion of Barkhousen noise in Chapter 5 shows, a very small change in the applied field can have a significant affect on the critical current and the maximum critical current may well occur at a magnetic field that is intermediate between the applied field values of adjacent steps. There is also the problem of reproducibility between films. The ‘double peak’ structure is strongly dependent upon the magnetic structure of the cobalt layer and there is often a significant difference in the critical current vs. applied field behaviour of two otherwise identical tracks in the same bilayer, see figure 6·33 for an extreme example of this. Thus direct comparisons between the behaviour of two films is regrettably limited until films are deposited with a greater degree of control over the magnetic structure of the cobalt layer.

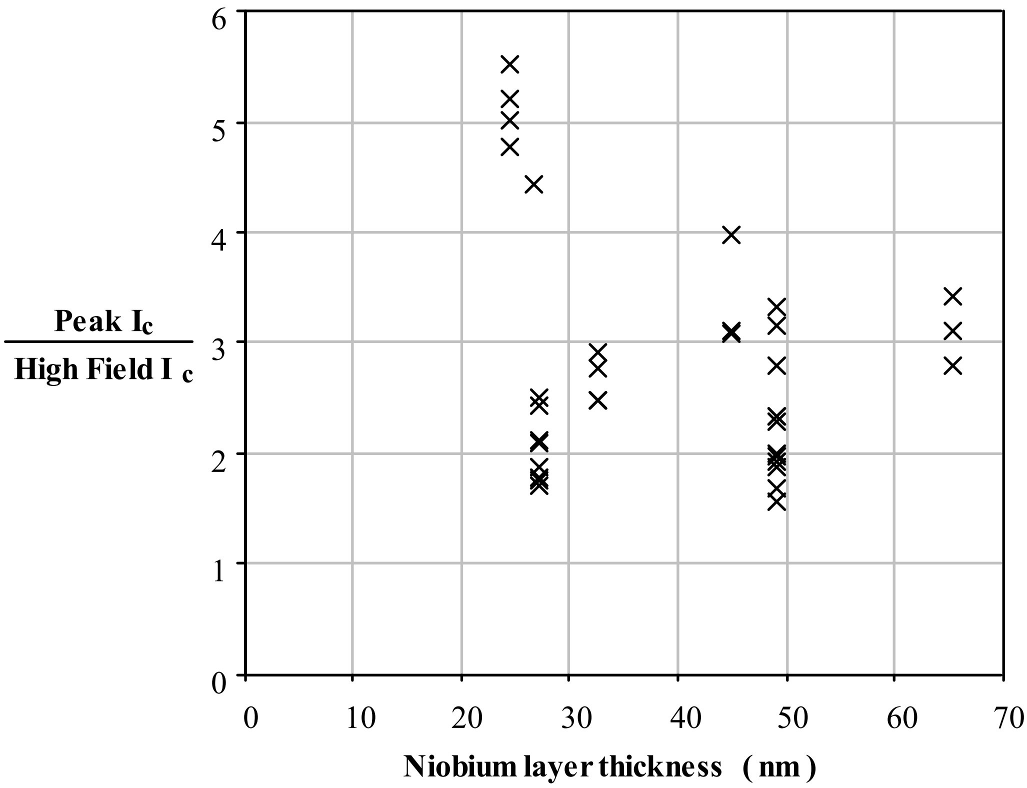

Figure 6·27 Maximum critical current in the double peak structure vs. niobium layer thickness for a 10 μm by 1 μm tracks in Nb/Co bilayers with (52 ± 16) nm of cobalt at 4.2K. There is a 34% error in the niobium layer thickness and though the measured critical currents are accurate to within a fraction of a percent there will be some discrepancy between the measured and true maximum critical current as described in the text.

Changing cobalt layer thickness

Provided that the cobalt layer is thick enough to form a ferromagnetic layer neither mechanism suggests any significant variation in the critical current vs. applied field measurement with the thickness of the cobalt layer. There will be some change in the profile of the stray field as it will tend to diverge more as the cobalt layer becomes thinner. This would tend to increase the stray field near the electrical contacts while decreasing it at the centre of the track. The change in the stray field profile could give rise to a stronger 'double peak' structure in the critical current vs. applied field measurement depending upon where the critical region is in the track. However we find that reducing the cobalt layer thickness beyond a critical limit has a dramatic change in the critical current vs. applied field behaviour of the Nb/Co bilayer, see

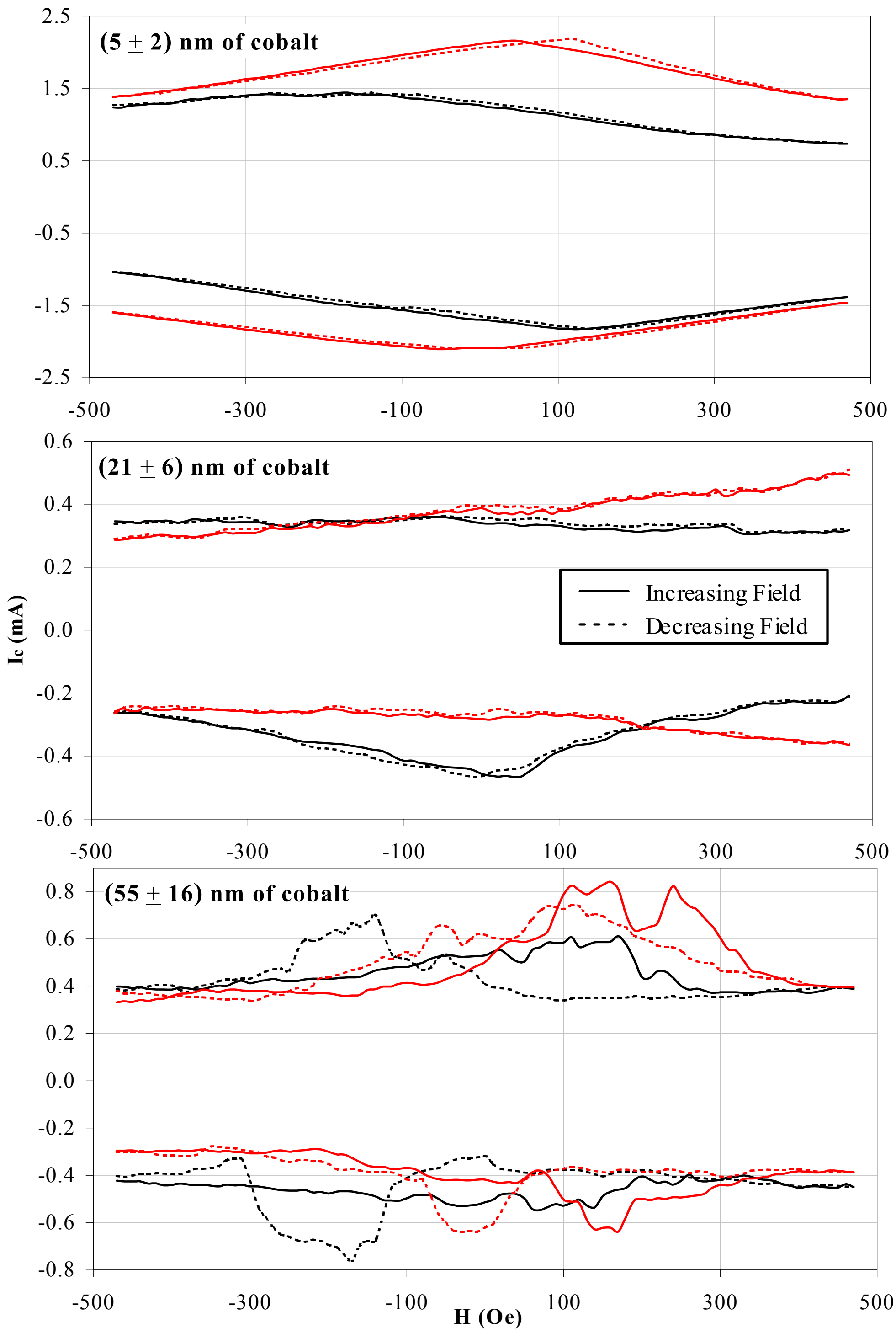

Figure 6·28 Critical current vs. applied field for two 10 μm by 2 μm tracks in a Nb/Co bilayer with (27 ± 9) nm of niobium and the cobalt thickness shown.

figure 6·28. Both the form and the magnitude of the critical current vs. applied field behaviour change. This effect is observed in the full range of measured track widths, from 1 μm to 5 μm wide.

For thin cobalt layers the critical current vs. applied field behaviour observed is very similar to that seen in a niobium film, as shown in figure 5·2. There is a small difference between the two, the thin cobalt layer gives rise to a slight offset in the value of the applied field which gives the peak critical current between the increasing and decreasing magnetic field sweeps. The thin cobalt layer gives a smaller magnetic hysteresis in the critical current than a thicker layer. If the cobalt layer is thinner than 25 nm then the hysteresis in the critical current vs. applied field behaviour has a maximum of approximately 10% while for a cobalt layer of 52 nm the hysteresis is approximately 100%, see figure 6·29. In this case the hysteresis is defined for each value of magnetic field as the change in critical current between the increasing and decreasing field sweeps relative to the minimum of the two. There also seems to be a trend of increasing hysteresis with increasing track width for the thin cobalt layers. This is due to a larger separation in the value of the applied field between the peak critical current on either increasing or decreasing the applied field rather than a change in the critical current vs. applied field behaviour.

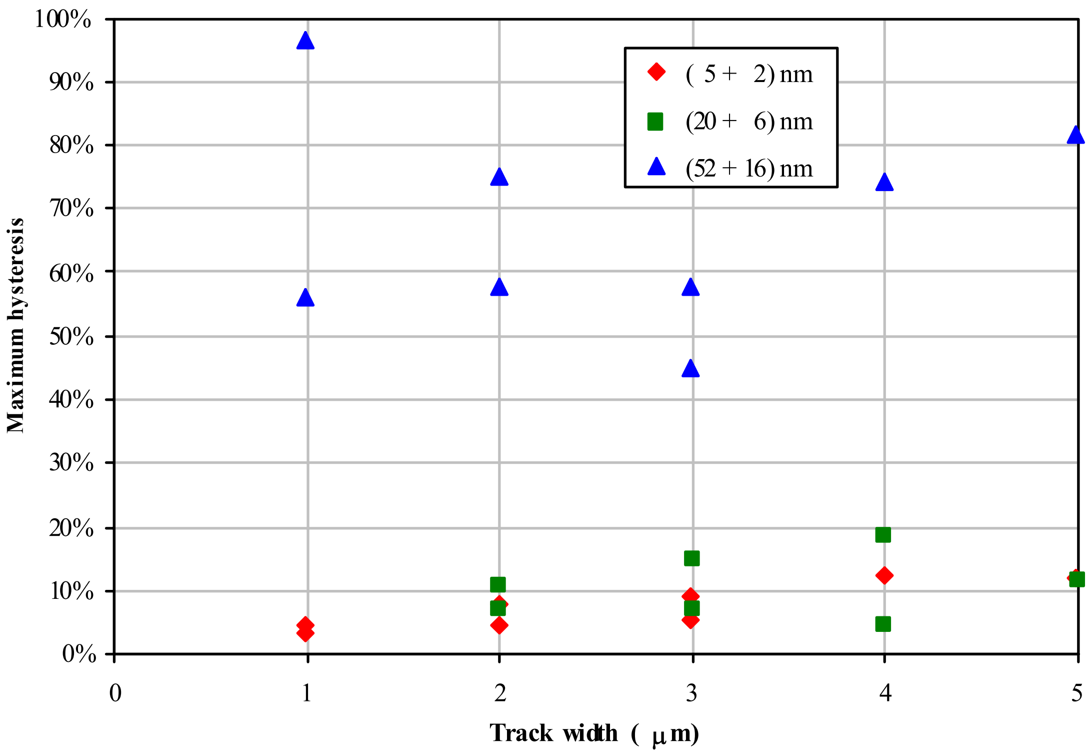

Figure 6·29 Maximum hysteresis, as defined in the text above, vs. track width for Nb/Co bilayers with (27 ± 9) nm of niobium and the cobalt thickness shown.

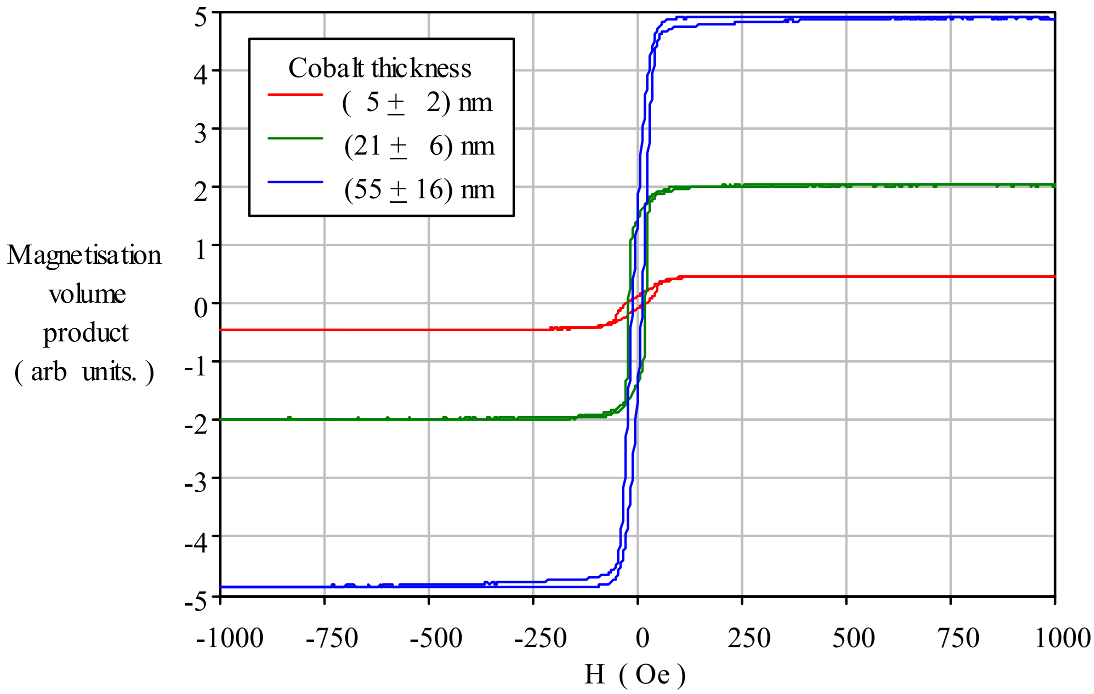

Figure 6·30 Magnetisation hysteresis loops of unpatterned 10 mm by 5 mm Nb/Co bilayers with (27 ± 9) nm of niobium and the cobalt thickness shown at room temperature.

The change in the critical current vs. applied field behaviour with cobalt layer thickness must be due to a change in the magnetic structure within the cobalt layer. If the cobalt layer is sufficiently thin then the magnetisation rotates out of the plane of the film, which would dramatically alter both the domain structure and the stray field. However this transition normally only occurs when the film is a few nanometres thick, rather than a few tens of nanometers. One would expect any change in the direction of magnetisation to be reflected in the magnetisation hysteresis curves, as shown in figure 6·30, if the magnetisation lies out of the plane of the film the saturation magnetisation in the plane of the film will be reduced. As figure 6·30 shows the saturation magnetisation measured along the long axis of an unpatterned 10 mm by 5 mm film scales with the thickness of the cobalt layer. This implies that if the magnetisation is out of the plane of the film it must be to a similar degree for all three cobalt layer thicknesses. It is possible that there is an interfacial layer composed of a mixture of cobalt and niobium, which means that the ferromagnetic cobalt layer is actually much thinner than the deposited cobalt thickness. If this were the case then the linear regression fit obtained from the cobalt layer thickness vs. saturation magnetisation data would go to zero magnetisation at a positive cobalt layer thickness. This assumes that the interfacial layer thickness is constant, a reasonable

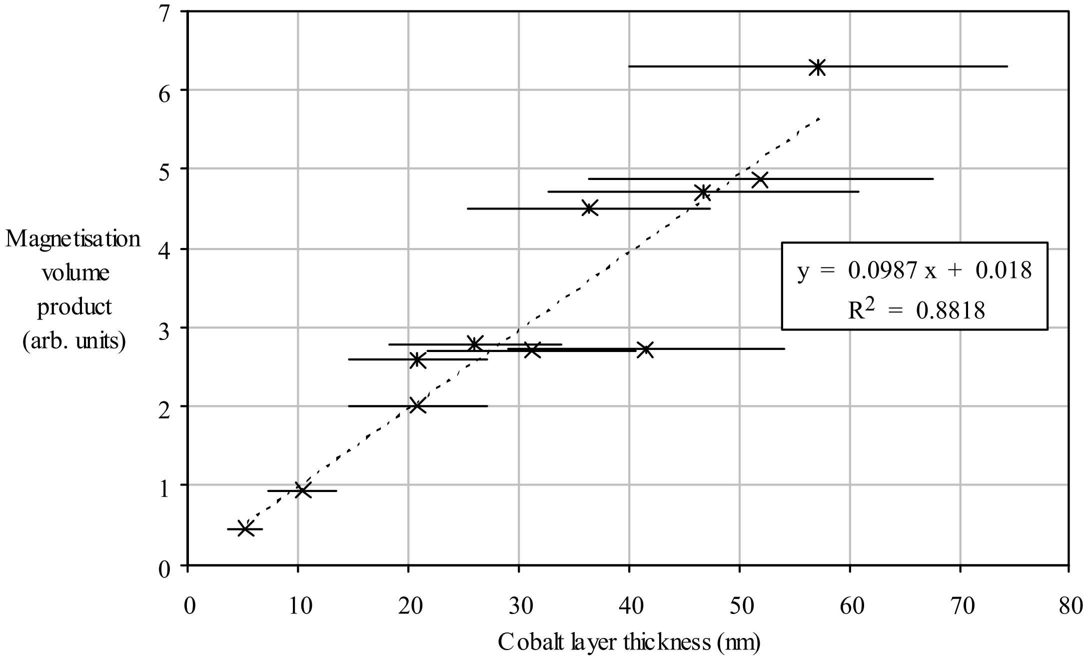

Figure 6·31 Cobalt thickness vs. magnetisation measurements at room temperature for unpatterned 10 mm by 5 mm Nb/Co bilayers. The linear regression line, with equation, is also shown.

assumption as the interfacial layer would form as the sputtered cobalt atoms become embedded in the niobium film and this process would depend upon the deposition power and pressure far more strongly than the deposition time. As figure 6·31 shows the maximum thickness for the interfacial layer is limited to 3 nm at most, which could explain the behaviour of the film with (5 ± 2) nm of cobalt but not the thicker cobalt layers that show the same behaviour.

As shown in figure 6·31, the coercive field of the three cobalt layers, at room temperature, is essentially unchanged. One would expect that the magnetisation hysteresis loops at 4.2 K would have a similar shape, just as they do at room temperature. Equally the polarisation of the cobalt layer would be the same at 4.2 K, as it is at room temperature. Thus, at first glance, the stray field cannot be responsible for the change in the critical current vs. applied field behaviour on changing the cobalt layer thickness. The change in the critical current vs. applied magnetic field behaviour can be explained in terms of a change in the magnetic structure of the cobalt layer. As the cobalt layer becomes thinner the effect of interfacial and edge pinning forces on the domain structure becomes more important. Thus at a critical thickness the domain structure within the track becomes dominated by the 'spike' domains at the edge of the film, see figure 5·15 for an illustration of this domain structure. The 'spike' domains act as closure domains, limiting the stray field and so suppressing this contribution to the 'double peak' structure. The 'spike' domains also suppress the percolation of additional critical current. Once the 'spike' domains have become large and fixed there is no significant change in the number of domain walls at the coercive field compared to saturation, as shown in figure 6·32. Equally the stray field would become very small at all applied fields due to the closure domains at the edge of the electrical connections. This means that there can be no significant change in the critical current. The offset in the normal suppression of the critical current in a superconducting layer in an applied magnetic field can be explained as the result of the internal field within the cobalt, which reflect the magnetisation curve of the film, adding to the applied field at the cobalt/niobium interface. The importance of the 'spike' domains also explains the intermediate behaviour of tracks in a Nb/Co bilayer with (26 ± 7) nm of cobalt where two theoretically identical tracks show very different behaviour, see figure 6·33. The 'spike' domains would be very sensitive to conditions at the edges of the track.

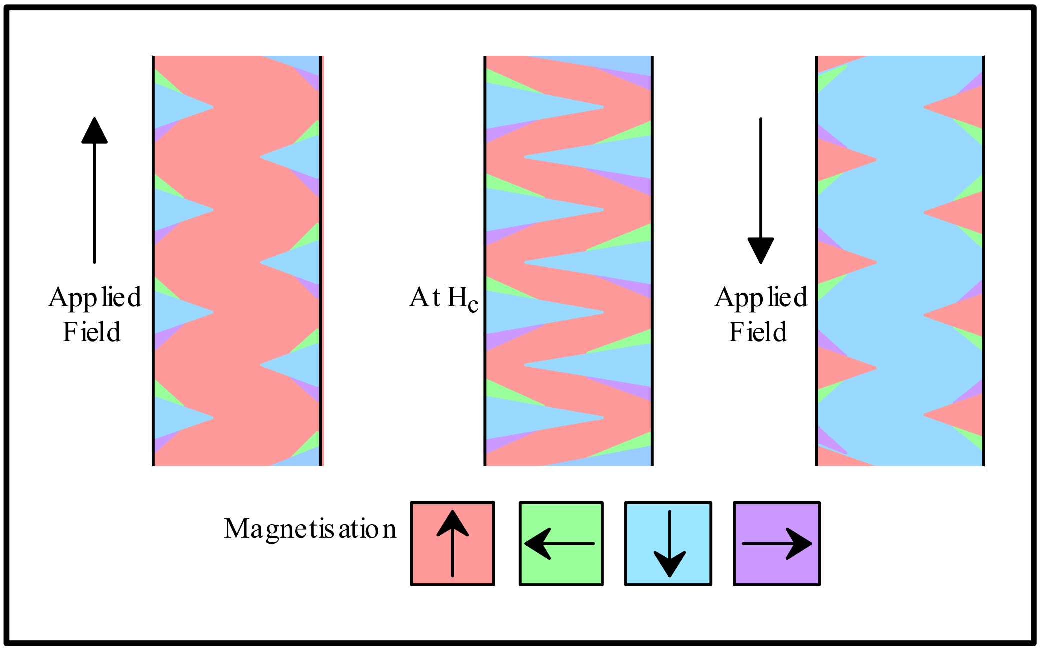

Figure 6·32 Schematic of the reversal of magnetisation by growth of spike domains.

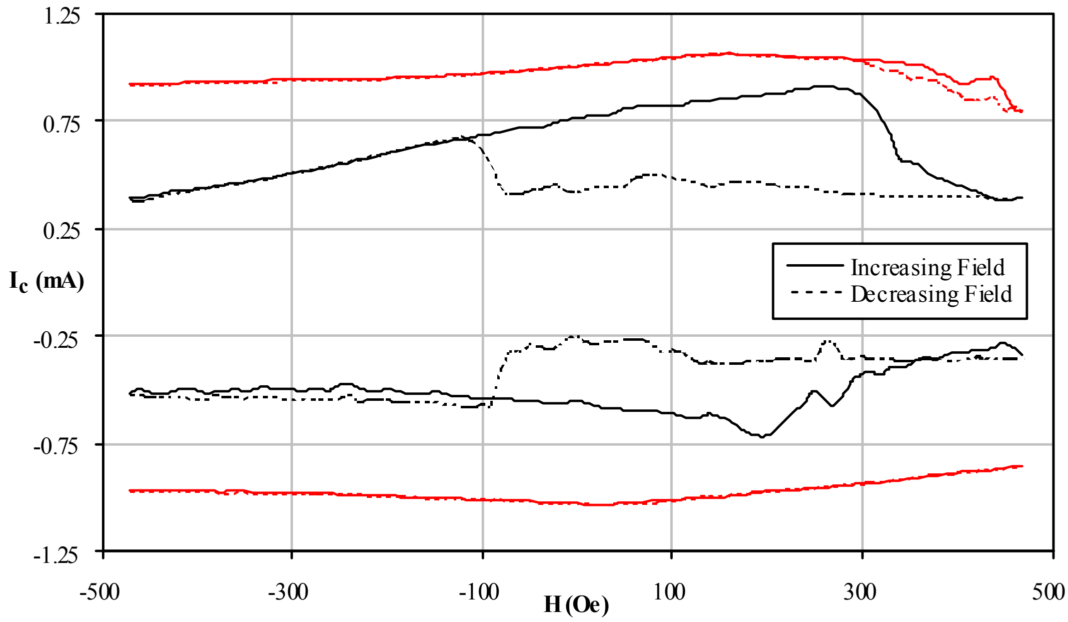

Figure 6·33 Critical current vs. applied field for two 10 μm by 2 μm tracks with 1 μm by 1 μm constriction in a Nb/Co bilayer with (27 ± 9) nm of niobium and (26 ± 7) nm of cobalt.

Niobium/iron bilayers

One might expect that there should be little difference between the critical current vs. applied field behaviour of two superconductor/ferromagnet bilayers with different ferromagnetic materials, especially with ferromagnets as similar as cobalt and iron. The stray field would depend upon the magnetisation of the ferromagnetic layer while each ferromagnet has a different exchange energy and spin imbalance. The extent to which the exchange interaction extends into the superconductor and the critical current vs. applied field behaviour will depend upon the superconducting layer so the change in the behaviour should be simply a change in magnitude. Increased stray field and/or increased spin-imbalance would give rise to larger peaks. The saturation polarisation of iron is 2.16 T while the saturation polarisation of cobalt is 1.76 T and the saturation polarisation depends upon the spin imbalance and the spin density. Thus the exchange interaction in the superconductor due to the iron will be stronger than that due to cobalt and one would expect that the stray field from the iron, given that iron is magnetically far softer than cobalt, would be at least similar in magnitude.

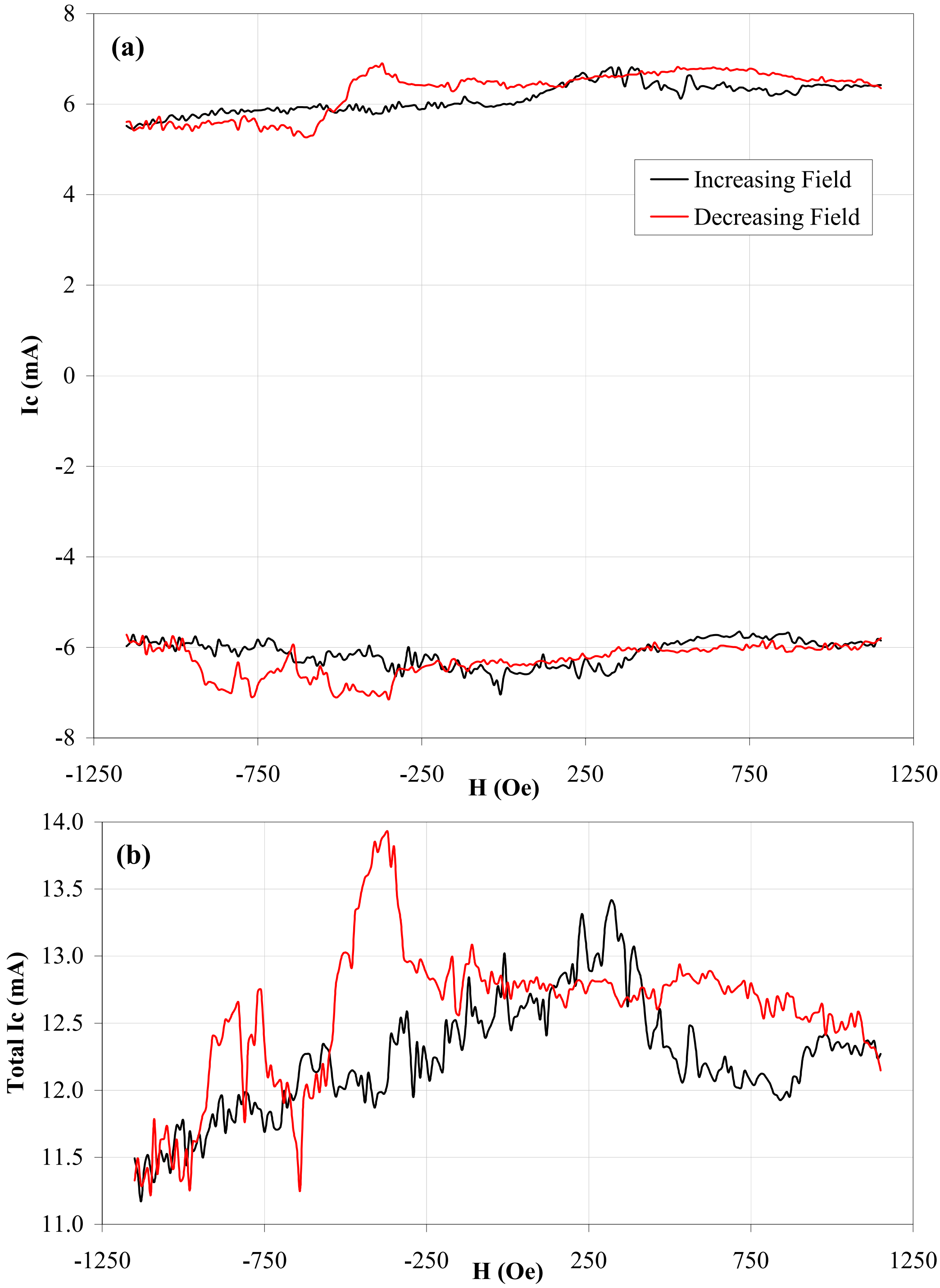

Figure 6·34 Critical current vs. applied field for a 10 μm by 1 μm track in a Nb/Fe bilayer with (139 ± 23) nm of niobium and (105 ± 12) nm of iron. Part (b) shows the detail of the total critical current vs. applied field.

significantly smaller 'double peak' structure for the Nb/Fe bilayers. In fact the peak height is approximately that which one would expect from stray field alone. The absence of any significant effect from the exchange interaction is easily understood in terms of the domain pattern in the iron layer. Unlike cobalt, where there is a single easy axis, there are several magnetic easy directions, at right angles to each other, in iron. Thus at the coercive field closure domains easily form and one would expect 90° domain walls to be far more common than they are in a cobalt layer, where they would only occur in the spike domains at the edge of the film. Beneath a 90° domain wall there would be no decrease in the exchange interaction in the superconductor. As a particle with spin enters a region where the spin is defined, either by a magnetic field or the exchange interaction, the spin of the particle must lie along the defined axis. The spin of a particle in free space must be either parallel or antiparallel to the magnetic field, as shown in the Stern-Gerlach experiment. If the spin of the particle has been previously defined then the spin is projected onto the newly defined axis using the spinor transformation, where the probability that the electron enters the new spin state is given by $\cos^2\left(\frac{\theta}{2}\right)$ with θ the angle between the two. Thus when projecting onto an axis at 90° to the original spin an equal proportion of the particles will enter both of the new spin states. The spin imbalance on one side of a 90° domain wall has no influence on the spin imbalance on the other side. There is no reduction in the exchange interaction beneath a 90° domain wall and so no increase in the critical current. Any 'double peak' structure in a niobium/iron bilayer will be limited to the affects of the stray field. Thus the Nb/Fe bilayer provides a measure of the affect of the stray field on the track.

SUMMARY

In this Chapter we have discussed the systematic changes in the niobium/cobalt bilayers and the measurement conditions, changing the maximum applied field, the field direction, the temperature, track width, layer thickness and changing the cobalt for iron. These changes have provided additional data to support the hypothesis that the stray field in the system is not solely responsible for the 'double peak' structure in the critical current vs. applied magnetic field measurements. Instead the percolation model, where additional 'supercurrent' is carried in the regions beneath 180° domain walls where the ferromagnetic exchange interaction in the superconductor is reduced, is also required to explain the data.

Evidence for the importance of the percolation model can be found in several experiments. The most important of these include the sensitivity to small changes in the magnetic field, the temperature variation of the critical current with temperature, the change in the critical current behaviour on adding a constriction and replacing the cobalt with iron. The sensitivity to small changes in the magnetic field was discussed in chapter 5 and at the beginning of this chapter. Almost all the experiments discussed show some evidence of this effect.

When we look at the temperature dependence of the critical current vs. magnetic field data we find that the stray field required to give the difference between the maximum critical current of the 'double peak' structure and the critical current at high magnetic field must change considerably with temperature. The temperature dependence can be explained using the exchange interaction mechanism as the volume beneath the domain wall that carries the additional critical current will depend upon the decay length of the exchange interaction in the superconductor. The decay length will in turn depend upon the temperature and, possibly, the local magnetic field. The data suggests that the decay length increases as the temperature is reduced, implying that the decay length depends upon the diffusion of quasiparticles.

Cutting a constriction in the track does not significantly change the stray field as the high field critical current density does not change but the constriction does give rise to a much stronger 'double peak' structure in the critical current vs. applied field measurement. In the track without a constriction we observe what looks like a pair of 'double peak' structures, switching at different applied fields. As the domain walls move through the cobalt layer different regions of the track can become the critical region, the first region of the track to go normal, giving rise to multiple 'double peak' structures. The constriction localises the critical region and so gives a single well defined 'double peak'. As the stray field depends upon the magnetisation of the cobalt layer the field which gives maximum critical current would be uniform across the track.

Iron tends to form 90° domain walls, beneath which there is no reduction in the exchange interaction, the Nb/Fe system illustrates the stray field behaviour without a contribution from the exchange interaction. This has proven to be small, as the rough calculation in chapter 5 indicated, implying that some other mechanism must be responsible for the significant changes in the critical current with applied field observed in the Nb/Co system.

We still have no conclusive proof that the exchange interaction, by means of the additional current carrying regions beneath 180° domain walls, is the cause of the 'double peak' structure in the critical current vs. applied field measurements of Nb/Co bilayers. In fact it is probable that both percolation beneath 180° domain walls and stray field both contribute to the change in critical current. The data shown in this chapter does show that the exchange interaction makes a significant contribution to the 'double peak' structure, which cannot be interpreted as simply due to stray field.

Chapter Seven

CONCLUSIONS

All things have a root and a top,
All events have an end and a beginning;
Whoever understands correctly
What comes first and what follows
Draws nearer to Tao.

The Study of the Ancients

This chapter brings together the results from the previous two chapters. Most of these conclusions were summarised at the end of the chapters. Some possibilities for further work are also given.

In this work I have attempted to demonstrate that it is possible to actively control the superconducting properties of superconductor/ferromagnet (S/F) heterostructures by changing the magnitude of the local ferromagnetic exchange interaction in the superconductor. The local exchange interaction in the superconductor is the sum of the exchange interaction from each ferromagnetic region, taking into account a phase that depends upon the direction that the region is magnetised and exponential decay with distance. The local exchange interaction, which can also be viewed as a spin-imbalance in the superconductor, reduces the superconducting gap parameter (Δ) and so the superconducting critical temperature (T_c) and critical current (I_c). Ferromagnetic regions with antiparallel magnetisations tend to reduce the local exchange interaction and so decrease the suppression of T_c. The extreme example of this effect is an antiferromagnet/superconductor heterostructure where, although the individual magnetic ions give rise to the same strength of the exchange interaction, the T_c is higher than that of a similar S/F heterostructure.

The 'Double Peak' Structure

I have measured the change in the superconducting properties of niobium/cobalt bilayers as a magnetic field is applied along the direction that the current is flowing. The strong uniaxial magnetocrystalline anisotropy in cobalt means that it forms antiparallel domains at the coercive field (H_C) thus there is a region beneath the 180° domain walls where the local exchange interaction is reduced. This creates a web of regions in the superconductor, at H_C, with a higher T_c than the rest of the niobium layer. Thus one would expect the critical current of the bilayer to be larger at H_C than at both zero and high applied field. This gives rise to a 'double peak' structure which is a component in the change of the critical current with applied field. Unfortunately other mechanisms also come into play as the magnetic field is changed and they must also be considered as possible sources for the 'double peak' structure.

Stray field from the edges of the cobalt layer can cut the track and so reduce T_c. There are two components of stray field to be considered, the stray field from the cobalt layer of the track and the stray field from the cobalt layer of the electrical connections to the track. Stray field from the track itself will go to a minimum at high applied field as the magnetisation tends to align with the applied field. Thus the magnitude of the flux cutting the superconducting layer goes to a minimum at high applied field. This component of the stray field actually gives the opposite of the 'double peak' structure, reducing the critical current at H_C, relative to the critical current at high applied fields. The stray field from the electrical connections is the sum of the individual stray fields from each piece of the edge of the electrical connections and so it will be roughly proportional to the magnetisation of the cobalt layer. The stray field adds to the applied field at high applied field but just before H_C the two will be antiparallel and so the local magnetic field will be small and may go to zero. Thus the stray magnetic field from the electrical connections can give the 'double peak' component in the measurement of the critical current as a function of the applied field.

A further possibility for the 'double peak' structure is the motion of flux vortices in the superconducting layer. There are three reasons why this mechanism is extremely unlikely to give the 'double peak' structure. Firstly the 'double peak' is not observed in the measurement of the critical current as a function of applied field for a plain niobium film. The cobalt layer would increase the local field and so merely intensify the feature rather than creating it. Second, the current flows parallel to the applied field and in this case there is no Lorentz force. The vortices must kink before they experience a Lorentz force and this process is very unpredictable, unlikely to give a simple 'double peak' structure. Finally the critical current before any magnetic field is applied is less than the critical current at H_C. If the flux vortices were responsible for the 'double peak' structure the opposite would be true as the number of flux vortices only goes to a minimum at H_C rather than to zero.

Exchange Interaction or Stray Field?

We have two mechanisms that give rise to the 'double peak' structure in the measurement of the critical current as a function of the applied field of the niobium/cobalt bilayers, the exchange interaction and the stray field. These mechanisms react differently to changes in the measurement conditions or the structure of the device. The contribution to the 'double peak' structure of the two mechanisms could not be quantified for comparison with the measurements of the niobium/cobalt bilayers that were made. However it was still possible to determine their relative importance and prove that at least a large proportion of the 'double peak' structure was due to the exchange interaction, showing that the basic concept is valid.

The first thing to consider is the amount of stray flux that the cobalt layer over the electrical connections generates. Measurement of a scale model suggests that the stray field strength at maximum applied field is only 125 Oe. I have measured critical currents at H_C that are approximately five times the critical current measured at high applied fields, as shown in figure 5·14. This implies that the upper critical field of the bilayer, given the change in critical current with applied field of a plain niobium layer shown in figure 5·2, is only approximately 800 Oe. However one can see, at fields larger than those that give the 'double peak' structure, that a change in the applied field of 250 Oe only reduces the critical current by 2%. This means that the stray field must be approximately 9 kOe for it to give the observed 'double peak' structure. The problem of the magnitude of the stray flux can also be seen in the change of the critical current with applied field as the temperature is changed, as demonstrated in Chapter 6 . The data shown in figures 6·10 and 6·11 implies that the stray field must have changed with temperature if the stray field mechanism is the sole cause of the 'double peak' structure. However the magnetisation of the cobalt layer does not significantly change over such a small temperature change, see figure 6·8. Thus the stray field cannot be the sole cause of the 'double peak' structure.

It is also important to consider the noise in the 'double peak' structure on repeated sweeps of the magnetic field, which is shown in figure 5·21. There is considerably more noise, both in relative and absolute terms, near H_C and within the 'double peak' structure than at high applied field. This implies that near H_C one observes the affect of Barkhousen noise as well as electrical noise on the critical current. The magnetisation of a ferromagnetic layer does not change smoothly but instead in a series of small steps as the domain walls move between pinning sites, this gives rise to Barkhousen noise. The position and motion of the domain walls depends critically upon the initial state, the domain structure at a given applied field will change with each sweep of the magnetic field. In both mechanisms the critical current depends upon the local domain structure. However, the stray field from the electrical connections near H_C is an average over multiple domains. Hence a small change in the position of the domain walls could not have given rise to the dramatic changes in the critical current that were observed, as much as 55% in 0.5 Oe. The sensitivity to small changes in the domain structure can easily be explained using the exchange interaction mechanism. The critical current of a piece of the bilayer would only increase if the region with suppressed exchange interaction beneath the domain wall bridged it. A small change in the position of a domain wall could prevent or create such a bridge and so have given rise to the observed changes in the critical current on repeated sweeps of the magnetic field. Thus the exchange interaction mechanism explains the sensitivity of the bilayers to small changes in the applied field in a way that the stray field mechanism can not.

The importance of the exchange interaction mechanism in explaining the behaviour of the niobium/cobalt bilayers in a magnetic field can also be seen in the effect of changing the track width, shown in figures 6·16 to 6·19. One would expect that doubling the width of the track would double the critical current, a constant critical current density (J_c). Instead I find that the critical current does not increase as much as it should, especially in the high field case. This implies that the J_c of the edge of the track was higher than that of the centre and that the edge of the track was not as strongly affected by the change in the magnetic field as the centre. The change in the track width would give a small change in the local magnetic field due to the change in the shape anisotropy but this cannot explain the amount of the difference and the change in the behaviour. However due to pinning forces in a thin film, domains will persist at the edge of the cobalt layer even at high applied fields. These 'spike' domains, shown schematically in figure 5·15, will reduce the exchange interaction at the edge of the track at all applied fields. At high applied fields the edge of the track would carry the majority of the critical current, while at H_C this effect would be far less noticeable as the centre of the track would also contain multiple domain walls. Thus the exchange interaction mechanism can explain both why the average J_c of the track falls with increasing track width and why this effect is far stronger at high applied field than it is at H_C.

The cases given above show that the exchange interaction is the source of a significant part of the 'double peak' behaviour I observed in the change of the critical current with applied magnetic field. It is possible to obtain an estimate of the 'double peak' structure generated by stray field alone by replacing the cobalt with iron. Unlike cobalt, iron has several magnetically easy directions and so the magnetisation of adjacent domains tends to be perpendicular rather than antiparallel and there is no cancellation of the exchange interaction beneath a 90°domain wall. As shown in figure 6·34, the 'double peak' structure in a niobium/iron bilayer is far smaller that in a similar Nb/Co bilayer.

Further Work

The evidence shows that the exchange interaction does have a significant effect on the on the critical current and that the exchange interaction can be controlled by changing the magnetisation of the ferromagnetic regions. However the niobium/cobalt bilayers are limited both by the Barkhousen noise, the thickness of the layers and the magnetic structure of the cobalt layer. The Barkhousen noise means that the applied magnetic field at which the critical current goes to a maximum will not remain the same between sweeps of the magnetic field. A very small change in the thickness of the niobium layer gives a significant change in the superconducting transition temperature of the bilayer, as shown in figure 6·23. Finally small changes in the magnetic structure of the cobalt layer, which in turn depends upon the pinning sites, can give significant changes in the behaviour of the bilayer.

The Barkhousen noise is an inevitable consequence of the formation of a domain structure. This can possibly be overcome by using more than one ferromagnetic layer, as in the structures proposed by Oh and Tagirov [Oh 1997, Tagirov 1999]. In these structures the two ferromagnetic layers have either parallel or antiparallel magnetisations. Although the layers will form domains while they are switching between states, there will be no domains in the ferromagnetic layers in these two states. Given that the critical current will only be measured in these states the device will essentially be free of Barkhousen noise.

If the interface between the niobium and cobalt layers is improved then a small change in the critical current will not have such a significant effect on the superconducting transition temperature of the bilayer, to the limit of a specular interface. This will allow the selection of a superconducting layer thickness such that the magnetic field will switch the heterostructure between the normal and the superconducting state at any specified temperature, probably 4.2 K. Equally control of the interface will give control of the magnetic structure of the ferromagnetic layer and so improve the reproducibility between tracks.

It may also possible to quantify the contributions of the exchange interaction and the stray field to the 'double peak' structure in order to properly model the additional critical current in the regions of reduced exchange interaction. Possibly the simplest way of doing this is to increase the length of the track and so the separation between the electrical contacts. Assuming that the magnetic structures are the same for each track the stray field will show the standard inverse square behaviour as the two poles are separated. It should also be possible to extract the strength of the stray field. Equally, assuming that the voltage signal can be measured and that the magnetisation lies in the plane of the film, it may be possible to use a smooth unpatterned ferromagnetic layer. The current would still flow through the superconductor up to the limit of the critical current but the absence of any edges would mean no surface poles and so no stray field.

I have only suggested a few possibilities for further work. Now that the concept of controlling the superconducting properties of a superconductor/ferromagnet heterostructure by means of the exchange interaction has been shown to be practical, many other devices will, no doubt, be proposed.

BIBLIOGRAPHY

Chapter One - Introduction

D.B. Chrisey, M.S. Osofsky, J.S. Horwitz, R.J. Soulen, B. Woodfield, J. Byers, G.M. Daly, P.C. Dorsey, J.M. Pond, M. Johnson and R.C.Y Auyeung (1997) *IEEE Trans. App. Supercon.* **7**(2) 2,067

Z.W. Dong, R. Ramesh, T. Venkatesan, M. Johnson, Z.Y. Chen, S.P. Pai, V. Talyansky, R.P. Sharma, R. Shreekala, C.J. Lobb and R.L. Greene (1997) *App. Phys. Lett.* **71**(12) 1,718

K.E. Gray (1981) "Nonequilibrium Superconductivity, Phonons and Kapitza Boundaries" (New York and London, Plenum Press)

J.J. Hauser, H.C. Theuerer and N.R. Werthamer (1966) *Phys. Rev.* **142**(1) 118

K. Lee, W. Wang, I. Iguchi, B. Friedman, T. Ishibashi and K. Sato (1999) *App. Phys. Lett.* **75**(8) 1,149

S. Oh, D. Youm and M.R. Beasley (1997) *App. Phys. Lett.* **71**(16) 2,376

C.P. Poole Jr. (2000) "Handbook of Superconductivity" (San Diego and London, Academic Press)

R.J. Soulen Jr., M.S. Osofsky, D.B. Chrisey, J.S. Horwitz, D. Koller, R.M. Sroud, J. Kim, C.R. Eddy, J.M. Byers, B.F. Woodfield, G.M. Daly, T.W. Clinton, M. Johnson and R.C.Y. Auyeung (1997) *Inst. Phys. Conf. Series* **158** 789

L.R. Tagirov (1999) *Phys. Rev. Lett.* **83**(10) 2,058

M. Tinkham (1996) "Introduction to Superconductivity" (New York, McGraw Hill)

V.A. Vas'ko, V.A. Larkin, P.A. Kraus, K.R. Nikolaev, D.E. Grupp, C.A. Nordman and A.M. Goldman (1997) *Phys. Rev. Lett.* **78**(6) 1,134

N.-C. Yeh, R.P. Vasquez, C.C. Fu, A.V. Samoilov, Y. Li and K. Vakili (1999-II) *Phys. Rev. B* **60**(14) 10,522

Chapter Two - Theory of Superconductors and Ferromagnets

A. Abrikosov (1957) *Zh. Eksp. Teor. Fiz.* **32** 1,442, [(1957) *JETP Lett.* **5** 1,174]

A. Andreev (1964) *Zh. Eksp. Teor. Fiz.* **46** 1,823 [(1964) *Sov. Phys. JETP* **19** 1,228]

H. Arie, E. Kume and I. Iguchi (1997-I) *Phys. Rev. B* **56**(5) 2,387

A.G. Aronov (1976) *Zh. Eksp. Teor. Fiz*. **24**(1) 37 [(1976) *JETP Lett*. **24**(1) 32]

J. Bardeen, L.N. Cooper and J.R. Schrieffer (1957) *Phys. Rev.* **108** 1,175

D. Belitz and T.R. Kirkpatrick (1999) *Phys. Rev. B* **60**(5) 3,485

J. Chang and D. Scalapino (1978) *J. Low Temp. Phys*. **31** 1

L.N. Cooper (1961) *Phys. Rev. Lett.* **6** 89

D.J. Craik and R.S. Tebble (1965) "Ferromagnetism and Ferromagnetic Domains" (Amsterdam, North-Holland Publishing)

S. Datta and B. Das (1990) *App. Phys. Lett*. **56** 665

F. Dyson (1955) *Phys. Rev*. **98** 349

R.I. Dzhioev, B.P. Zakharchenya, V.L. Korenev and M.N. Stepanova (1997) *Phys. Solid State* **39**(11) 1,765

L. Esaki, P. Stilles and S. von Molnar (1967) *Phys. Rev. Lett*. **19** 852

S.M. Faris, S.I. Raider, W.J. Gallagher and R.E. Drake (1983) *IEEE Trans. Magn.* **MAG-19**(3) 1,293

G. Feher and A. Kip (1955) *Phys. Rev*. **98** 337

A. Fert and S.-F. Lee (1997) *J. Magn. Magn. Mater.* **165** 115

P.G. de Gennes (1964) *Rev. Mod. Phys.* **38** 225

V.L. Ginzburg and L.D. Landau (1950) *Zh. Eksp. Teor. Fiz.* **20** 1,064

L.P. Gor'kov (1958) *Zh. Eksp. Teor. Fiz.* **34** 735 [(1958) *Sov. Phys. JETP* **7** 505]

K.E. Gray (1981) "Nonequilibrium Superconductivity, Phonons and Kapitza Boundaries" (New York and London, Plenum Press)

J. Gregg, W. Allen, N. Viart, R. Kirschman, C. Sirisathitkul, J.-P. Schille, M. Gester, S. Thompson, P. Sparks, V. Da Costa, K. Ounadjela, M. Skvarla (1997) *J. Magn. Magn. Mater.* **175** 1

C. Grimaldi and P. Fulde (1996) *Phys. Rev. Lett.* **77**(12) 2,550

C. Grimaldi and P. Fulde (1997–I) *Phys. Rev. B* **56**(5) 2,751

J.J. Hauser and H.C. Theuerer (1965) *Phys. Lett.* **14** 270

B.D. Hunt, R.P. Robertazzi and R.A. Buhrman (1985) *IEEE Trans. Magn.* **MAG-21**(2) 717

M. Johnson and R. Silsbee (1985) *Phys. Rev. Lett*. **55**(17) 1,790

M. Johnson and R. Silsbee (1988) *Phys. Rev. B* **37**(10) 5,312 and 5,326

M. Johnson and J. Clarke (1990) *J. App. Phys*. **67** 6,141

M. Johnson (1993) *Phys. Rev. Lett*. **70**(14) 2,142

M. Johnson (1994) *J. App. Phys*. **75**(10) 6,714

M. Johnson (1996) *J. Magn. Magn. Mater*. **156**(1-3) 321

B. Josephson (1962) *Phys. Lett.* **1** 251

M. Julliere (1975) *Phys. Lett*. **54A**(3) 225

T. Jungwirth and A.H. MacDonald (1998) *Solid State Comm.* **108**(3) 127

A. Knigavko and B. Rosenstein (1998) *Phys. Rev. B* **58**(14) 9,354

T. Kobayashi, K. Hasimoto, U. Kabasawa and M. Tonouchi (1989) *IEEE Trans. Magn.* **MAG-21** 927

F. London and H. London (1935) *Proc. Roy. Soc. (London)* **A149** 71

K. Machida and T. Ohmi (1998) *J. Phys. Soc. Japan* **67**(4) 1,122

J. Mannhart (1996) *Supercon. Sci. Tech.* **9**(2) 49

J.M. Martinis, G.C. Hilton, K.D. Irwin and D.A. Wollman (2000) *Nuc. Instr. Meth. Phys. Res. A* **444** 23

W. Meissner and R. Ochsenfeld (1933) *Naturwissenschaften* **21** 787

R. Meservey, P.M. Tedrow and P. Fulde (1970) *Phys. Rev. Lett*. **25**(18) 1,270

R. Meservey, D. Paraskevopoulos and P.M. Tedrow (1976) *Phys. Rev. Lett.* **37**(13) 858

R. Meservey and P.M. Tedrow (1994) *Phys. Rep.* **238**(4) 173

J. Moodera, R. Meservey and X. Hao (1993) *Phys. Rev. Lett*. **70** 853

J. Moodera, T. Wong, L. Kinder and R. Meservey (1995) *Phys. Rev. Lett*. **74** 3,273

N.F. Mott (1936) *Proc. R. Soc.* **153** 699

H. Onnes (1911) *Leiden Comm.* **120b**, **122b**, **125c**

C.S. Owen and D.J. Scalapino (1972) *Phys. Rev. Lett.* **28** 1,559

W.H. Parker (1975) *Phys. Rev. B* **12** 3,667

R.D. Parks (1964) "Superconductivity" (New York, Marcel Dekker)

C.P. Poole Jr. (2000) "Handbook of Superconductivity" (San Diego and London, Academic Press)

G. Prinz (1995) *Physics Today* **48**(4) 58

C.W. Schneider, R. Schneider, R. Moerman, G.J. Gerritsma, and H. Rogalla (1997) *Inst. Phys. Conf. Ser.* **158** 437

S. Shapiro (1963) *Phys. Rev. Lett.* **11** 80

R. Silsbee, A. Janossy and P. Monod (1979) *Phys. Rev. B*. **19** 4,382

M.B. Stearns (1977) *J. Magn. Magn. Mater.* **5** 167

P.M. Tedrow and R. Meservey (1971) *Phys. Rev. Lett*. **26**(4) 192

P.M. Tedrow and R. Meservey (1973) *Phys. Rev. Lett*. **7**(1) 318

P.M. Tedrow, J.S. Moodera and R. Meservey (1982) *Solid State Comm.* **44**(5) 587

W. Thompson, F. Holtzberg and T. McGuire (1971) *Phys. Rev. Lett*. **26** 1,308

M. Tinkham (1996) "Introduction to Superconductivity" (New York, McGraw Hill)

K.D. Usadel (1970) *Phys. Rev. Lett.* **25** 507

D. V. Vier and S. Schultz (1983) *Phys. Lett*. **98a** 238

N.R. Werthamer (1963) *Phys. Rev.* **132**(6) 2,440

R. Wiesendanger, H. Güntherodt, G. Güntherodt, R. Gambino and R. Ruf (1990) *Phys. Rev. Lett*. **65** 247

E.L. Wolf (1985) "Principles of Electron Tunneling Spectroscopy" (New York, Oxford University Press)

T. Wong, J.T.C. Yeh and D.N. Langenberg (1976) *Phys. Rev. Lett*. **37**(3) 150

S. Zhang and P.M. Levy (1996) *Phys. Rev. Lett.* **77**(5) 916

S. Zhang and P.M. Levy (1998) *Phys. Rev. B* **57** 5,336

I. Žutić and S. Das Sarma (1999-II) *Phys. Rev. B* **60**(24) R16,322

Chapter Three - Coexistence of Superconductivity and Magnetism

J. Aarts, J.M.E. Geers, E. Bruck, A.A. Golubov and R. Coehoorn *Phys. Rev. B* **56** 2779

A.A. Abrikosov and L.P. Gor'kov (1960) *Zh. Eksp. Teor. Fiz.* **39** 1,781 [(1961) *Sov. Phys. JETP* **12** 1,243]

P.W. Anderson and H. Suhl (1959) *Phys. Rev.* **116** 898

H. Arie, E. Kume and I. Iguchi (1997-I) *Phys. Rev. B* **56**(5) 2,387

A.G. Aronov (1976) *Zh. Eksp. Teor. Fiz.* **71** 371 [(1976) *Sov. Phys. JETP* **44**(1) 193]

M.A. Bari, O. Cabeza, L. Capogna, P. Woodall, C.M. Muirhead and M.G. Blamire (1997) *IEEE Trans. App. Supercon.* **7**(2) 2,304

L.N. Bulaevskiĭ, A.I. Rusinov and M.L. Kulić (1979) *Solid State Comm.* **30** 59

L.N. Bulaevskiĭ, A.I. Buzdin, M.L. Kulić and S.V. Panjukov (1985) *Adv. in Phys.* **34**(2) 175

A.I. Buzdin and L.N. Bulaevskiĭ (1988) *Zh. Eksp. Teor. Fiz.* **67**(3) 576, [(1988) *Sov. Phys. JETP* **94** 256]

C.L. Chien, J.S. Jiang, J.Q. Xiao, D. Davidovic and D.H. Reich (1997) *J. App. Phys.* **81**(8) 5,358

D.B. Chrisey, M.S. Osofsky, J.S. Horwitz, R.J. Soulen, B. Woodfield, J. Byers, G.M. Daly, P.C. Dorsey, J.M. Pond, M. Johnson and R.C.Y Auyeung (1997) *IEEE Trans. App. Supercon.* **7**(2) 2,067

T.W. Clinton and M. Johnson (1997) *App. Phys. Lett.* **70**(9) 1,170

T.W. Clinton and M. Johnson (1998) *J. App. Phys.* **83**(11) 6,777

T.W. Clinton and M. Johnson (1999) *J. App. Phys.* **85**(3) 1,637

T.W. Clinton and M. Johnson (2000) *App. Phys. Lett.* **76**(15) 2,116

E.A. Demler, G.B. Arnold and M.R. Beasley (1997-II) *Phys. Rev. B* **55**(22) 15,174

G. Deutscher and D. Feinberg (2000) *App. Phys. Lett.* **76**(4) 487

M.J. DeWeert and G.B. Arnold (1989) *Phys. Rev. B* **39**(16) 11,307

Z.W. Dong, R. Ramesh, T. Venkatesan, M. Johnson, Z.Y. Chen, S.P. Pai, V. Talyansky, R.P. Sharma, R. Shreekala, C.J. Lobb and R.L. Greene (1997) *App. Phys. Lett.* **71**(12) 1,718

Z.W. Dong, S.P. Pai, R. Ramesh, T. Venkatesan, M. Johnson, Z.Y. Chen, A. Cavanaugh, Y.G. Zhao, X.L. Jiang, R.P. Sharma, S. Ogale and R.L. Greene (1998) *J. App. Phys.* **83**(11) 6,780

W. Dupont, E. Ziemniak and K.D. Usadel (1983) *J. Low Temp. Phys.* **52**(1-2) 41

O. Entin-Wohlman (1975) *Phys. Rev. B* **12**(11) 4,860

V.I. Fal'ko, C.J. Lambert and A.F. Volkov (1999) *Pis'ma Zh. Eksp. Teor. Fiz.* **69**(7) 532 [(1999) *JETP Lett.* **69**(7) 532]

W.A. Fertig, D.C. Johnston, L.E. DeLong, R.W. McCallum, M.B. Maple and B.T. Matthias (1977) *Phys. Rev. Lett.* **38** 387

P. Fulde and R.A. Ferrel (1964) *Phys. Rev. A* **135** 550

P.G. de Gennes and G. Sarma (1963) *J. App. Phys.* **34** 1,380

V.L. Ginzburg (1956) *Zh. Eksp. Teor. Fiz.* **31** 202

M. Giroud, H. Courtois, K. Hasselbach, D. Mailly and B. Pannetier (1998-II) *Phys. Rev. B* **58**(18) R11,872

A.A. Golubov (1999) *Physica C* **326-327** 46

C. Grimaldi and P. Fulde (1997-I) *Phys. Rev. B* **56**(5)5 2,751

L.P. Guo, Y.J. Tian, J.Z. Liu, S.F. Xu, L. Li, Z.X. Zhao, Z.H. Chen, D.F. Cui, H.B. Lu, Y.L. Zhou and G.Z. Yang (1995) *App. Phys. Lett.* **66** 3,356

D.P. Hampshire (1998) *Physica C* **304** 1

N. Hass, M. Covington, W.L. Feldmann, L.H. Greene, M. Johnson (1994) *Physica C* **235-240** 1,905

J.J. Hauser, H.C. Theuerer and N.R. Werthamer (1966) *Phys. Rev.* **142**(1) 118

G. Jakob, V.V. Moschalkov and Y. Bruynseraede (1995) *App. Phys. Lett.* **66**(19) 2,564

F.J. Jedema, B.J. van Wees, B.H. Hoving, A.T. Filip and T.M. Klapwijk (1999-II) *Phys. Rev. B* **60**(24) 16,549

J.S. Jiang, D. Davidovi, D.H. Reich and C.L. Chien (1996) *Phys. Rev. Lett.* **74**(2) 314

M. Johnson (1993) *Phys. Rev. Lett*. **70**(14) 2,142

M. Johnson (1994) *App. Phys. Lett.* **65**(11) 1,460

M. Johnson (1995) *J. Magn. Magn. Mater.* **148** 349

M.J.M. de Jong and C.W.J. Beenakker (1995) *Phys. Rev. Lett.* **74**(9) 1,657

M. Julliere (1975) *Phys. Lett*. **54A**(3) 225

A. Kadigrobov, R.I. Shekhter, M. Jonson and Z.G. Ivanov (1999-I) *Phys. Rev. B* **60**(21) 14,593

M. Kasai, T. Ohno, Y. Kanke, Y. Kozono, M. Hanazono and Y. Sugita (1990) *Jpn. J. App. Phys.* **29**(12) L2,219

M. Kasai, Y. Kanke, T. Ohno and Y. Kozono (1992) *J. App. Phys.* **72**(11) 5,344

D. Koller, M.S. Osofsky, D.B. Chrisey, J.S. Horwitz, R.J. Soulen Jr., R.M. Stroud, C.R. Eddy, J. Kim, R.C.Y. Auyeung, J.B. Byers, B.F. Woodfield, G.M. Daly, T.W. Clinton and M. Johnson (1998) *J. App. Phys.* **83**(11) 6,774

P. Koorevaar, Y. Suzuki, R. Coehoorne and J. Aarts (1994) *Phys. Rev. B* **49** 441

V.N. Krivoruchko and M.A. Belogolovskiĭ (1993) *Pis'ma Zh. Eksp. Teor. Fiz.* **58**(8) 662 [(1993) *JETP Lett.* **58**(8) 642]

M.L. Kulić (1981) *Phys. Rev. A* **83** 46

M.D. Lawrence and N. Giordano (1999) *J. Phys. Cond. Matt.* **11** 1,089

L. Lazar, K. Westerholt, H. Zabel, L.R. Tagirov, Y.V. Goryunov, N.N. Garif'yanov and I.A. Garifullin (2000-I) *Phys. Rev. B* **61**(5) 3,711

K. Lee, W. Wang, I. Iguchi, B. Friedman, T. Ishibashi and K. Sato (1999) *App. Phys. Lett.* **75**(8) 1,149

S.F. Lee, Y. Liou, Y.D. Yao, W.T. Shih and C. Yu (2000) *J. App. Phys.* **87**(9) 5,564

B.T. Matthias, H. Suhl and E. Corenzwit (1958) *Phys. Rev. Lett.* **1** 92

B.T. Matthias and H. Suhl (1960) *Phys. Rev. Lett.* **4**(2) 51

J.E. Mattson, C.D. Potter, M.J. Conover, C.H. Sowers and S.D. Bader (1997) *J. Vac. Sci. Tech. A* **15**(5) 2,793

L.V. Mercaldo, S.M. Anlage and L. Maritato (1999-II) *Phys. Rev. B* **59**(6) 4,455

R.L. Merrill and Q. Si (1999) *Phys. Rev. Lett.* **83**(25) 5,326

D. Mou, A.M. Grishin and K.V. Rao (1998) *J. App. Phys.* **83**(11) 7,327

T. Mühge, K. Westerholt, H. Zabel, N.N. Garif'yanov, Y.V. Goryunov, I.A. Garifullin and G.G. Khaliullin (1997-I) *Phys. Rev. B* **55**(14) 70

T. Mühge, N.N. Garif'yanov, Y.V. Goryunov, K. Theis-Bröhl, K. Westerholt, I.A. Garifullin and H. Zabel (1998) *Physica C* **296** 325

S. Oh, D. Youm and M.R. Beasley (1997) *App. Phys. Lett.* **71**(16) 2,376

V.T. Petrashov, V.N. Antonov, S.V. Maksimov and R.S. Shaĭkhaĭdarov (1994) *Pis'ma Zh. Eksp. Teor. Fiz.* **59**(8) 523 [(1994) *JETP Lett.* **59**(8) 551]

P. Przysłupski, T. Nishizaki, N. Kobayashi, S. Koleśnik, T. Skośkiewicz and E. Dynowska (1999) *Physica B* **259-261** 820

Z. Radović, L. Dobrosavljević-Grujić, A.I. Buzdin, J.R. Clem (1988) *Phys. Rev. B* **38**(4) 2388

C. Rau, C. Lui, A. Schmalzbauer and G. Xing (1986) *Phys. Rev. Lett.* **57** 2,311

M. Rubinstein, P. Lubitz, W. Carlos, P. Broussard, D. Christey, J. Horowitz and J. Krebs (1993) *Phys. Rev. B* **47** 15,350

C.A.R. Sá de Melo (1997) *Phys. Rev. Lett.* **79**(10) 1,933

T. Senthil, M.P.A. Fisher, L. Balents and C. Nayak (1998) *Phys. Rev. Lett.* **81**(21) 4,704

Q. Si (1997) *Phys. Rev. Lett.* **78**(9) 1,767

R.J. Soulen Jr., M.S. Osofsky, D.B. Chrisey, J.S. Horwitz, D. Koller, R.M. Sroud, J. Kim, C.R. Eddy, J.M. Byers, B.F. Woodfield, G.M. Daly, T.W. Clinton, M. Johnson and R.C.Y. Auyeung (1997) *Inst. Phys. Conf. Series* **158** 789

R.J. Soulen Jr., J.M. Byers, M.S. Osofsky, B. Nadgorny, T. Ambrose, S.F. Cheng, P.R. Broussard, C.T. Tanaka, J. Nowak, J.S. Moodera, A. Barry and J.M.D. Coey (1998) *Science* **282**(5,386) 85

S. Stadler, Y.U. Idzerada, Z. Chen, S.B. Ogale and T. Venkatesan (2000) *J. App. Phys.* **87**(9) 6,767

R.M. Stroud, J. Kim, C.R. Eddy, D.B. Chrisey, J.S. Horwitz, D. Koller, M.S. Osofsky, R.J. Soulen Jr. and R.C.Y. Auyeung (1998) *J. App. Phys.* **83**(11) 7,189

C. Strunk, C. Sürgers, U. Paschen and H.v. Löhneysen (1994) *Phys. Rev. B* **49**(6) 4,053

S. Takahashi, H. Imamura and S, Maekawa (1999) *Phys. Rev. Lett.* **82**(19) 3,911

M. Tachiki, A. Koyani, H. Matsumoto and H. Umezawa (1979) *Solid State Comm.* **32** 599

L.R. Tagirov (1998) *Physica C* **307** 145

L.R. Tagirov (1999) *Phys. Rev. Lett.* **83**(10) 2,058

J.E. Tkaczyk and P.M. Tedrow (1988) *Phys. Rev. Lett.* **61**(10) 1,253

J.E. Tkaczyk and P.M. Tedrow (1992-I) *Phys. Rev. B* **46**(13) 8,344

S.K. Upadhyay, A. Palanisami, R.N. Louie and R.A. Buhrman (1998) *Phys. Rev. Lett.* **81**(15) 3,247

V.A. Vas'ko, V.A. Larkin, P.A. Kraus, K.R. Nikolaev, D.E. Grupp, C.A. Nordman and A.M. Goldman (1997) *Phys. Rev. Lett.* **78**(6) 1,134

M. Vélez, M.C. Cyrille, S. Kim, J.L. Vicent and I.K. Schuller (1999) *Phys. Rev. B* **59**(22) 14,659

G. Verbanck, C.D. Potter, R. Schad, P. Belien, V.V. Moshchalkov and Y. Bruynseraede (1994) *Physica C* **235-240** 3,295

H.K. Wong, B.Y. Yin, H.Q. Yang, J.B. Ketterson and J.E. Hillard (1986) *J. Low Temp. Phys.* **63** 307

N.-C. Yeh, R.P. Vasquez, C.C. Fu, A.V. Samoilov, Y. Li and K. Vakili (1999-II) *Phys. Rev. B* **60**(14) 10,522

H.L. Zhao and S. Hershfield (1995) *Phys. Rev. B.* **52**(5) 3,632

J.-X. Zhu (1999) *Physica C* **323** 65

J.-X. Zhu, B. Friedman and C.S. Ting (1999-II) *Phys. Rev. B* **59**(14) 9,558

Chapter Four - Experimental Methods

F. Altmann and D. Katzer (1999) *Thin Solid Films* **344** 609

M.G. Blamire, R.E. Somekh, Z.H. Barber, G.W. Morris and J.E. Evetts (1988) *J. App. Phys.* **64**(11) 6,396

FEI Company (1996) "Focused ion beam workstation user's guide" 7451 N.E. Evergreen Parking, Hillsboro, OR, USA

L.P. Guo, Y.J. Tian, J.Z. Liu, S.F. Xu, L. Li, Z.X. Zhao, Z.H. Chen, D.F. Cui, H.B. Lu, Y.L. Zhou and G.Z. Yang (1995) *App. Phys. Lett.* **66** 3,356

K.H. Huang (1991) Ph.D Thesis, Dept. Materials Science and Metallurgy, University of Cambridge, Cambridge, U.K.

S.B. Kaplan, C.C. Chi and D.N. Langenberg (1976) *Phys. Rev. B* **14**(11) 4,854

J.W. Loram, T.E. Whall and P.J. Ford (1970) *Phys. Rev. B* **2**(4) 357

R.W. Moseley (2000) Ph.D Thesis, Dept. Materials Science and Metallurgy, University of Cambridge, Cambridge, U.K.

H.S. Peiser, H.P. Rooksey and A.J.C. Wilson (1955) “X-Ray Diffraction by Polycrystalline Materials” (London, The Institute of Physics)

M.J. Vasile, R. Nassar, J. Xie and H. Guo (1999) *Micron* **30** 235

R.J. Young (1993) *Vacuum* **44** 353

Chapter Five - Characterisation of Niobium/Cobalt Bilayers

H. Arie, E. Kume and I. Iguchi (1997-I) *Phys. Rev. B* **56**(5) 2,387

C.P. Bean (1962) *Phys. Rev. Lett.* **8** 250

G. Burnell (1998) Ph.D Thesis, Dept. Materials Science and Metallurgy, University of Cambridge, Cambridge, U.K.

L. Callegaro, V. Lacquaniti, S. Maggi, E. Puppin, O. Rampado, S. Ricci and R. Steni (2000) *Philosophical Magazine B* **80**(5) 1,127

S. Chikazumi with the assistance of C.D. Graham Jr. (1997) “Physics of Ferromagnetism” 2nd Edition (Oxford, Clarendon Press)

T.W. Clinton and M. Johnson (1997) *App. Phys. Lett.* **70**(9) 1,170

D.J. Craik and R.S. Tebble (1965) “Ferromagnetism and Ferromagnetic Domains” (Amsterdam, North-Holland)

F.E. Harper and M. Tinkham (1968) *Phys. Rev.* **172** 441

K.H. Huang (1991) Ph.D Thesis, Dept. Materials Science and Metallurgy, University of Cambridge, Cambridge, U.K.

M. Johnson (1995) *J. Magn. Magn. Mater.* **148** 349

G.W.C. Kaye and T.H. Laby (1995) “Tables of Physical and Chemical Constants” 16th Edition (Harlow Essex, Longman)

T. Mühge, N.N. Garif’yanov, Y.V. Goryunov, K. Theis-Bröhl, K. Westerholt, I.A. Garifullin and H. Zabel (1998) *Physica C* **296** 325

C. Muirhead (2001) Private communication

H.S. Peiser, H.P. Rooksey and A.J.C. Wilson (1955) “X-Ray Diffraction by Polycrystalline Materials” (London, The Institute of Physics)

J.H. Quateman (1986) *Phys. Rev. B* **34** 1,948

Chapter Six – Systematic Changes

D. Dimos, P. Chaudhari and J. Mannhart (1990) *Phys. Rev. B* **41**(7) 4,038

B.T. Matthias and H. Suhl (1960) *Phys. Rev. Lett.* **4**(2) 51

R.W. Moseley (2000) Ph.D Thesis, Dept. Materials Science and Metallurgy, University of Cambridge, Cambridge, U.K.

Z. Radović, L. Dobrosavljević-Grujić, A.I. Buzdin, J.R. Clem (1988) *Phys. Rev. B* **38**(4) 2388

N.A. Rutter (2001) Ph.D Thesis, Dept. Materials Science and Metallurgy, University of Cambridge, Cambridge, U.K.

P. Šmilauer (1991) *Contemporary Physics* **32**(2) 89

Chapter Seven – Conclusions

S. Oh, D. Youm and M.R. Beasley (1997) *App. Phys. Lett.* **71**(16) 2,376

L.R. Tagirov (1999) *Phys. Rev. Lett.* **83**(10) 2,058

Appendix A

Paper

The woods are lovely, dark and deep,
but I have promises to keep. And miles to go
before I sleep.

Robert Frost

Active Supercurrent Control in Superconductor/Ferromagnet Heterostructures

Robert J. Kinsey, Gavin Burnell, Mark G. Blamire

Abstract—**Several recent papers predict that the critical temperature of superconducting/ferromagnet heterostructure can be controlled by varying the exchange field of the ferromagnet within the superconductor, providing a means of controlling the superconducting properties. This paper reports the first experimental observation of this effect: we show that the critical temperature and critical current of a Nb/Co bilayer can be controlled by a small magnetic field, on the order of a few tens of kA/m. In these devices, the suppression of T_c is minimised at the coercive field of the Co layer implying that with a sufficiently fine domain structure the net exchange field in the superconductor is reduced. These structures offer the potential for active control of the superconducting properties in both low and high T_c materials through the application of very small magnetic fields.**

Index Terms—**Magnetic Materials, Superconducting Devices, Superconducting Films**

I. Introduction

The proximity effect in superconductor/ferromagnet (S/F) multilayers has been extensively studied. The strong exchange interaction of the ferromagnet extends into the superconductor in a manner similar to the extension of the superconducting order parameter into the ferromagnet. This exchange interaction breaks the spin degeneracy in the superconductor, reducing the superconducting order parameter. This leads to a number of experimentally observed effects, including oscillations in superconducting transition temperature (T_c) as a function of layer thickness [1], [2], the possibility of π-phase Josephson junctions [3] and, when the magnetic field is applied parallel to the ferromagnetic layers, an enhanced critical field [4].

Recent theoretical studies suggest that active control of the magnetization of the ferromagnetic layers in S/F heterostructures can be used to modify the superconducting properties. The proposed heterostructures have a pair of ferromagnetic layers with antiparallel magnetizations at low field and parallel at high field. One way of achieving this is to have the ferromagnetic layers on either side of the superconductor with one layer pinned by the exchange interaction to a single direction by an antiferromagnetic layer (see Fig. 1a) [5]. Alternatively the ferromagnetic layers can be separated with a normal metal spacer with a thickness such that in the zero field state the exchange coupling induces antiparallel alignment [6], as in giant magnetoresistive structures (see Fig 1b).

When the two ferromagnetic layers have antiparallel magnetizations the exchange interaction in the superconductor is reduced. This reduces the pair breaking potential to give an increased T_c, relative to that when the magnetizations are parallel. Alternatively, if the ferromagnet contained multiple domains with antiparallel magnetizations the same increase in T_c would be observed, this was suggested as an explanation for the ferromagnetic superconductors [7].

We report here on measurements of the superconducting properties of niobium/cobalt bilayers with a small magnetic field applied parallel to the track. After saturating the cobalt layer the T_c is higher when a small magnetic field is applied in the opposite direction than it is at zero field. On increasing the field still further, saturating the cobalt again, T_c falls to the original value. This gives rise to a double peak structure that is stable over repeated cycles of the magnetic field, reflecting the magnetization of the Co layer. We propose that the cobalt layer forms antiparallel domains at the coercive field such that the local ferromagnetic exchange interaction in

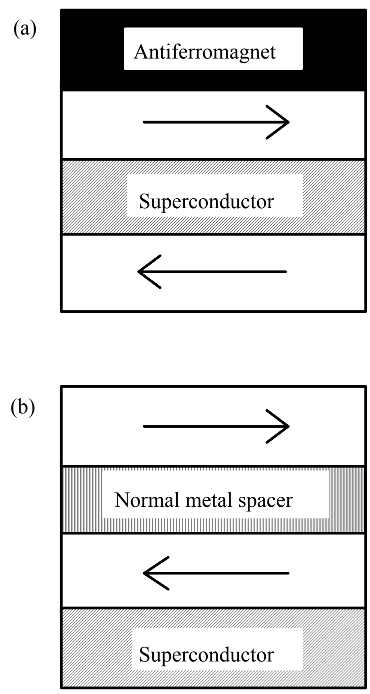

Fig. 1. Two theoretical structures that have been predicted to show an increased T_c when the two ferromagnetic layers, shown with arrows

Manuscript received 17 September 2000. This work was supported by the Engineering and Physical Sciences Research Council (EPSRC) of the United Kingdom.

R. J. Kinsey, G. Burnell and M. G. Blamire are with the IRC in Superconductivity, University of Cambridge, Cambridge, CB3 0HE. (fax: +44 1223 334373, e-mail: rjk20@cam.ac.uk)

the niobium layer is reduced, and hence the T_c is enhanced.

II. Experimental Details

We have measured the superconducting and magnetic properties of niobium/cobalt bilayers. The bilayers consist of (54 ± 9) nm of Co on between 15 and 65 nm of Nb. The bilayers were sputter deposited on r-plane sapphire in a UHV system with a base pressure of 5.10^{-9} mbar. The niobium was deposited at a rate of (16 ± 5) nm min^{-1} and the cobalt at (11 ± 3) nm min^{-1}. The magnetic properties were determined using an unpatterned bilayer at room temperature with a vibrating sample magnetometer (VSM) and at cryogenic temperatures with a SQUID magnetometer. The bilayers were magnetically soft, with a coercive field (H_c) at room temperature between 1.2 kA/m and 2.0 kA/m, increasing to around 5.2 kA/m at 6 K.

The bilayers were then patterned with standard photolithography and Ar^+ milling into 1 µm by 10 µm tracks, with the associated connections and contact pads. The superconducting properties were measured using a quasi-DC transport current with the magnetic field applied in the direction of current flow. The T_c was determined as the temperature at which the conductivity of the track became infinite, measured with a 1 µA transport current. The superconducting critical current (I_c) was determined as the current at which the voltage exceeded 5 µV, approximately three times the noise in the voltage signal.

X-ray diffraction studies of the cobalt layer gives a crystallite size of (56 ± 4) nm. Lorentz microscopy, which shows the domain walls in ferromagnetic materials, also shows that the magnetically soft cobalt layer has a range of domain sizes with some smaller than 1 µm.

III. Results

Fig. 2 shows the shows the effect of a small magnetic field on a track of a Nb/Co bilayer at (5.40 ± 0.05) K. This is above the T_c of the as–deposited film, which is (5.24 ± 0.05) K. The cobalt layer was saturated with the application of –40 kA/m. As the magnetic field was increased to +40 kA/m the track switched from the normal to the superconducting state at +5 kA/m, and then switched back into the normal state at +20 kA/m. This transition into the superconducting state and back into the normal state also occurs when the field is swept in the opposite direction. The maximum I_c occurs at approximately ±8 kA/m, depending on the direction of the magnetic field sweep. This produces the double peak structure shown in Fig. 2b. The double peak structure is stable over repeated sweeps of the magnetic field. Before the magnetic field was applied the critical current was intermediate, between the maximum and minimum values.

The magnetic hysteresis loop of an unpatterned 5 mm by 10 mm film with the same thickness of niobium, at 6 K, is shown in Fig. 2c. The difference in shape anisotropy between the unpatterned film and the patterned chip (which includes the track, connections and contact pads) will shift the magnetic fields at which the features occur. None the less the suppression of I_c in the track appears to follow closely the magnetization of the cobalt layer.

The range of temperatures over which the niobium layer can be switched between the normal and the superconducting state by the application of the magnetic field is only on the order of 0.5 K. This limits the maximum critical current and so the voltage step that occurs on sweeping the magnetic field. The double peak structure in I_c, caused by the change in T_c, persists at lower temperatures. This offers a device with a larger voltage signal. The data shown in Fig. 3 was taken from a Nb/Co bilayer with a niobium thickness of (63 ± 18) nm, an as deposited T_c of (8.42 ± 0.05) K and a resistance of 5.2 Ω at 10 K. Fig. 3a shows the change in the critical current with the magnetic field sweeps. If a constant current, slightly greater than the I_c at high field, is passed through the track then it is possible to obtain a significant change in the voltage signal as the I_c of the track becomes larger than chosen current (see Fig. 3b). In this case the

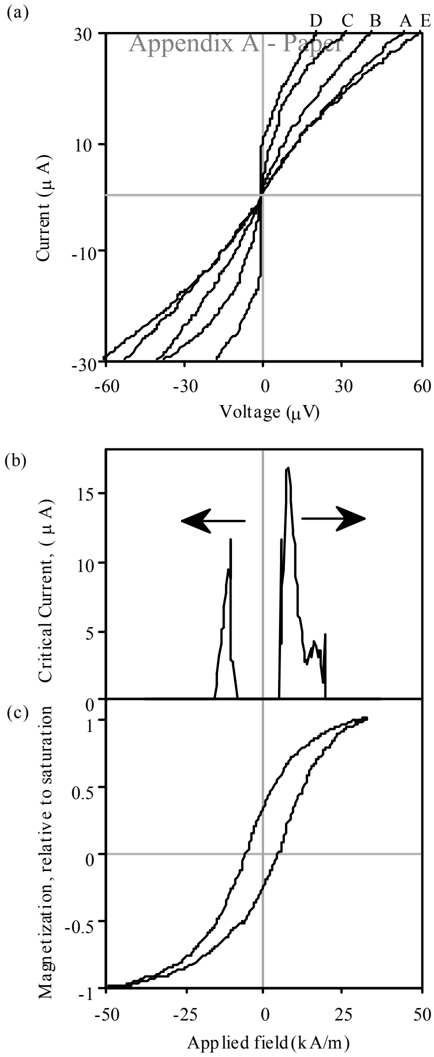

Fig. 2. Superconducting and magnetic measurements of a Nb/Co bilayer with (31 ± 9) nm of niobium at (5.40 ± 0.05) K, slightly above the as-deposited T_c of (5.24 ± 0.05) K. The magnetic field was applied parallel to the track and increased in the direction showed by the arrow. (a) Current vs. voltage characteristics of a 1 µm wide by 10 µm long track after poling at –37 kA/m. The field was successively increased to –32 kA/m (A), –10 kA/m (B), 0 kA/m (C), 10 kA/m (D) and 32 kA/m (E). (b) Critical current vs. magnetic field for the same track. (c) Magnetization vs. applied field loop of an unpatterned 5 mm by 10 mm film of the same thickness at 6 K

indicating the magnetization in the low field state, have antiparallel magnetizations [5], [6].

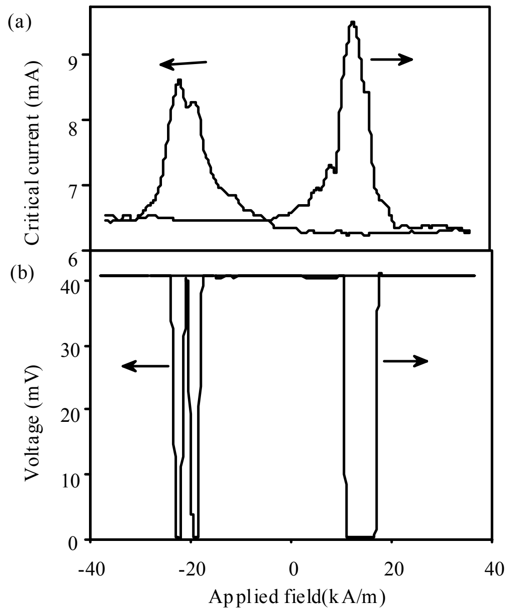

Fig. 3. Superconducting measurements of a Nb/Co bilayer with (63 ± 18) nm of niobium at 4.2 K. This track has an as deposited T_c of (8.42 ± 0.05) K. Magnetic field is applied parallel to the track and increased in the direction shown by the arrow. (a) Change in the critical current of the track as the magnetic field is swept between saturation of the cobalt layer. (b) Change in the voltage signal at an applied current of 8 mA during the magnetic field sweep. This shows the switching between the normal and superconducting state when a current density of (12.7 ± 3.7) MA/cm^2 flows through the track

chosen current is 8 mA, compared to the peak I_c of 9 mA and the minimum I_c of 6.4 mA, which produces a voltage step of (40.5 ± 0.2) mV.

IV. Discussion

While we believe that the double peak structure is caused by the proximity effect we have also considered the possibility of other mechanisms causing the effect. Fig. 4 shows the effect of a small magnetic field on a (17 ± 6) nm thick Nb track with a T_c of (7.1 ± 0.05) K. The I_c is reduced by 18% by the application of 40 kA/m, with no evidence of a double peak structure or any other effect dependent on the magnetic history of the device. This enables us to discount any purely superconducting effect, such as flux flow.

The superconducting properties of the bilayer will also be affected by any stray field from the cobalt layer. This needs to be considered in two parts. The stray field for the cobalt layer on the track itself will be a maximum at H_c. The magnetic field is applied parallel to the track and so the magnetizations will tend to align with the track when the cobalt is saturated. This minimizes the field at the edge of the track. Thus any stray field from the cobalt layer on the track will tend to reduce I_c at H_c rather than increase it as is observed. It is possible that this stray field is responsible for some of the structure seen in the peaks (see Fig. 2b and 3a) .

The stray field from the cobalt layer on the connections to the track is of more concern as it will act to increase the magnetic field near the track when the cobalt is saturated. This would give additional suppression of T_c when the cobalt is saturated and so could give the double peak structure. In order to determine the magnitude of the magnetic field a scale model of the track and connections was made from iron, with a room temperature magnetization approximately 1.1 times the magnetization of the cobalt at 4.2 K, and the field was measured at room temperature (see Fig. 5). The measurements show that the magnetic field over the track does increase but only by 20% at most. Removing the track increases the amount of stray field, as the flux will tend to follow the cobalt and so the niobium layer is screened, and the maximum field is only still twice the applied field, the worst case. In the worst case there is zero field at H_c and 80 kA/m at the maximum applied field. Applying this result to the niobium track (Fig. 4) gives a peak I_c that is 1.56 times as large as that at a large applied field. As Fig. 6 shows the bilayers display a much larger response, the local magnetic field would have to be approximately 4 times the applied

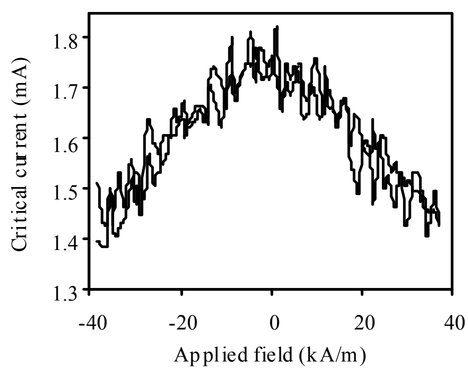

Fig. 4. Critical current vs. applied field measurement of a (17 ± 6) nm thick niobium track at 4.2 K. This track has a T_c of (7.1 ± 0.05) K. The field was applied parallel to the track

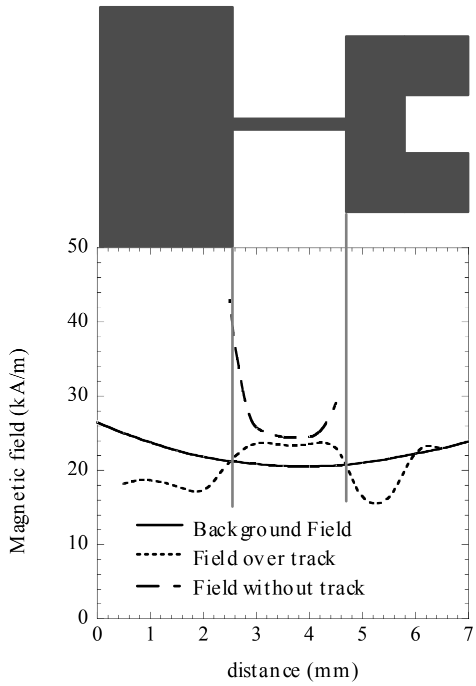

Fig. 5. Determination of the change in the magnetic field caused by the ferromagnetic layer. The portion of the S/F device shown was scaled up and the magnetic field was measured at room temperature. The solid line shows the background field before the ferromagnet was placed between the poles. The dotted line shows the field over the track. The dashed line shows the field between the current and voltage connections when the track is removed.

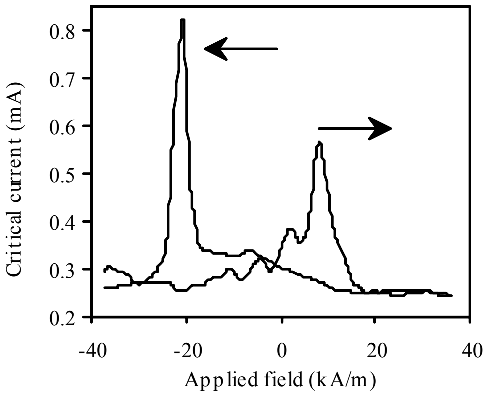

Fig. 6. Critical current vs. applied field measurement of a bilayer with (24 ± 8) nm of Nb track at 4.2 K. This track has a T_c of (5.9 ± 0.05) K. The field was applied parallel to the track. The direction of increasing field is shown by the arrow.

field.

We believe that the double peak structure in T_c and hence I_c is caused by the reduction in the local ferromagnetic exchange field as the cobalt layer forms antiparallel domains at H_c. This domain structure, shown schematically in Fig. 7, is equivalent to the theoretical structures shown in Fig. 1. When the cobalt layer is saturated the strong ferromagnetic exchange interaction gives a large pair breaking potential in the niobium and so a considerable reduction in T_c. However at H_c domains nucleate and grow until the whole cobalt layer has reversed magnetization. The ferromagnetic exchange interaction in the niobium layer will be at a minimum directly beneath the domain walls separating the antiparallel domains. This creates a web of regions with a slightly higher T_c through which the additional critical current flows.

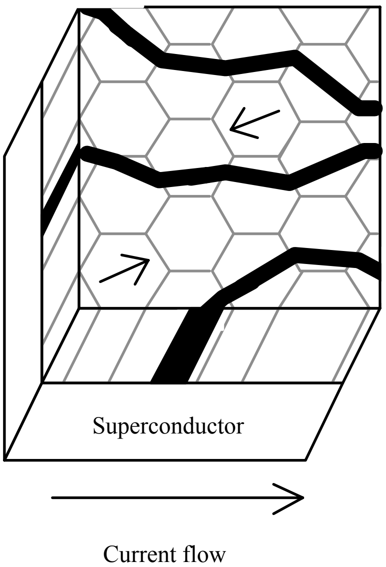

Fig. 7. Schematic of a portion of the S/F bilayer near H_c, The grain boundaries are shown in gray and the domain walls are shown as thick black lines. The strong uniaxial magnetocrystalline anisotropy in cobalt means that the magnetization of each grain lies on a single axis so the domain wall changes direction in each grain, giving a variable domain size. The arrows indicate the magnetization of a single grain.

An alternative way to look at this is to consider a single Cooper pair. The exchange interaction shifts the energy of one spin with respect to the other, reducing the energy gap. However if the Cooper pair extends over two antiparallel domains then the two electrons will both be changed by the same amount and the energy gap will remain the same, giving an increased T_c in that region.

The ability of this structure to act as a superconducting switch is illustrated by Fig. 3. The ferromagnetic layer is easily saturated by a field of a few tens of kA/m and the switching field is close to ten kA/m. The switching voltage obtained depends on the thickness of the niobium layer and the track width. These parameters are limited by the need for a niobium layer thick enough to still be superconducting at the operating temperature and a track wide enough for multiple domains to easily form.

V. Conclusions

We have measured the ferromagnetic and superconducting properties of Nb/Co bilayers in a magnetic field of a few tens of kA/m applied parallel to the track. There is a peak in T_c at a field that we believe is the H_c of the track. This results in a double peak structure that is stable over repeated sweeps of the magnetic field. As other mechanisms will not give this result we believe that it is due to the interaction of the superconductor and the exchange interaction in the ferromagnet.

This is the first experimental measurement of the active control of superconductivity by means of the ferromagnetic exchange interaction. The domain structure formed by the cobalt layer at H_c reduces the local exchange interaction in the niobium layer. This in turn gives an increased T_c and so I_c.

This track can act as a uniaxial low magnetic field superconducting switch. This shows that engineered structures, as shown in Fig. 1, have the potential to be practical devices.

References

[1] C. Strunk, C. Surgers, U. Paschen and H. von Lohneysen, "Superconductivity in layered Nb/Gd film," *Phys. Rev. B*, vol. 49, pp. 4053-4063, 1994.

[2] J.S. Jiang, D. Davidovi, D.H. Reich, C.L. Chien, "Oscillatory superconducting transition temperature in Nb/Gd multilayers," *Phys. Rev. Lett.*, vol. 74, pp. 314-317, 1996.

[3] T. Muhge et al., "Magnetizm and Superconductivity of Fe/Nb/Fe Trilayers," *Phys. Rev. B*, vol. 55, pp. 8945-8954, 1997.

[4] C.L. Chien, J.S. Jiang, J.Q. Xiao, D. Davidovic and D.H. Reich, "Proximity and coupling effects in superconductor/ferromagnet multilayers," *J. App. Phys.*, vol. 81, pp. 5358-5363, 1997.

[5] L.R. Tagirov, "Low-Field Superconducting Spin Switch Based on a Superconductor/Ferromagnet Multilayer," *Phys. Rev. Lett.*, vol. 83, pp. 2058-2061, 1999.

[6] S. Oh, D. Youm, and M.R. Beasley, "A superconductive magnetoresistive memory element using controlled exchange interaction," *App. Phys. Lett.*, vol. 71, pp. 2376-2378, 1997.

[7] A.I. Buzdin, and L.N. Bulaevskii, "Ferromagnetic film on the surface of a superconductor: possible onset of inhomogenious magnetic ordering," *Sov. Phys. JETP*, vol. 67B, pp. 576-578, 1987.

Appendix B

SUPPLEMENTARY DATA

Selah

Sample ID	Niobium thickness (nm)			Cobalt thickness (nm)		
9773a	13·8	±	13·7	50·3	±	15·9
9773b	18·4	±	18·2	50·3	±	15·9
9773c	22·9	±	22·8	50·3	±	15·9
9773d	34·4	±	34·2	50·3	±	15·9
9773e	45·9	±	45·5	50·3	±	15·9
9853a	16·4	±	5·5	51·9	±	15·6
9853b	24·5	±	8·2	51·9	±	15·6
9853c	32·7	±	11·0	51·9	±	15·6
9853d	40·9	±	13·7	51·9	±	15·6
9853Co		—		51·9	±	15·6
9859a	29·5	±	15·6	54·8	±	15·6
9859b	44·3	±	23·4	54·8	±	15·6
9859c	59·1	±	31·2	54·8	±	15·6
9859Co		—		54·8	±	15·6
9859Nb	76·3	±	40·3		—	
9958a	17·7	±	6·0		—	
9958b	32·7	±	11·0		—	
9958c	49·1	±	16·5		—	
9958d	65·5	±	22·0		—	
10073a	14·2	±	5·3	51·9	±	15·6
10073b	16·2	±	6·0	51·9	±	15·6
10073c	28·3	±	6·6	51·9	±	15·6
10073d	26·1	±	7·2	51·9	±	15·6
10073e	32·6	±	7·9	51·9	±	15·6
10122a	19·4	±	6·5	54·5	±	6·2
10122b	21·8	±	7·3	54·5	±	6·2
10122c	24·3	±	8·2	54·5	±	6·2
10122d	26·7	±	9·0	54·5	±	6·2
10122e	29·2	±	9·8	54·5	±	6·2
10186a	28·2	±	6·2	29·4	±	6·2
10186b	28·2	±	6·2	39·3	±	8·3
10186c	28·2	±	6·2	49·1	±	10·4
10186d	28·2	±	6·2	58·9	±	12·5
10186e	28·2	±	6·2		—	
10191a	27·9	±	6·9	26·3	±	6·9
10191b	27·9	±	6·9	35·1	±	9·2
10191c	27·9	±	6·9	43·9	±	11·5
10191d	27·9	±	6·9	52·7	±	13·8
10191e	27·9	±	6·9		—	
10354a	60·3	±	13·0	46·0	±	6·5
10354b	40·2	±	8·7	46·0	±	6·5

Sample ID	Niobium thickness (nm)			Cobalt thickness (nm)		
10354c	30·1	±	6·5	46·0	±	6·5
10354d	40·2	±	8·7	36·8	±	5·2
10354e	40·2	±	8·7		—	
10354f		—		46·0	±	6·5
10409a	58·3	±	15·4	31·2	±	9·4
10409b	58·3	±	15·4	41·6	±	12·5
10409c	58·3	±	15·4	51·9	±	15·6
10409e	58·3	±	15·4		—	
10409g		—		58·6	±	6·9
10466a	65·5	±	22·0	311·7	±	93·8
10554a	27·3	±	9·2	20·8	±	6·3
10554b	163·6	±	55·0	10·4	±	3·1
10554c	27·3	±	9·2	5·2	±	1·6
10554d	27·3	±	9·2	51·9	±	15·6

Table B1 Calculated niobium and cobalt layer thickness for all the Nb/Co bilayers deposited for this work.

Sample 9614 consists of a Nb/Fe bilayer with (139·1 ± 23·4) nm of niobium and (104·9 ± 12·3) nm of iron. Sample 10409f of (127 ± 6) nm of copper.

Sample run 10275 was used to construct the thinned tracks and so a niobium bilayer was used with an aluminium mask and etch stop layer. Within the etched region the niobium layer was (32·7 ± 11·0) nm thick while outside it this was supplemented with an additional (81·8 ± 27·5) nm of Nb. The bottom cobalt layer had a thickness of (23·0 ± 10·5) nm, (28·7 ± 13·1) nm, (40·2 ± 18·4) nm, (51·7 ± 23·6) nm and (63·2 ± 28·9) nm for samples 10275a to 10275e respectively.

Sample runs 10432 and 10466 were attempts to manufacture spin valve structures in place of a simple cobalt layer, though they were unsuccessful. They consisted of the following structures:

10432a: (65·5 ± 22·0) nm of Nb, (31·2 ± 9·4) nm of Co, (4·3 ± 0·8) nm of Cu, (31·2 ± 9·4) nm of Co

10432b: (81·8 ± 27·5) nm of Nb, (31·2 ± 9·4) nm of Co, nine repeats of [(4·3 ± 0·8) nm of Cu, (31·2 ± 9·4) nm of Co]

10466a: (65·5 ± 22·0) nm of Nb, (311·7 ± 93·8) nm of Co

10466b: (49·1 ± 16·5) nm of Nb, (31·2 ± 9·4) nm of Co, nine repeats of [(1·8 ± 0·3) nm of Cu, (31·2 ± 9·4) nm of Co]

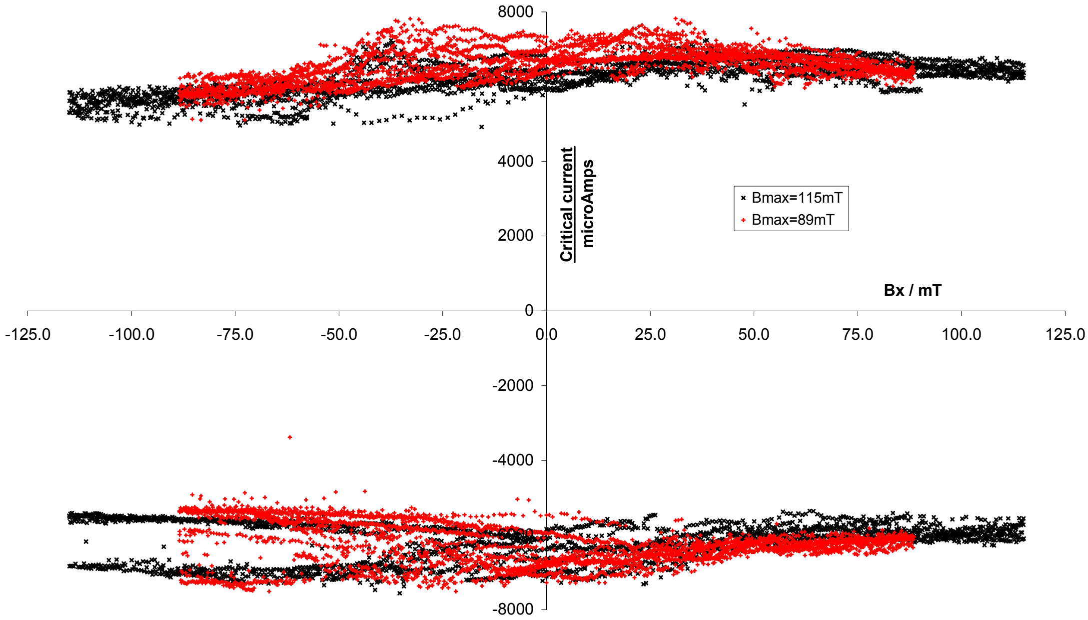

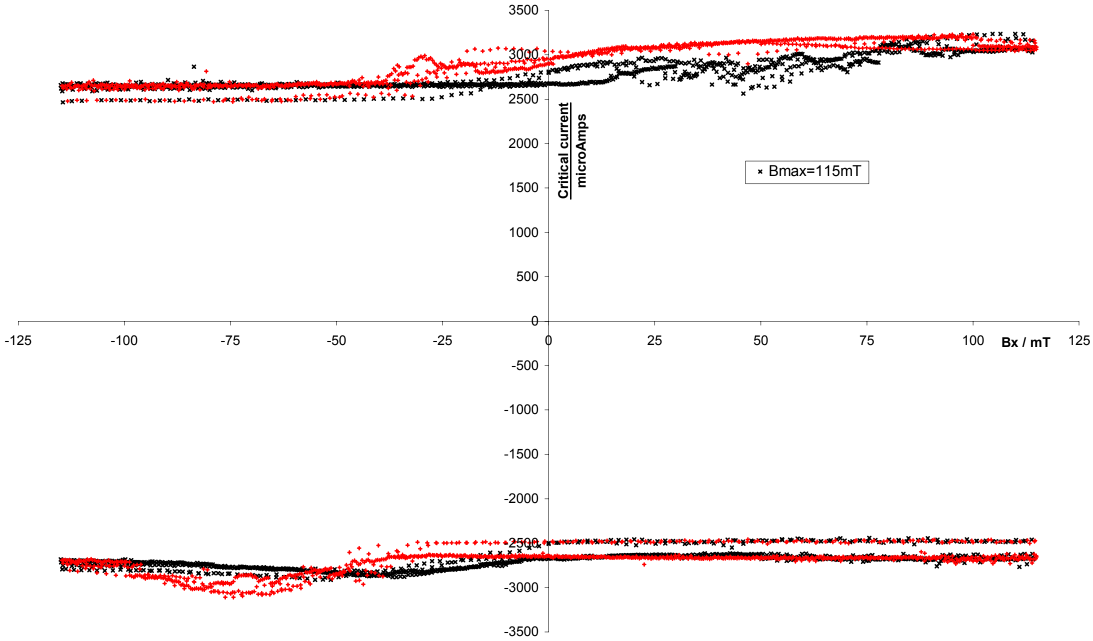

Figure B1 Sample 9614, one micron wide tracks, field applied in the x-direction at 4·2K.

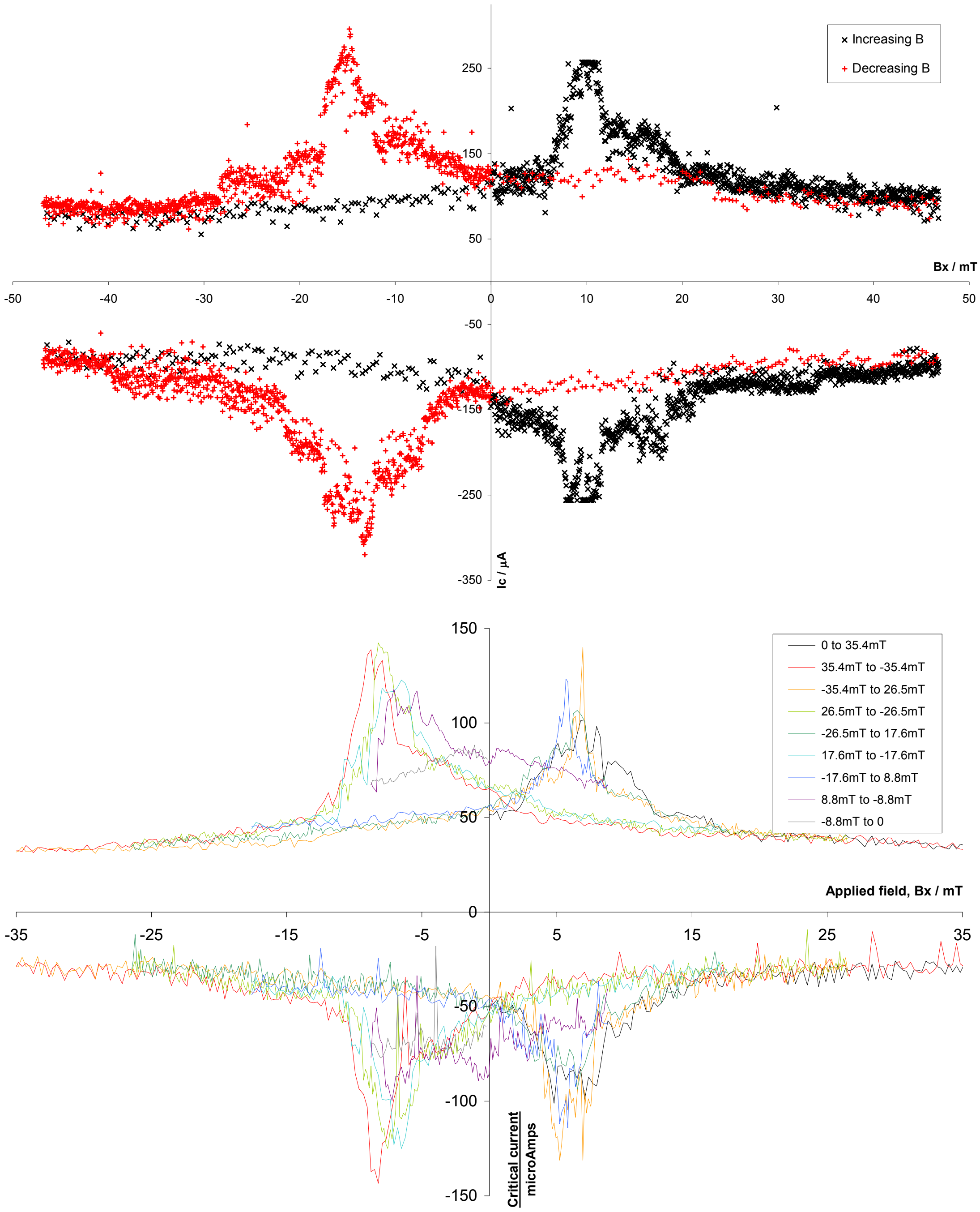

Figure B2 Sample 9467b, one micron wide tracks, field applied in the x-direction at 4·2K.

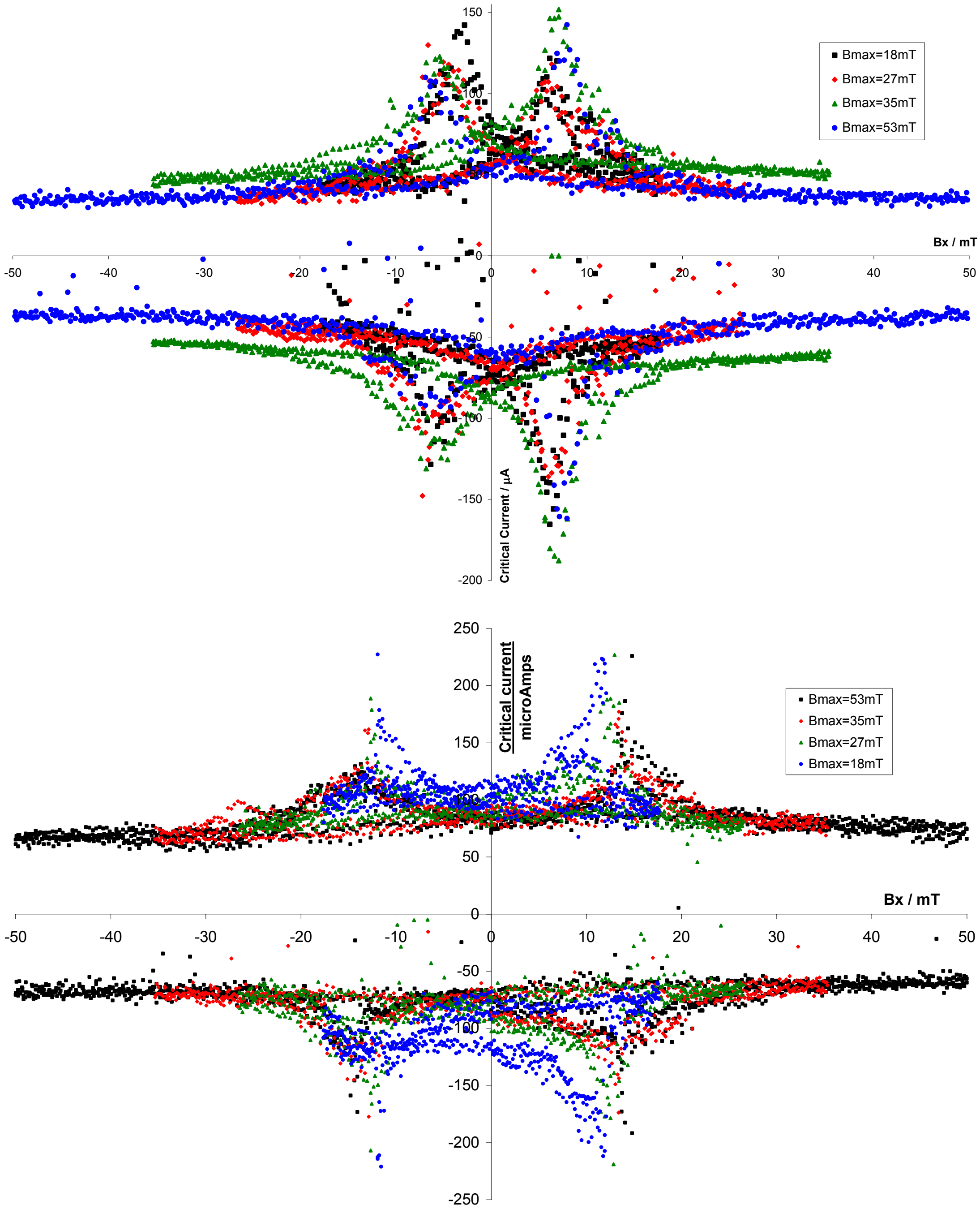

Figure B3 Sample 9467b, one micron wide tracks, field applied in the x-direction at 4·2K.

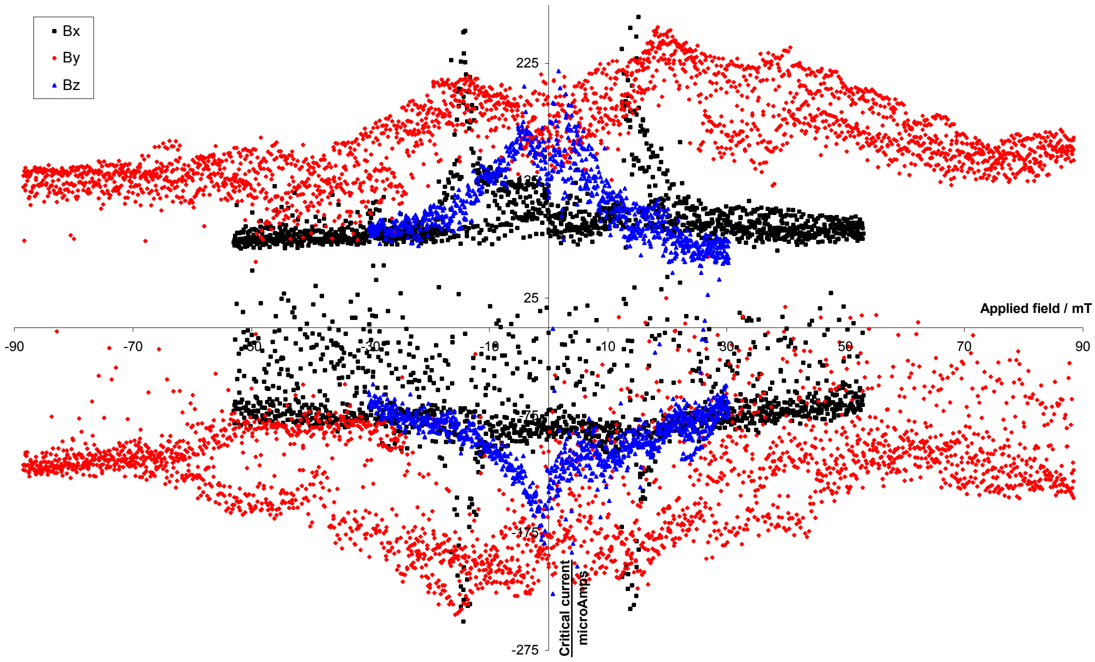

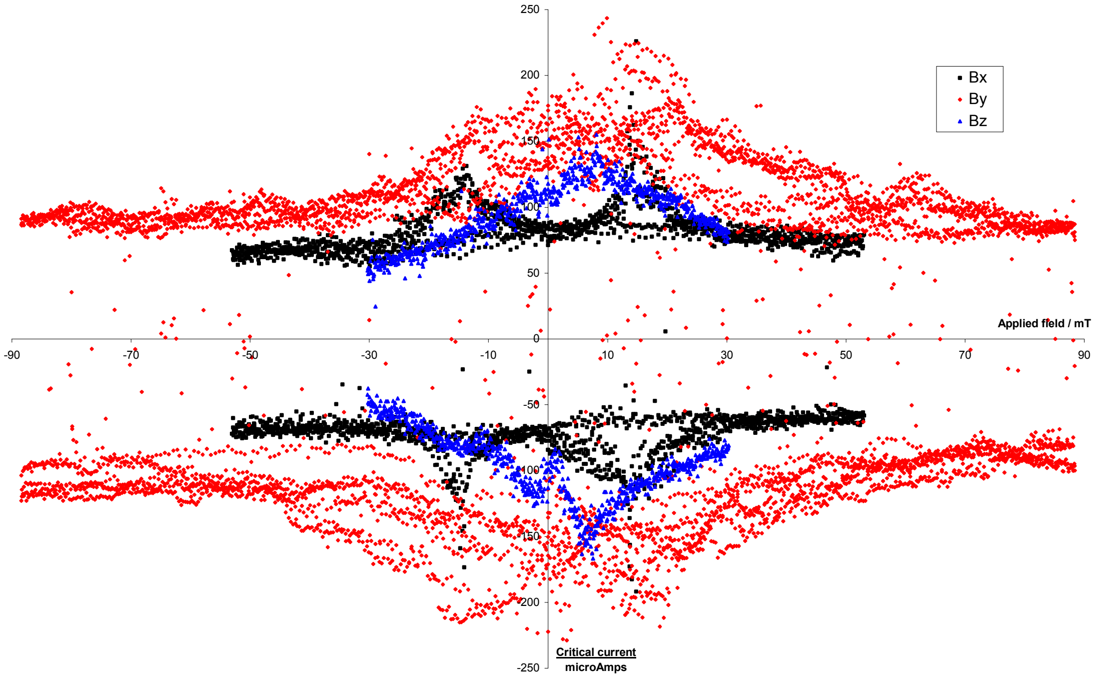

Figure B4 Sample 9467b, one micron wide tracks, field applied in the three orthogonal directions at 4·2K.

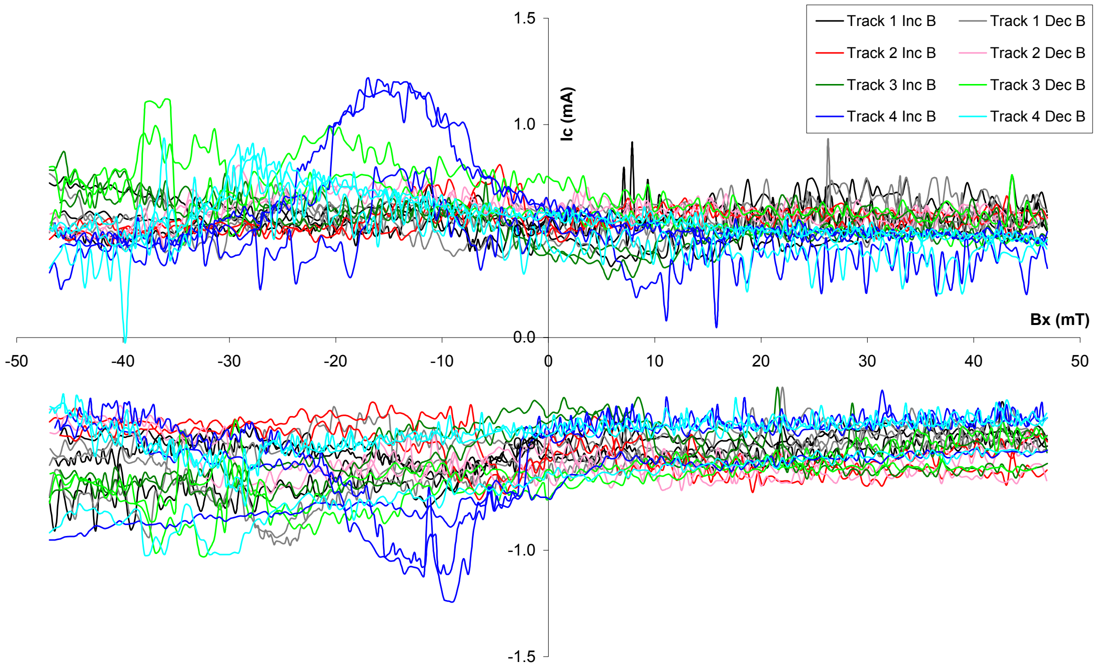

Figure B5 Sample 9773d, two micron wide tracks, field applied in the x-direction at 4·2K.

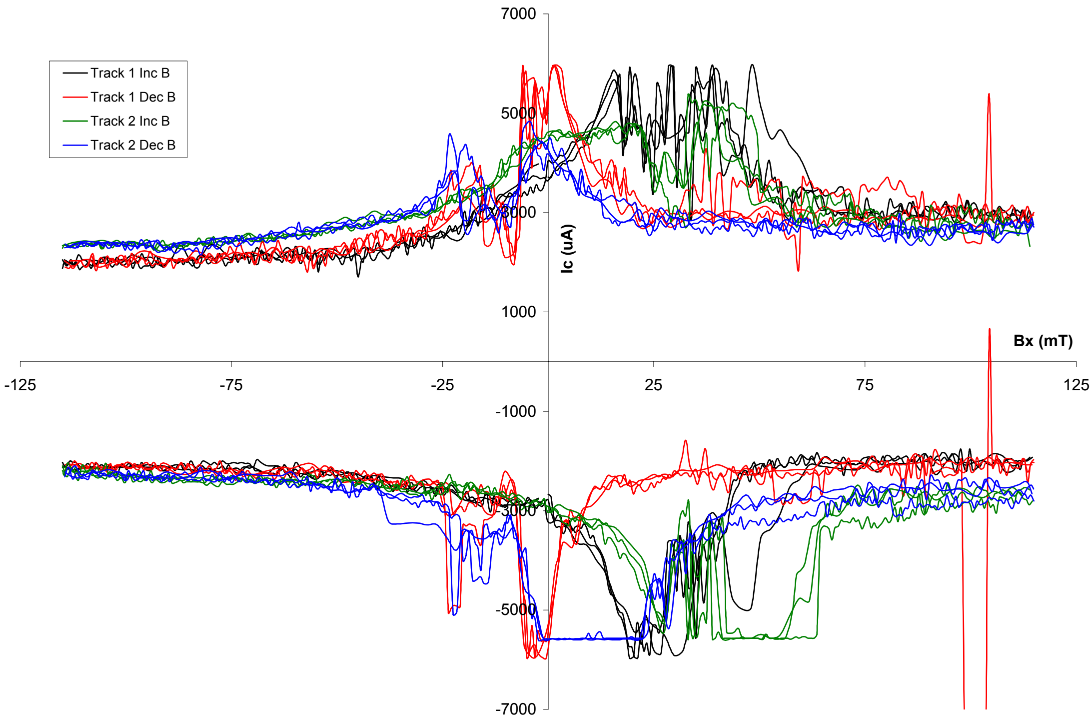

Figure B6 Sample 9773e, two micron wide tracks, field applied in the x-direction at 4·2K.

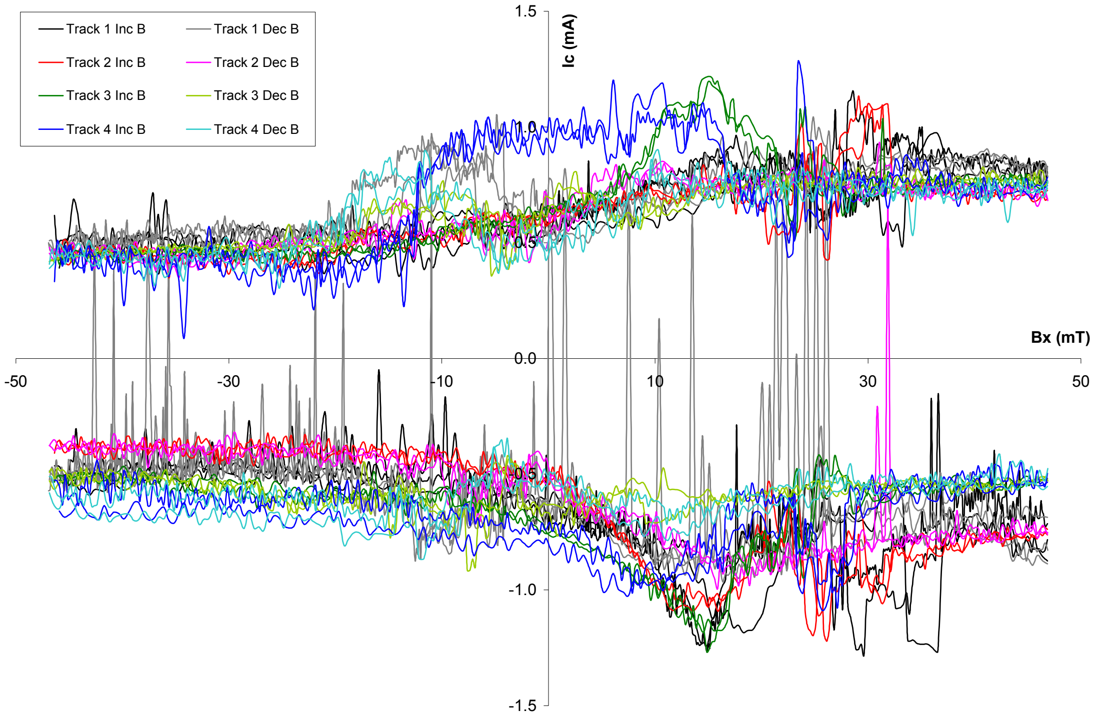

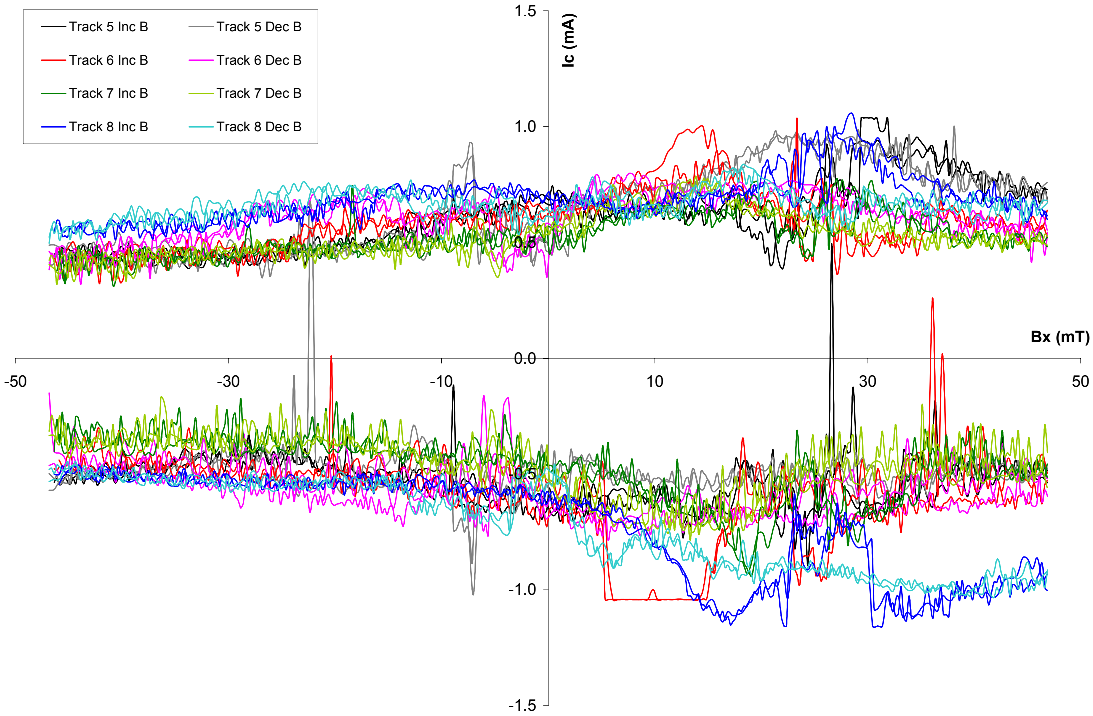

Figure B7 Sample 9853b, two micron wide tracks, field applied in the x-direction at 4·2K.

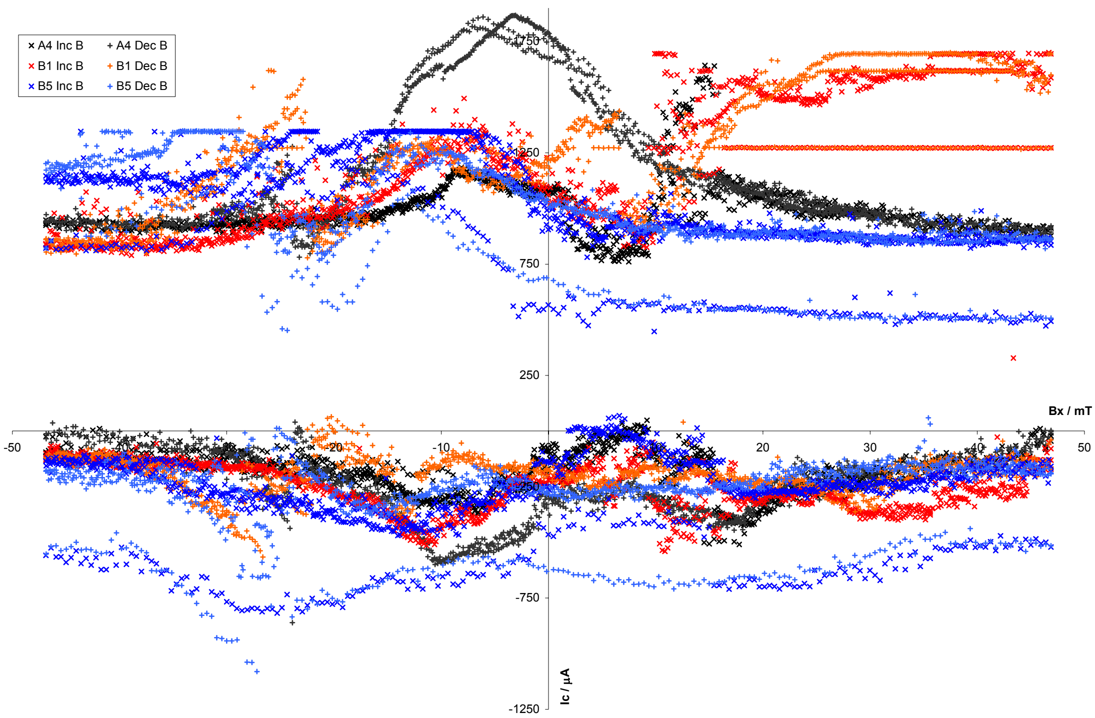

Figure B7 Sample 9853b, two micron wide tracks, field applied in the x-direction at 4·2K.

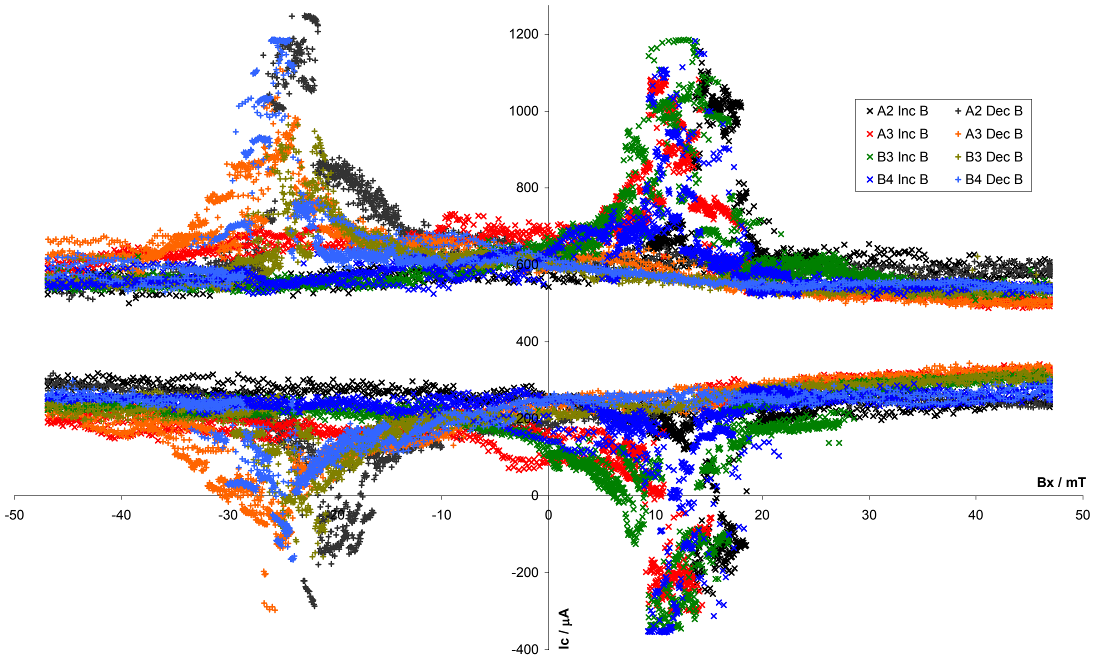

Figure B8 Sample 9853b, two micron wide tracks with a one micron wide and half micron long constriction, field applied in the x-direction at 4·2K.

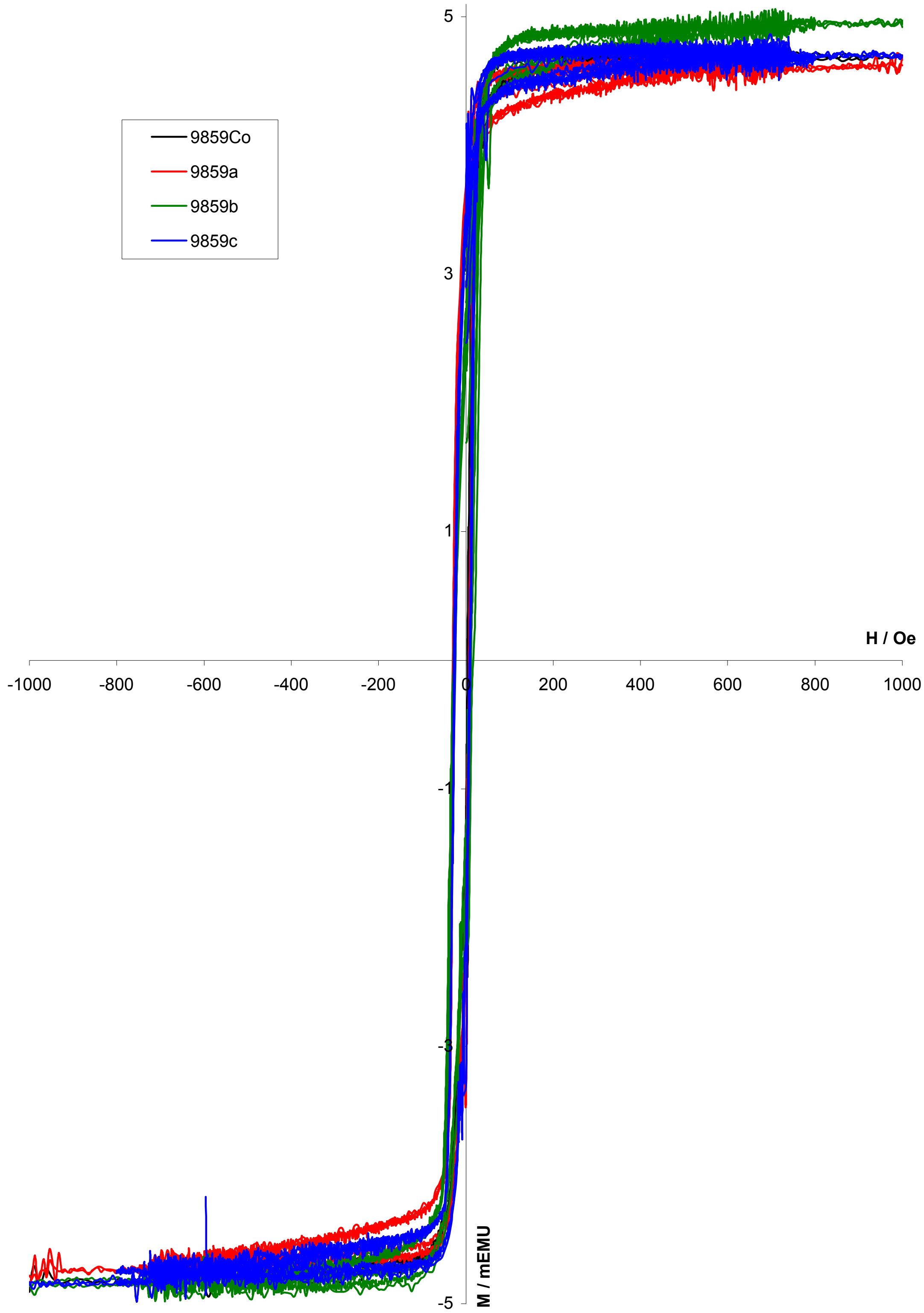

Figure B9 Samples 9859, unpatterned 10mm by 5mm film, field applied along the long axis at room temperature.

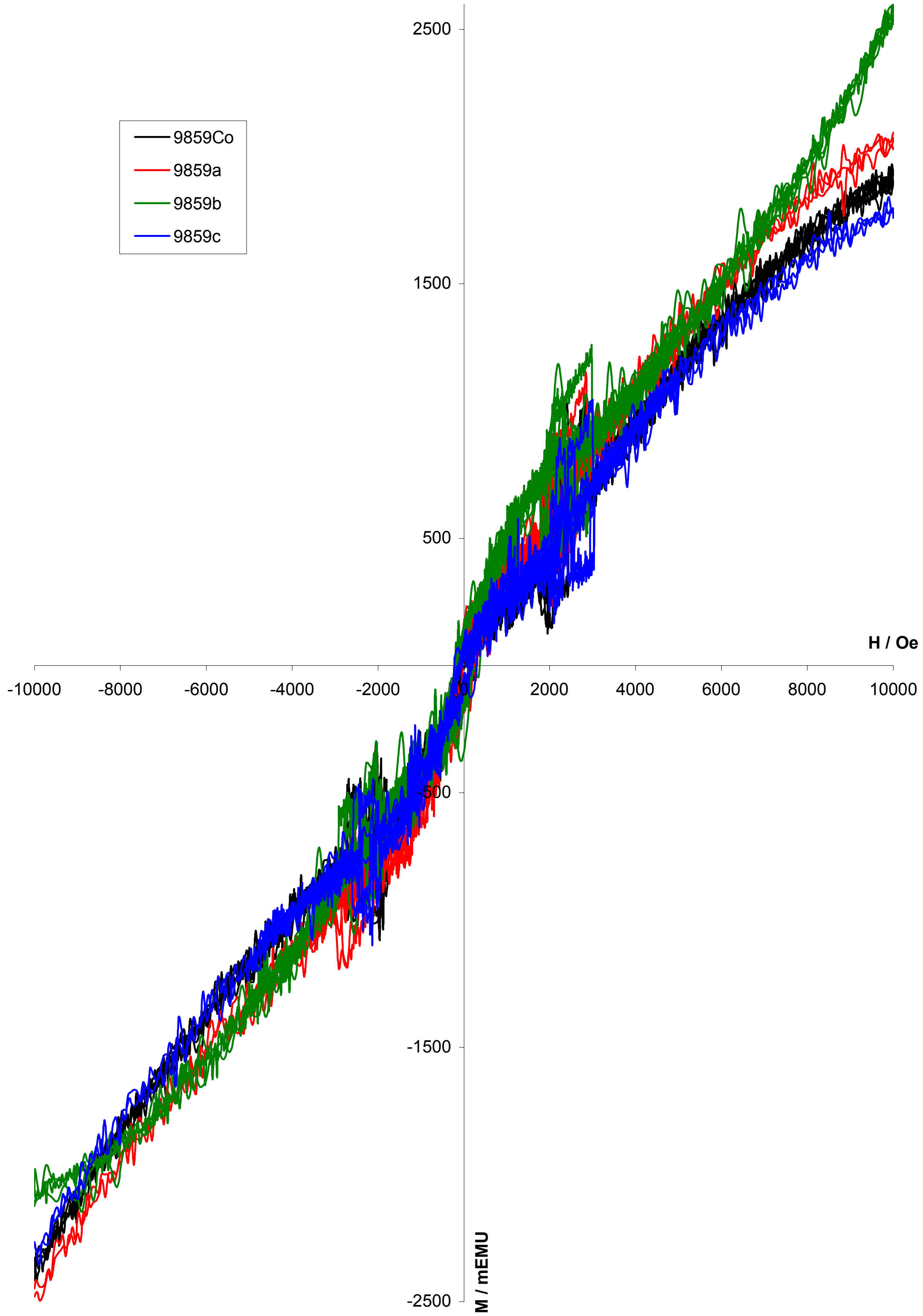

Figure B10 Samples 9859, unpatterned 10mm by 5mm film, field applied along the short axis at room temperature.

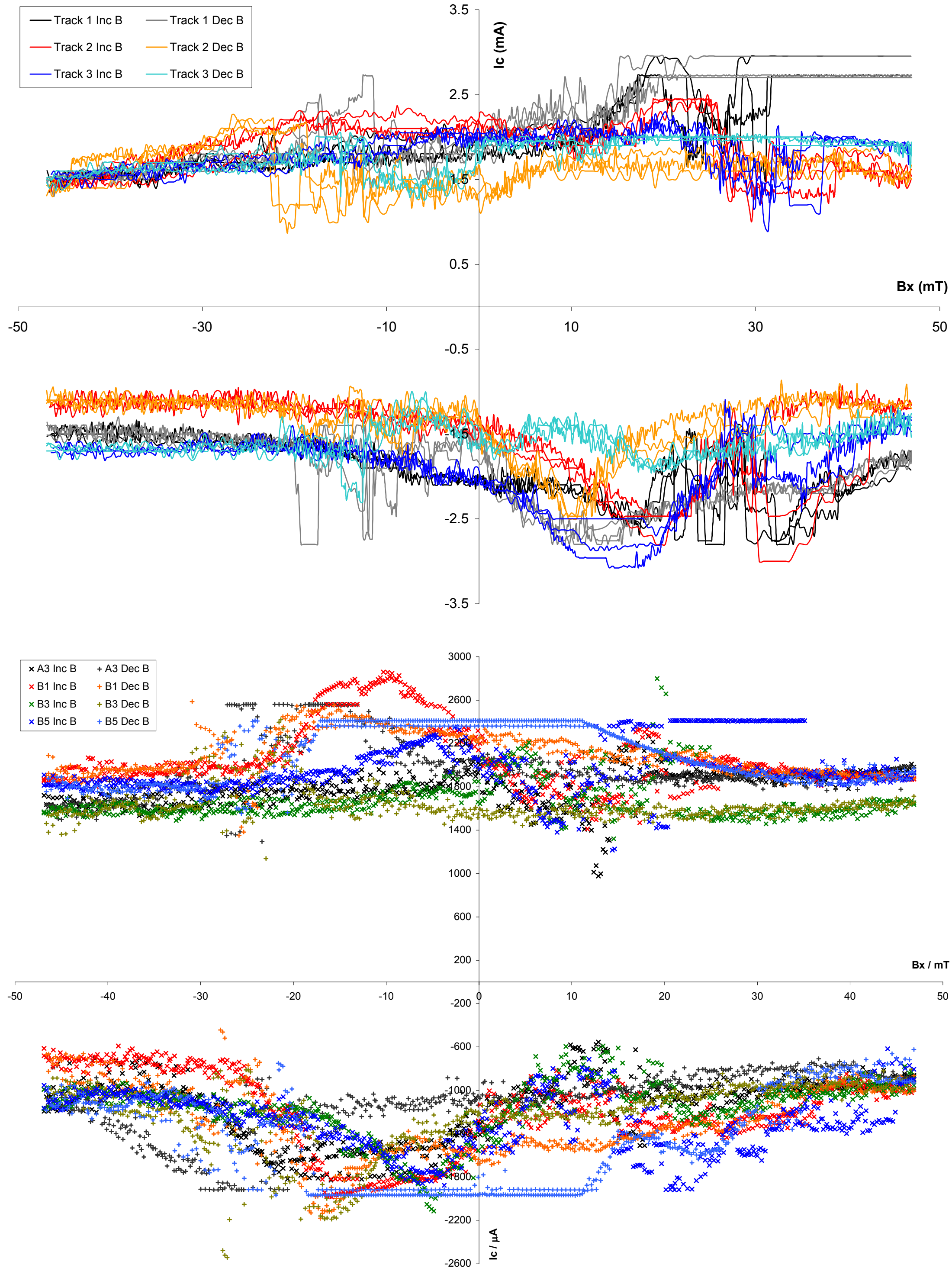

Figure B11 Sample 9859a, two micron wide tracks, field applied in the x-direction at 4·2K.

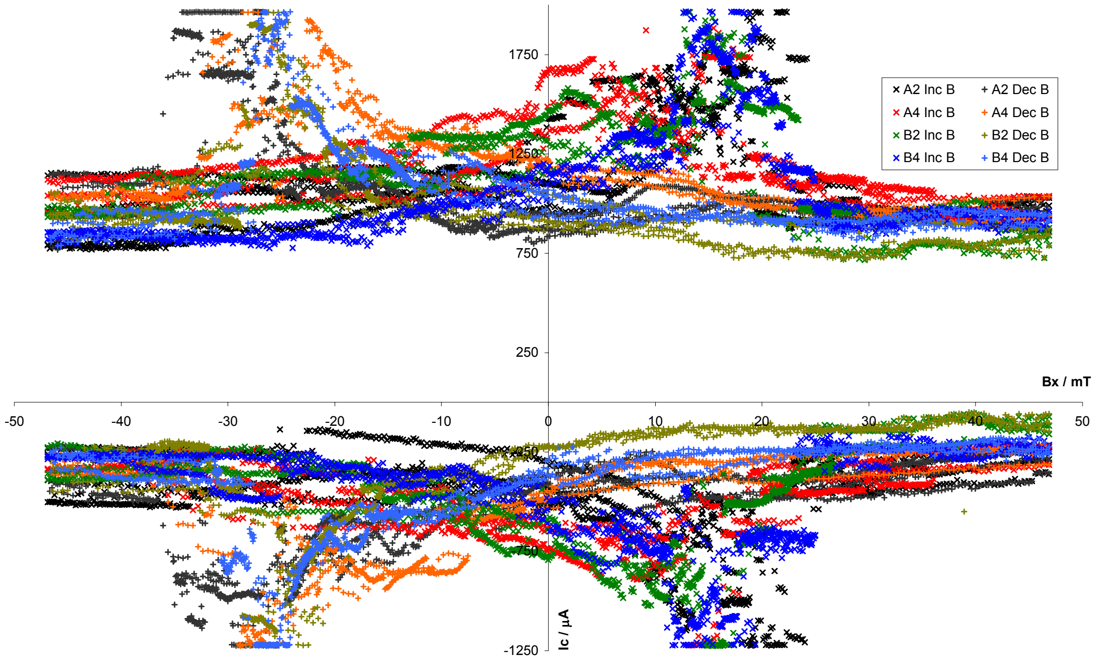

Figure B12 Sample 9859a, two micron wide tracks with a one micron wide and half micron long constriction, field applied in the x-direction at 4·2K.

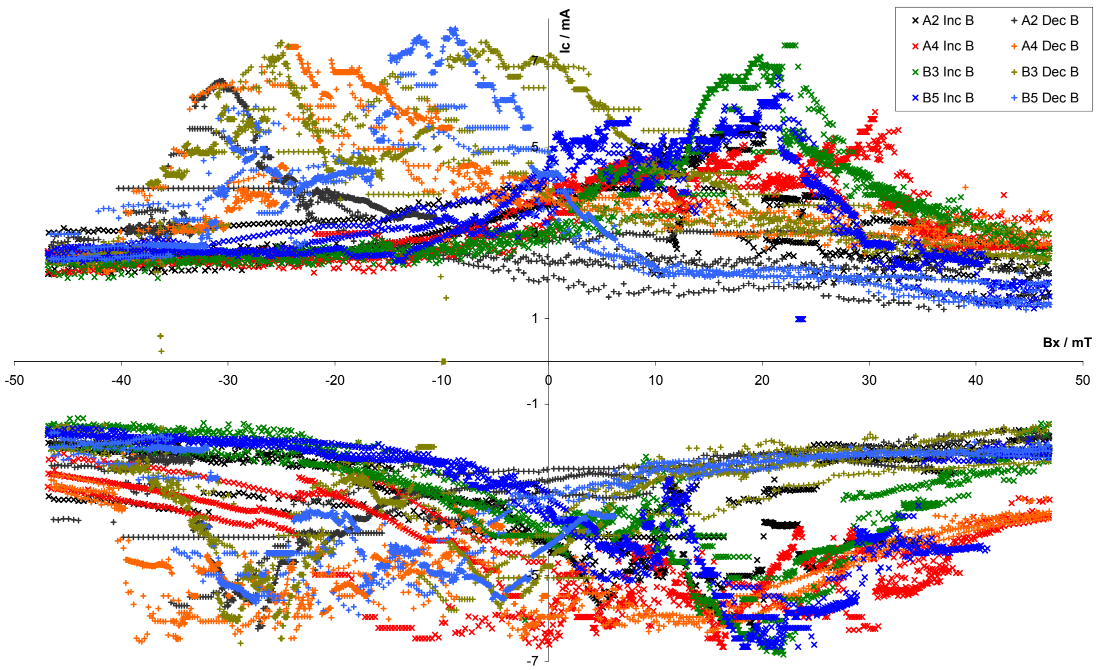

Figure B13 Sample 9859b, two micron wide tracks with a one micron wide and half micron long constriction, field applied in the x-direction at 4·2K.

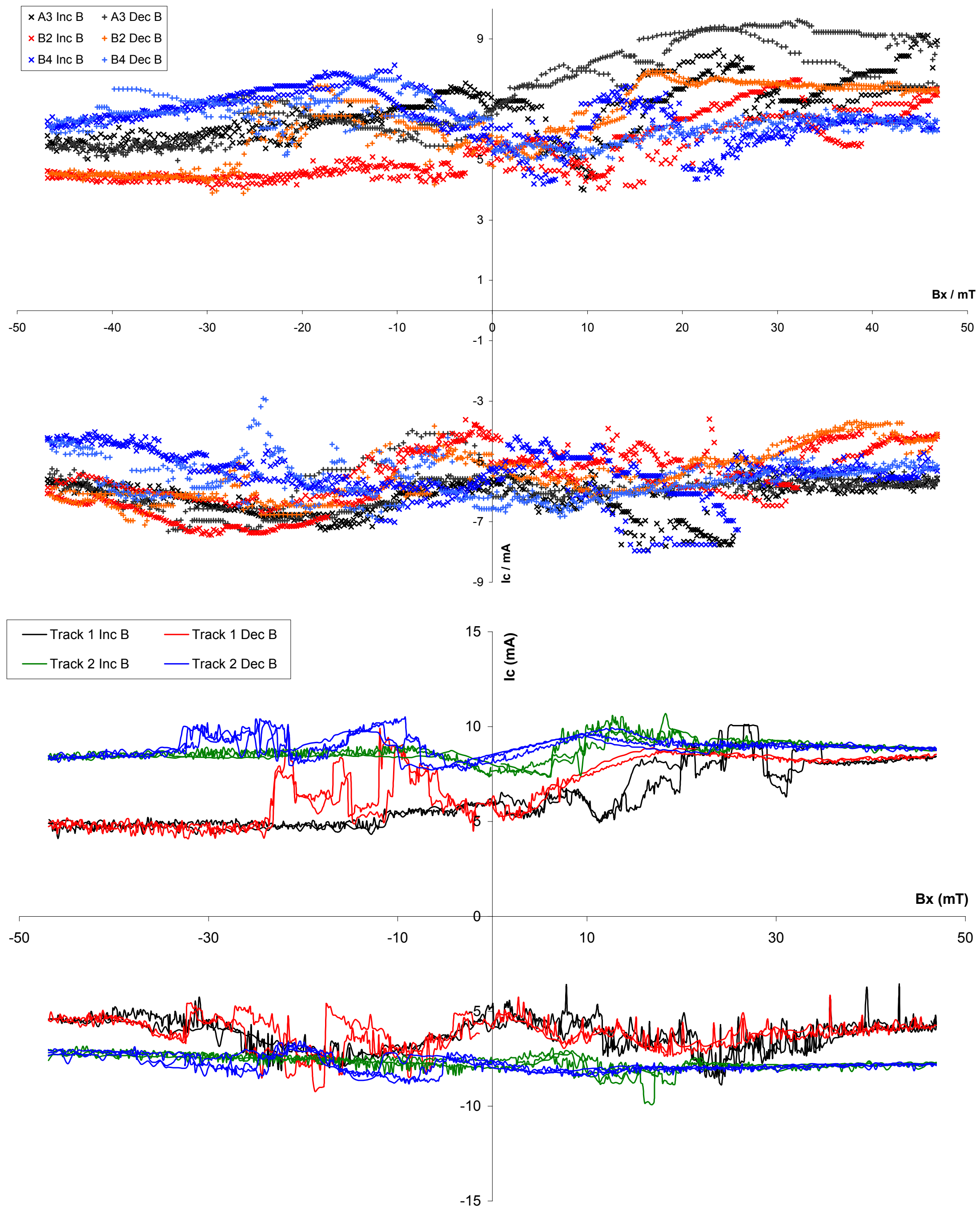

Figure B14 Sample 9859b, two micron wide tracks, field applied in the x-direction at 4·2K.

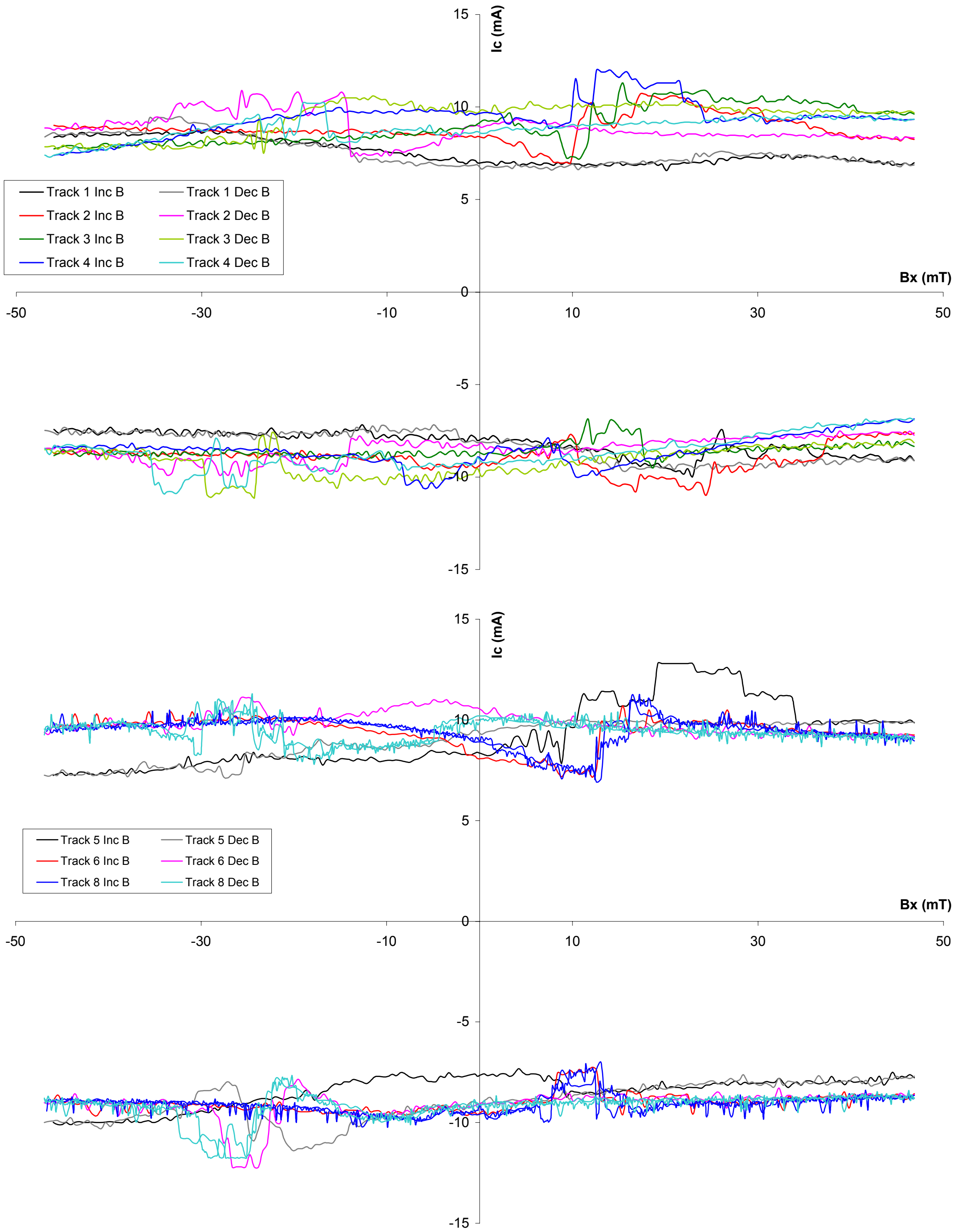

Figure B15 Sample 9859c, two micron wide tracks, field applied in the x-direction at 4·2K.

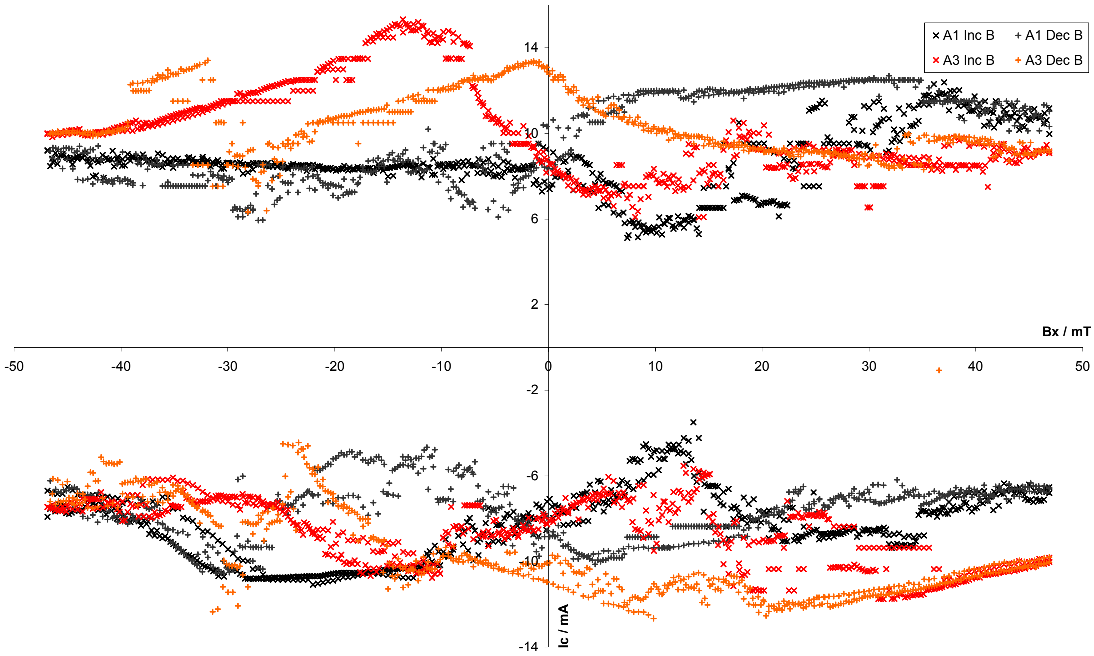

Figure B16 Sample 9859c, two micron wide tracks, field applied in the x-direction at 4·2K.

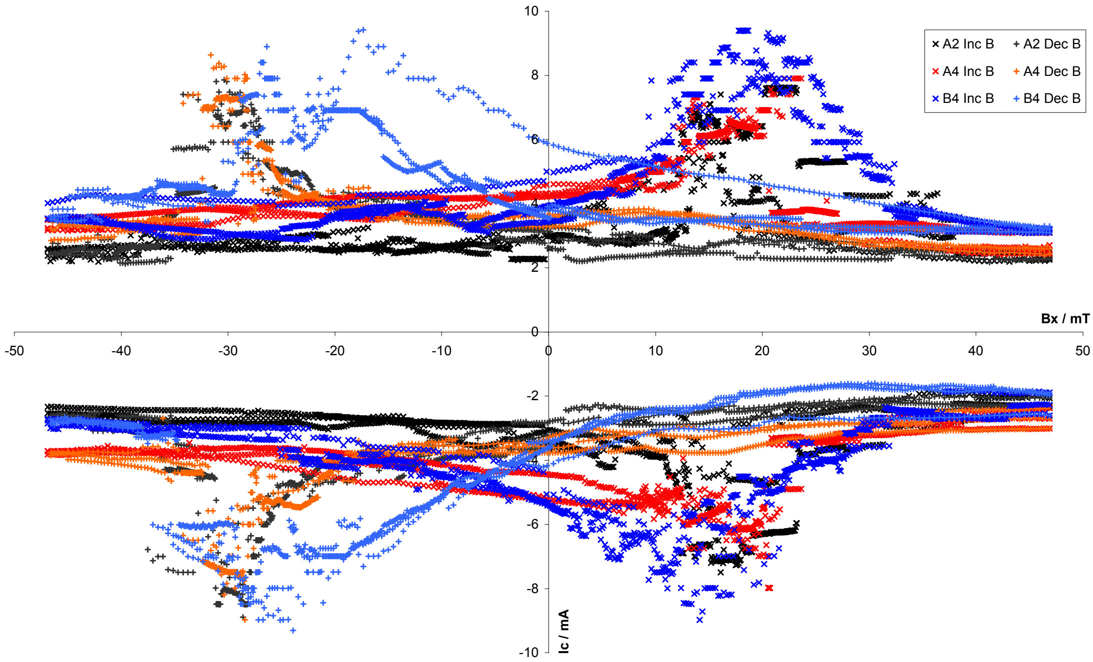

Figure B17 Sample 9859c, two micron wide tracks with a one micron wide and half micron long constriction, field applied in the x-direction at 4·2K.

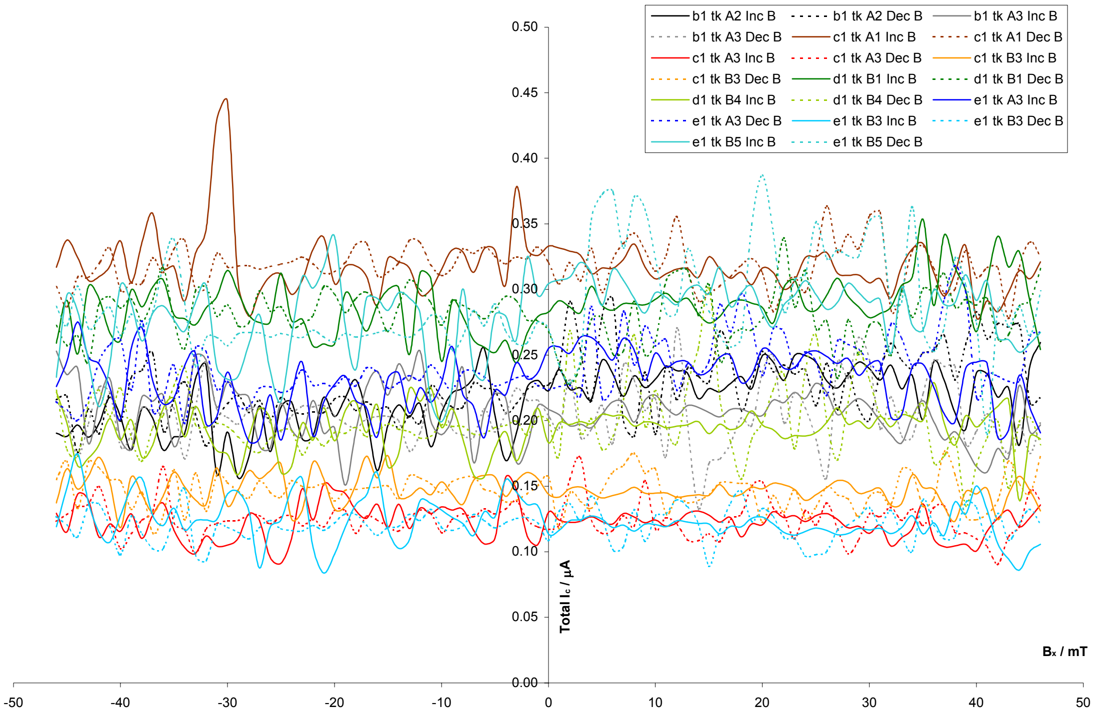

Figure B18 Samples 10073b to e, two micron wide tracks, field applied in the x-direction at 4·2K.

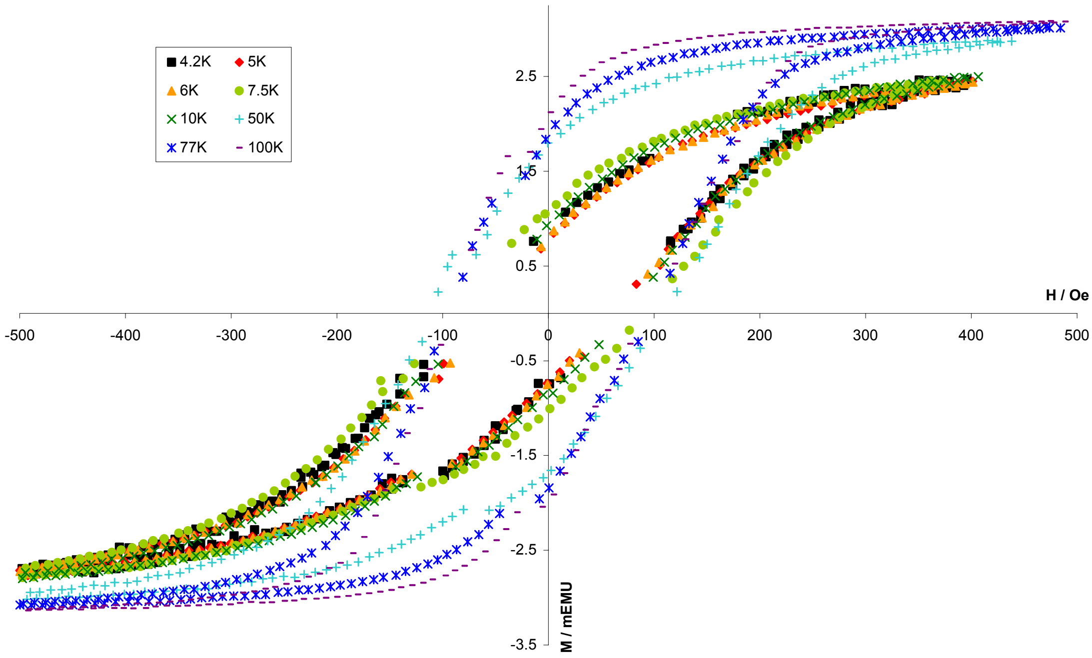

Figure B19 Samples 10122d1, unpatterned 10mm by 5mm film, field applied along the long axis.

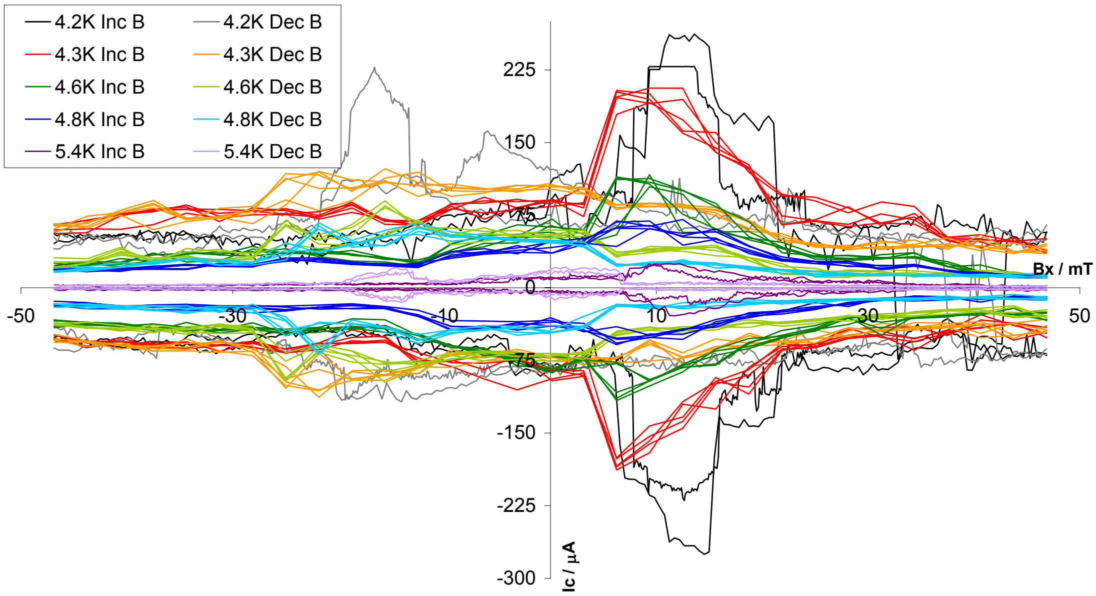

Figure B20 Sample 10122d, one micron wide track, field applied in the x-direction at the temperature shown.

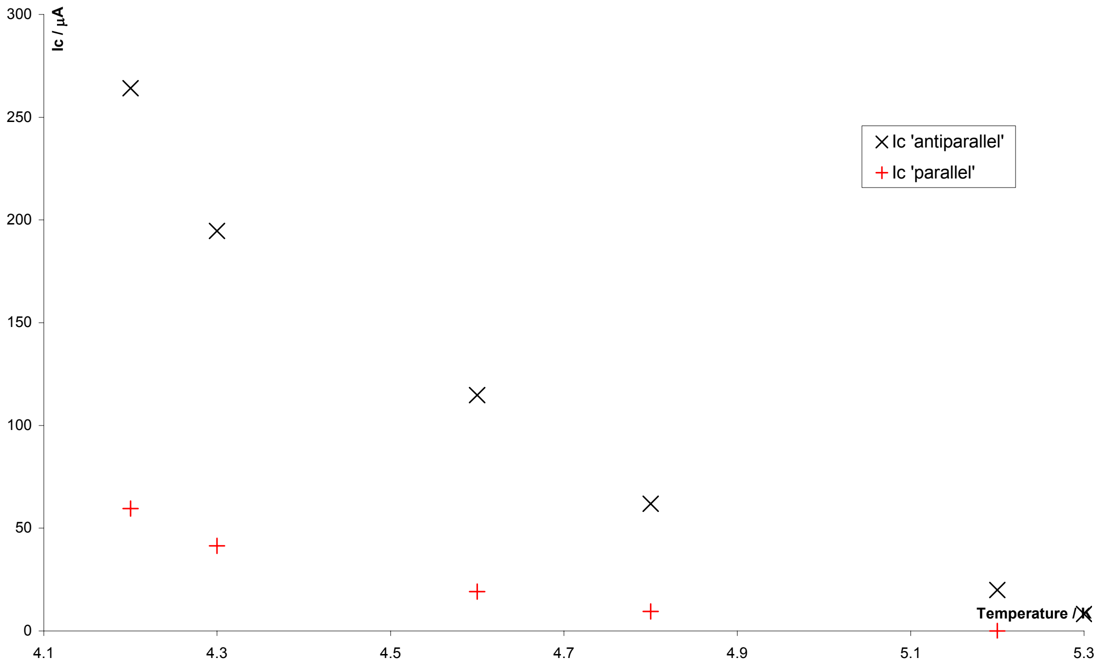

Figure B21 Sample 10122d, one micron wide track, field applied in the x-direction with the field either at maximum or else the maximum critical current.

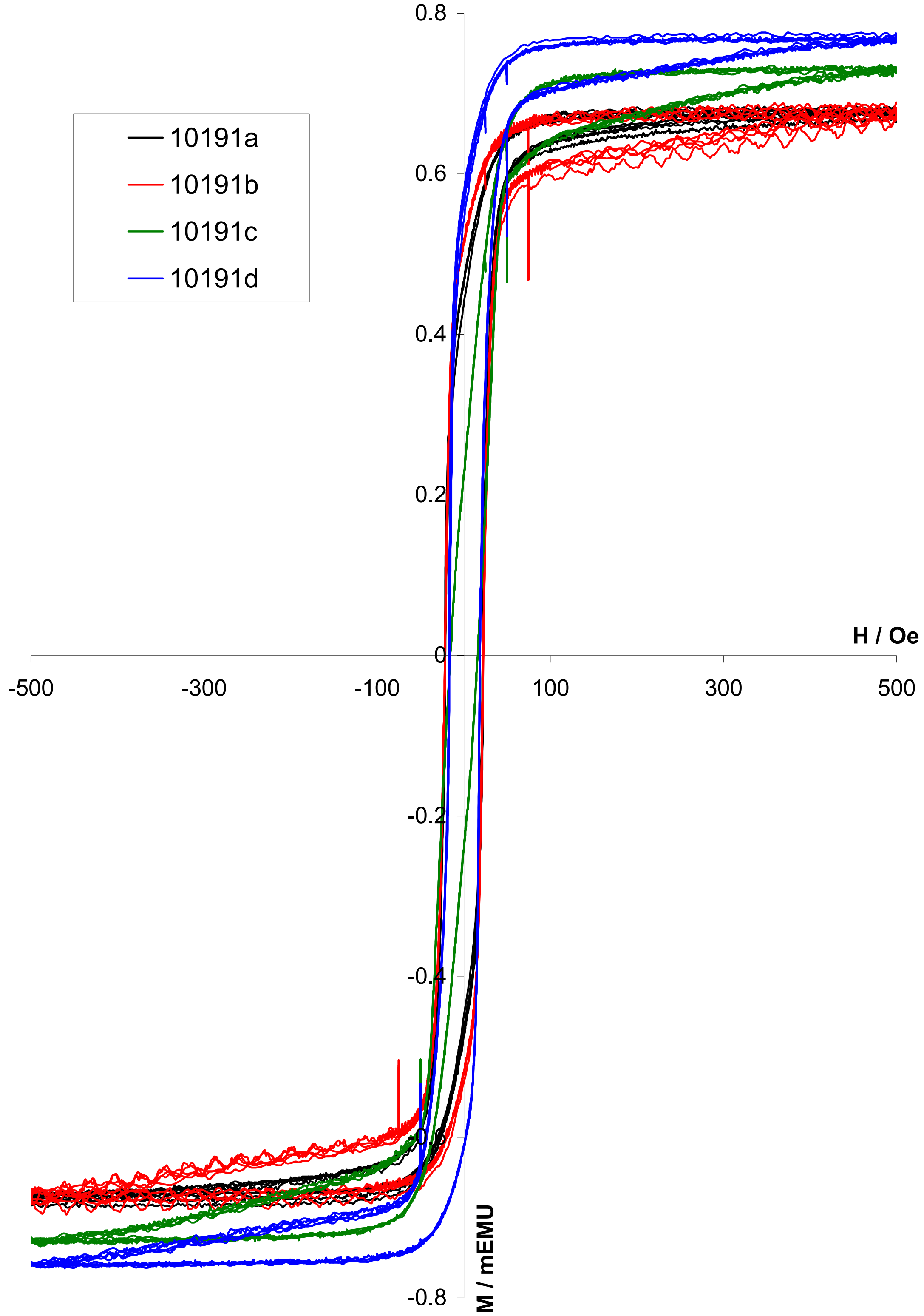

Figure B22 Samples 10191, unpatterned 10mm by 5mm film, field applied along the long axis at room temperature.

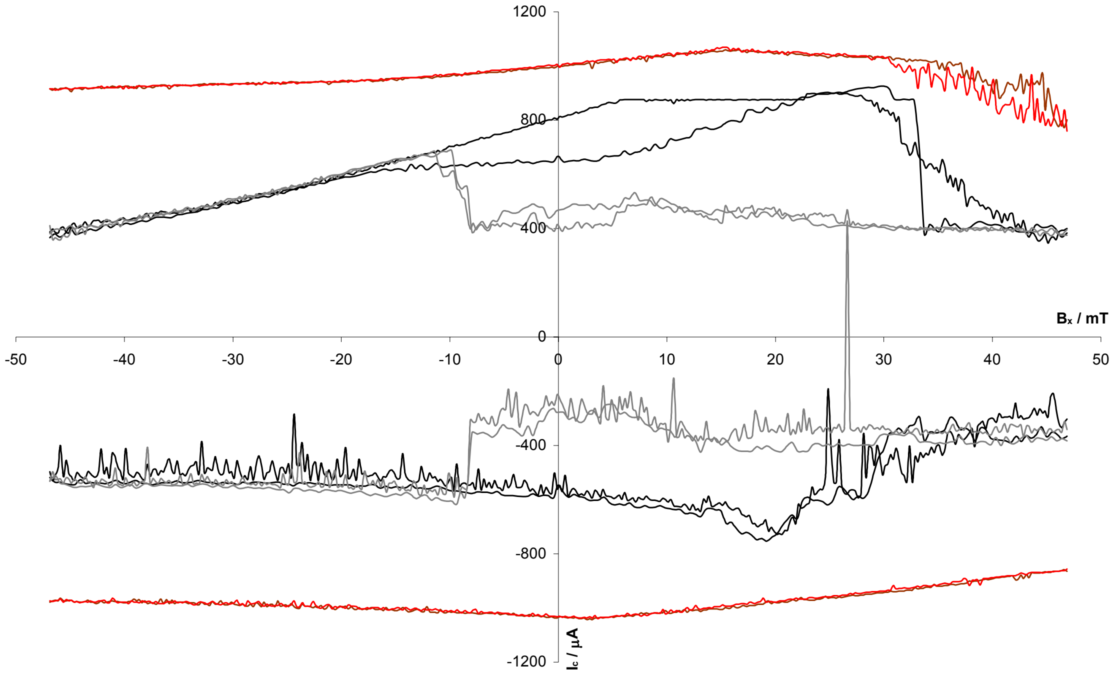

Figure B23 Sample 10191a, two micron wide tracks with a one micron wide and one micron long constriction, field applied in the x-direction at 4·2K.

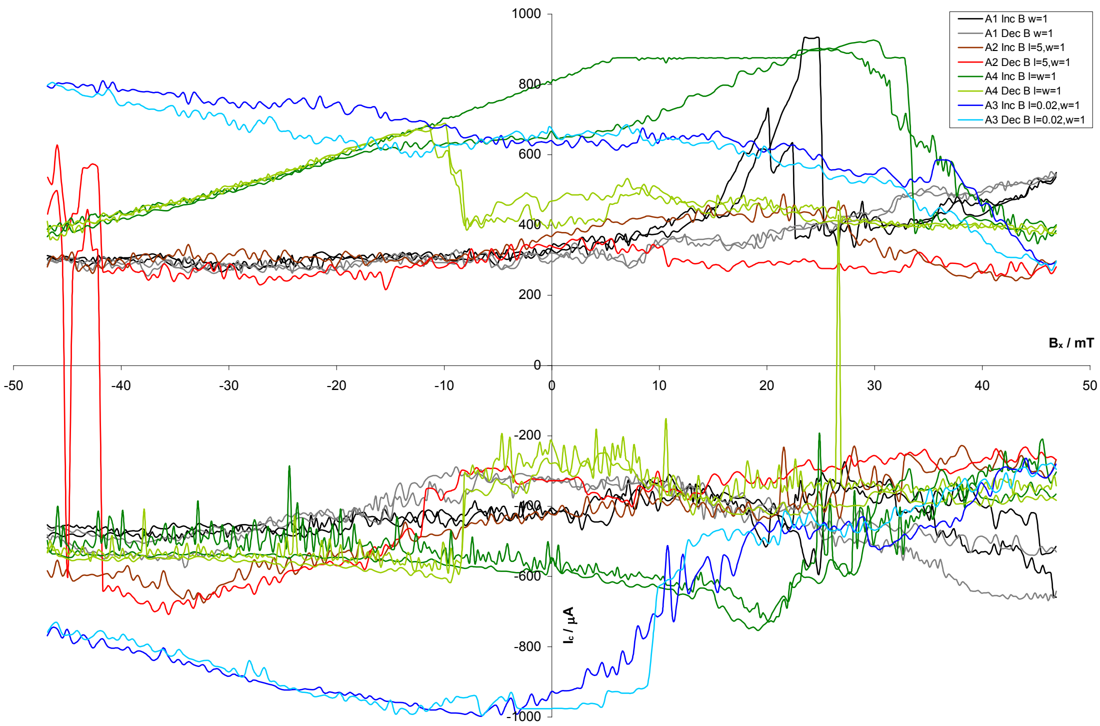

Figure B24 Sample 10191a, two micron wide tracks with a one micron wide constriction with the length shown, field applied in the x-direction at 4·2K.

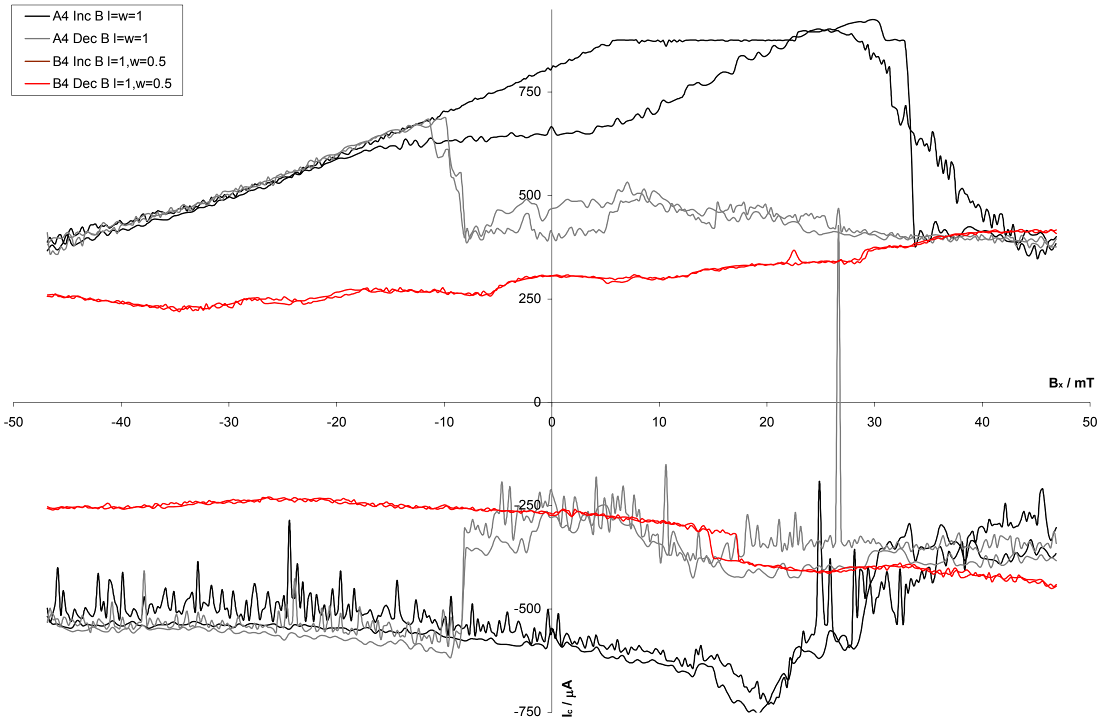

Figure B25 Sample 10191a, two micron wide tracks with a one micron long constriction with the width shown, field applied in the x-direction at 4·2K.

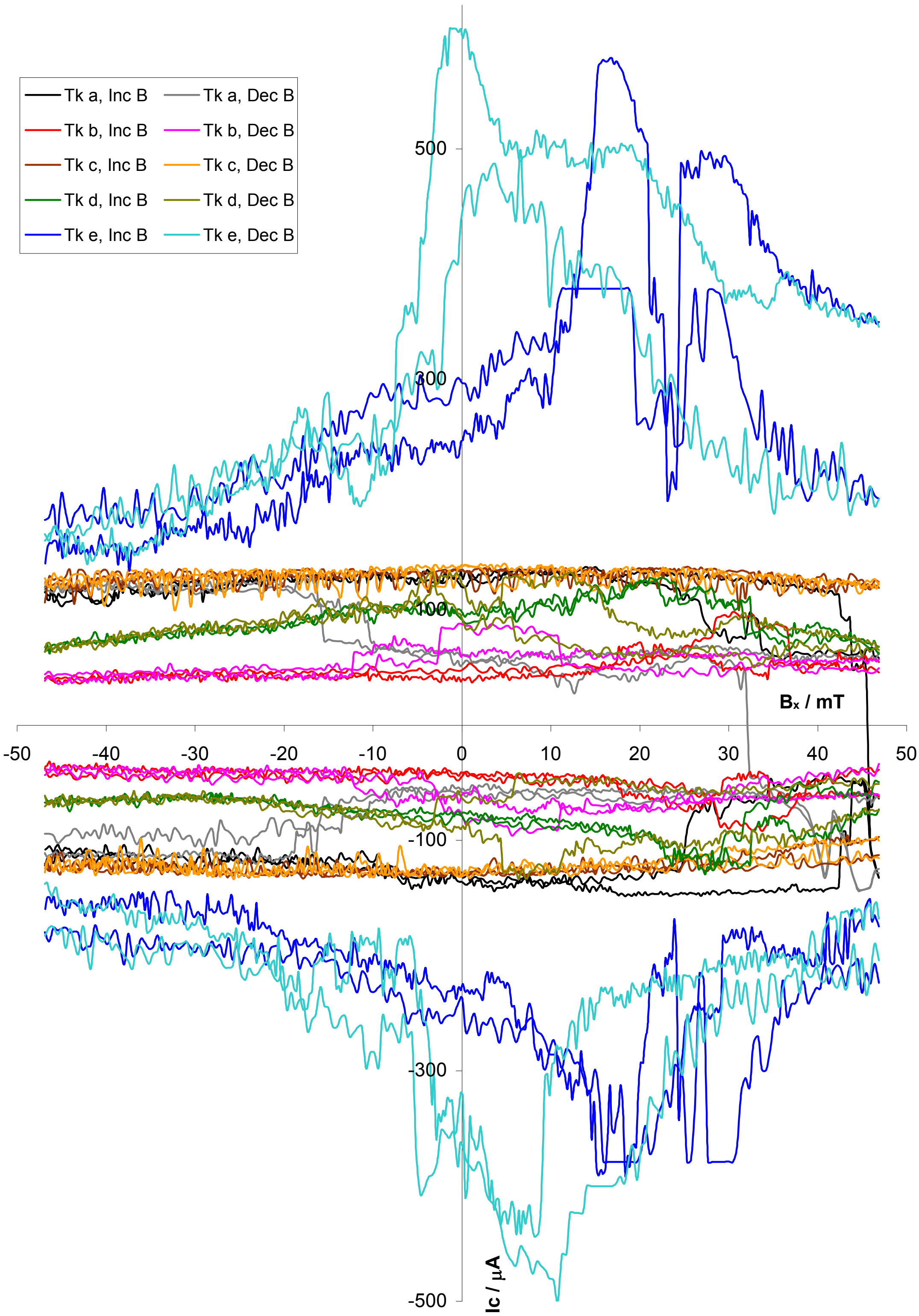

Figure B26 Sample 10191b, one micron wide track, field applied in the x-direction at 4·2K.

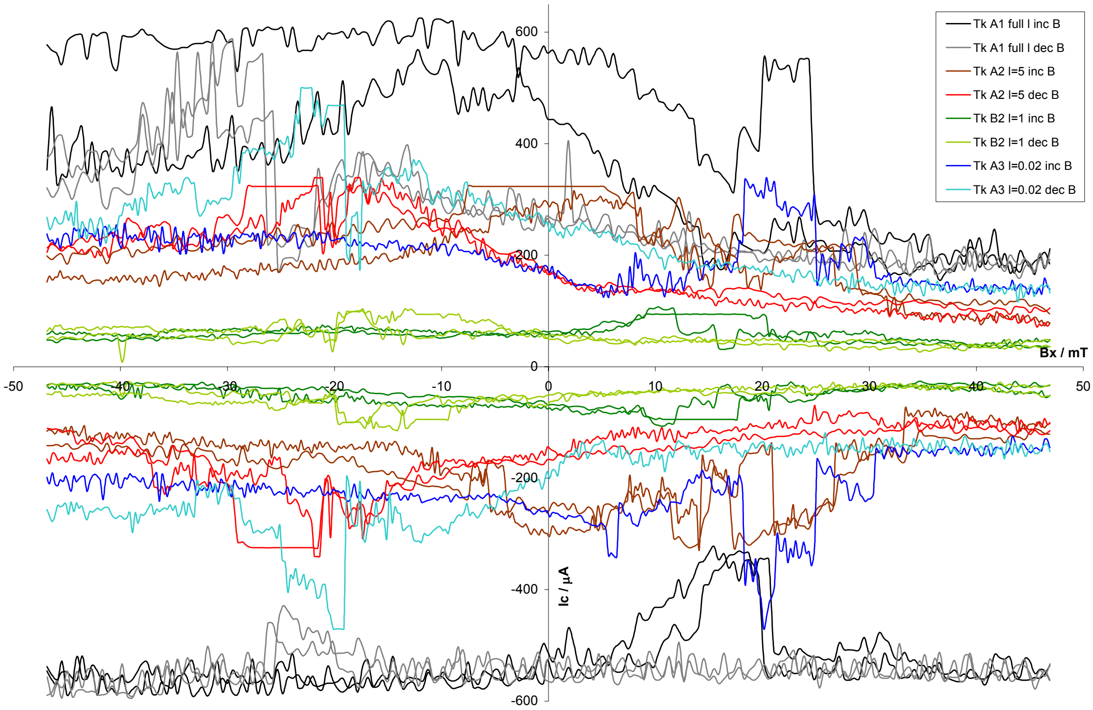

Figure B27 Sample 10191c, two micron wide tracks with a one micron wide constriction with the length shown, field applied in the x-direction at 4·2K.

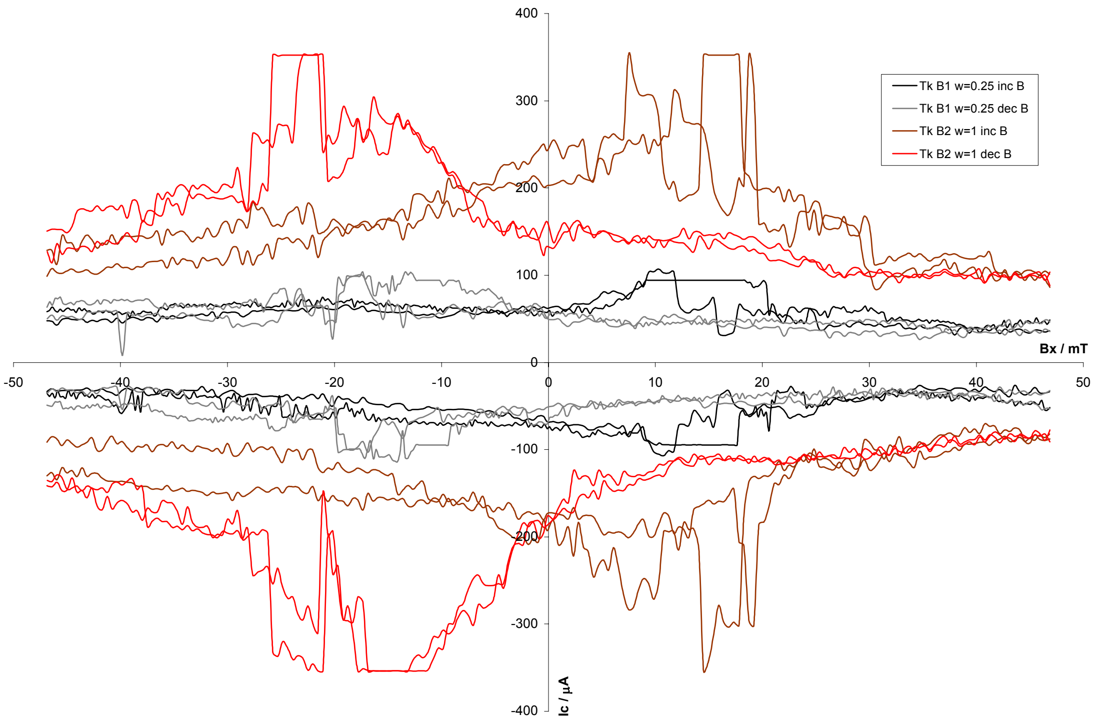

Figure B28 Sample 10191c, two micron wide tracks with a one micron long constriction with the width shown, field applied in the x-direction at 4·2K.

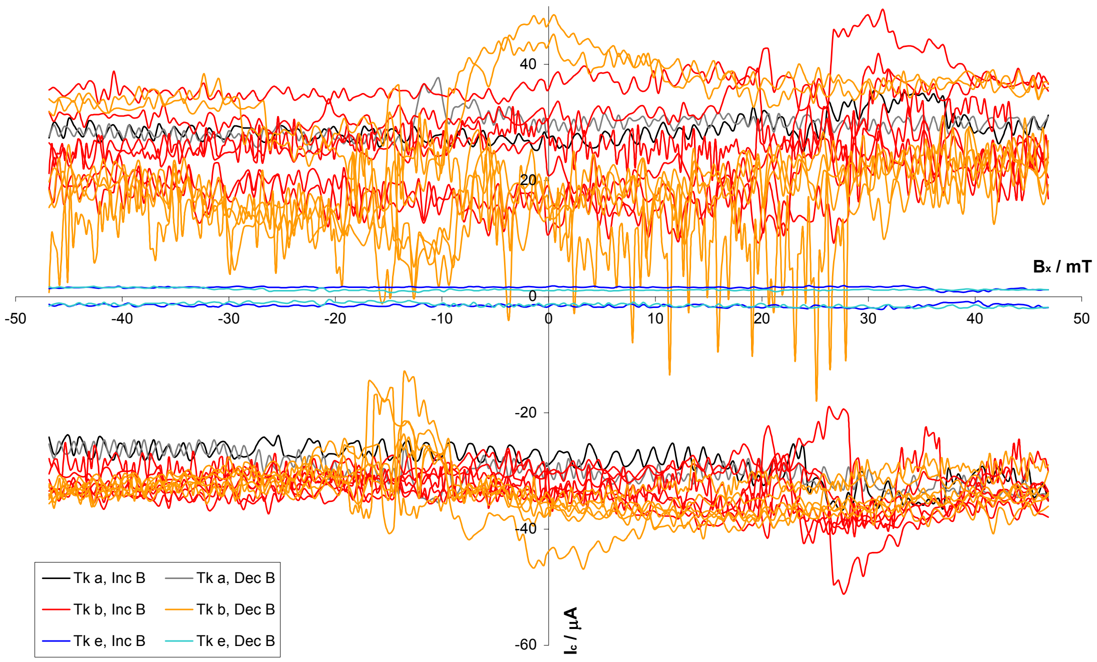

Figure B29 Sample 10191d, one micron wide track, field applied in the x-direction at 4·2K.

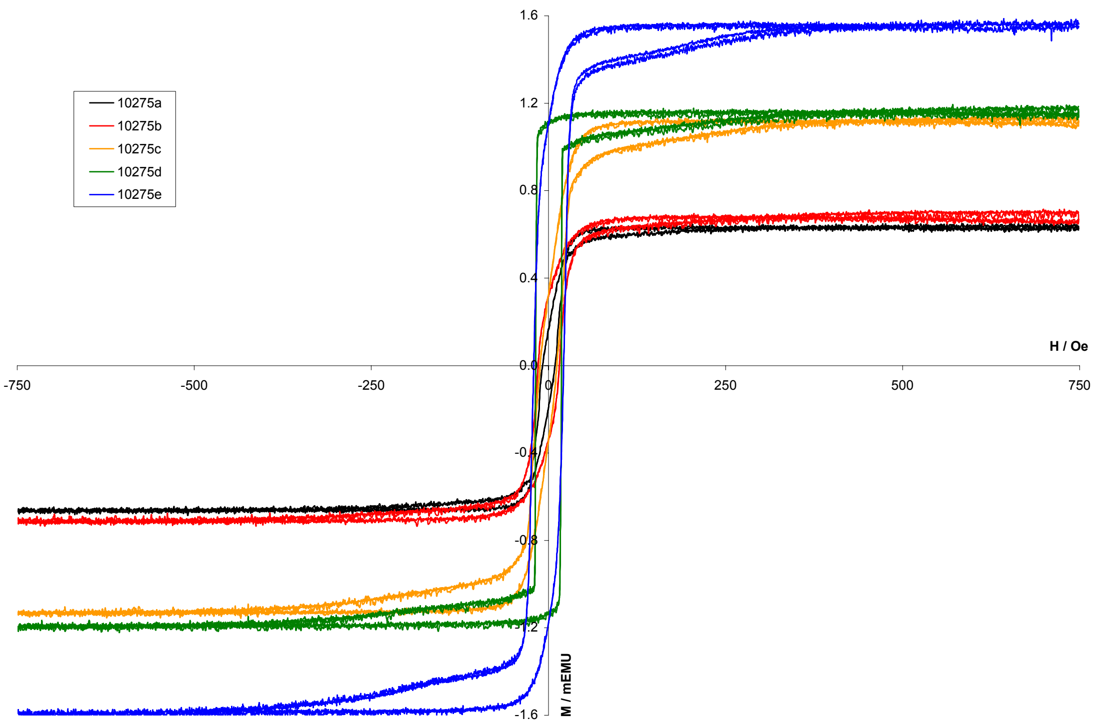

Figure B30 Samples 10275, unpatterned 10mm by 5mm film, field applied along the long axis at room temperature.

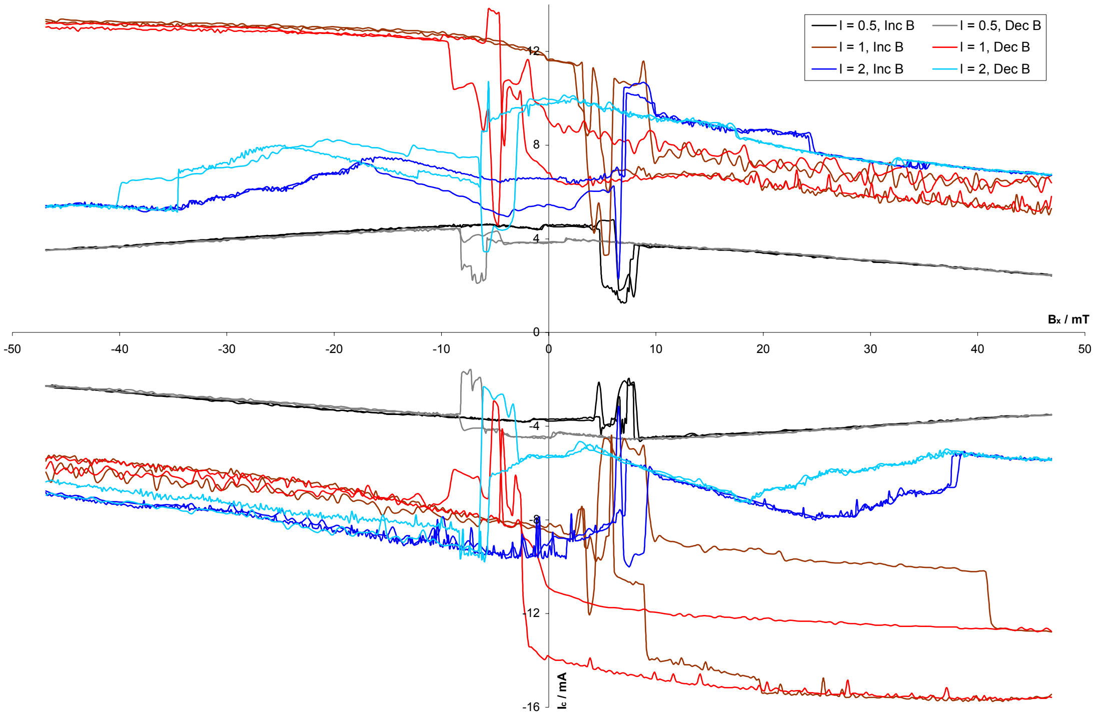

Figure B31 Sample 10275c, two micron wide tracks with a one micron wide constriction with the length given, field applied in the x-direction at 4·2K.

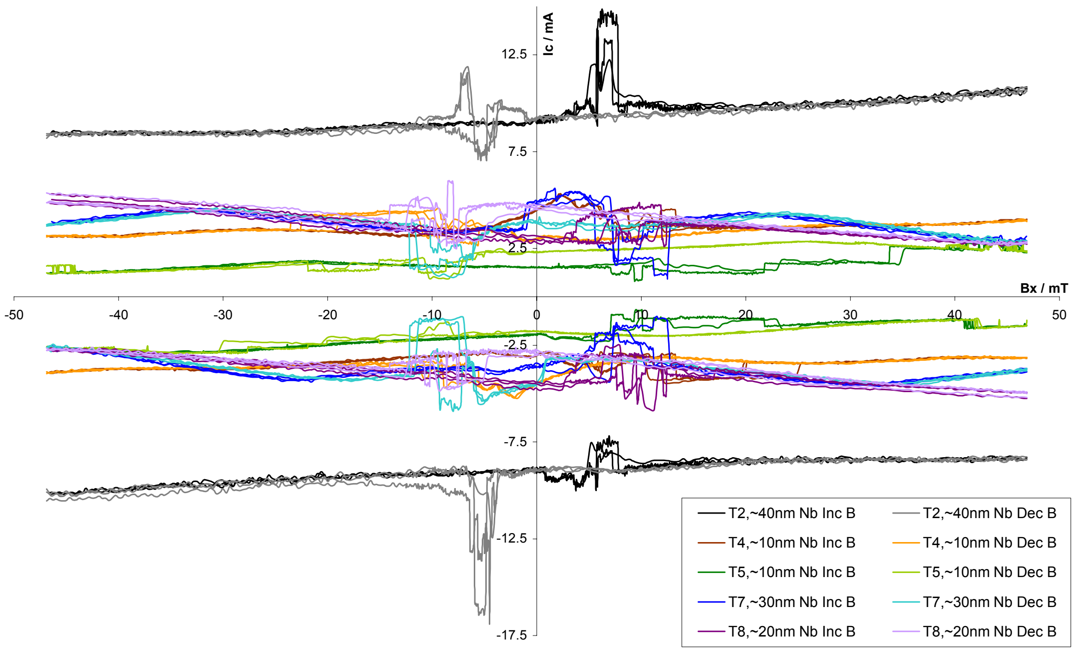

Figure B32 Sample 10275c, two micron wide tracks with the niobium thinned to the thickness shown over one micron, field applied in the x-direction at 4·2K.

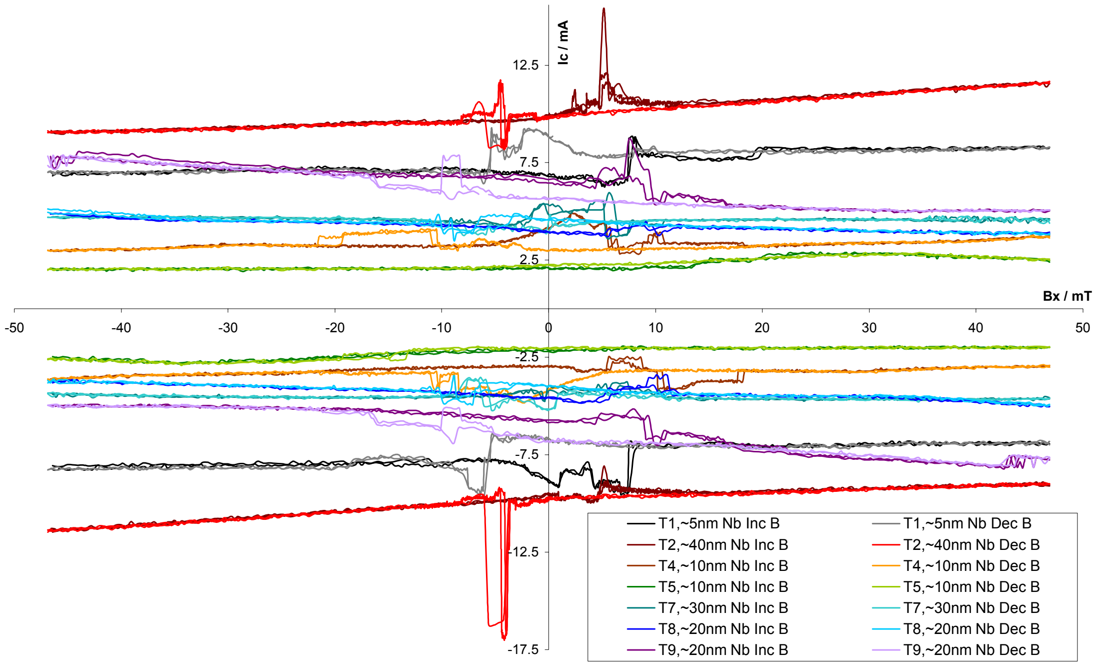

Figure B33 Sample 10275c, high voltage criterion, two micron wide tracks with the niobium thinned to the thickness shown over one micron, field applied in the x-direction at 4·2K.

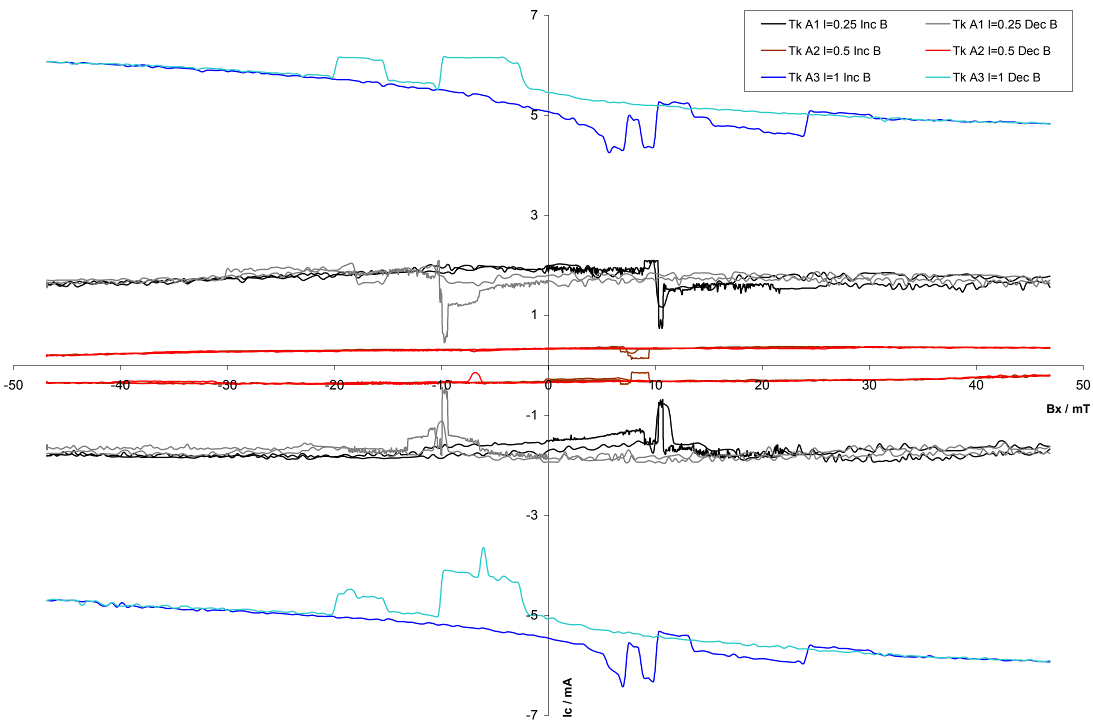

Figure B34 Sample 10275d, two micron wide tracks with a one micron wide constriction with the length given, field applied in the x-direction at 4·2K.

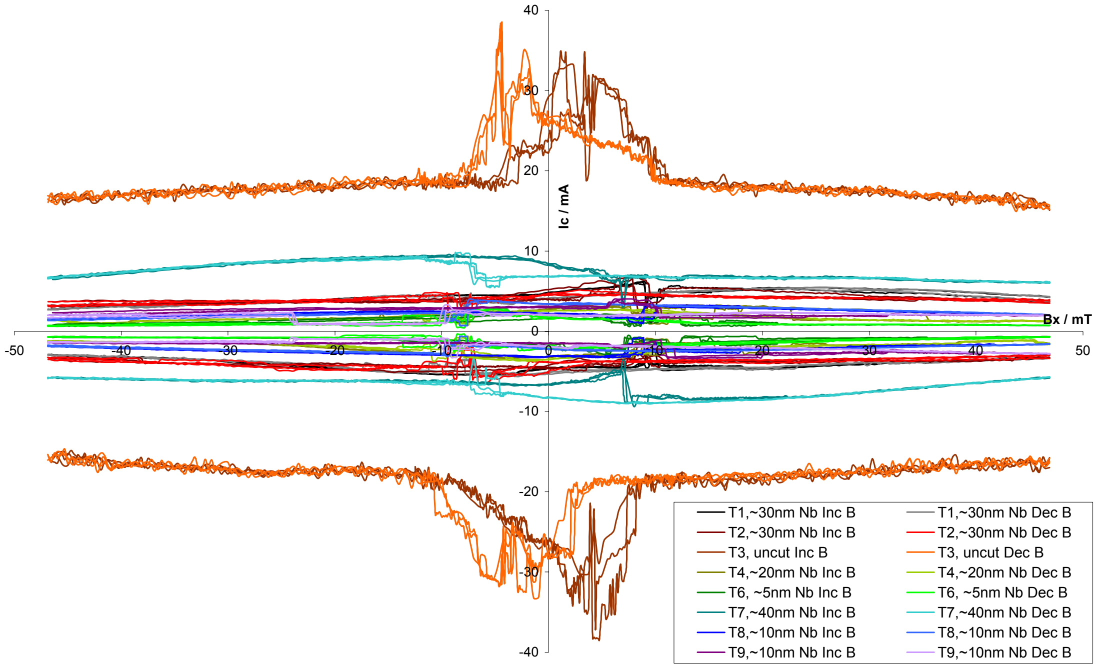

Figure B35 Sample 10275d, two micron wide tracks with the niobium thinned to the thickness shown over one micron, field applied in the x-direction at 4·2K.

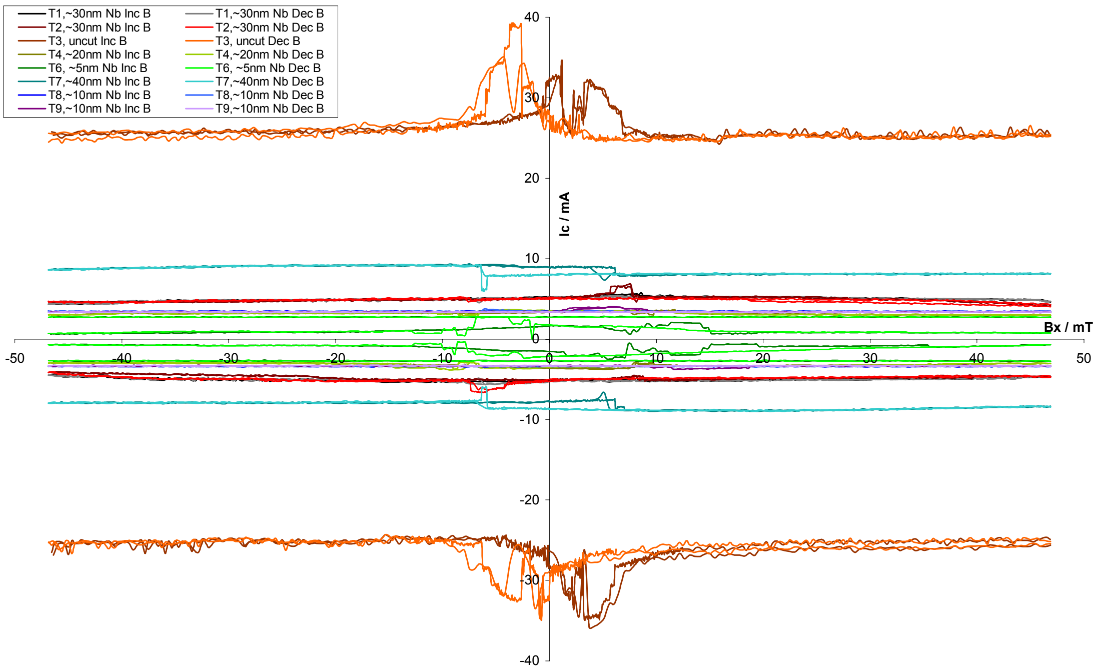

Figure B36 Sample 10275d, high voltage criterion, two micron wide tracks with the niobium thinned to the thickness shown over one micron, field applied in the x-direction at 4·2K.

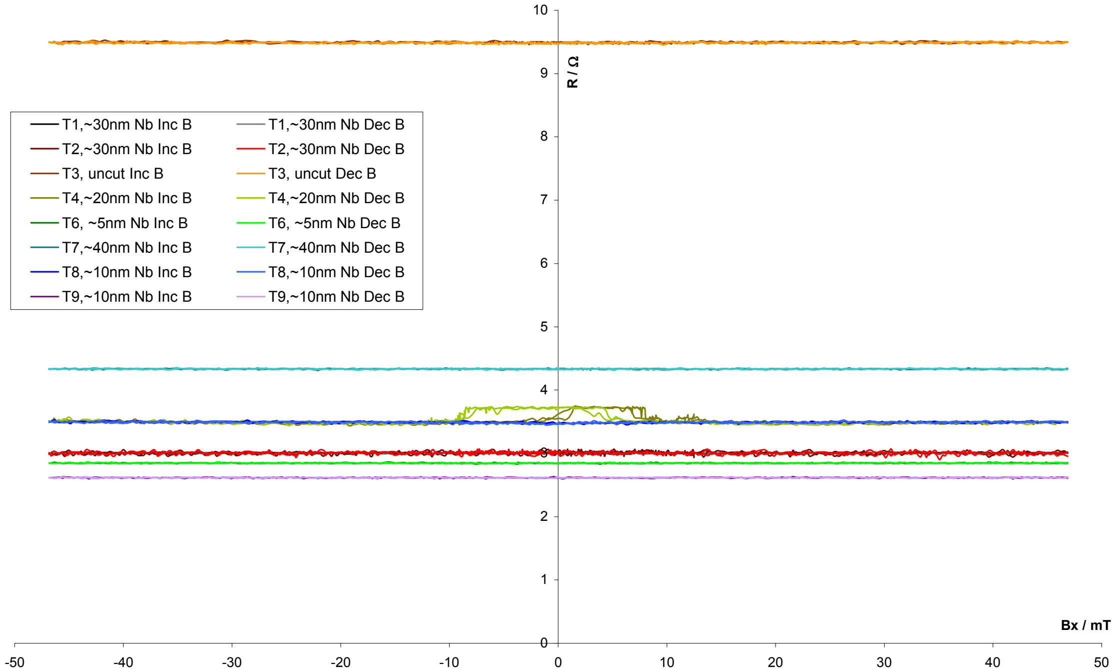

Figure B37 Sample 10275d, two micron wide tracks, field applied in the x-direction at 4·2K.

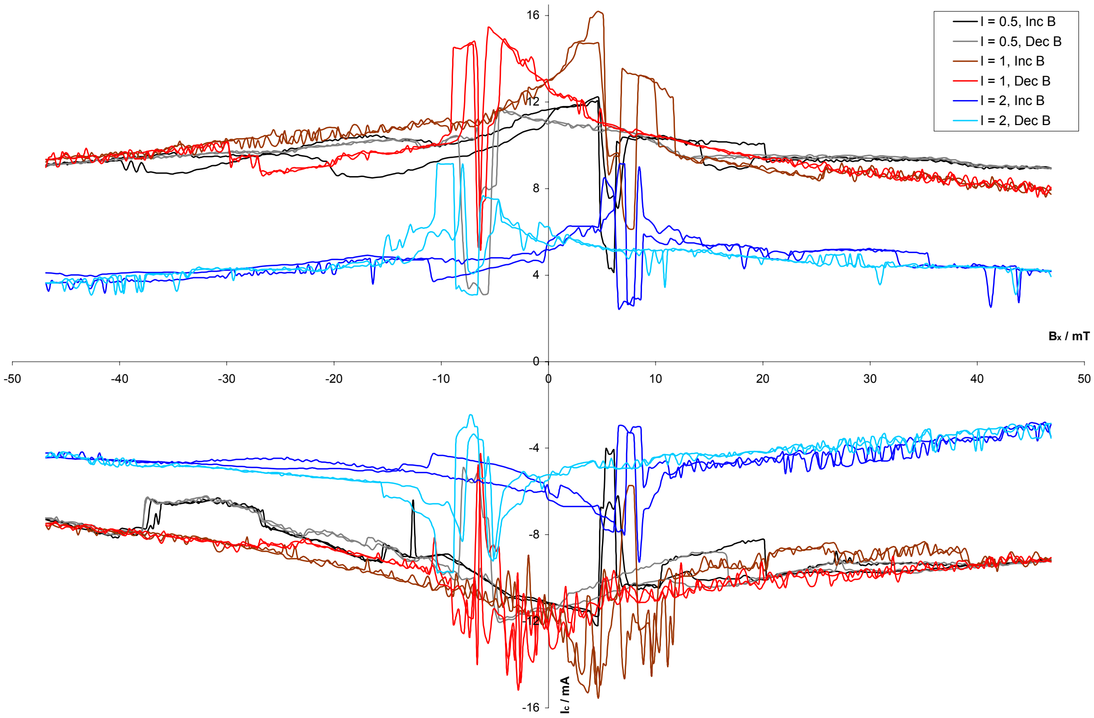

Figure B38 Sample 10275e, two micron wide tracks with a one micron wide constriction with the length given, field applied in the x-direction at 4·2K.

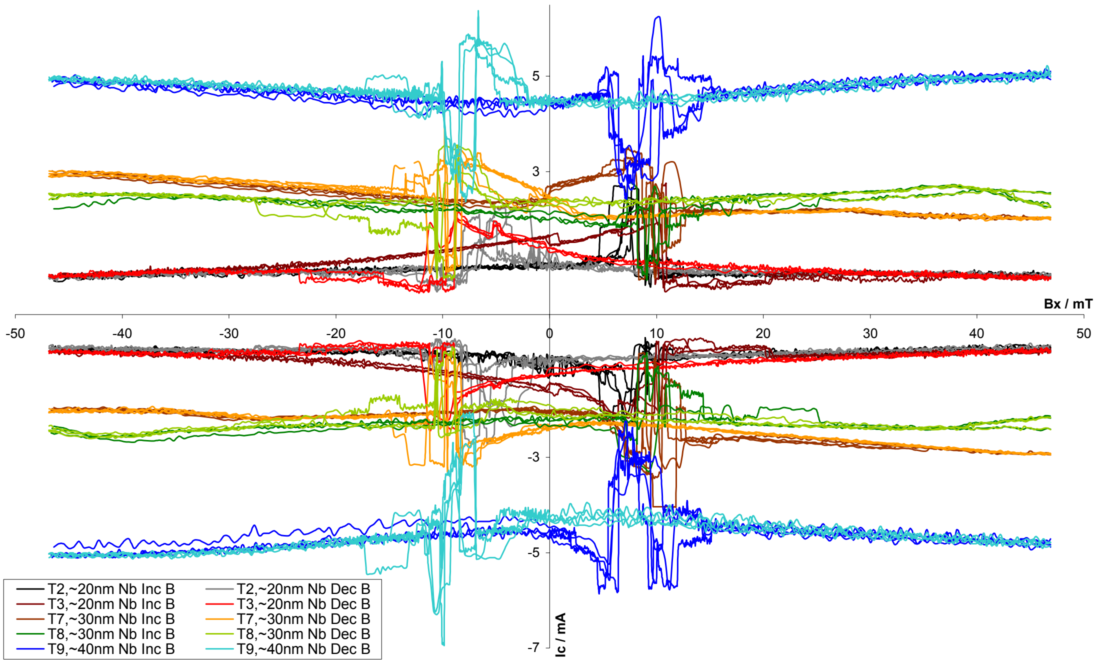

Figure B39 Sample 10275e, high voltage criterion, two micron wide tracks with the niobium thinned to the thickness shown over one micron, field applied in the x-direction at 4·2K.

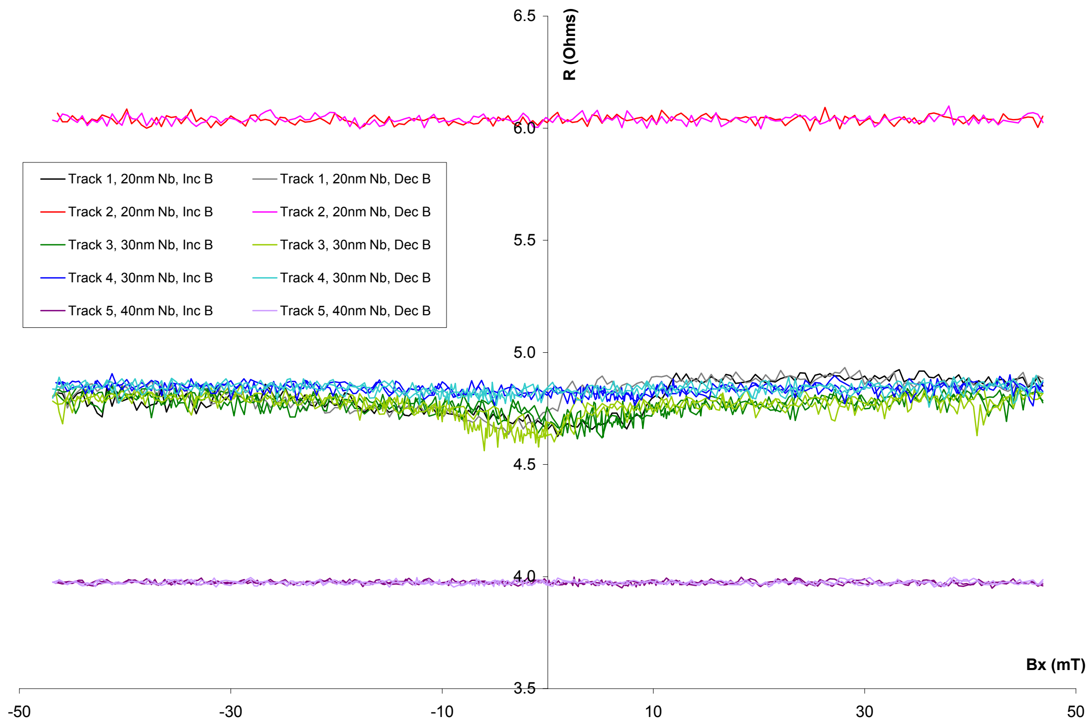

Figure B40 Sample 10275e, two micron wide tracks, field applied in the x-direction at 4·2K.

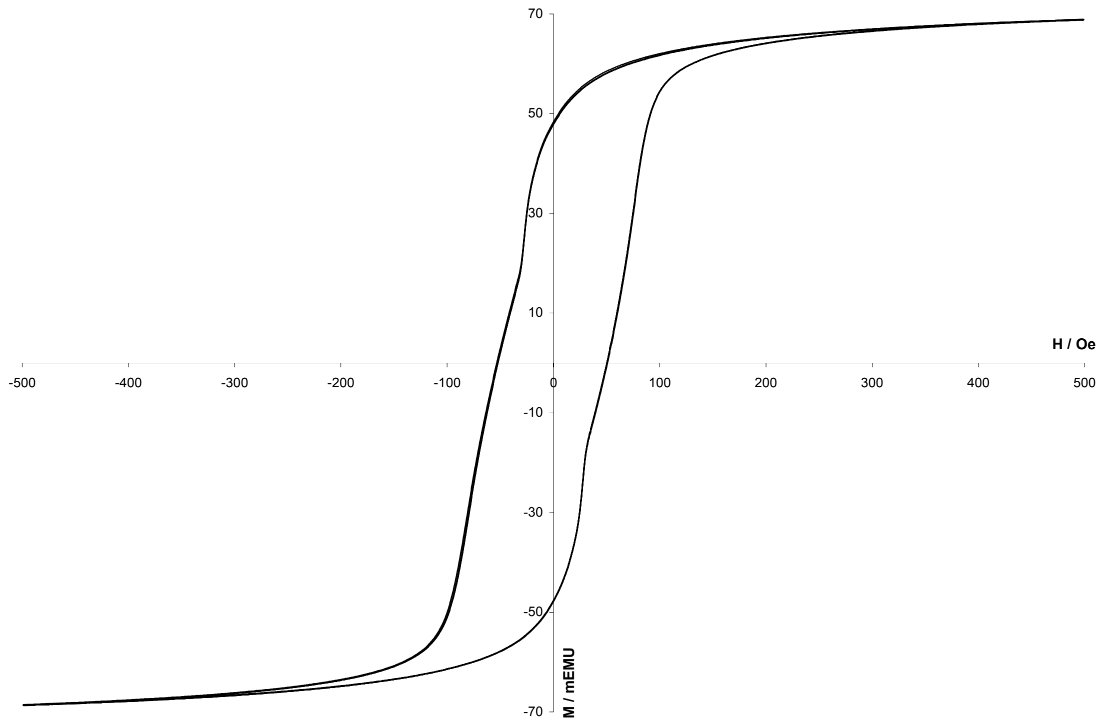

Figure B41 Samples 10323, unpatterned 10mm by 5mm film, field applied along the long axis at room temperature.

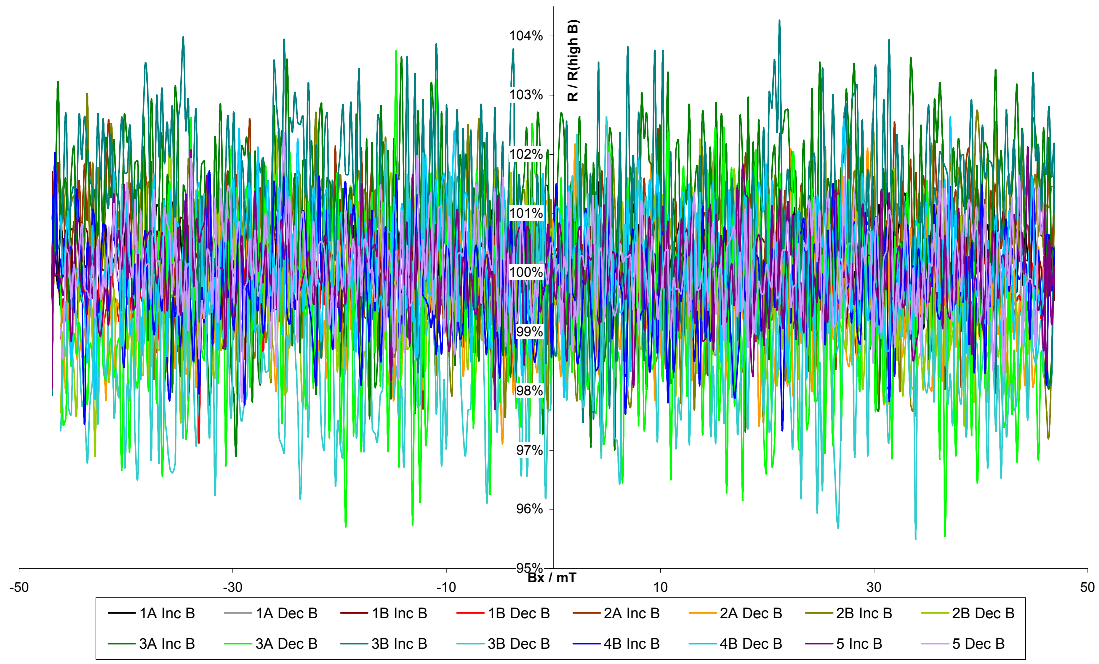

Figure B42 Sample 10354a, track width as shown, field applied in the x-direction at 4·2K.

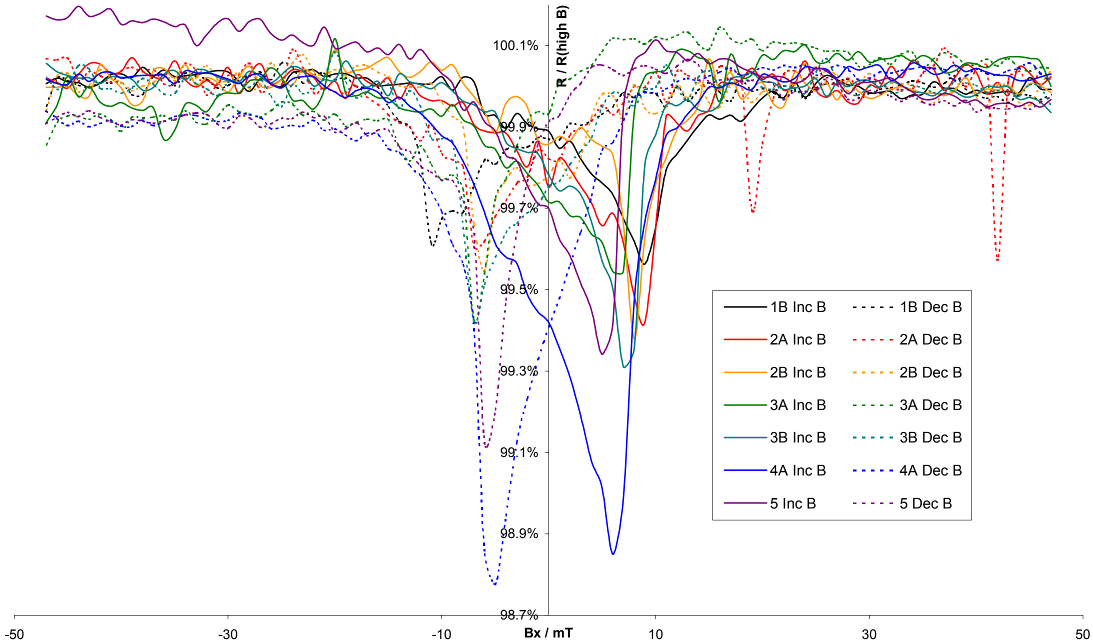

Figure B43 Sample 10354f, track width as shown, field applied in the x-direction at 4·2K.

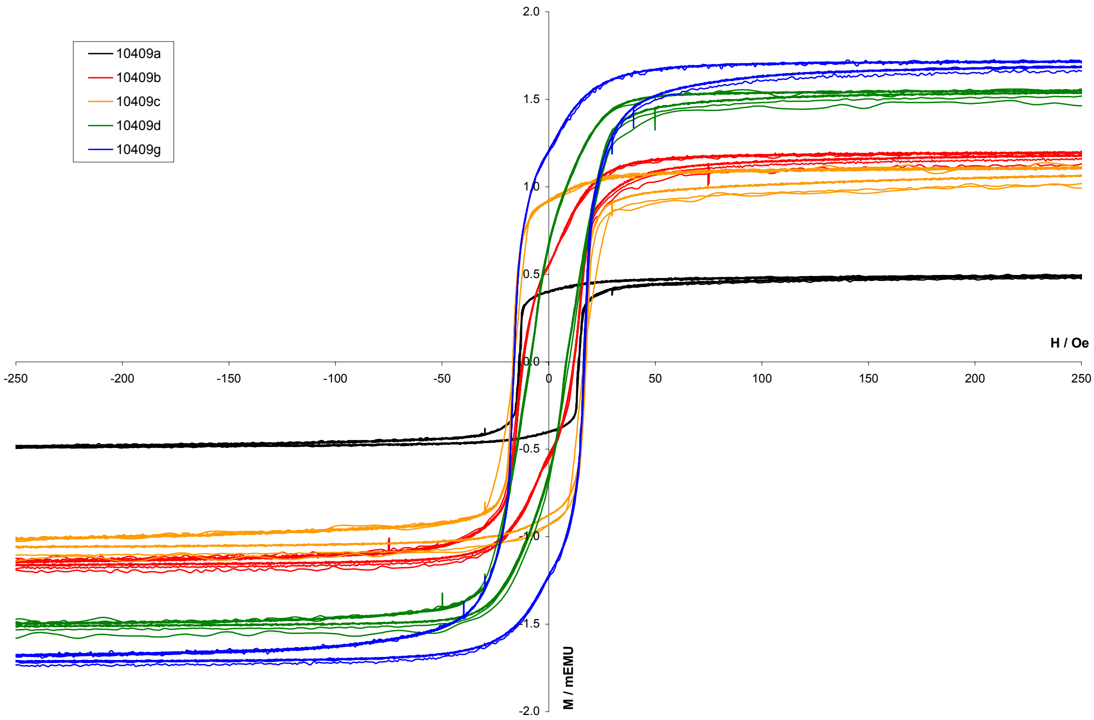

Figure B44 Samples 10409, unpatterned 10mm by 5mm film, field applied along the long axis at room temperature.

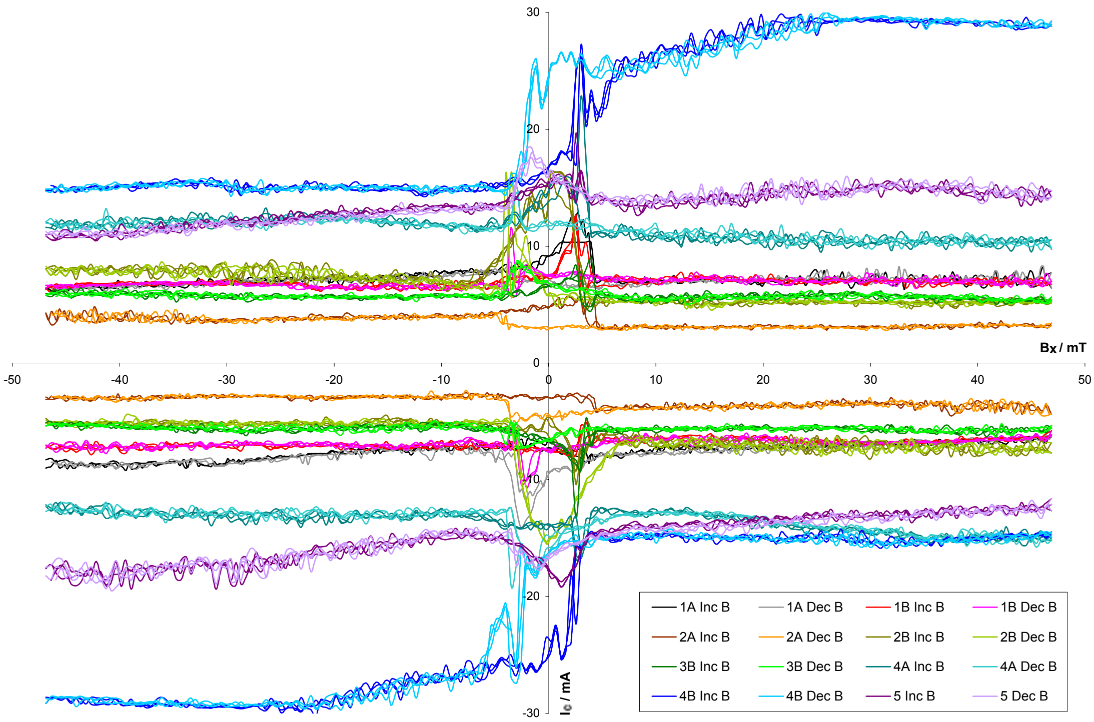

Figure B45 Sample 10409a, track width as shown, field applied in the x-direction at 4·2K.

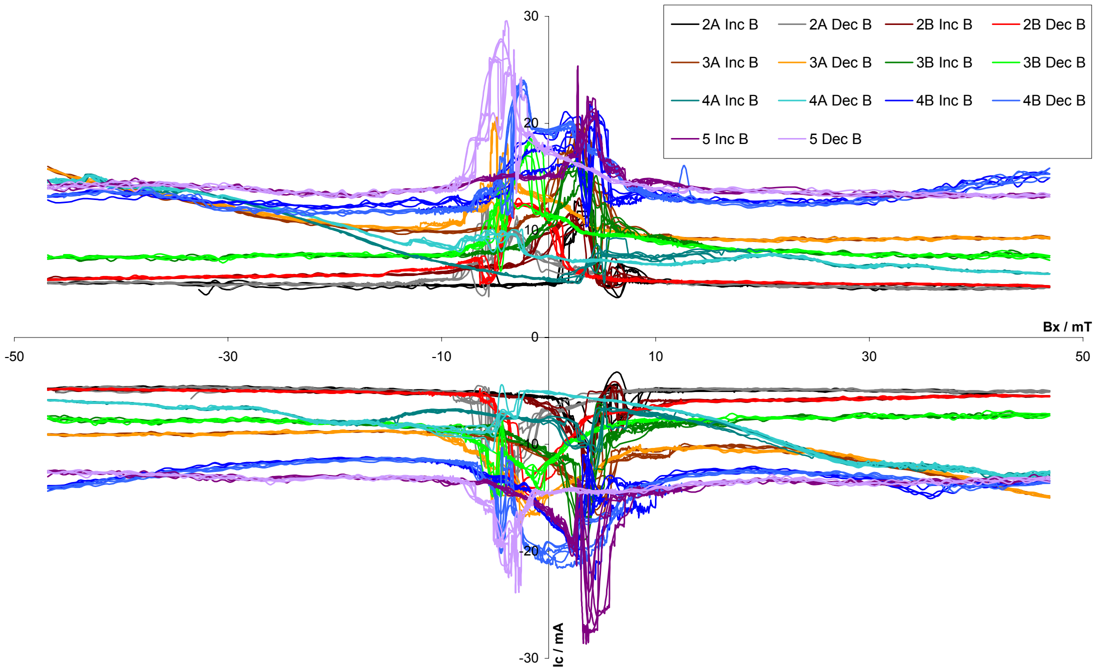

Figure B46 Sample 10409b, track width as shown, field applied in the x-direction at 4·2K.

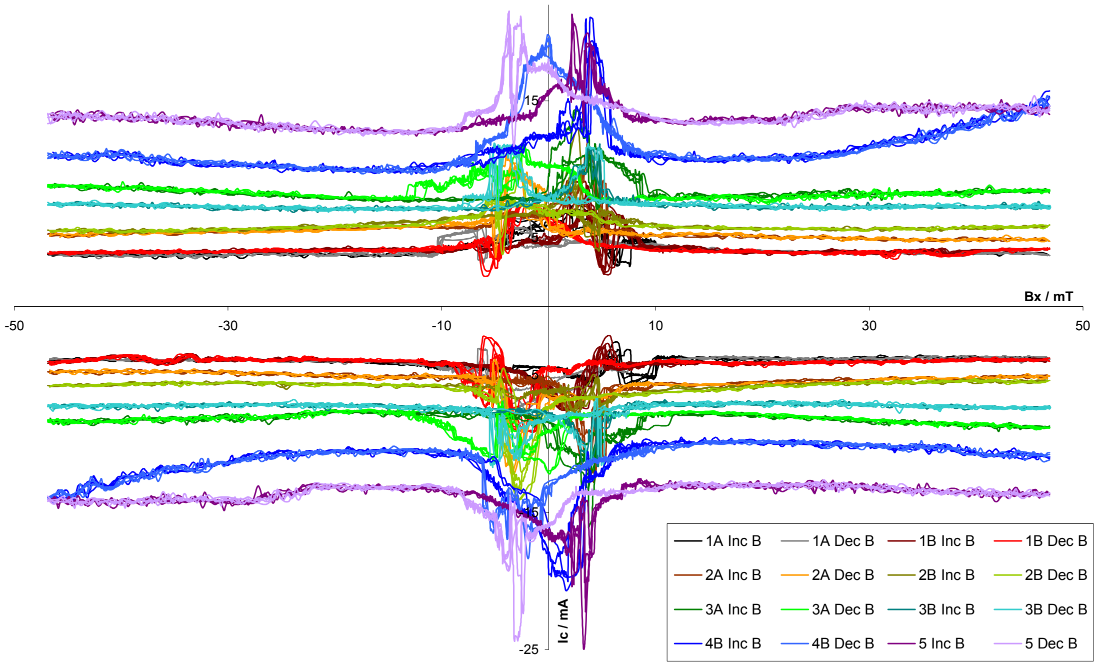

Figure B47 Sample 10409c, track width as shown, field applied in the x-direction at 4·2K.

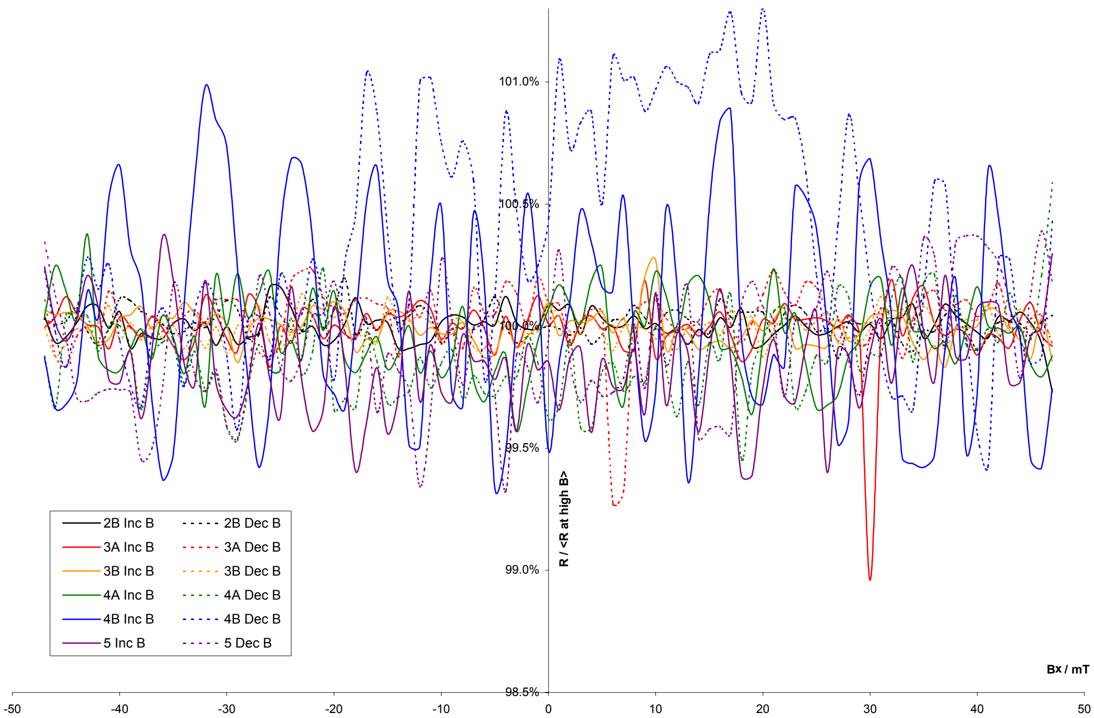

Figure B48 Sample 10409e, track width as shown, field applied in the x-direction at 4·2K.

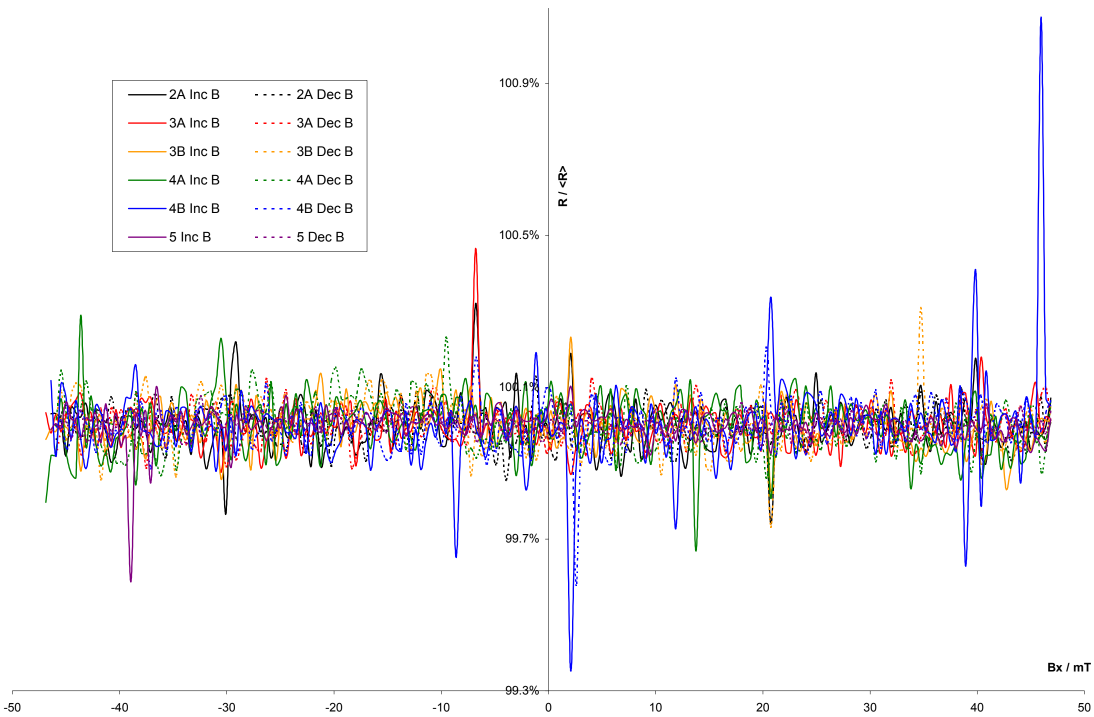

Figure B49 Sample 10409f, track width as shown, field applied in the x-direction at 4·2K.

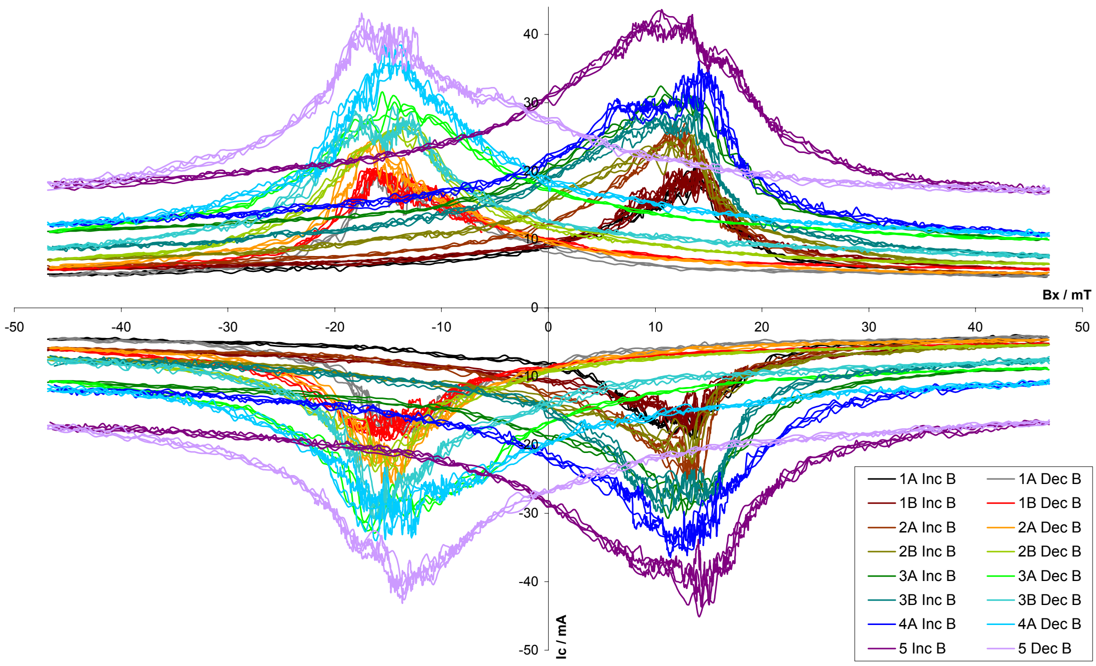

Figure B50 Sample 10432b, track width as shown, field applied in the x-direction at 4·2K.

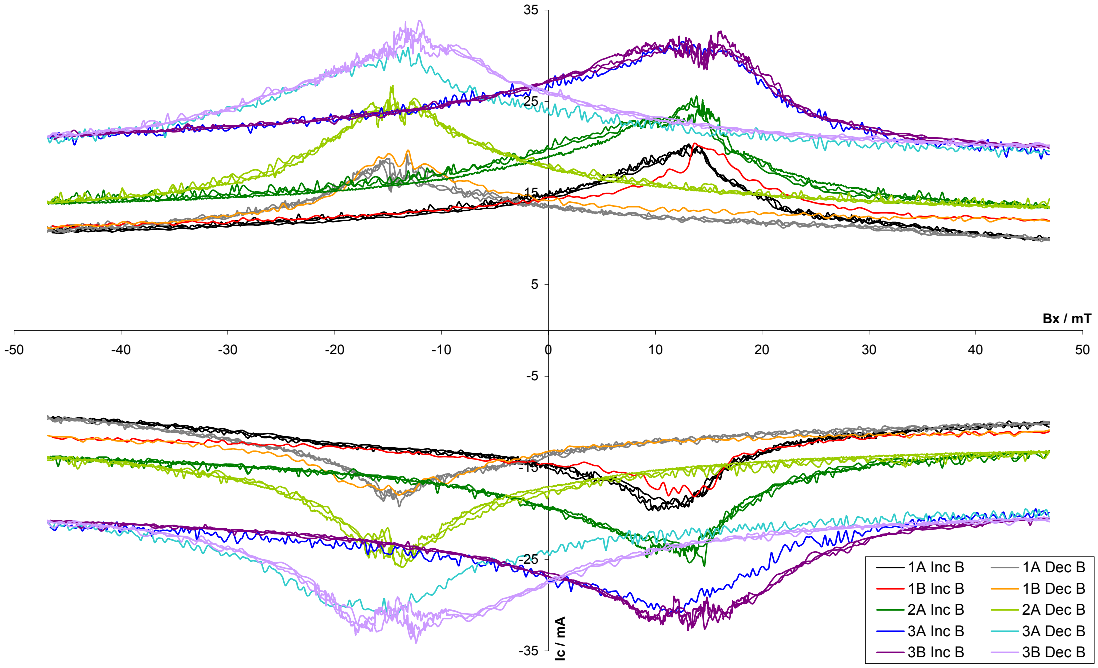

Figure B51 Sample 10432b, high voltage criterion, track width as shown, field applied in the x-direction at 4·2K.

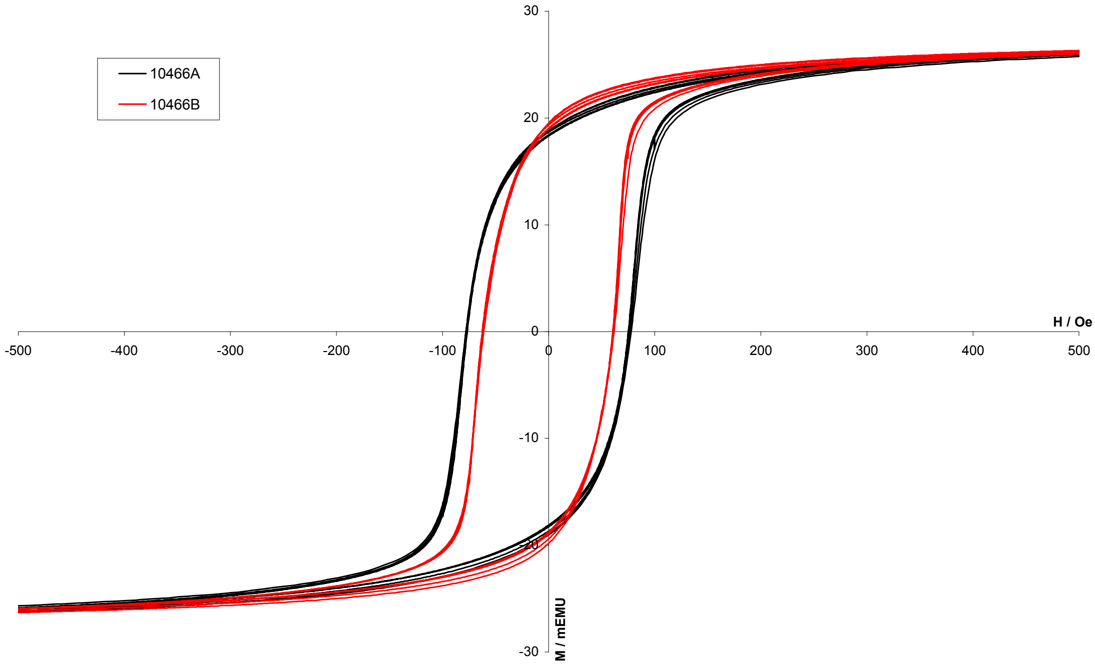

Figure B52 Samples 10466, unpatterned 10mm by 5mm film, field applied along the long axis at room temperature.

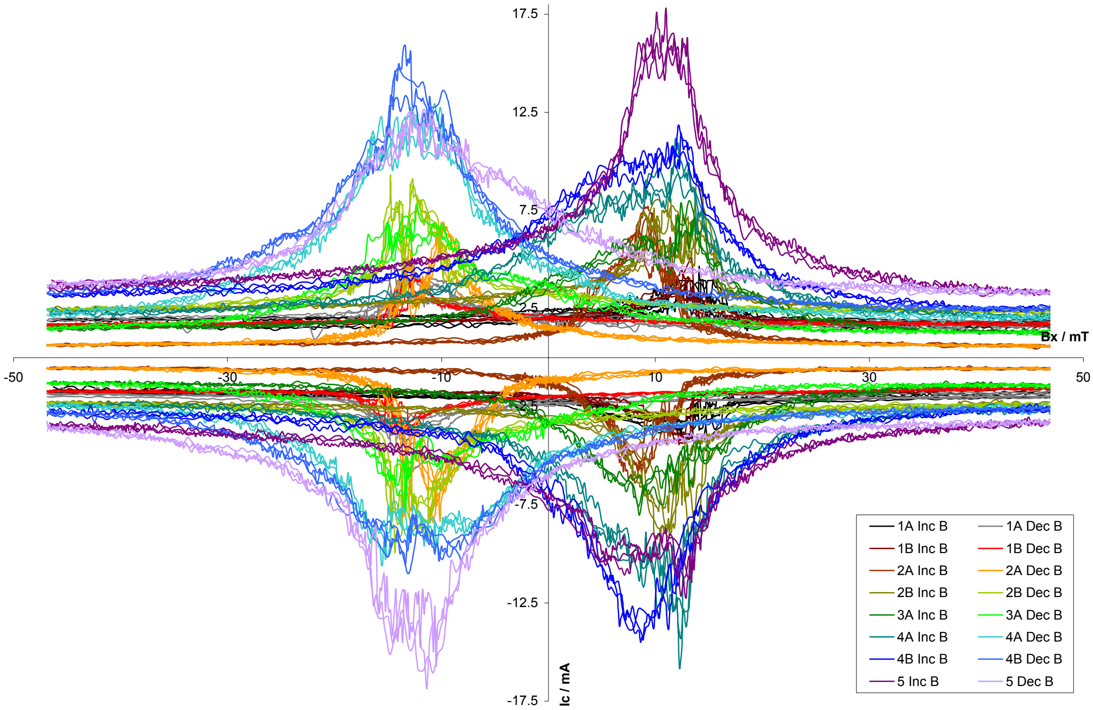

Figure B53 Sample 10466a, track width as shown, field applied in the x-direction at 4·2K.

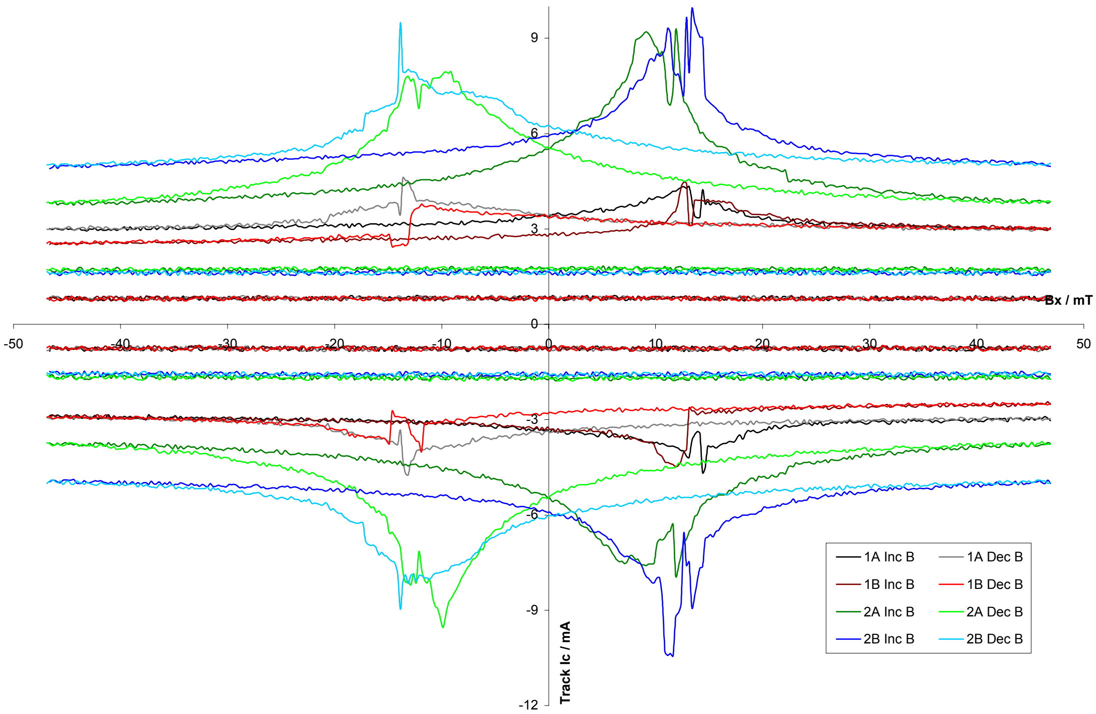

Figure B54 Sample 10466a, high voltage criterion, track width as shown, field applied in the x-direction at 4·2K.

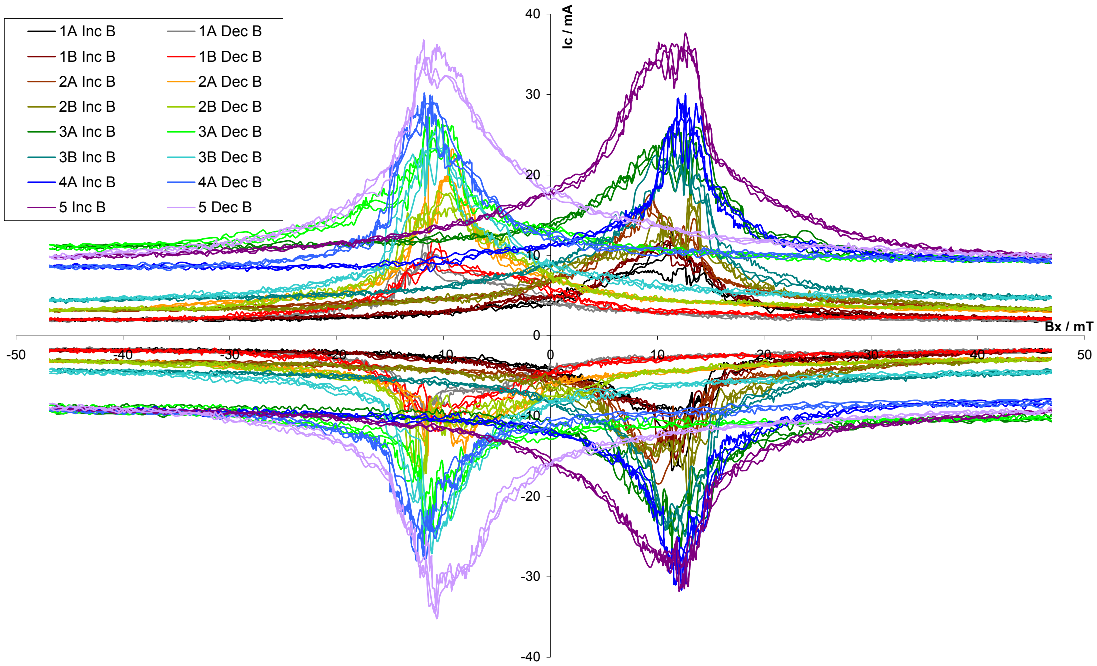

Figure B55 Sample 10466b, track width as shown, field applied in the x-direction at 4·2K.

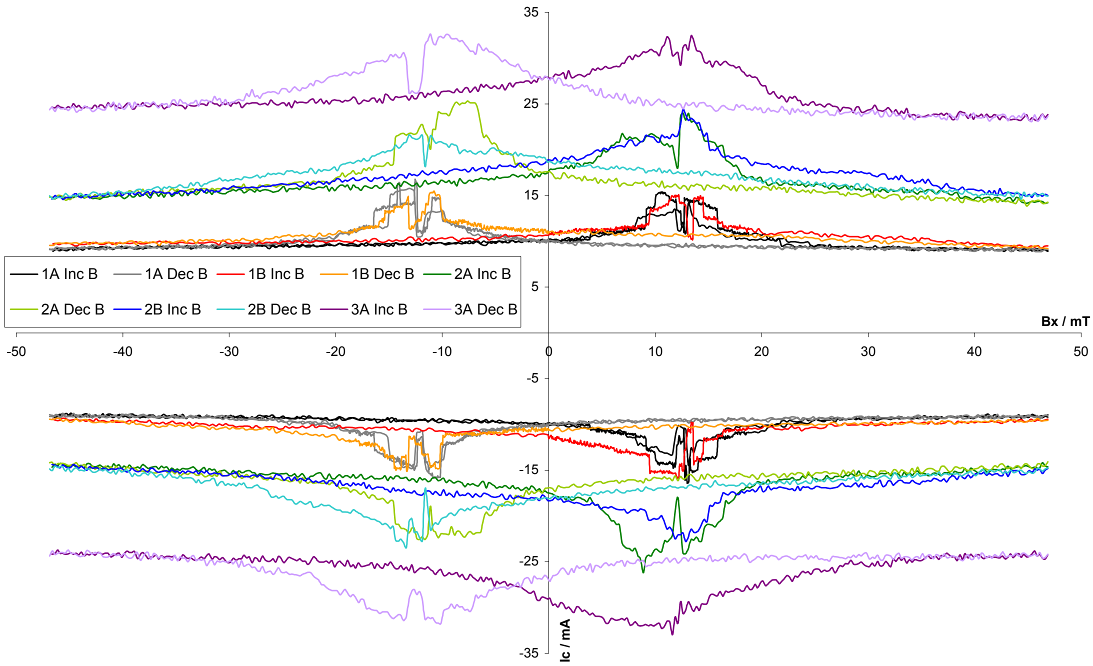

Figure B56 Sample 10466b, high voltage criterion, track width as shown, field applied in the x-direction at 4·2K.